

**ARMY RESEARCH LABORATORY**



**Relative Accuracies of Wind, Virtual Temperature, and  $C_2$   
Profiler Measurements at the Atmospheric Profiler  
Research Facility, White Sands Missile Range, NM**

**by J. Hines  
F. Eaton  
W. Hatch  
S. McLaughlin  
Battlefield Environment Directorate**

**W. Flowers  
L. Parker-Sedillo  
E. Santantonio  
G. Hoidale  
Science and Technology Corporation**

ARL-TR-1003

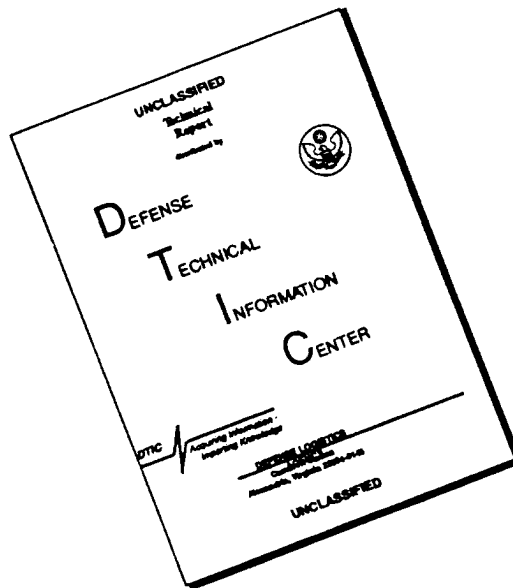
April 1996

*Approved for public release; distribution unlimited.*

19960614 059

DTIC QUALITY INSPECTED 1

# DISCLAIMER NOTICE



**THIS DOCUMENT IS BEST QUALITY AVAILABLE. THE COPY FURNISHED TO DTIC CONTAINED A SIGNIFICANT NUMBER OF PAGES WHICH DO NOT REPRODUCE LEGIBLY.**

## **NOTICES**

### **Disclaimers**

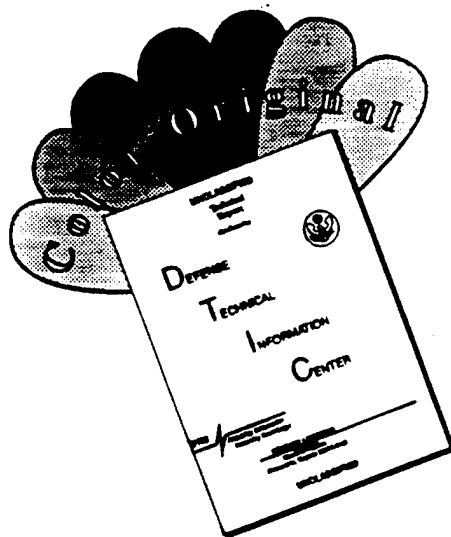
The findings in this report are not to be construed as an official Department of the Army position, unless so designated by other authorized documents.

The citation of trade names and names of manufacturers in this report is not to be construed as official Government indorsement or approval of commercial products or services referenced herein.

### **Destruction Notice**

When this document is no longer needed, destroy it by any method that will prevent disclosure of its contents or reconstruction of the document.

# DISCLAIMER NOTICE



THIS DOCUMENT IS BEST QUALITY AVAILABLE. THE COPY FURNISHED TO DTIC CONTAINED A SIGNIFICANT NUMBER OF COLOR PAGES WHICH DO NOT REPRODUCE LEGIBLY ON BLACK AND WHITE MICROFICHE.

# REPORT DOCUMENTATION PAGE

Form Approved  
OMB No. 0704-0188

Public reporting burden for this collection of information is estimated to average 1 hour per response, including the time for reviewing instructions, searching existing data sources, gathering and maintaining the data needed, and completing and reviewing the collection of information. Send comments regarding this burden estimate or any other aspect of this collection of information, including suggestions for reducing this burden, to Washington Headquarters Services, Directorate for Information Operations and Reports, 1215 Jefferson Davis Highway, Suite 1204, Arlington, VA 22202-4302, and to the Office of Management and Budget, Paperwork Reduction Project (0704-0188), Washington, DC 20503.

<b>1. AGENCY USE ONLY (Leave blank)</b>		<b>2. REPORT DATE</b> April 1996	<b>3. REPORT TYPE AND DATES COVERED</b> Final	
<b>4. TITLE AND SUBTITLE</b> Relative Accuracies of Wind, Virtual Temperature, and C <sub>n</sub> <sup>2</sup> Profiler Measurements at the Atmospheric Profiler Research Facility, White Sands Missile Range, NM			<b>5. FUNDING NUMBERS</b>	
<b>6. AUTHOR(S)</b> J. Hines, F. Eaton, W. Hatch, S. McLaughlin (ARL/BED) W. Flowers, L. Parker-Sedillo, E. Santantonio, G. Hoidale (STC)				
<b>7. PERFORMING ORGANIZATION NAME(S) AND ADDRESS(ES)</b> Science and Technology Corporation Las Cruces, NM 88005			<b>8. PERFORMING ORGANIZATION REPORT NUMBER</b> ARL-TR-1003	
<b>9. SPONSORING/MONITORING AGENCY NAME(S) AND ADDRESS(ES)</b> U.S. Army Research Laboratory Battlefield Environment Directorate Attn: AMSRL-BE-E White Sands Missile Range, NM 88002-5501			<b>10. SPONSORING/MONITORING AGENCY REPORT NUMBER</b> ARL-TR-1003	
<b>11. SUPPLEMENTARY NOTES</b>				
<b>12a. DISTRIBUTION / AVAILABILITY STATEMENT</b> Approved for public release; distribution unlimited.			<b>12b. DISTRIBUTION CODE</b> A	
<b>13. ABSTRACT (Maximum 200 words)</b>  Three wind profiling radars are being used at the Atmospheric Profiler Research Facility at White Sands Missile Range, NM, to obtain vertical profiles of wind, virtual temperature, and the refractive index structure parameter C <sub>n</sub> <sup>2</sup> from the boundary layer to the lower stratosphere. To assess the accuracy of the wind data measured with the 50-, 404-, and 924-MHz profilers, statistical intercomparisons were made of the winds measured by the three systems for 5 days during the spring of 1993 when there were complete data sets from the three systems. To assess the accuracy of vertical profiles of virtual temperature data measured with Radio Acoustic Sounding Systems (RASS) associated with each of the three wind profilers, comparisons were made with profiles of virtual temperature computed from the 21 radiosonde runs (spanning 13 days) during the spring of 1993 when there were data from all three RASS systems. Seven systems are used to obtain vertical profiles of C <sub>n</sub> <sup>2</sup> : 50-, 404-, and 924-MHz profilers, sodar, tower systems, a tethered balloon system, and FM-CW radar. The capability of each system to measure C <sub>n</sub> <sup>2</sup> is demonstrated.				
<b>14. SUBJECT TERMS</b> profiler, wind, temperature, radar, C <sub>n</sub> <sup>2</sup> , sodar			<b>15. NUMBER OF PAGES</b> 182	
			<b>16. PRICE CODE</b>	
<b>17. SECURITY CLASSIFICATION OF REPORT</b> Unclassified	<b>18. SECURITY CLASSIFICATION OF THIS PAGE</b> Unclassified	<b>19. SECURITY CLASSIFICATION OF ABSTRACT</b> Unclassified	<b>20. LIMITATION OF ABSTRACT</b> SAR	

# Contents

<b>Executive Summary</b> .....	9
<b>1. Introduction</b> .....	11
<b>2. Measurement Sites</b> .....	13
<b>3. Wind</b> .....	15
3.1 <i>System Comments</i> .....	17
3.1.1 50-MHz Profiler .....	18
3.1.2 404-MHz Profiler .....	18
3.1.3 924-MHz Profiler .....	18
3.2 <i>Availability of Data</i> .....	19
3.3 <i>Quality Control</i> .....	20
3.3.1 Raw Data .....	21
3.3.2 Consensus Method .....	21
3.3.3 Continuity Method .....	22
3.4 <i>Averaging</i> .....	24
3.4.1 Volume .....	24
3.4.2 Temporal .....	24
3.5 <i>Relative Accuracies</i> .....	26
3.5.1 Analyses .....	26
3.5.2 Statistics .....	64
3.6 <i>Meteorological Conditions</i> .....	74
3.6.1 7 Mar 93 .....	75
3.6.2 16 May 93 .....	75
3.6.3 17 May 93 .....	76
3.6.4 21 May 93 .....	76
3.6.5 25 May 93 .....	77
3.7 <i>Discussion</i> .....	77
3.7.1 7 Mar 93 .....	77
3.7.2 16 May 93 .....	78
3.7.3 17 May 93 .....	78
3.7.4 21 May 93 .....	78
3.7.5 25 May 93 .....	79
<b>4. Virtual Temperature</b> .....	81
4.1 <i>System Comments</i> .....	82
4.1.1 50-MHz Profiler .....	83
4.1.2 404-MHz Profiler .....	83

4.1.3	924-MHz Profiler	83
4.1.4	Radiosonde	84
4.2	<i>Availability of Data</i>	84
4.3	<i>Quality Control</i>	85
4.4	<i>Spatial and Temporal Averaging</i>	86
4.5	<i>Relative Accuracies</i>	99
4.5.1	Altitude Dependence	102
4.5.2	Stability (Day Versus Night) Dependence	103
4.6	<i>Meteorological Conditions</i>	103
4.6.1	13 May 93	103
4.6.2	14 May 93	104
4.6.3	18 May 93	104
4.6.4	26 May 93	105
4.6.5	27 May 93	105
4.6.6	3 Jun 93	105
4.6.7	5 Jun 93	106
4.6.8	9 Jun 93	106
4.6.9	10 Jun 93	107
4.6.10	11 Jun 93	107
4.6.11	14 Jun 93	108
4.6.12	15 Jun 93	108
4.6.13	17 Jun 93	109
4.7	<i>Discussion</i>	109
<b>5.</b>	<b>Refractive Index Structure Parameter</b>	<b>111</b>
5.1	<i>System Comments</i>	112
5.1.1	50-MHz Radar Profiler	113
5.1.2	Sodar	115
5.1.3	Tower Systems	120
5.1.4	Tethered Balloon System (Tethersonde)	126
5.1.5	FM-CW Radar	129
5.2	<i>Availability of Data</i>	136
5.3	<i>Quality Control</i>	136
5.4	<i>Volume and Temporal Averaging</i>	136
5.5	<i>Summary</i>	136
<b>6.</b>	<b>Conclusions</b>	<b>139</b>
	<b>References</b>	<b>141</b>
	<b>Acronyms and Abbreviations</b>	<b>145</b>

<b>Bibliography</b> .....	147
<b>Appendices</b>	
<i>Appendix A. Range Gate Information for the Wind Profilers</i> .....	149
<i>Appendix B. Range Gate Information for the Virtual Temperature Profilers</i> .....	157
<i>Appendix C. SAS Statistical Runs for Table 17</i> .....	163
<b>Distribution</b> .....	173

### Figures

1. Aerial view of the APRF. The FM-CW radar is located at the extreme left; the 50-MHz radar is located at the right-center .....	14
2. Horizontal separation of the axes of the antenna beams for each of the three wind profiling radars as a function of altitude .....	17
3. Availability of wind, temperature, and $C_n^2$ data from the three radar profilers, APRF complex, WSMR, Jan to Jun 93 .....	20
4. Vertical measurement range for the four wind profiler systems, APRF complex, WSMR .....	25
5. Wind barb to wind speed conversion .....	27
6. Hourly average vertical profiles of wind speed and wind direction, as measured with the (a) 50- and (b) 404- (high mode) MHz profilers, APRF complex, WSMR, 0000 to 1200 MST, 7 Mar 93 .....	28
7. Hourly average vertical profiles of wind speed and wind direction, as measured with the (a) 50- and (b) 404- (high mode) MHz profilers, APRF complex, WSMR, 1200 to 2400 MST, 7 Mar 93 .....	29
8. Hourly average vertical profiles of wind speed and wind direction, as measured with the (a) 50- and (b) 404- (low mode) MHz profilers, APRF complex, WSMR, 0000 to 1200 MST, 7 Mar 93 .....	30
9. Hourly average vertical profiles of wind speed and wind direction, as measured with the (a) 50- and (b) 404- (low mode) MHz profilers, APRF complex, WSMR, 1200 to 2400 MST, 7 Mar 93 .....	31
10. Hourly average vertical profiles of wind speed and wind direction, as measured with the (a) 50- and (b) 404- (high mode) MHz profilers, APRF complex, WSMR, 0000 to 1200 MST, 16 May 93 .....	32
11. Hourly average vertical profiles of wind speed and wind direction, as measured with the (a) 50- and (b) 404- (high mode) MHz profilers, APRF complex, WSMR, 1200 to 2400 MST, 16 May 93 .....	33
12. Hourly average vertical profiles of wind speed and wind direction, as measured with the (a) 50- and (b) 404- (low mode) MHz profilers, APRF complex, WSMR, 0000 to 1200 MST, 16 May 93 .....	34

13.	Hourly average vertical profiles of wind speed and wind direction, as measured with the (a) 50- and (b) 404- (low mode) MHz profilers, APRF complex, WSMR, 1200 to 2400 MST, 16 May 93 . . . . .	35
14.	Hourly average vertical profiles of wind speed and wind direction, as measured with the (a) 924- and (b) 404- (low mode) MHz profilers, APRF complex, WSMR, 0000 to 1200 MST, 16 May 93 . . . . .	36
15.	Hourly average vertical profiles of wind speed and wind direction, as measured with the (a) 924- and (b) 404- (low mode) MHz profilers, APRF complex, WSMR, 1200 to 2400 MST, 16 May 93 . . . . .	37
16.	Hourly average vertical profiles of wind speed and wind direction, as measured with the (a) 924- and (b) 50-MHz profilers, APRF complex, WSMR, 0000 to 1200 MST, 16 May 93 . . . . .	38
17.	Hourly average vertical profiles of wind speed and wind direction, as measured with the (a) 924- and (b) 50-MHz profilers, APRF complex, WSMR, 1200 to 2400 MST, 16 May 93 . . . . .	39
18.	Hourly average vertical profiles of wind speed and wind direction, as measured with the (a) 50- and (b) 404- (high mode) MHz profilers, APRF complex, WSMR, 0000 to 1200 MST, 17 May 93 . . . . .	40
19.	Hourly average vertical profiles of wind speed and wind direction, as measured with the (a) 50- and (b) 404- (high mode) MHz profilers, APRF complex, WSMR, 1200 to 2400 MST, 17 May 93 . . . . .	41
20.	Hourly average vertical profiles of wind speed and wind direction, as measured with the (a) 50- and (b) 404- (low mode) MHz profilers, APRF complex, WSMR 0000 to 1200 MST, 17 May 93 . . . . .	42
21.	Hourly average vertical profiles of wind speed and wind direction, as measured with the (a) 50- and (b) 404- (low mode) MHz profilers, APRF complex, WSMR, 1200 to 2400 MST, 17 May 93 . . . . .	43
22.	Hourly average vertical profiles of wind speed and wind direction, as measured with the (a) 924- and (b) 404- (low mode) MHz profilers, APRF complex, WSMR, 0000 to 1200 MST, 17 May 93 . . . . .	44
23.	Hourly average vertical profiles of wind speed and wind direction, as measured with the (a) 924- and (b) 404- (low mode) MHz profilers, APRF complex, WSMR, 1200 to 2400 MST, 17 May 93 . . . . .	45
24.	Hourly average vertical profiles of wind speed and wind direction, as measured with the (a) 924- and (b) 50-MHz profilers, APRF complex, WSMR, 0000 to 1200 MST, 17 May 93 . . . . .	46
25.	Hourly average vertical profiles of wind speed and wind direction, as measured with the (a) 924- and (b) 50-MHz profilers, APRF complex, WSMR, 1200 to 2400 MST, 17 May 93 . . . . .	47
26.	Hourly average vertical profiles of wind speed and wind direction, as measured with the (a) 50- and (b) 404- (high mode) MHz profilers, APRF complex, WSMR, 0000 to 1200 MST, 21 May 93 . . . . .	48
27.	Hourly average vertical profiles of wind speed and wind direction, as measured with the (a) 50- and (b) 404- (high mode) MHz profilers, APRF complex, WSMR, 1200 to 2400 MST, 21 May 93 . . . . .	49

28.	Hourly average vertical profiles of wind speed and wind direction, as measured with the (a) 50- and (b) 404- (low mode) MHz profilers, APRF complex, WSMR, 0000 to 1200 MST, 21 May 93 . . . . .	50
29.	Hourly average vertical profiles of wind speed and wind direction, as measured with the (a) 50- and (b) 404- (low mode) MHz profilers, APRF complex, WSMR, 1200 to 2400 MST, 21 May 93 . . . . .	51
30.	Hourly average vertical profiles of wind speed and wind direction, as measured with the (a) 924- and (b) 404- (low mode) MHz profilers, APRF complex, WSMR, 0000 to 1200 MST, 21 May 93 . . . . .	52
31.	Hourly average vertical profiles of wind speed and wind direction, as measured with the (a) 924- and (b) 404- (low mode) MHz profilers, APRF complex, WSMR, 1200 to 2400 MST, 21 May 93 . . . . .	53
32.	Hourly average vertical profiles of wind speed and wind direction, as measured with the (a) 924- and (b) 50-MHz profilers, APRF complex, WSMR, 0000 to 1200 MST, 21 May 93 . . . . .	54
33.	Hourly average vertical profiles of wind speed and wind direction, as measured with the (a) 924- and (b) 50-MHz profilers, APRF complex, WSMR, 1200 to 2400 MST, 21 May 93 . . . . .	55
34.	Hourly average vertical profiles of wind speed and wind direction, as measured with the (a) 50- and (b) 404- (high mode) MHz profilers, APRF complex, WSMR, 0000 to 1200 MST, 25 May 93 . . . . .	56
35.	Hourly average vertical profiles of wind speed and wind direction, as measured with the (a) 50- and (b) 404- (high mode) MHz profilers, APRF complex, WSMR, 1200 to 2400 MST, 25 May 93 . . . . .	57
36.	Hourly average vertical profiles of wind speed and wind direction, as measured with the (a) 50- and (b) 404- (low mode) MHz profilers, APRF complex, WSMR, 0000 to 1200 MST, 25 May 93 . . . . .	58
37.	Hourly average vertical profiles of wind speed and wind direction, as measured with the (a) 50- and (b) 404- (low mode) MHz profilers, APRF complex, WSMR, 1200 to 2400 MST, 25 May 93 . . . . .	59
38.	Hourly average vertical profiles of wind speed and wind direction, as measured with the (a) 924- and (b) 404- (low mode) MHz profilers, APRF complex, WSMR, 0000 to 1200 MST, 25 May 93 . . . . .	60
39.	Hourly average vertical profiles of wind speed and wind direction, as measured with the (a) 924- and (b) 404- (low mode) MHz profilers, APRF complex, WSMR, 1200 to 2400 MST, 25 May 93 . . . . .	61
40.	Hourly average vertical profiles of wind speed and wind direction, as measured with the (a) 924- and (b) 50-MHz profilers, APRF complex, WSMR, 0000 to 1200 MST, 25 May 93 . . . . .	62
41.	Hourly average vertical profiles of wind speed and wind direction, as measured with the (a) 924- and (b) 50-MHz profilers, APRF complex, WSMR, 1200 to 2400 MST, 25 May 93 . . . . .	63
42.	Composite scatter diagram of the horizontal wind speed estimated from the 50- and 404- (high mode) MHz data from the APRF complex, WSMR, 7 Mar, 16, 17, 21, and 25 May 93 . . . . .	66

43.	Composite scatter diagram of the horizontal wind speed estimated from the 50- and 404- (low mode) MHz data from the APRF complex, WSMR, 7 Mar, 16, 17, 21, and 25 May 93 . . . . .	67
44.	Composite scatter diagram of the horizontal wind speed estimated from the 924- and 404- (low mode) MHz data from the APRF complex, WSMR, 16, 17, 21, and 25 May 93 . . . . .	68
45.	Composite scatter diagram of the horizontal wind speed estimated from the 924- and 50-MHz data from the APRF complex, WSMR, 16, 17, 21, and 25 May 93 . . . . .	69
46.	Virtual temperature vertical profiles computed from 924- (+), 404- (•), and 50- (▲) MHz RASS profilers, APRF complex, and radiosonde (—) data, Oasis Site, WSMR, 13 May 93 . . . . .	88
47.	Virtual temperature vertical profiles computed from 924- (+), 404- (•), and 50- (▲) MHz RASS profilers, APRF complex, and radiosonde (—) data, Oasis Site, WSMR, 14 May 93 . . . . .	89
48.	Virtual temperature vertical profiles computed from 924- (+), 404- (•), and 50- (▲) MHz RASS profilers, APRF complex, and radiosonde (—) data, Oasis Site, WSMR, 14 and 18 May 93 . . . . .	90
49.	Virtual temperature vertical profiles computed from 924- (+), 404- (•), and 50- (▲) MHz RASS profilers, APRF complex, and radiosonde (—) data, Oasis Site, WSMR, 18 and 26 May 93 . . . . .	91
50.	Virtual temperature vertical profiles computed from 924- (+), 404- (•), and 50- (▲) MHz RASS profilers, APRF complex, and radiosonde (—) data, Oasis Site, WSMR, 27 May and 3 Jun 93 . . . . .	92
51.	Virtual temperature vertical profiles computed from 924- (+), 404- (•), and 50- (▲) MHz RASS profilers, APRF complex, and radiosonde (—) data, Oasis Site, WSMR, 5 Jun 93 . . . . .	93
52.	Virtual temperature vertical profiles computed from 924- (+), 404- (•), and 50- (▲) MHz RASS profilers, APRF complex, and radiosonde (—) data, Oasis Site, WSMR, 9 Jun 93 . . . . .	94
53.	Virtual temperature vertical profiles computed from 924- (+), 404- (•), and 50- (▲) MHz RASS profilers, APRF complex, and radiosonde (—) data, Oasis Site, WSMR, 10 Jun 93 . . . . .	95
54.	Virtual temperature vertical profiles computed from 924- (+), 404- (•), and 50- (▲) MHz RASS profilers, APRF complex, and radiosonde (—) data, Oasis Site, WSMR, 11 and 14 Jun 93 . . . . .	96
55.	Virtual temperature vertical profiles computed from 924- (+), 404- (•), and 50- (▲) MHz RASS profilers, APRF complex, and radiosonde (—) data, Oasis Site, WSMR, 15 Jun 93 . . . . .	97
56.	Virtual temperature vertical profiles computed from 924- (+), 404- (•), and 50- (▲) MHz RASS profilers, APRF complex, and radiosonde (—) data, Oasis Site, WSMR, 17 Jun 93 . . . . .	98
57.	Radar signal power measured with the north/south beam of the 50-MHz radar, APRF, 0600 UTC on 16 May to 0500 UTC on 17 May 93. The received power ranges from -191 to -124 dB . . . . .	116

58.	Vertical profile of calibrated $C_n^2$ data derived from the 50-MHz radar signal power, APRF, 0000 to 0100 UTC, 17 May 93 . . . . .	117
59.	The corresponding wind profile for the period shown in figure 58 emphasizes the resolution of the 50-MHz system . . . . .	118
60.	Received power backscatter measured by the sodar during four meteorological conditions: (a) rainfall, (b) convective plumes, (c) inversion, and (d) neutral period, APO, 22 Jul 94. The color scale ranges from the darkest red, corresponding to a return of $\geq +100$ -dB signal, to black, corresponding to a 0-dB signal . . . . .	121
61.	Diurnal variation of calibrated $C_n^2$ data derived from sodar data taken at three heights, APO, 12 Jun 94 . . . . .	122
62.	Diurnal variation of integrated path $C_n^2$ scintillometer measurements, APRF, 4 and 20 m AGL, 0000 to 2400 MST, 20 Mar 95 . . . . .	124
63.	Diurnal variation of $C_n^2$ measured with five spatial temperature probes at five levels of a 4-m tower, LCMS Site, 16 Jun 94 . . . . .	125
64.	Vertical profile of $C_n^2$ measured with a tethersonde sensor at Isabell Site. The data were acquired during the ascent portion of the flight, 0955 to 1249 MST, 19 Aug 92 . . . . .	127
65.	Vertical profiles of $C_n^2$ measured with a tethersonde at Isabell Site, and a sodar and five tower-mounted spatial temperature probes at the APRF, 19 Aug 92. The tethersonde data were acquired during the ascent portion of the flight from 0955 to 1008 MST. The sodar and spatial temperature probe data represent a 15-min average from 1000 to 1015 MST . . . . .	128
66.	Vertical profiles of $C_n^2$ measured with a tethersonde at Isabell Site and a sodar at the APRF, 13 Jan 93. The tethersonde data were acquired during the ascent portion of the flight from 1048 to 1116 MST. The sodar data represent a 30-min average from 1045 to 1115 MST. Calibration data were obtained with a spatial temperature probe at the 2-m level of a tower at the Isabell Site. The data were obtained over a 10-min period just prior to the tethersonde flight . . . . .	129
67.	FM-CW Radar, WSMR (view toward the west with the 924-MHz wind profiler in the foreground and the Organ Mountains in the background) . . . . .	131
68.	Block diagram displaying the calibration technique for the FM-CW radar . . . . .	134
69.	Boundary layer backscatter measured by the FM-CW radar during a 1-h midday convective period, APRF, 26 Aug 92 . . . . .	135

### Tables

1.	Beam parameters for the 924-, 404-, and 50-MHz profilers . . . . .	15
2.	Range and resolution of the 924-, 404-, and 50-MHz profilers . . . . .	16
3.	Maximum radial wind speed components along the axis of the vertical and oblique beams of the three radar wind profilers . . . . .	17
4.	Operational periods for the three modes of the 924-MHz profiler, APRF complex, WSMR, 30 Mar to 18 Jun 93 . . . . .	20
5.	Control parameters for the continuity method of quality control of the wind data . . . . .	23

6.	Statistical comparisons of the 50- and 404- (high mode) MHz wind speeds, APRF complex, WSMR, 1993 . . . . .	70
7.	Statistical comparisons of the 50- and 404- (low mode) MHz wind speeds, APRF complex, WSMR, 1993 . . . . .	71
8.	Statistical comparisons of the 404- (low mode) and 924-MHz wind speeds, APRF complex, WSMR, 1993 . . . . .	71
9.	Statistical comparisons of the 50- and 924-MHz wind speeds, APRF complex, WSMR, 1993 . . . . .	72
10.	Composite statistical summary of the 50- and 404- (high mode) MHz wind profiler wind speed comparison, APRF complex, WSMR, 7 Mar, 16, 17, 21, and 25 May 93 . . . . .	72
11.	Composite statistical summary of the 50- and 404- (low mode) MHz wind profiler wind speed comparison, APRF complex, WSMR, 7 Mar, 16, 17, 21, and 25 May 1993 . . . . .	73
12.	Composite statistical summary of the 404- (low mode) and 924-MHz wind profiler wind speed comparison, APRF complex, WSMR, 16, 17, 21, and 25 May 93 . . . . .	73
13.	Composite statistical summary of the 50- and 924-MHz wind profiler wind speed comparison, APRF complex, WSMR, 16, 17, 21, and 25 May 93 . . . . .	74
14.	RASS characteristics for the three radar profilers . . . . .	83
15.	Radiosonde releases from Oasis Site for which there were virtual temperature data from all three profiler systems . . . . .	84
16.	Control parameters for the continuity method of quality control of the RASS data . . . . .	85
17.	Statistical summary of the RASS and radiosonde temperature data comparisons, APRF complex/Oasis Site, WSMR . . . . .	100
18.	Temporal distribution of 21 radiosonde releases during May and Jun 93, Oasis Site, WSMR . . . . .	103
19.	Features of the 50-MHz, sodar, tower, FM-CW and tethered balloon systems . . . . .	113
20.	Characteristics of the ARL FM-CW radar . . . . .	132

### Appendix Tables

A-1.	Gates for the 50-MHz wind profiler . . . . .	150
A-2.	High-mode gates for the 404-MHz wind profiler . . . . .	153
A-3.	Low-mode gates for the 404-MHz wind profiler . . . . .	154
A-4.	Gates for the 924-MHz wind profiler . . . . .	155
B-1.	Gates for the 50-MHz RASS system and the mean air temperature for each gate as determined from radiosondes released from Oasis Site from Jan 92 through Mar 93 . . . . .	158
B-2.	Gates for the 404-MHz RASS system and the mean air temperature for each gate as determined from radiosondes released from Oasis Site from Jan 92 through Mar 93 . . . . .	160
B-3.	Gates for the 924-MHz RASS system . . . . .	161

## Executive Summary

An integrated system for the continuous measurement of vertical profiles of wind, temperature, and refractive index structure parameter from the surface to the stratosphere is under development by the U.S. Army Research Laboratory (ARL) Battlefield Environment Directorate. The major components of the system are 50-, 404-, and 924-MHz radar wind profilers, a sodar, a 152-m instrumented meteorological tower, a tethered balloon system, and a frequency modulated continuous wave radar located at the Atmospheric Profiler Research Facility (APRF) at White Sands Missile Range (WSMR), NM. After the facility became operational in 1992, two requirements were to assess the accuracy of the wind and virtual temperature data obtained with the radar profilers and demonstrate the capability of the APRF to measure the refractive index structure parameter.

Assessment of the wind and virtual temperature from the radar profilers is a complicated task because there is no standard of comparison except, by historical precedent, rawinsondes. The location and low frequency of rawinsonde releases at WSMR limited their usefulness for this study, and the wind assessment was limited to a statistical intercomparison of the three radar profilers. The virtual temperature assessment of the radars was performed by comparison with closest radiosonde data because the height range of temperature data overlap amongst the three profilers was small. The assessment of the refractive index turbulence structure parameter was limited to a capability demonstration of the systems at the APRF because not all the systems were calibrated for the turbulence structure parameter, and thermosonde (special radiosonde packages equipped with spatial temperature probes) measurements were not available during the study period.

The evaluation period for this study was from Jan to Jul 93. The criteria of nearly continuous 24-h wind data from the profilers led to choosing five days in March and May for the wind comparisons. For the virtual temperature comparison, 21 rawinsonde releases from Oasis Site in May and June were chosen when corresponding virtual temperature data from all three radar profilers were available.

Extensive efforts were expended to ensure that data formats among the systems were consistent and nearly identical sample volumes were used for the statistical evaluation. All data were run through a continuity/pattern-matching quality-control algorithm to help ensure only high quality data were used in this study.

Statistical results, including Pearson product-moment (correlation) coefficients, F-tests, root mean square error values, and significance probabilities, are tabulated for individual days and composite data.

The 404- and 50-MHz profiler wind speeds compared quite well during the selected period with correlation coefficients of 0.92 or above. The 50- and the 924-MHz wind speeds compared less well, with a composite wind speed correlation of 0.80. The comparison between the 404- and 924-MHz wind speeds was the poorest with a correlation of 0.66; however, this result is statistically significant (not caused by randomness).

The virtual temperature statistics show a high correlation between all three radar profilers and the rawinsondes.

Detailed statistical comparisons of the turbulence measurements were not performed because a cohesive, calibrated data set from all the turbulence instrumentation was not available. The bulk of data to date seem to indicate general agreement among the various instruments, particularly among optical and spatial temperature instruments.

# 1. Introduction

The U.S. Army Research Laboratory (ARL) Battlefield Environment Directorate is developing an integrated system for the continuous measurement of vertical profiles of wind, temperature, and refractive index structure parameter ( $C_n^2$ ) tailored to ARL requirements. The system consists of 50-, 404-, and 924-MHz three-beam, wind-profiling radars; a sodar; 20- and 152-m towers; a tether sonde; and a frequency modulated continuous wave (FM-CW) radar and is located at the Atmospheric Profiler Research Facility (APRF) complex at White Sands Missile Range (WSMR), NM (Hines et al. 1993b). Each three-beam, wind-profiling radar is equipped with a Radio Acoustic Sounding System (RASS) to measure virtual temperature.

After the APRF complex became operational in early 1992, there were three requirements. The first requirement was to evaluate the 924-MHz system as a potential replacement for rawinsondes in profiling wind and temperature within a battlefield environment (Flowers et al. 1994a,b). The second requirement was to assess the accuracy of the wind and virtual temperature data obtained with the three three-beam radar profilers. The third requirement was to demonstrate the capability of the system to measure  $C_n^2$ .

The purpose of this report is to address the second and third requirements.

Assessing the accuracy of the profilers in use at the APRF for the measurement of wind and virtual temperature is a complicated task because there is no true standard of comparison. Biltoft (1991) suggests that the only feasible method for evaluating the performance of profiler systems is through field intercomparison tests and that certain statistics be used as figures of merit. However, the figures of merit require a reference instrument, and even the reference instrument would have its own measurement limitations.

Comparisons with rawinsonde data are certainly useful because the rawinsonde measurements are, by historical precedent, the current standard. At WSMR, the closest rawinsonde release point is 6 km from the APRF complex, and the frequency of the aperiodic releases is low. For wind, it was decided to limit the assessment of the relative accuracies of the 50-, 404-, and 924-MHz profilers to an intercomparison of the winds measured by the three systems.

Comparisons of the wind data from the three systems were limited to five days from Jan through mid-Jun 93 when there were complete data sets from the three systems. The comparisons are based on the Pearson product-moment (correlation) coefficient, the root mean square error (root MSE), the bias, and the F-test.

In the case of the RASS data, an intercomparison of virtual temperature data from the three RASS systems was not practical because the ranges of overlap were small. Therefore, for the 13 days when there were simultaneous radiosonde data from Oasis Site (approximately 6 km south-southwest of the APRF complex) and RASS data from all three profiler systems, the composite RASS vertical profile of virtual temperature was compared to the virtual temperature profile computed from the corresponding radiosonde run.

Even more difficult than the assessment of the relative accuracies of wind and temperature measurements is the assessment of the accuracy of measurements of  $C_n^2$ . Therefore, it was decided to concentrate on demonstrating the capability of all seven systems for obtaining vertical profiles of  $C_n^2$ .

The report is divided into three sections, one each for wind, virtual temperature, and  $C_n^2$ . The first section addresses the comparison of the 50- and 404-MHz (high and low modes as discussed in section 3.1.2) and 404-MHz (low mode) and 924-MHz profiler wind data. The second section is devoted to the comparison of the simultaneous radiosonde and composite RASS virtual temperature profiles. The third section centers on examples of measurements of  $C_n^2$  with the radar, sodar, tower, and tethered sonde system.

The applicable range gate information for the three wind profilers is listed in appendices A (wind) and B (virtual temperature).

## 2. Measurement Sites

The APRF complex is situated on the floor of the Tularosa basin (about 1220 m above mean sea level (MSL)) some 10 to 15 km east of the north-south oriented San Andres, San Augustine, and Organ Mountains. Individual mountain peaks extend as high as 1500 m above the basin floor.

Winds above the APRF are subject to lee waves off the mountains when the winds aloft are from the southwest through the northwest. Because one of the oblique beams of each of the three radars is directed toward the north or south and the other toward the east or west, small-scale vertical motion resulting from lee waves could be an important factor in wind-profiler measurements at the APRF. Other atmospheric factors expected to contribute to small-scale vertical motion variability are convective activity, gravity waves, and precipitation. Figure 1 shows the APRF complex with the FM-CW radar located at the extreme left and the 50-MHz profiler located in the right center.

The radiosondes, from which data were compared to the RASS virtual temperature data, were released from Oasis Site. Oasis Site is located approximately 6 km south-southwest of the APRF complex.

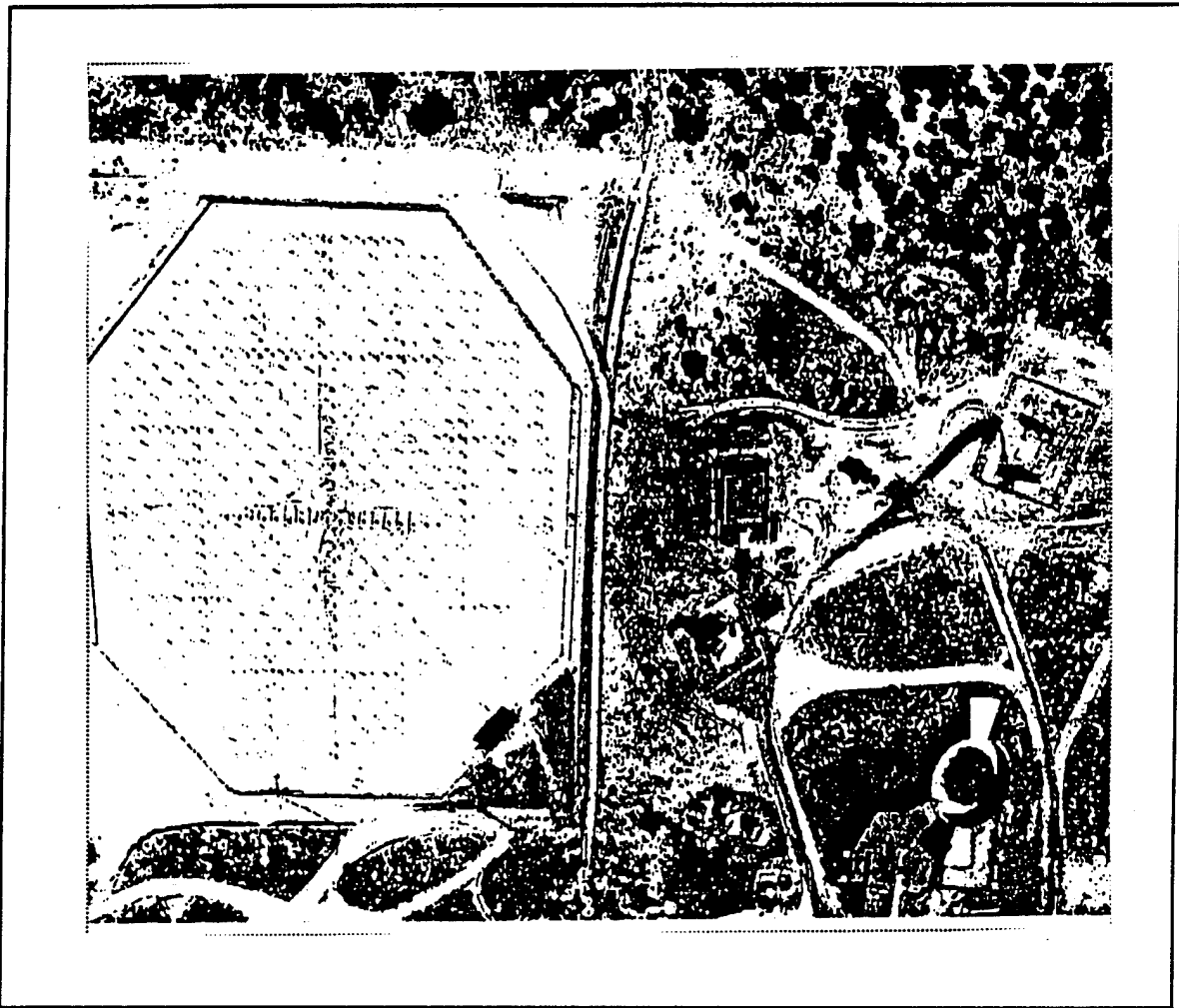


**Figure 1. Aerial view of the APRF. The FM-CW radar is located at the extreme left; the 50-MHz radar is located at the right center.**

### 3. Wind

As noted in the Introduction, there are multiple systems within the APRF complex for measuring the wind field: 50-, 404-, and 924-MHz radar wind profilers, a sodar, tower-mounted anemometers, a tethersonde, and FM-CW radar. Flowers et al. (1994a) reported on statistical intercomparisons of the data from the 924- and 404-MHz radars, the sodar, and the tower-mounted anemometers from the surface to just under 3 km above ground level (AGL). In this study, wind data from the low and high modes of the 404-MHz system are compared with data from the 50-MHz profiler in the range of 2,000 to 16,250 m AGL, and wind data from the 924-MHz system are compared with data from (a) the low mode of the 404-MHz system from 500 to 4000 m AGL and from (b) the 50-MHz system from 2000 to 4073 m AGL.

Each of the three wind-profiling radars at the APRF complex uses three antenna beams to measure the radial speed component along the axis of each beam. One beam of each system is directed vertically while the other two are directed off axis. The speeds along the oblique axes represent the contributions of horizontal wind and vertical motion.

Table 1 lists the beam parameters for the three profilers, and table 2 lists the vertical range and vertical and temporal resolution. More complete information on the APRF complex and instrumentation is provided in Hines et al. 1993b.

**Table 1. Beam parameters for the 924-, 404-, and 50-MHz profilers**

Profiler (MHz)	Beam Width	Oblique Beam Angle	Oblique Beam Azimuth
50	3.3°	15°	180°, 270° (± 2°)
404	4.0°	16.1°	90°, 360° (± 3°)
924	10.0°	20°	56°, 333° (± 3°)

**Table 2. Range and resolution of the 924-, 404-, and 50-MHz profilers**

Profiler (MHz)	Vertical Range <sup>a</sup> (m)	Vertical Resolution (m)	Temporal Resolution (min)
50	2000-18488	150	3
404 (low)	500-9250	375	6
404 (high)	7500-16250	1000	6
924	140-5089	101	1.5

<sup>a</sup>Midpoints of the gate extremes

The operation of three-beam profilers is predicated on the assumption that the windfield at a given altitude is uniform over the triangle defined by the three beams, a separation that can approach 5 km near the upper end of the range of the 50- and 404-MHz profilers (figure 2). If the vertical motion is not uniform across the triangle, it is not proper to use the single measurement of the vertical motion to estimate the horizontal wind components. Weber et al. (1992), determined that although three-beam systems cannot detect small-scale spatial variations across the antenna beams, the errors caused by the variations can be significant. The APRF profilers were not affected by the potential limitation. To estimate the horizontal wind (components or speed and direction), the contribution of the vertical motion was removed at the finest resolution scale.

In addition, there is a maximum wind speed that can be measured along the vertical and oblique beams. Table 3 lists the maxima.

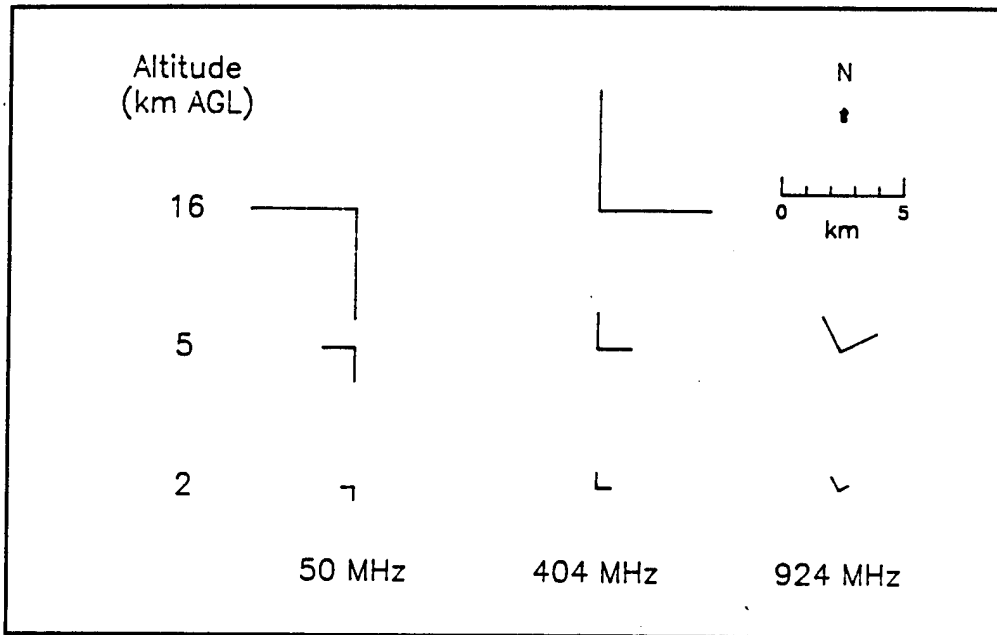


**Figure 2. Horizontal separation of the axes of the antenna beams for each of the three wind profiling radars as a function of altitude.**

**Table 3. Maximum radial wind speed components along the axis of the vertical and oblique beams of the three radar wind profilers**

Profiler/Mode (MHz)	Vertical Beam (m/s)	Oblique Beam (m/s)
50	6.84	20.51
404 - high	12.50	23.08
404 - low	12.62	15.61
924	10.10	10.10

### 3.1 System Comments

Brief sketches of the three wind-profiling radars are provided in subsections 3.1.1, 3.1.2, and 3.1.3.

### **3.1.1 50-MHz Profiler**

The 50-MHz profiler, manufactured by Tycho Technology, Inc., consists of three antenna beams. The beam sampling sequence is (1) 270°, (2) 180°, and (3) vertical.

The measurement of the radial speed along each antenna beam requires approximately 1 min; therefore, a measurement cycle is completed in 3 min. The 3-min cycling continues for approximately 24 min.

At that point, 1-min RASS temperature data are acquired for several minutes. Thus, RASS data are acquired at ½-h intervals.

### **3.1.2 404-MHz Profiler**

The 404-MHz profiler, manufactured by the UNISYS corporation, consists of three antenna beams and two operational modes: high and low altitude (table 2). The beam sampling sequence is (1) 90°, (2) 0°, and (3) vertical.

The measurement of the radial speed along each antenna beam requires approximately 1 min for each of the high and low modes. The measurement sequence is as follows: east/high, east/low, north/high, north/low, vertical/high, vertical/low. A measurement cycle is completed in 6 min, which equates to 10 cycles/h.

In addition, parallel processing allows RASS measurements to be made during the 1-min vertical/low period. Thus, RASS data are acquired at 6-min intervals.

### **3.1.3 924-MHz Profiler**

An earlier 924-MHz wind profiler, developed by the National Oceanic and Atmospheric Administration (NOAA) and used in the previous study (Flowers et al. 1994a), was shipped to NOAA in Boulder, CO, in late Aug 92 and was incorporated into ARL's Mobile Profiler System. The system was configured with a 2-m<sup>2</sup>, three-beam, phased-array antenna.

A replacement 924-MHz system with three separate microstrip antennas (1-m wide by 2-m long for the oblique beams and 2 by 2 m for the vertical beam) was installed at the APRF complex on 30 Mar 93.

The beam sampling sequence of the 924-MHz microstrip profiler system is (1) vertical, (2) 56°, and (3) 333°.

The measurement of the radial speed along each antenna beam requires approximately 30 s. Therefore, a measurement cycle is completed in 90-s. The 90-s cycling continues for approximately 25 min. The system was operated with height ranges of 3, 4, or 5 km (4 km was used throughout the comparison period).

At that point, 30-s RASS temperature data are acquired for approximately 5 min. Thus, RASS data are acquired at ½-h intervals.

### **3.2 Availability of Data**

Figure 3 summarizes the general features of the availability of the data between 1 Jan and mid-Jun 93 for each of the three radar profilers, a sodar (section 5.1.2), and tower systems (section 5.1.3). The only extended period when the 50-MHz system was not operating occurred between 17 Mar and 27 Apr when the system was down for maintenance. The data set for the 404-MHz profiler is virtually complete with only occasional periods of missing data.

As previously stated, the new 924-MHz system at the APRF operated at one of three height ranges (0 to 3 km, 0 to 4 km, and 0 to 5 km). Table 4 shows the periods during which each of the three modes was in operation.

So as not to bias the statistical results toward the evening hours when more data were generally available, the data sets were searched for the 24-h periods when there was a nearly full complement of wind data from all three radar profilers. The search resulted in the selection of five days for comparison of the 50- and 404-MHz systems: 7 Mar and 16, 17, 21, and 25 May 93. Of the five days, only the four days in May could be used for comparisons of the 924-MHz data with the 50- and 404-MHz data, because the 924-MHz system was not operational until 30 Mar (table 4).

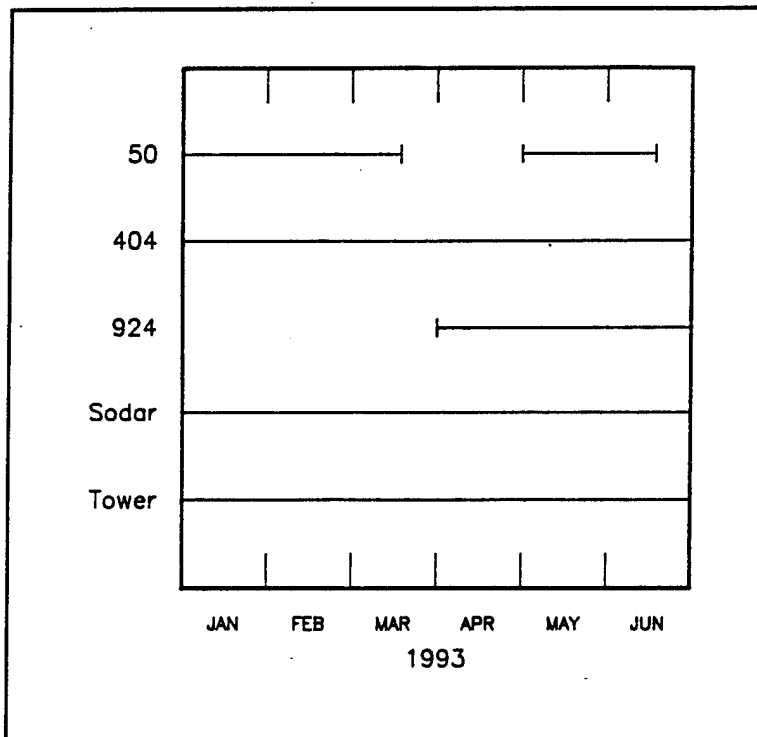


**Figure 3. Availability of wind, temperature, and  $C_n^2$  data from the three radar profilers, APRF complex, WSMR, Jan to Jun 93.**

**Table 4. Operational periods for the three modes of the 924-MHz profiler, APRF complex, WSMR, 30 Mar to 18 Jun 93**

Mode	Operational Periods (1993)
3 km	30 Mar (1706 MST) to 29 Apr (0705 MST)
5 km	29 Apr (1041 MST) to 2 May (1505 MST)
4 km	2 May (1618 MST) to 18 Jun (1635 MST)

### 3.3 Quality Control

Data from the three profilers can be contaminated by radio frequency (RF) noise and interference, echoes from unwanted targets, precipitation, and low signal-to-noise ratio (Wuertz and Weber 1989). The contaminants produce

"fliers" (individual points or clusters of "bad" data) that do not accurately reflect the atmospheric flow.

Before profiler data can be used effectively, the fliers must be flagged through a quality control or editing process. Two methods have been used for the quality control of the wind data from the APRF: (1) a consensus method whereby vertical wind profiles are temporally compared and (2) a continuity method that uses pattern recognition to look for consistency over time and height.

### **3.3.1 *Raw Data***

The raw data for the 50-MHz system consists of spectral moment (Law 1991) data for each minute for each of the three beams. The moment data for the vertical beam and appropriate beam geometry (elevation angle and azimuth) are used to obtain the horizontal wind speed and direction for the given 3-min period. The conversion is done within the 50-MHz system.

The moment data from the 404-MHz system are handled in an analogous manner, except the conversion is done external to the 404-MHz system at the APRF complex. The raw data become wind speed and direction over 6-min periods.

In the case of the 924-MHz system, the moment data are processed in basically the same manner as with the 50-MHz system. The internal processing results in a 30-s average for each of the U, V, and W components. Although the subsequent 90-s cycle data were recoverable, the time constraints placed on this study dictated the use of the system generated 30-min consensus data for the comparisons with the low-mode 404-MHz wind data.

### **3.3.2 *Consensus Method***

The consensus method of quality control (Fischler and Boles 1981) is employed at the APRF complex (by the 404-, 50-, and 924-MHz systems) to obtain operational, hourly-average, wind-barb vertical profiles of horizontal wind speed and direction. Basically, the consensus method looks for consistency over time and is best suited to nearly stationary wind fields with limited spurious data (Wuertz and Weber 1989).

The consensus method provides hourly averages of the raw moment data (3-, 6-, or 1.5-min) from each of the three beams at a given height based on two criteria: (1) the data points used in the average must fall within a certain range, and (2) there must be at least a predetermined minimum number of data points that fall within that range.

In the case of the 404-MHz system, a consensus average is established when 4 of the maximum of 10 6-min samples taken within an hour meet the established criteria. It could be that two markedly different speed groupings of four samples occur during the 1-h period, each meeting the criteria. In this case, the group that occurs latest in the hour would be selected. The hourly consensus-averaged moment data for each of the three beams, through the appropriate geometry, are used to compute the hourly-average wind speed and direction. If the vertical wind speed does not pass consensus and the oblique-beam data do, the vertical wind speed is assumed to be zero and the oblique-beam data are not corrected for vertical motion.

In the case of the 50-MHz data, if the hourly-average vertical wind speed exceeds 4 m/s (positive or negative), the horizontal wind for that hour is nulled out.

In the case of the 924-MHz profiler, the consensus average was applied to the individual 30-s U, V, and W components for 30-min periods. The consensus criteria for a given beam were that at least 50 percent of the maximum of 20 1.5-min samples in a given 30-min period agree to within  $1 \text{ m s}^{-1}$  in the case of the vertical beam and  $1.5 \text{ m s}^{-1}$  for the oblique beams. The consensus-averaged U and V components were combined to obtain the resultant 30-min wind speed and direction.

### **3.3.3 *Continuity Method***

Upon reviewing the data in Flowers et al. (1994b), it became clear that consensus averaging was not entirely satisfactory for estimating the hourly averaged winds. In an effort to circumvent some of the shortcomings of the consensus method, the continuity method of Weber et al. (1993) was adapted to the quality control of the data from all three profiler systems (Hines and Parker-Sedillo 1993a). Whereas the consensus method looks for consistency

over time, the continuity technique offered an attractive alternative in that both temporal and spatial (height) consistency are addressed.

The Weber et al. (1993) continuity method of quality control uses pattern recognition to flag discontinuous data points prior to the computation of the hourly average. Application of the continuity algorithm requires specification of five control parameters (Weber et al. 1993). Table 5 shows the values of the five control parameters used in this study.

**Table 5. Control parameters for the continuity method of quality control of the wind data**

Profiler <sup>a</sup> (MHz)	dx(h) (m)	dx(t) <sup>b</sup> (min)	dy <sup>c</sup> (ms <sup>-1</sup> )	gd <sup>d</sup> (ms <sup>-1</sup> )	nmin <sup>e</sup>
50	300 (gates=2)	6	4.0	40	30
404 - high	1000 (gates=1)	12	6.0	60	25
404 - low	750 (gates=2)	12	5.0	50	25
924	200 (gates=2)	30	3.5	35	10

<sup>a</sup>dx(h) = vertical width for neighboring points.

<sup>b</sup>dx(t) = temporal width for neighboring points.

<sup>c</sup>dy = the maximum difference in the U component, V component, and virtual temperature allowed per dx(h) and dx(t).

<sup>d</sup>gd = gross difference. Used to minimize computation time by allowing entire branches to be flagged all at once instead of point by point.

<sup>e</sup>nmin = size of the smallest allowable pattern detected by pattern recognition.

The continuity method consists of two parts, pattern recognition and quality control. The procedure can best be visualized by thinking of the data as a tree of continuous data. Individual data points are formed into discrete groupings, termed branches, of continuous data. The branches are compared with adjacent branches to form discrete patterns of continuous data. Adjacent branches within adjacent patterns are compared. If there is a discontinuity between the branches, the smaller of the two branches (in terms of the number of data points) is flagged as discontinuous data.

Further details on the implementation, use, and potential limitations of the algorithm are given by Weber and Wuertz (1991), Miller and Barth (1993), and Hines and Parker-Sedillo (1993a).

### **3.4 Averaging**

Because of differences in the vertical and temporal resolution of the three radar wind profilers, vectorial averaging was used to approximately equate the sampling volumes and periods.

#### **3.4.1 Volume**

Figure 4 shows the vertical ranges of measurement for the wind profiler systems located at the APRF. The vertical resolutions over these ranges run from 150 m for the 50-MHz system to 375 m for the low mode of the 404-MHz system, 1000 m for the high mode of the 404-MHz system, and 101 m for the 924-MHz system. To compare the 50-MHz wind data with the 404-MHz high-mode wind data, the wind data from a single 404-MHz high-mode wind gate would be compared with vectorially averaged wind data from the corresponding seven or so 50-MHz gates.

#### **3.4.2 Temporal**

As shown in table 1, the temporal resolutions of the 50- and 404-MHz profilers are 3 and 6 min, respectively. The quality controlled 3- and 6-min wind component data were vector averaged over 1-h periods. The 30-min quality controlled data from the 924-MHz profiler were also vector averaged over 1-h periods.

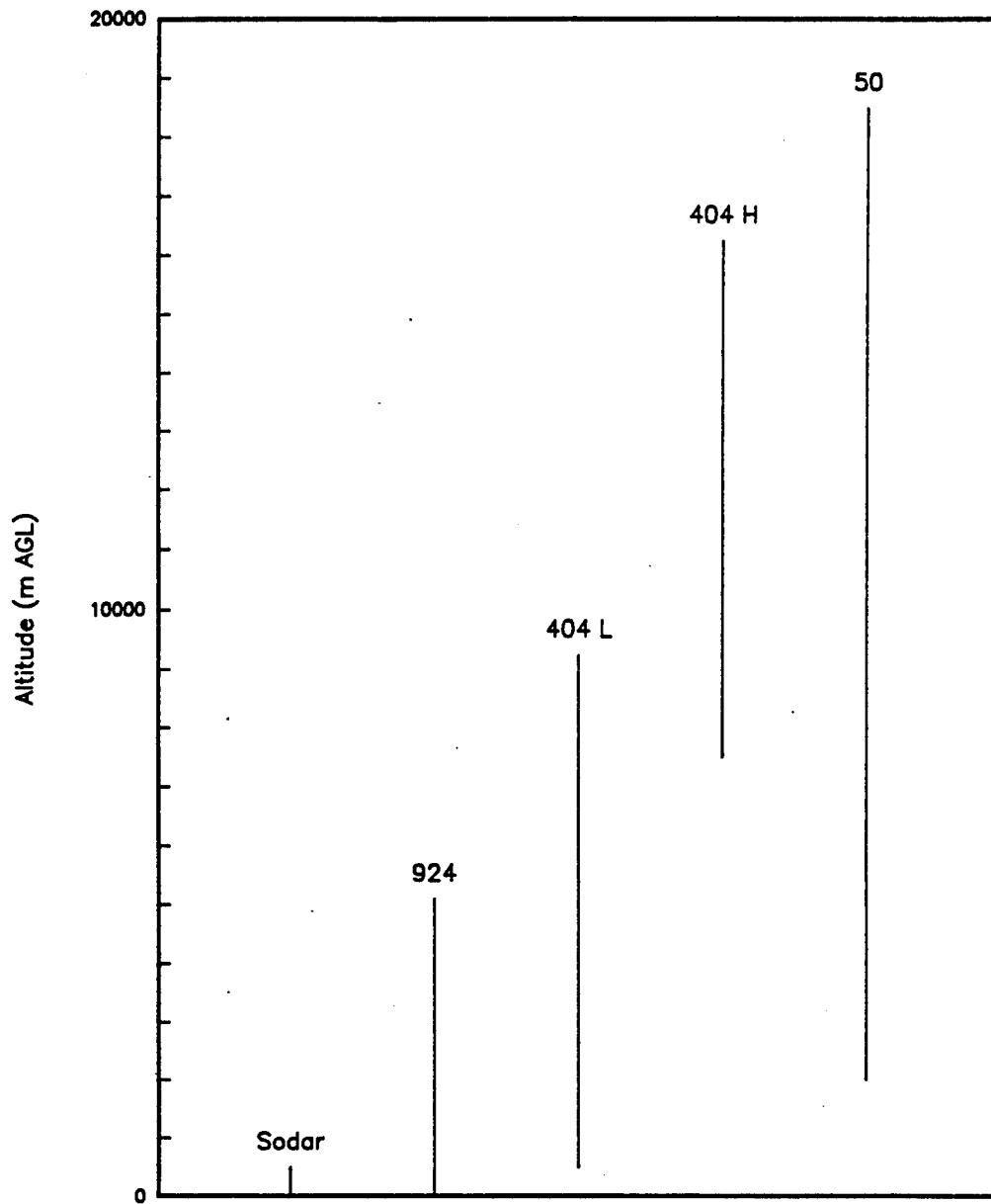


**Figure 4. Vertical measurement range for the four wind profiler systems, APRF complex, WSMR.**

## 3.5 Relative Accuracies

### 3.5.1 Analyses

The accuracy is limited by the atmosphere and the radar systems themselves. As pointed out by Hoehne (1980), the term precision implies repeated measurements of the same quantity by the same instrument. However, because of the natural variability of the atmosphere, it is not possible to make repeated measurements with one instrument. Therefore, the term "functional precision" was coined. Functional precision is the root mean square difference between measurements made by identical instruments at as nearly as possible the same time from as nearly as practical the same point in the atmosphere.

Implicit in the analyses of the profiler wind data is the assumption that the wind field is uniform across all antenna beams at a given height and over a specified averaging interval. Figure 2 shows the horizontal separation of the beams at 2, 5, and 16 m AGL.

"In the presence of significant vertical motion, it is necessary to use the measurement on the vertical antenna beam in order to remove the effects of that vertical motion on the horizontal wind component estimates." (Weber et al. 1992). In the troposphere, significant vertical motion may result from precipitation, gravity waves, and convective activity. However, such conditions occur infrequently in the troposphere. Within the boundary layer, a correction for vertical motion is more imperative because of low-level ground clutter interference (Wolfe et al. 1993).

As previously discussed, the data from all three wind-profiling radars have been corrected for vertical motion. The subhourly oblique radial speeds may be individually corrected using hourly-averaged vertical speeds or the individual subhourly vertical speeds. In this study, hourly-averaged vertical speeds were used, effectively smoothing subhourly mechanical turbulence.

Examination of the availability of wind data from the 50-MHz profiler from Feb to mid-Jun 93 revealed that more vertical profiles were missing during the day than during the night, especially from April to June. The same was true for the 404-MHz profiler but not to as great an extent. Much of the missing

data is attributable to air conditioner failure. When the air conditioner fails, the room temperature may rise. When the temperature exceeds a certain value, the 50-MHz system is automatically shut down. At night, if the room temperature cools to a certain value, the 50-MHz system will be reactivated.

To avoid biasing the comparison of the data from the three profilers toward the night, those days having a full complement of 24 hourly wind profiles for both profilers were identified. Data from the resultant five days were used as the basis of the statistical comparison of the wind data from the three profilers.

Graphical comparisons of the quality-controlled wind data from the three profilers are presented by means of hourly-averaged vertical profiles in which the wind speed and direction are depicted by means of barb plots. Figure 5 shows the conversion of wind barbs to wind speed. Figures 6 through 41 show the comparisons.

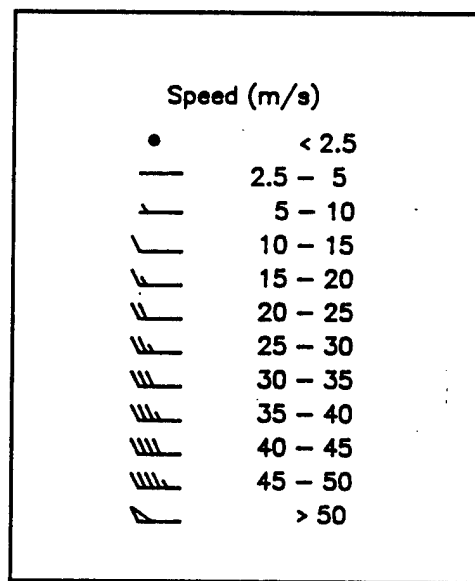


**Figure 5. Wind barb to wind speed conversion.**

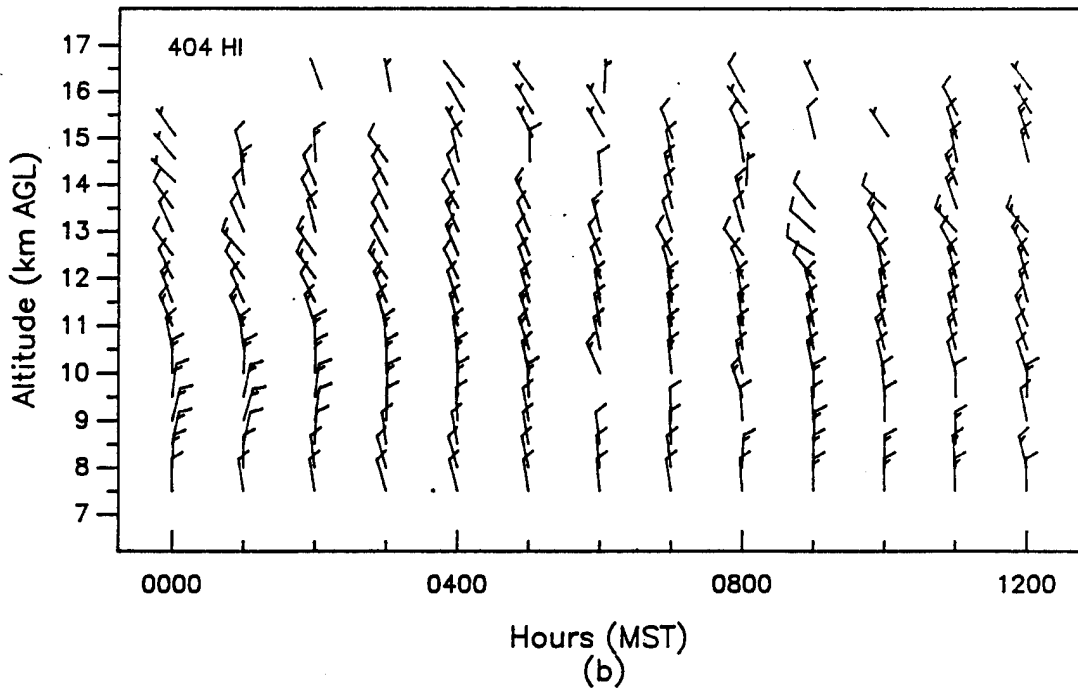
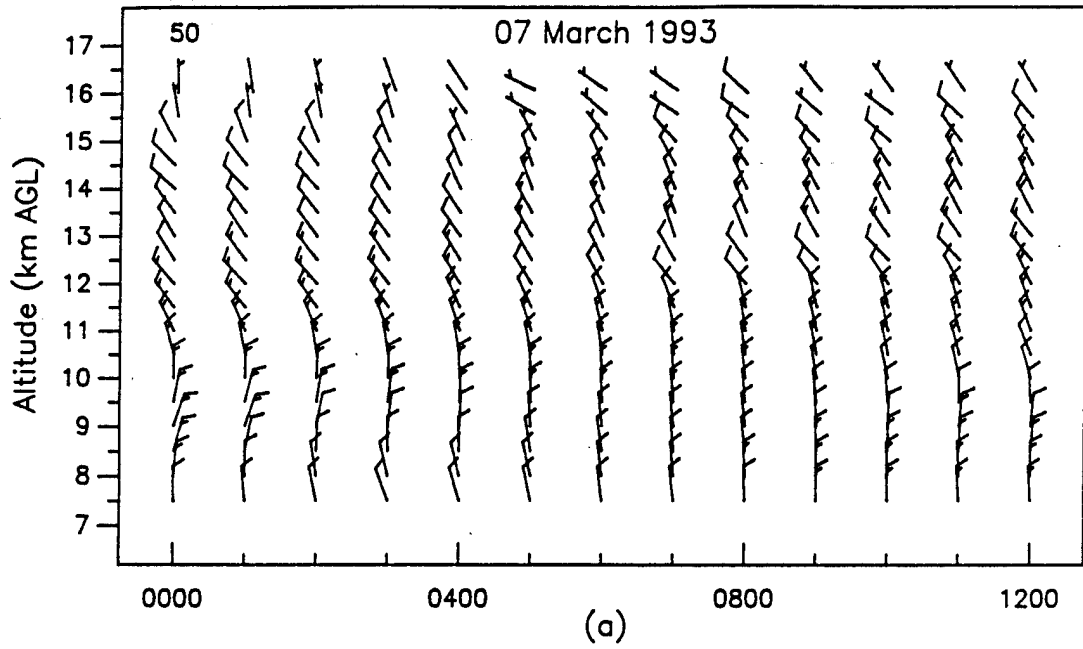


**Figure 6. Hourly average vertical profiles of wind speed and wind direction, as measured with the (a) 50- and (b) 404- (high mode) MHz profilers, APRF complex, WSMR, 0000 to 1200 MST, 7 Mar 93.**

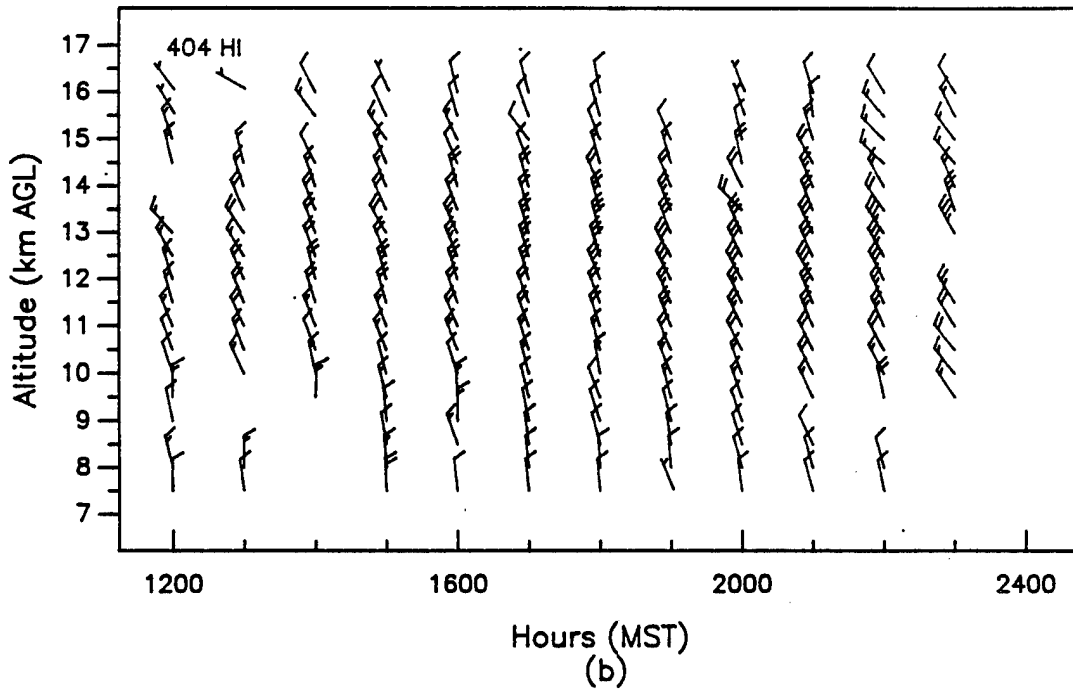
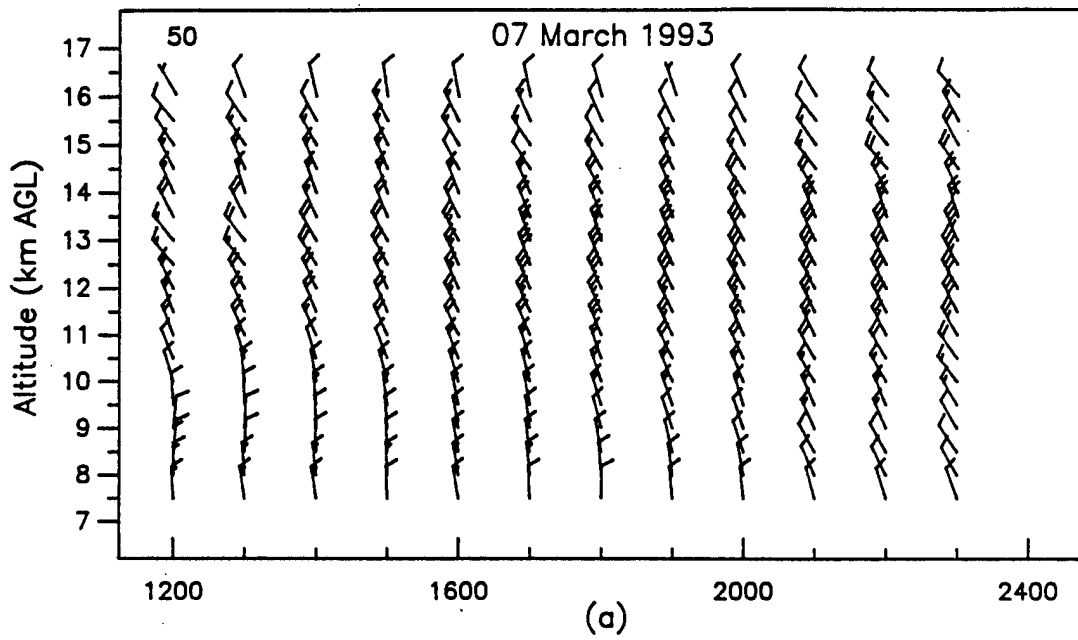


**Figure 7. Hourly average vertical profiles of wind speed and wind direction, as measured with the (a) 50- and (b) 404- (high mode) MHz profilers, APRF complex, WSMR, 1200 to 2400 MST, 7 Mar 93.**

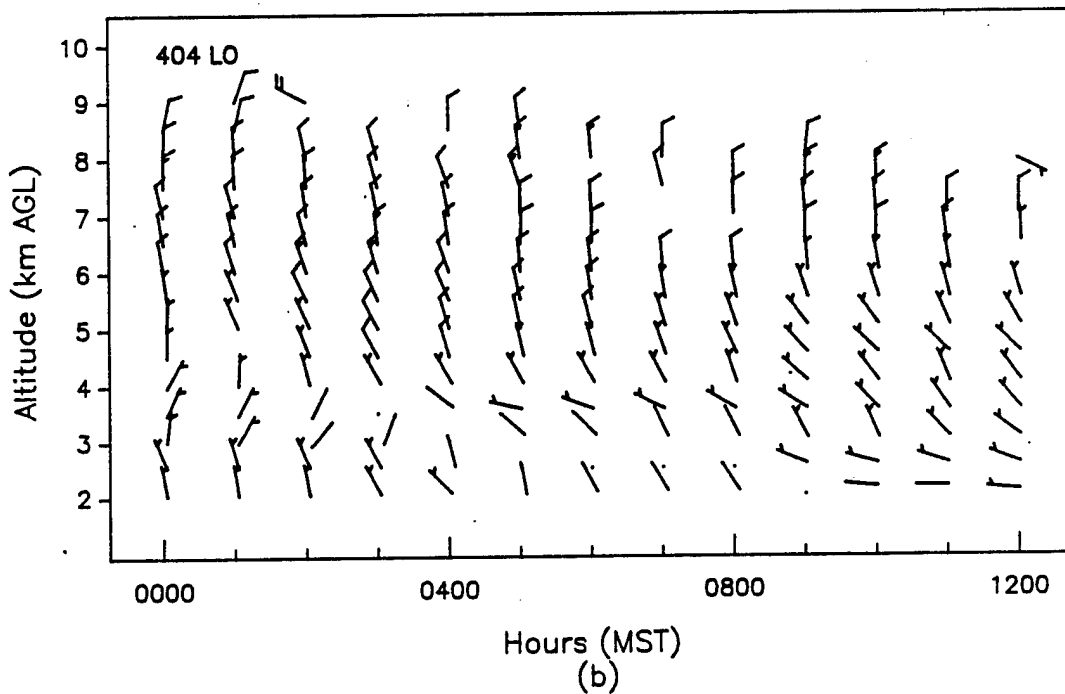
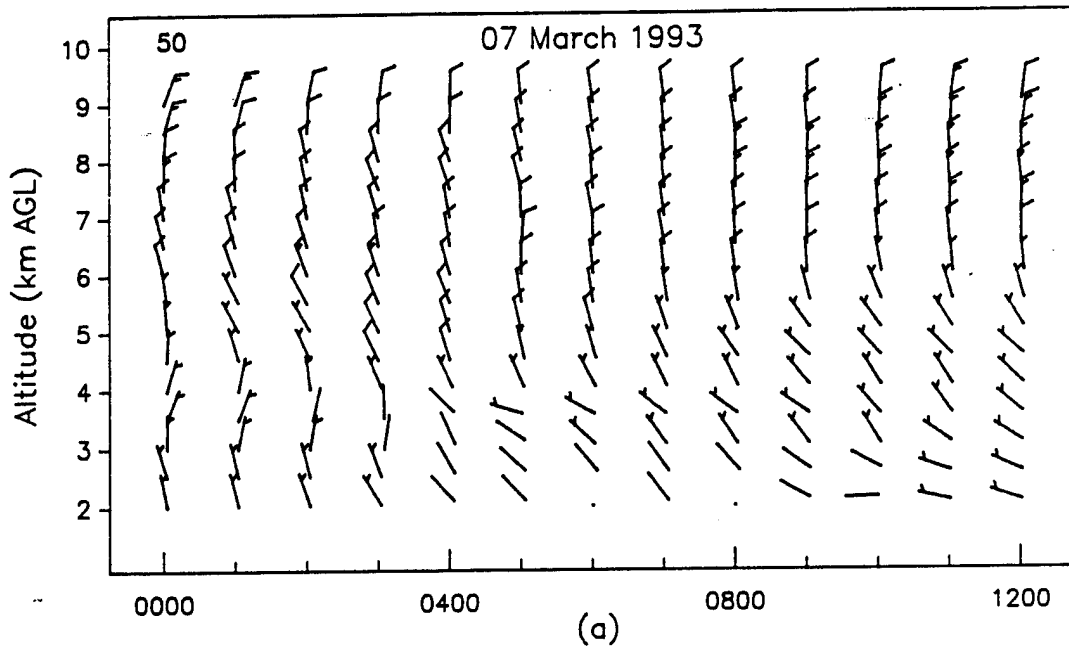


**Figure 8. Hourly average vertical profiles of wind speed and wind direction, as measured with the (a) 50- and (b) 404- (low mode) MHz profilers, APRF complex, WSMR, 0000 to 1200 MST, 7 Mar 93.**

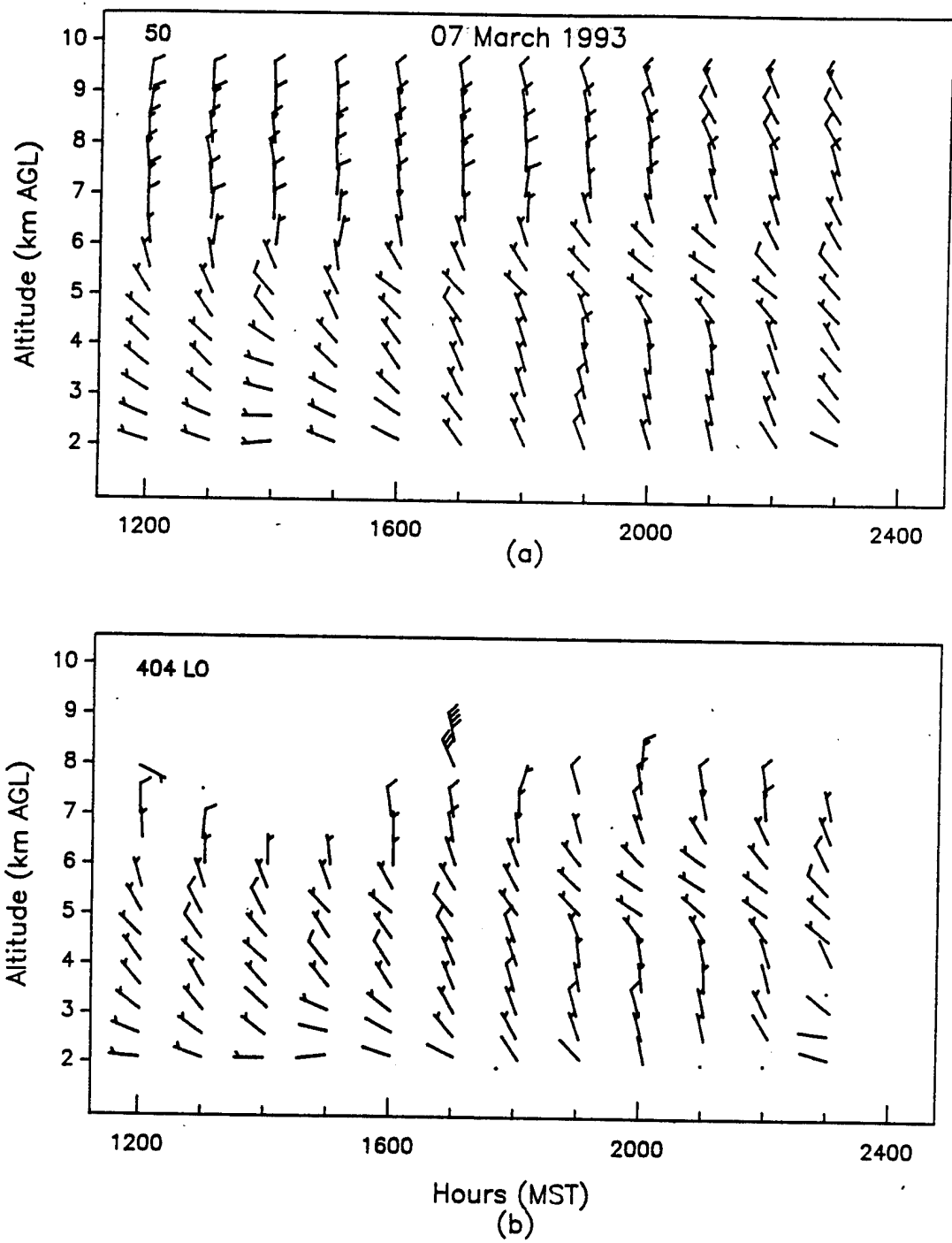


**Figure 9. Hourly average vertical profiles of wind speed and wind direction, as measured with the (a) 50- and (b) 404- (low mode) MHz profilers, APRF complex, WSMR, 1200 to 2400 MST, 7 Mar 93.**

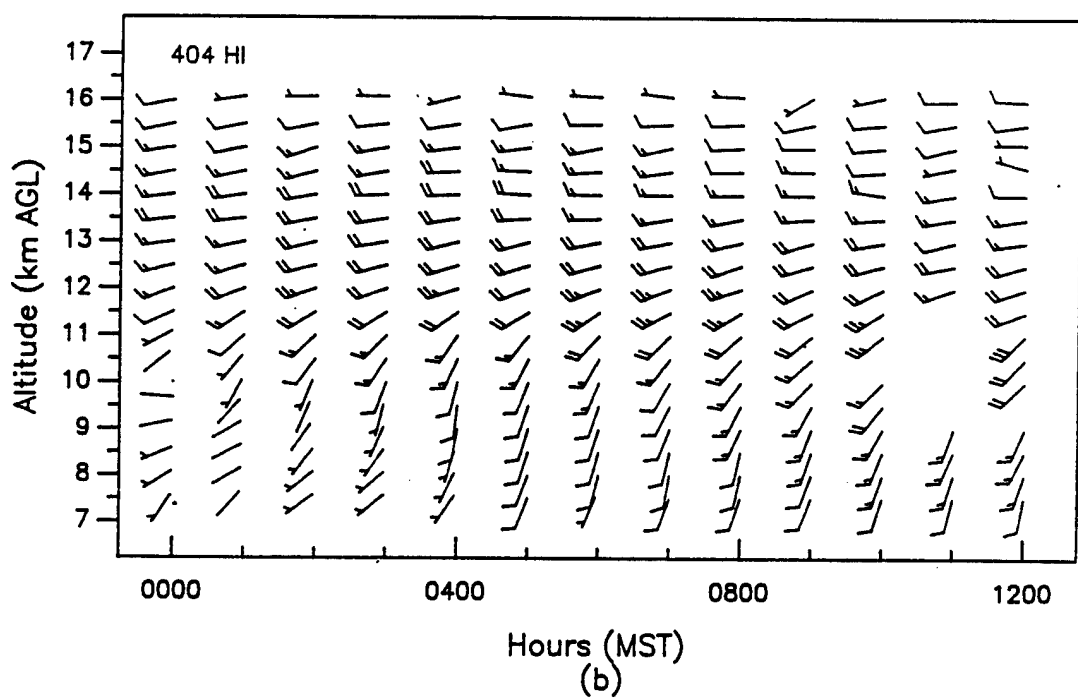
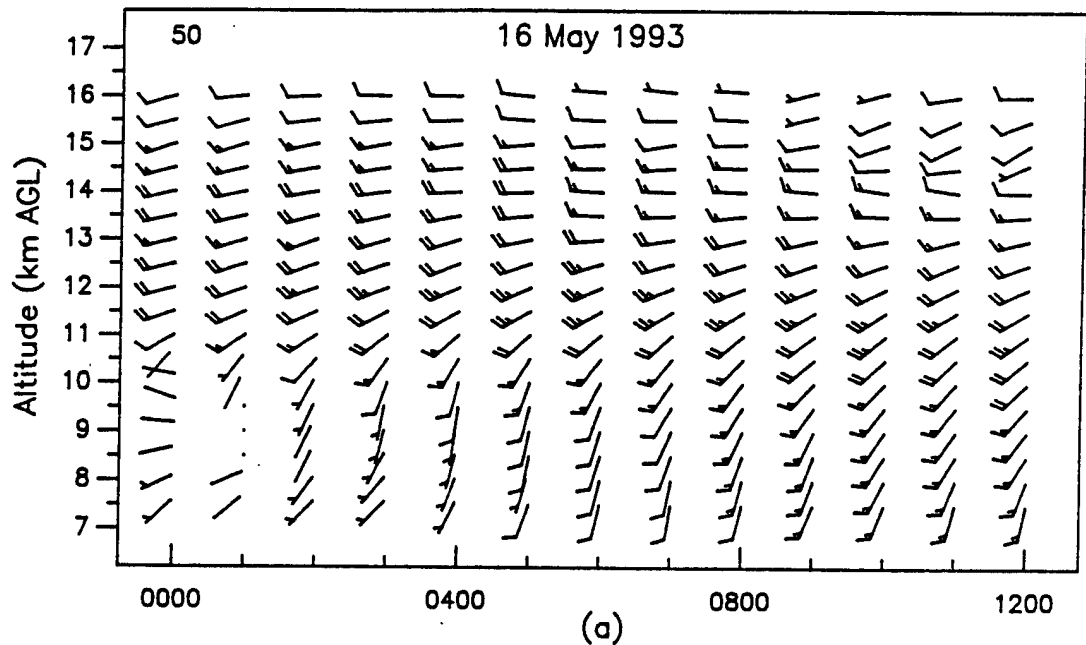


**Figure 10. Hourly average vertical profiles of wind speed and wind direction, as measured with the (a) 50- and (b) 404- (high mode) MHz profilers, APRF complex, WSMR, 0000 to 1200 MST, 16 May 93.**

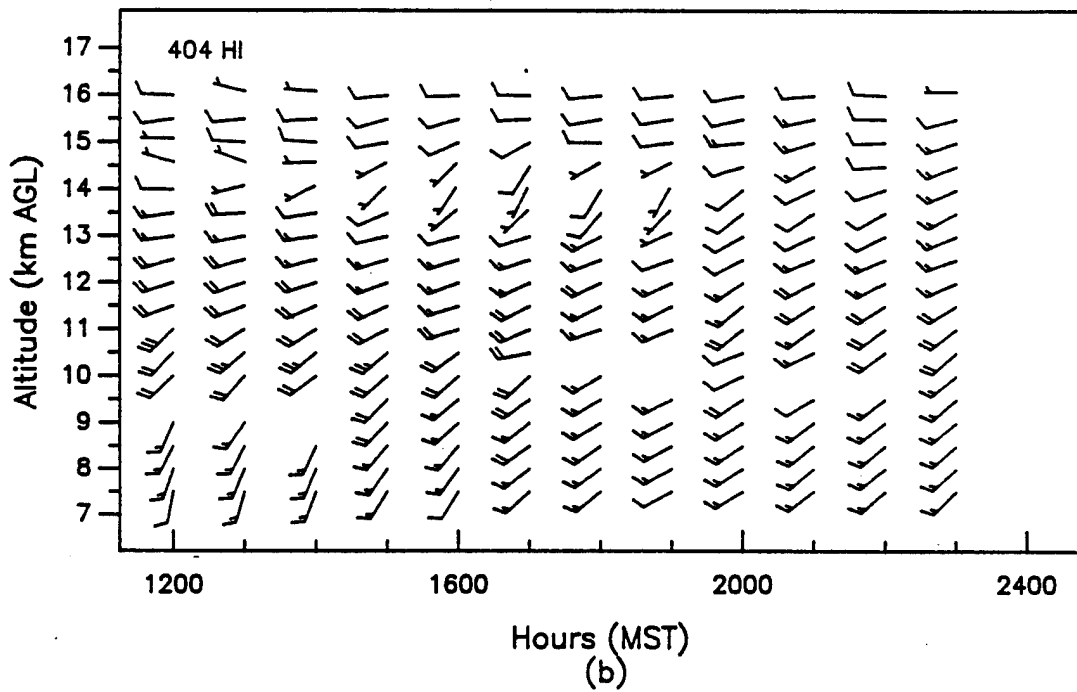
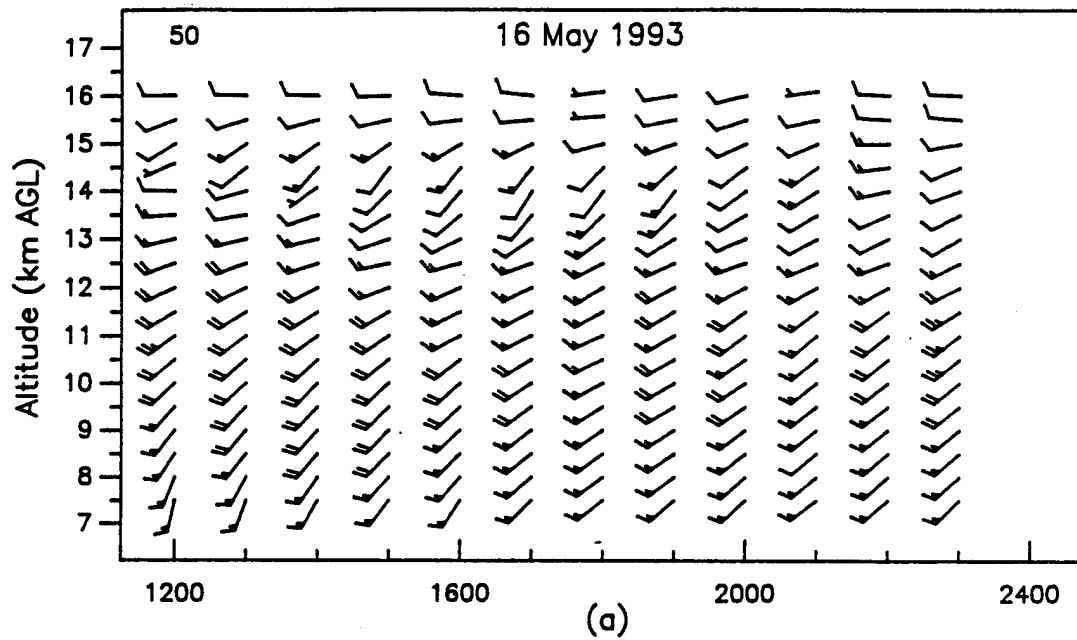


**Figure 11. Hourly average vertical profiles of wind speed and wind direction, as measured with the (a) 50- and (b) 404- (high mode) MHz profilers, APRF complex, WSMR, 1200 to 2400 MST, 16 May 93.**

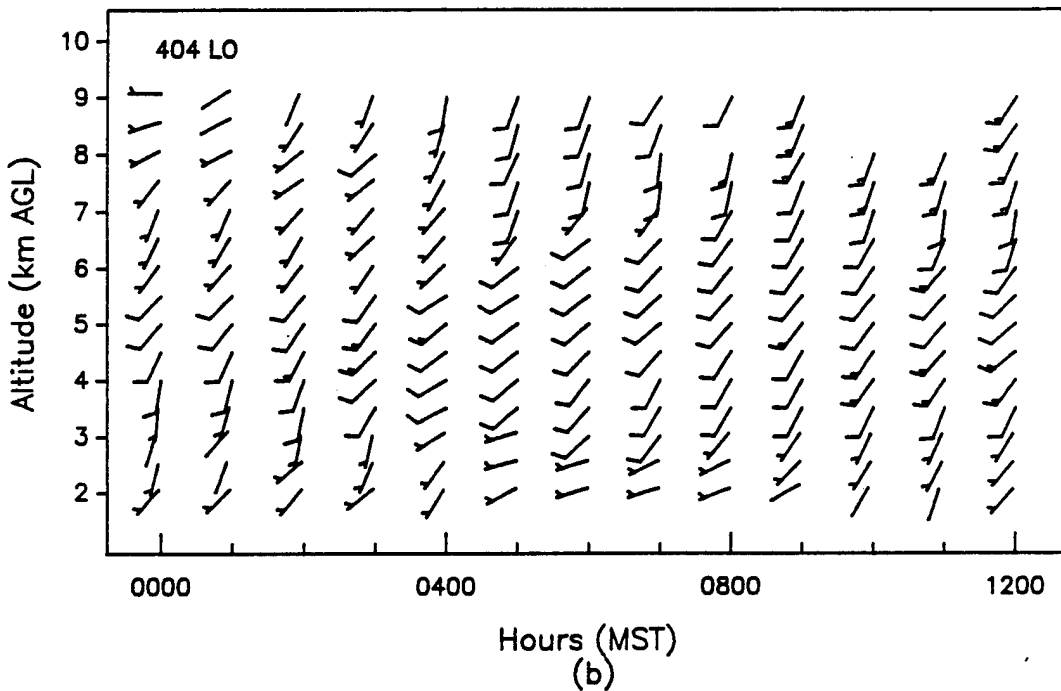
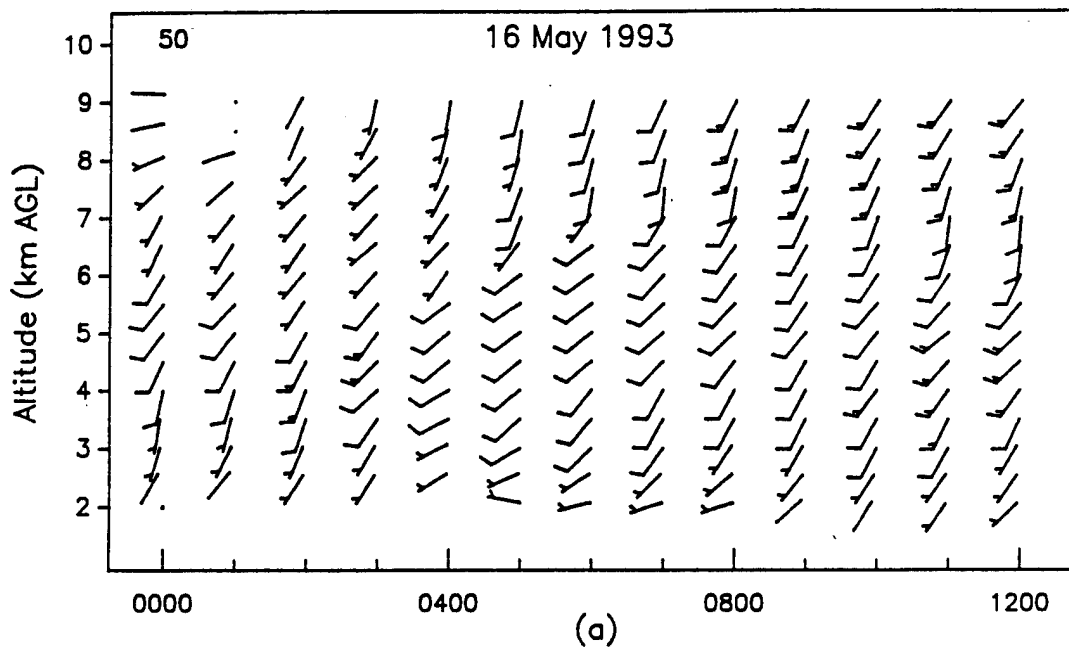


**Figure 12. Hourly average vertical profiles of wind speed and wind direction, as measured with the (a) 50- and (b) 404- (low mode) MHz profilers, APRF complex, WSMR, 0000 to 1200 MST, 16 May 93.**

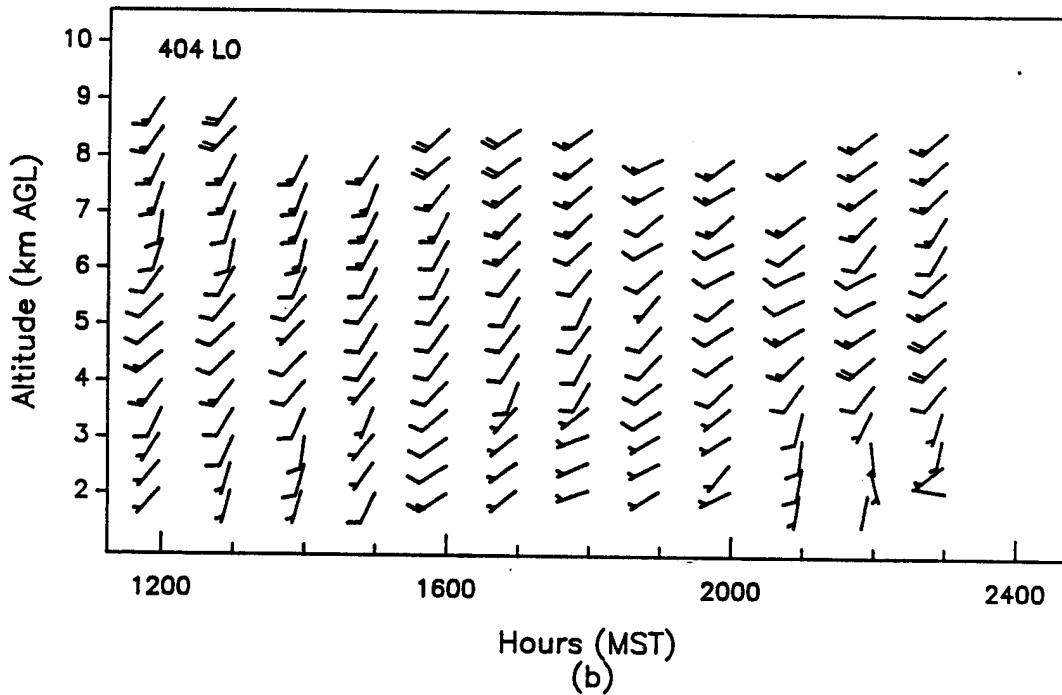
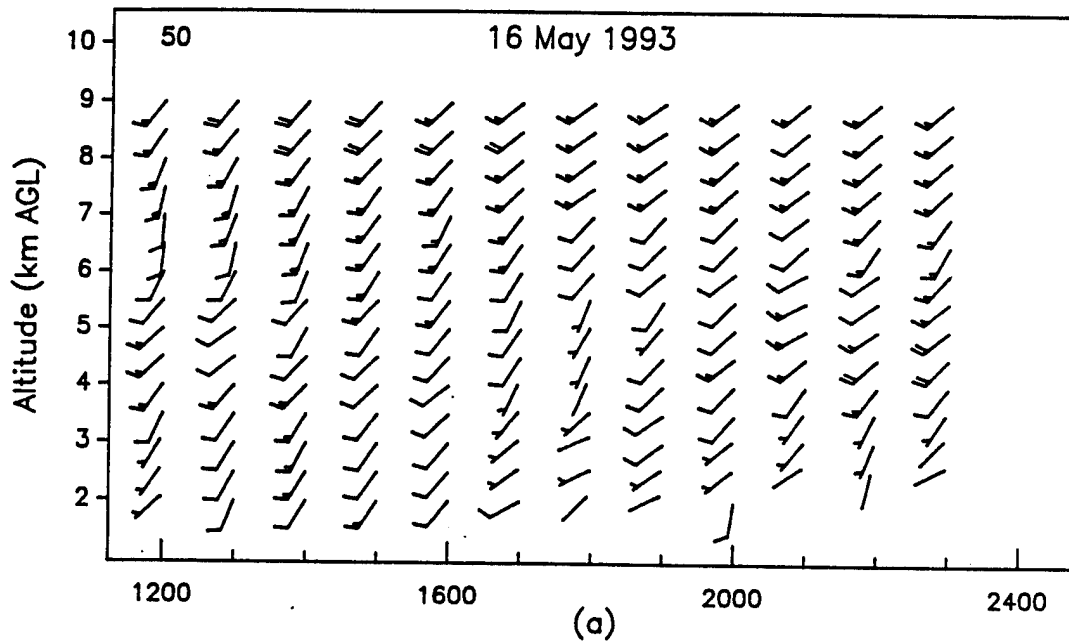


**Figure 13. Hourly average vertical profiles of wind speed and wind direction, as measured with the (a) 50- and (b) 404- (low mode) MHz profilers, APRF complex, WSMR, 1200 to 2400 MST, 16 May 93.**

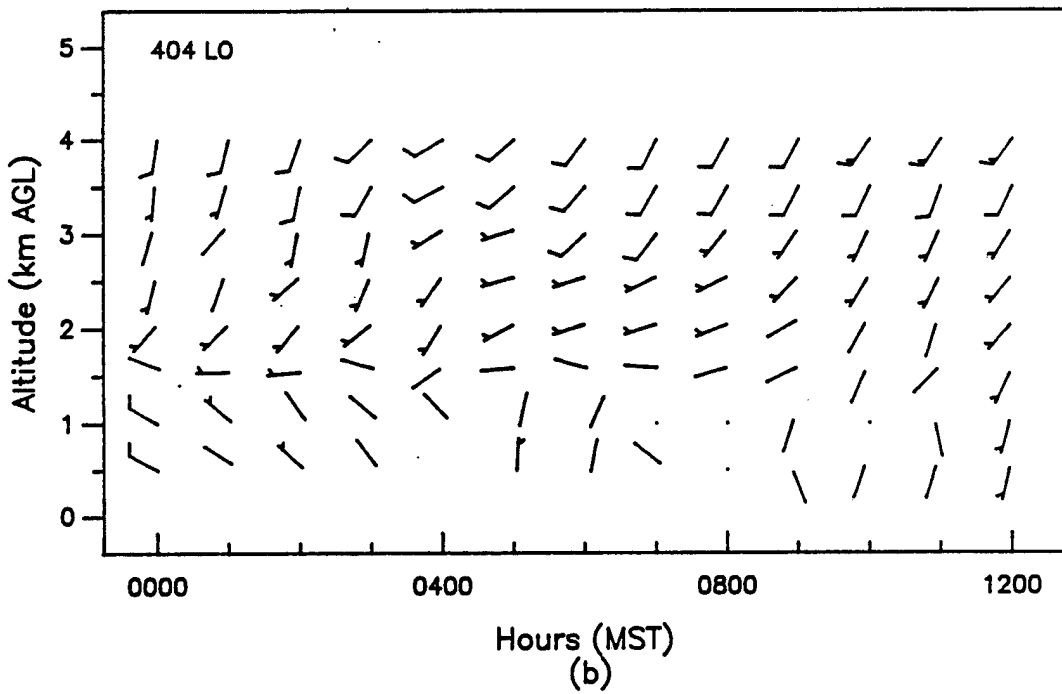
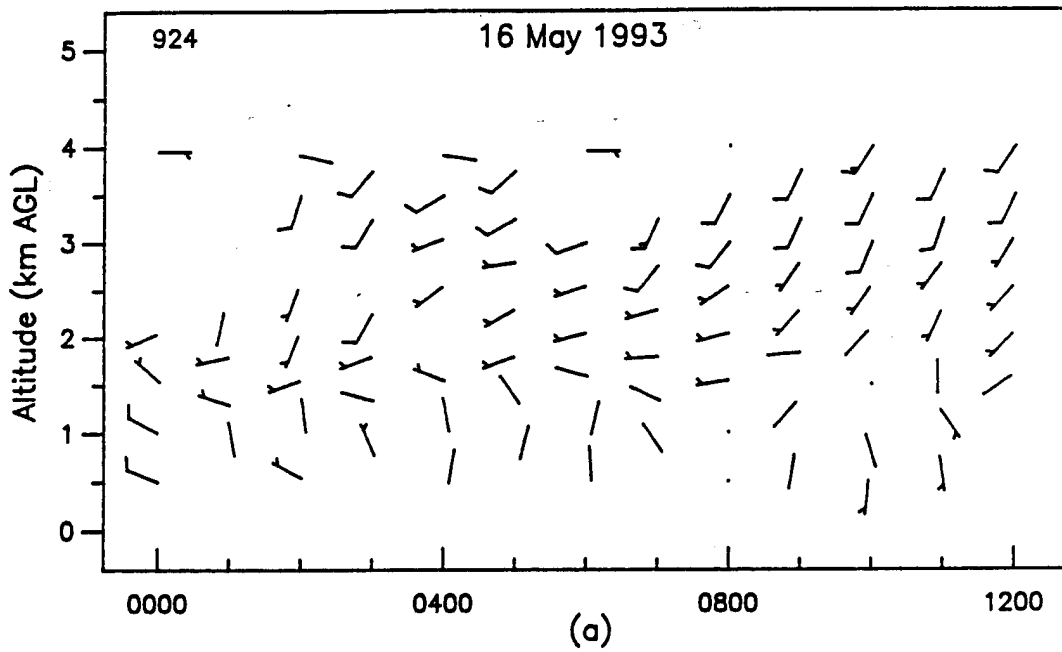


**Figure 14. Hourly average vertical profiles of wind speed and wind direction, as measured with the (a) 924- and (b) 404- (low mode) MHz profilers, APRF complex, WSMR, 0000 to 1200 MST, 16 May 93.**

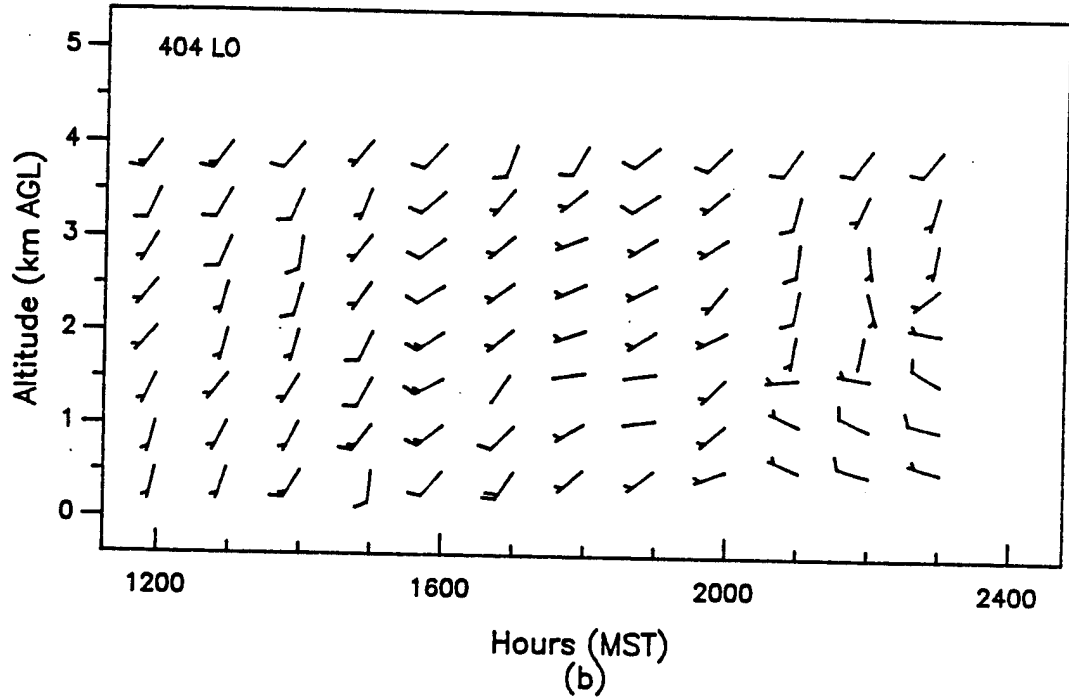
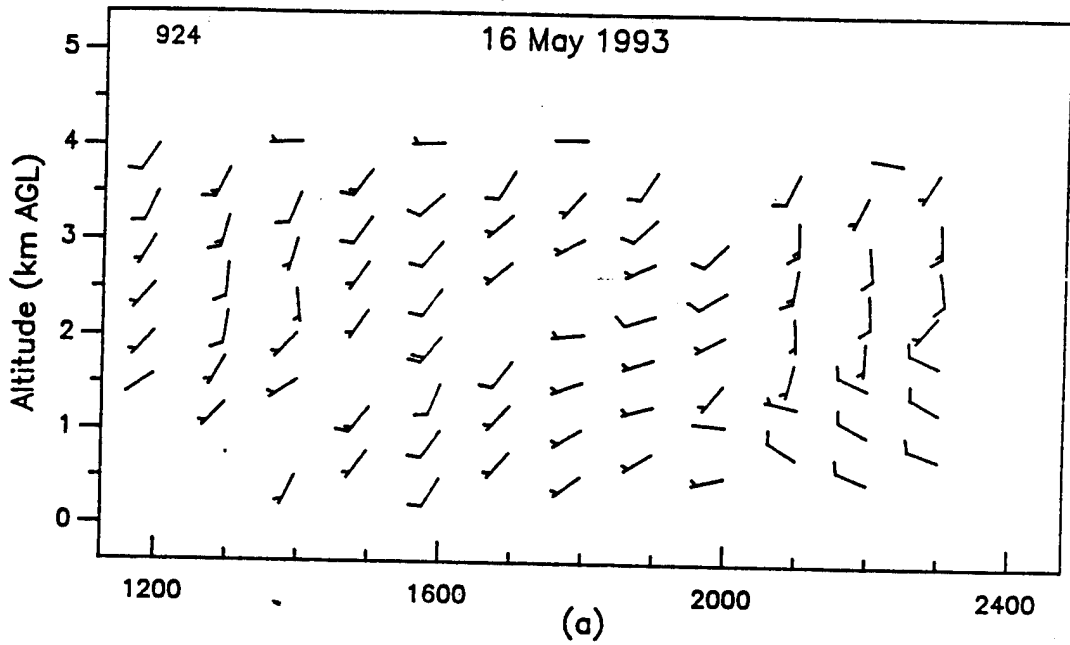


**Figure 15. Hourly average vertical profiles of wind speed and wind direction, as measured with the (a) 924- and (b) 404- (low mode) MHz profilers, APRF complex, WSMR, 1200 to 2400 MST, 16 May 93.**

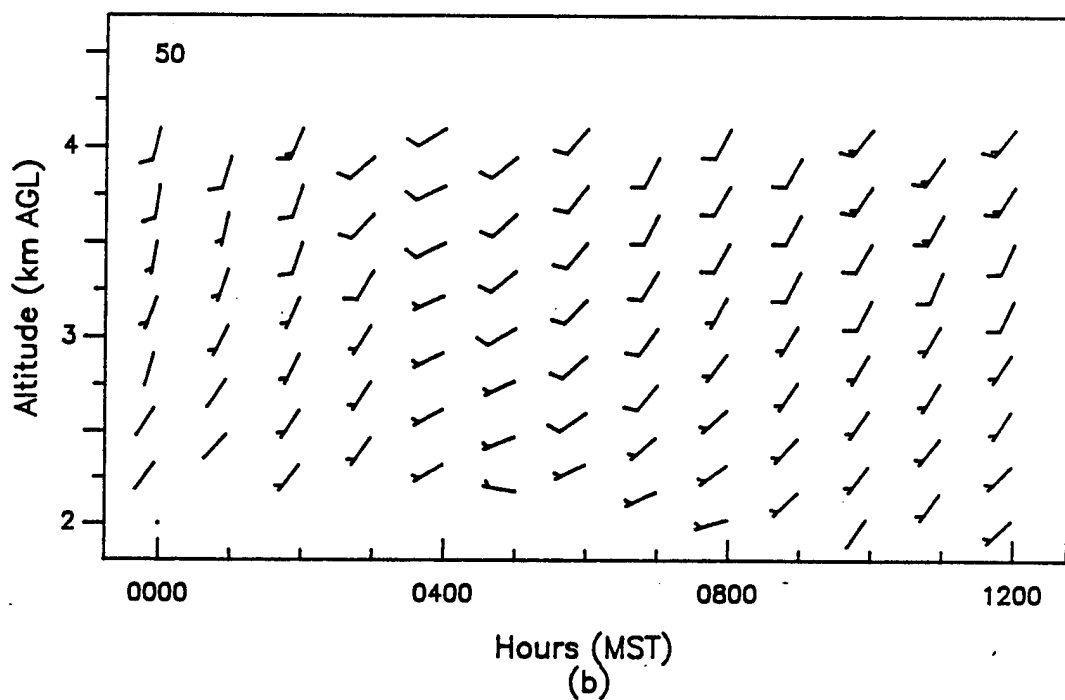
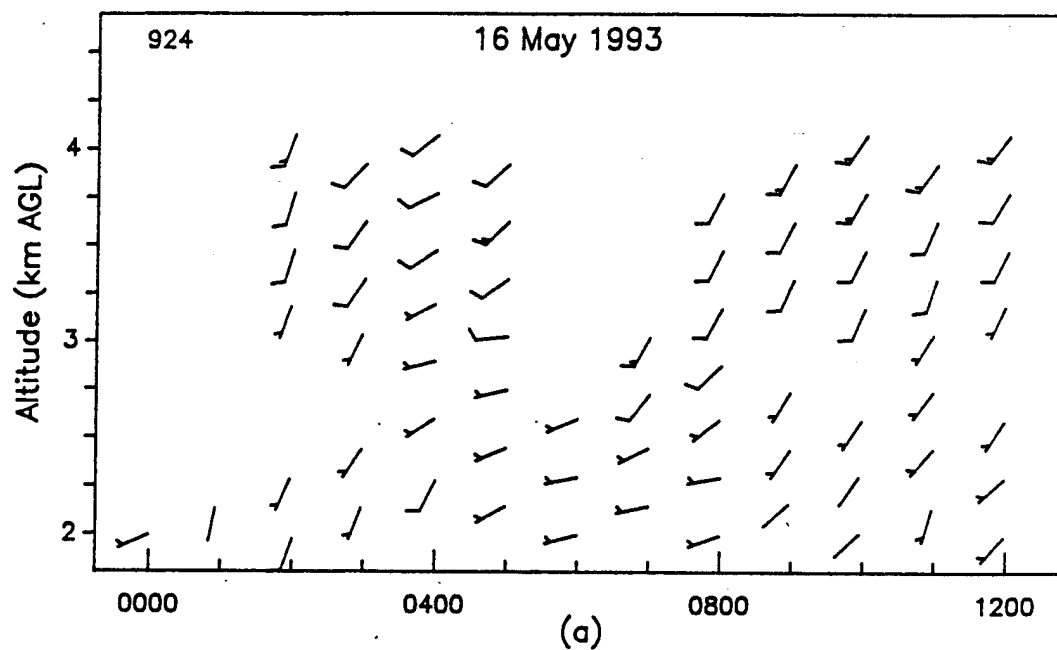


**Figure 16. Hourly average vertical profiles of wind speed and wind direction, as measured with the (a) 924- and (b) 50-MHz profilers, APRF complex, WSMR, 0000 to 1200 MST, 16 May 93.**

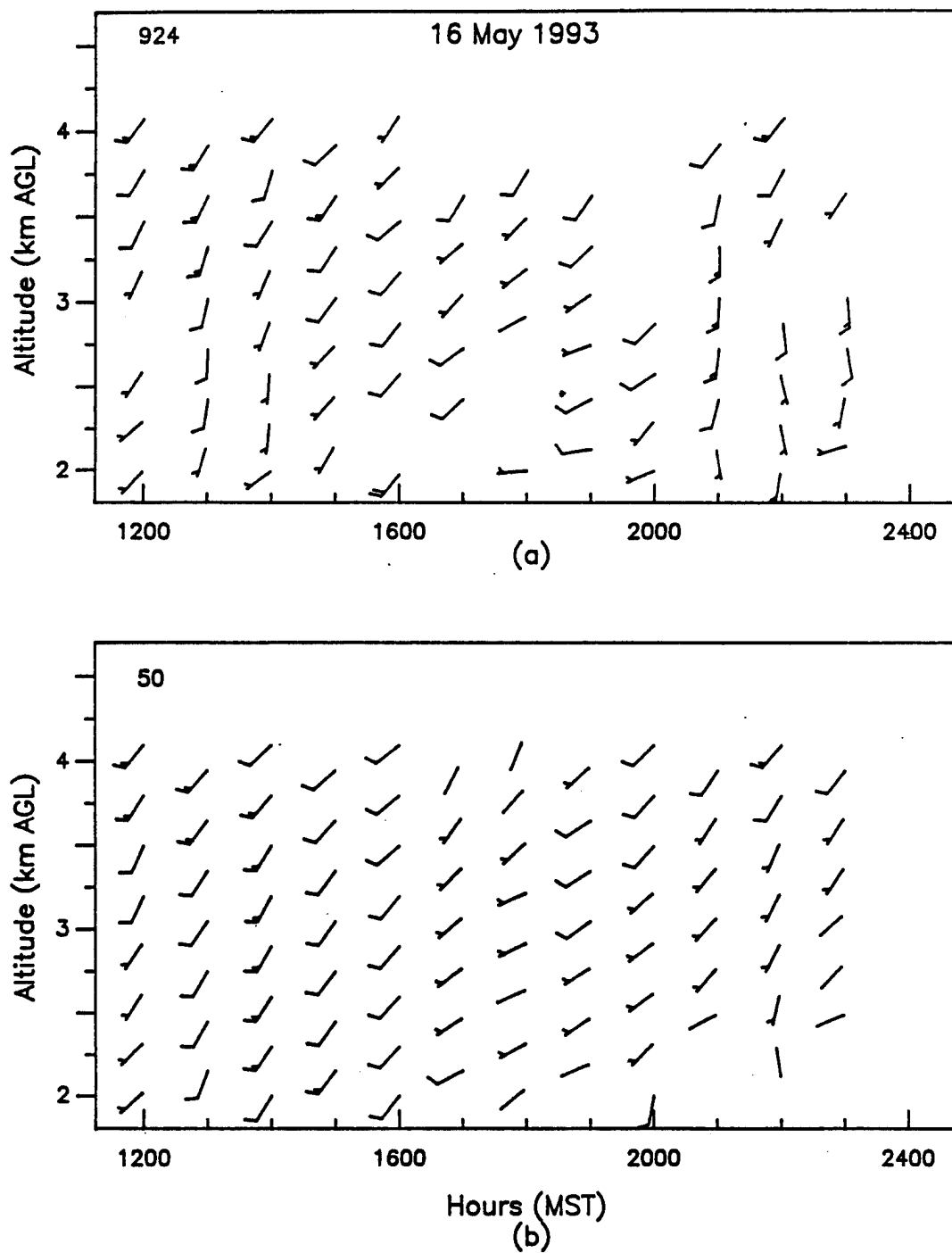


**Figure 17. Hourly average vertical profiles of wind speed and wind direction, as measured with the (a) 924- and (b) 50-MHz profilers, APRF complex, WSMR, 1200 to 2400 MST, 16 May 93.**

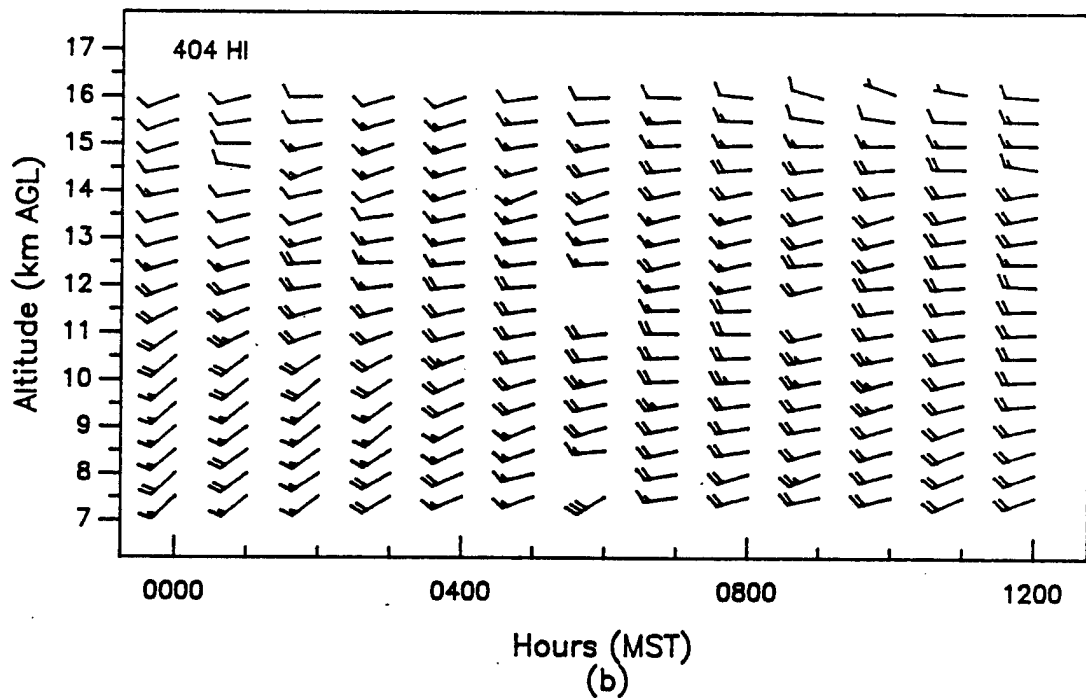
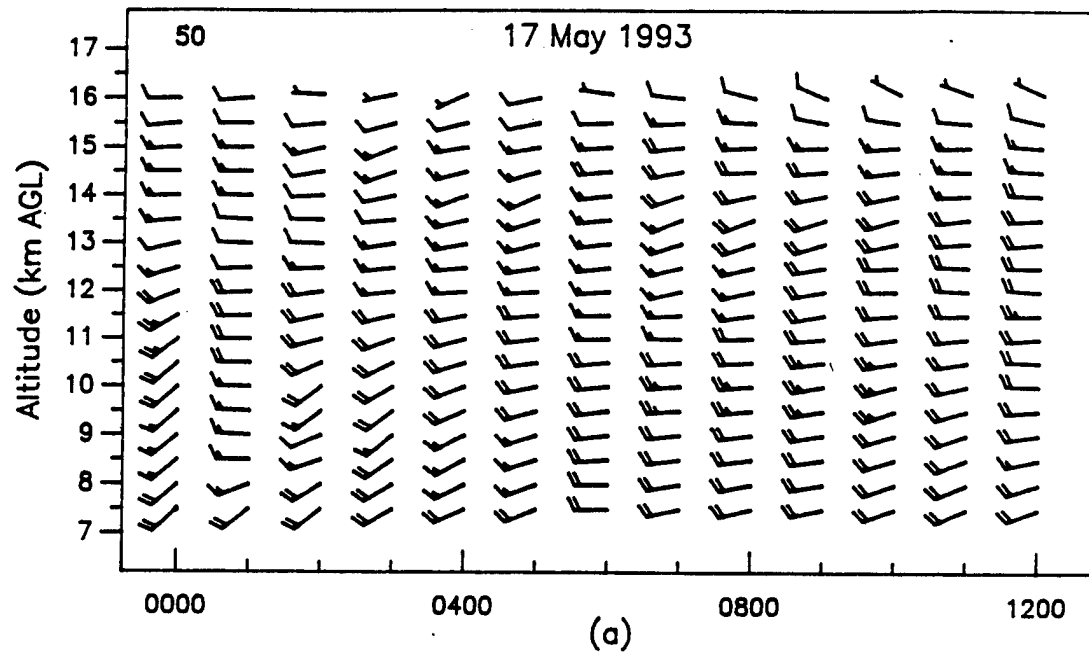


**Figure 18. Hourly average vertical profiles of wind speed and wind direction, as measured with the (a) 50- and (b) 404- (high mode) MHz profilers, APRF complex, WSMR, 0000 to 1200 MST, 17 May 93.**

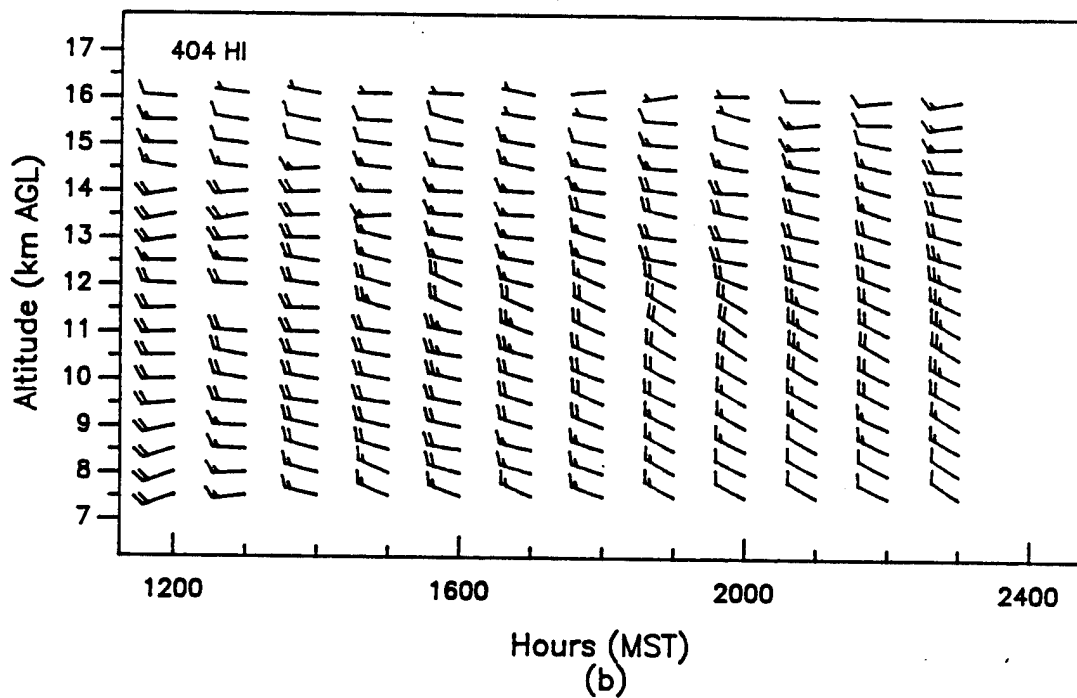
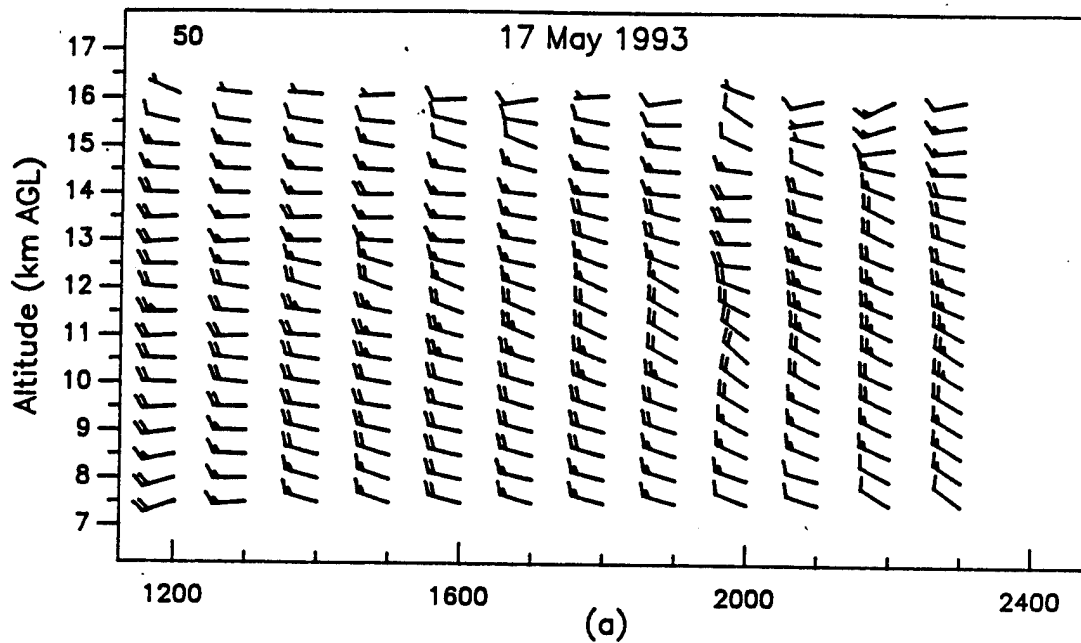
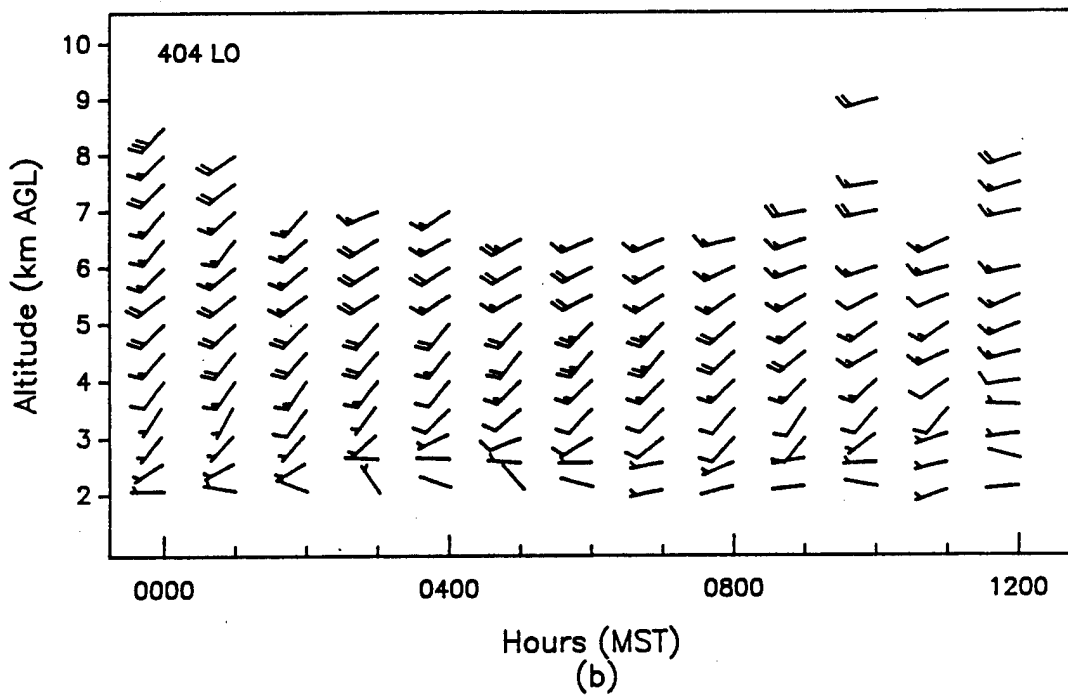
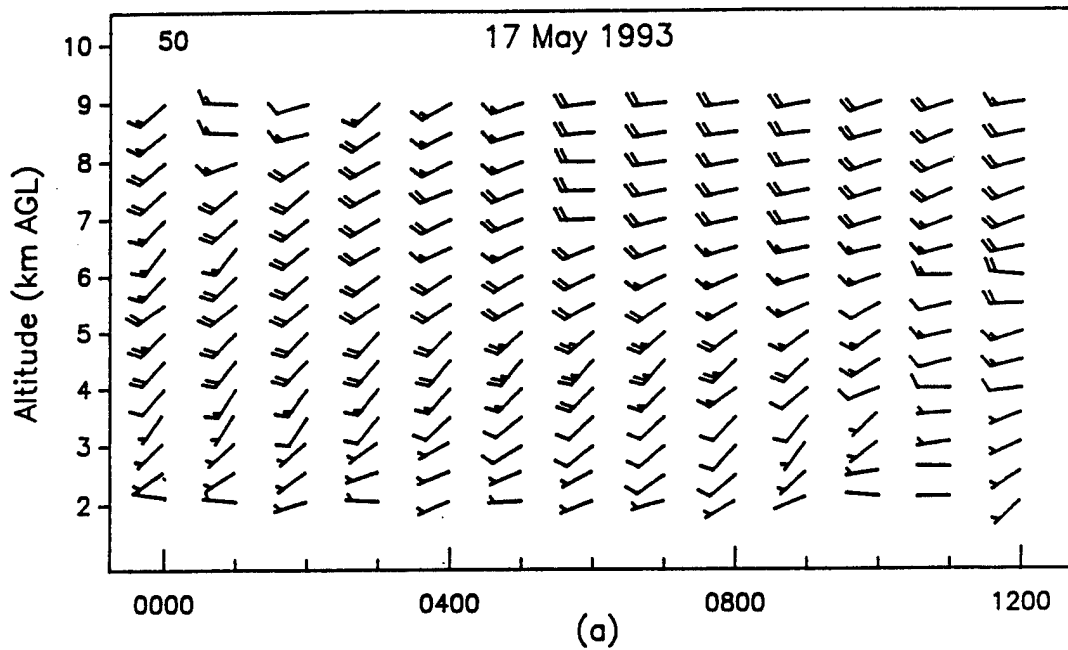
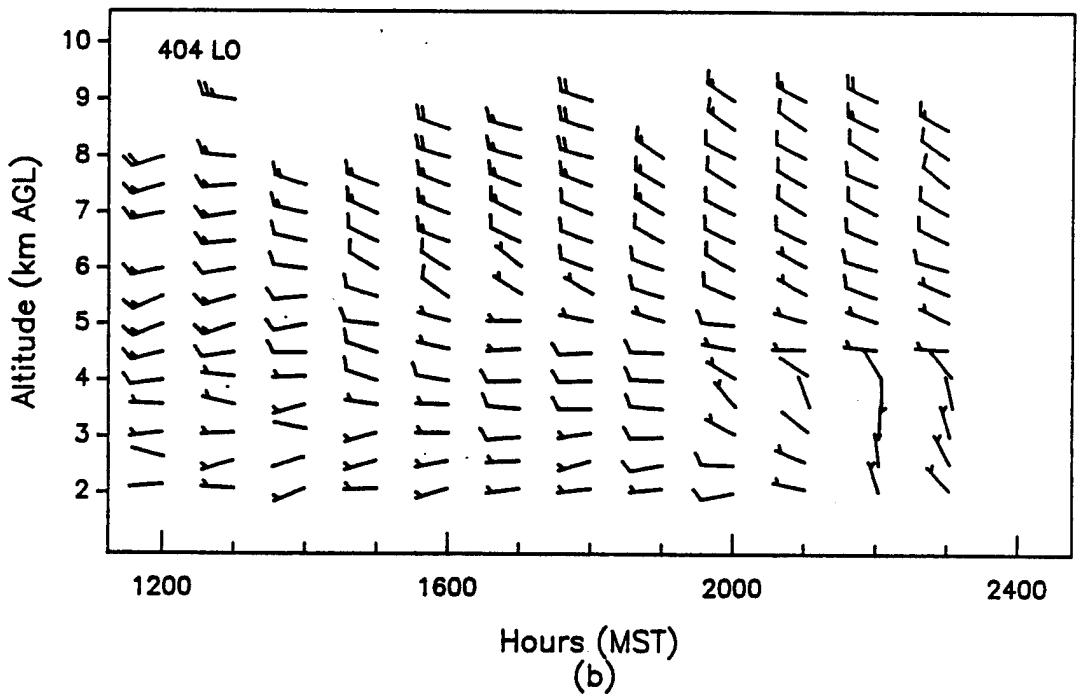
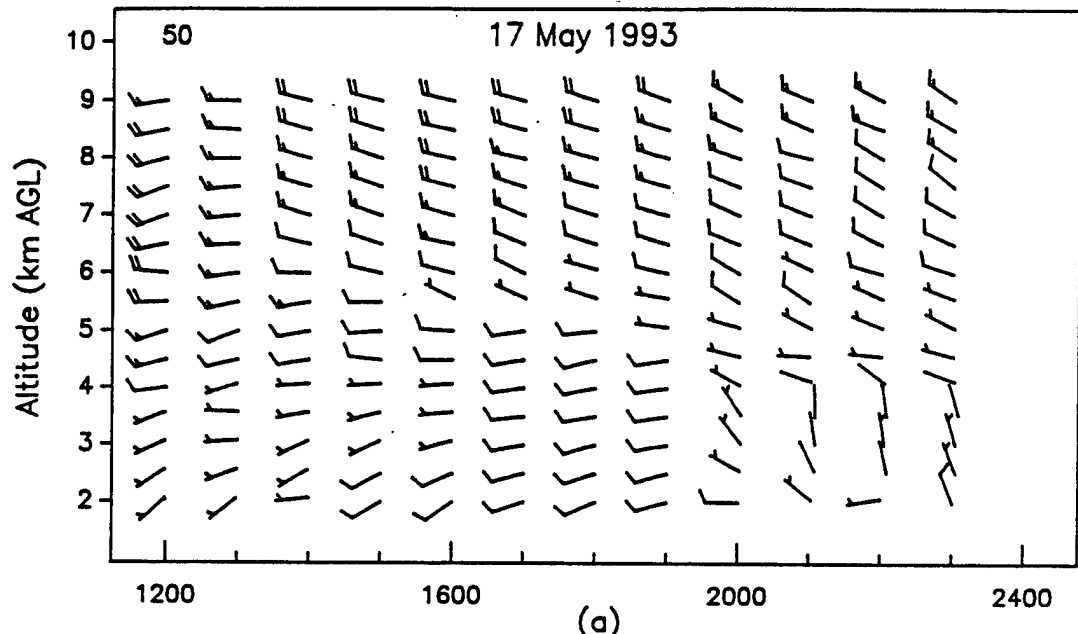


Figure 19. Hourly average vertical profiles of wind speed and wind direction, as measured with the (a) 50- and (b) 404- (high mode) MHz profilers, APRF complex, WSMR, 1200 to 2400 MST, 17 May 93.



**Figure 20. Hourly average vertical profiles of wind speed and wind direction, as measured with the (a) 50- and (b) 404- (low mode) MHz profilers, APRF complex, WSMR, 0000 to 1200 MST, 17 May 93.**



**Figure 21. Hourly average vertical profiles of wind speed and wind direction, as measured with the (a) 50- and (b) 404- (low mode) MHz profilers, APRF complex, WSMR, 1200 to 2400 MST, 17 May 93.**

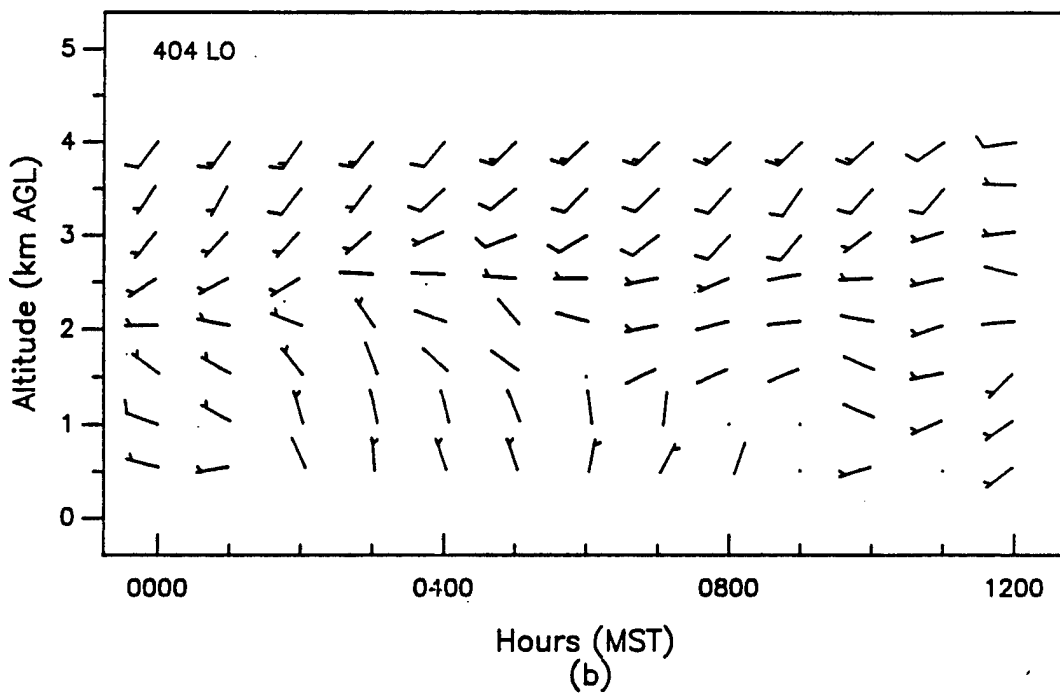
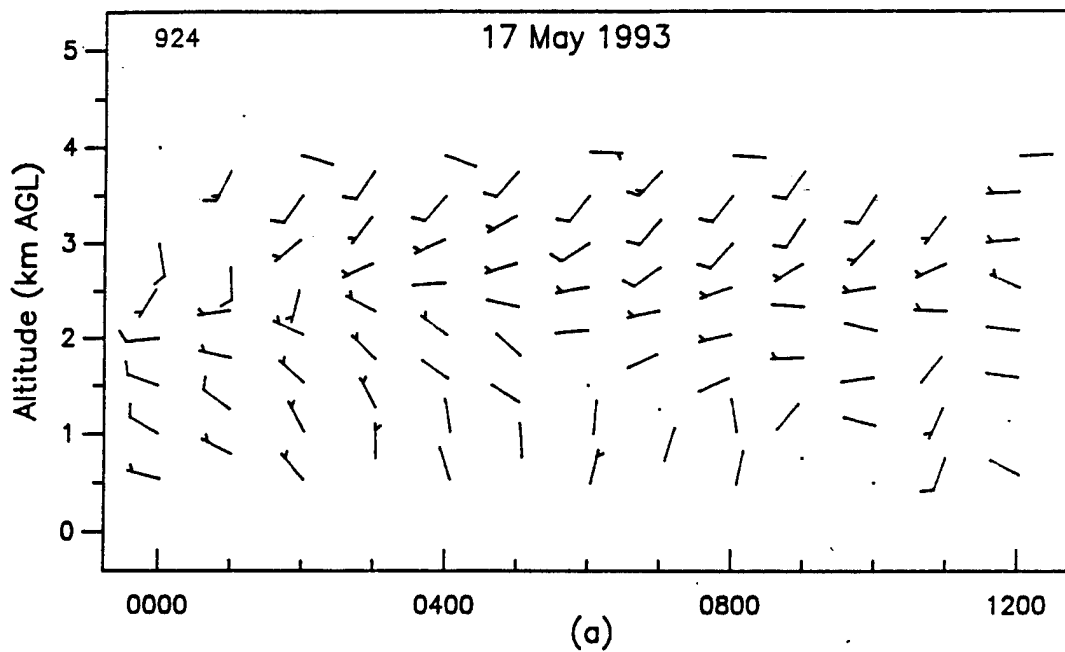


**Figure 22. Hourly average vertical profiles of wind speed and wind direction, as measured with the (a) 924- and (b) 404- (low mode) MHz profilers, APRF complex, WSMR, 0000 to 1200 MST, 17 May 93.**

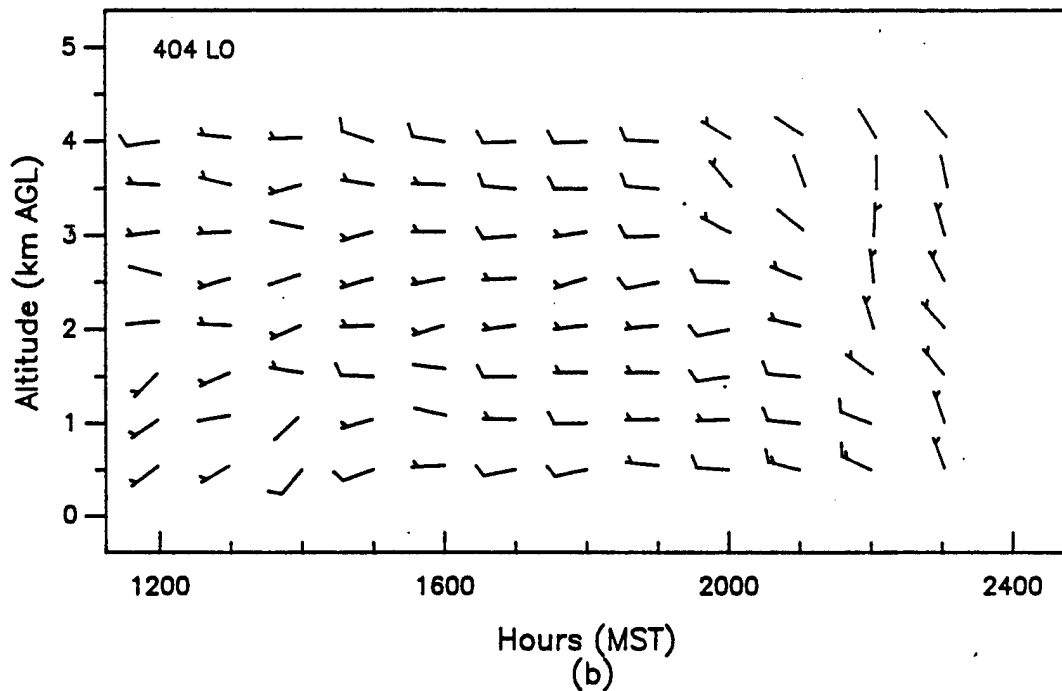
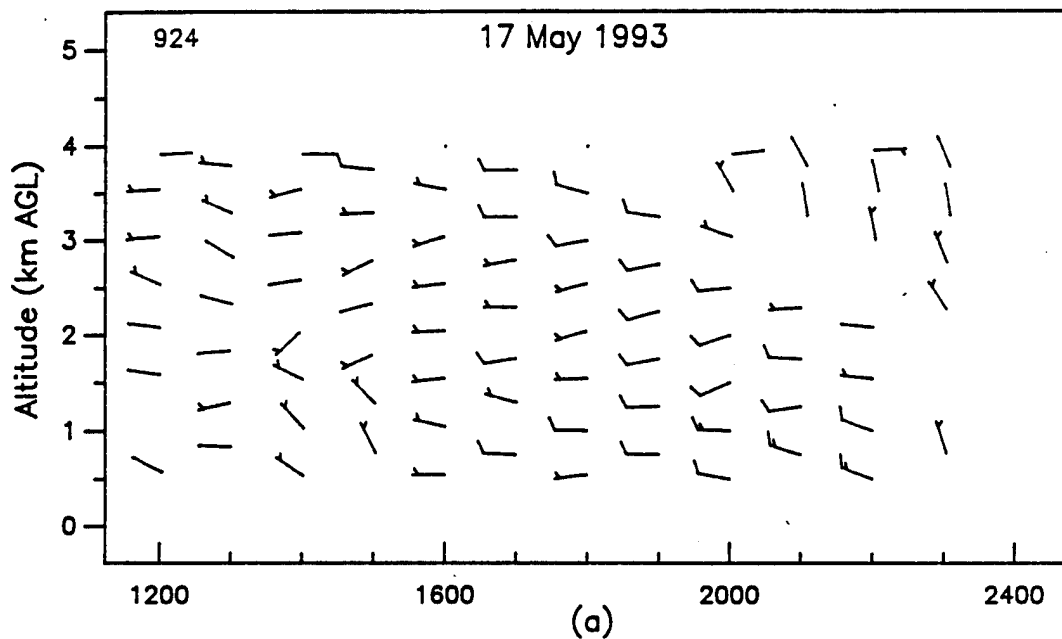


**Figure 23. Hourly average vertical profiles of wind speed and wind direction, as measured with the (a) 924- and (b) 404- (low mode) MHz profilers, APRF complex, WSMR, 1200 to 2400 MST, 17 May 93.**

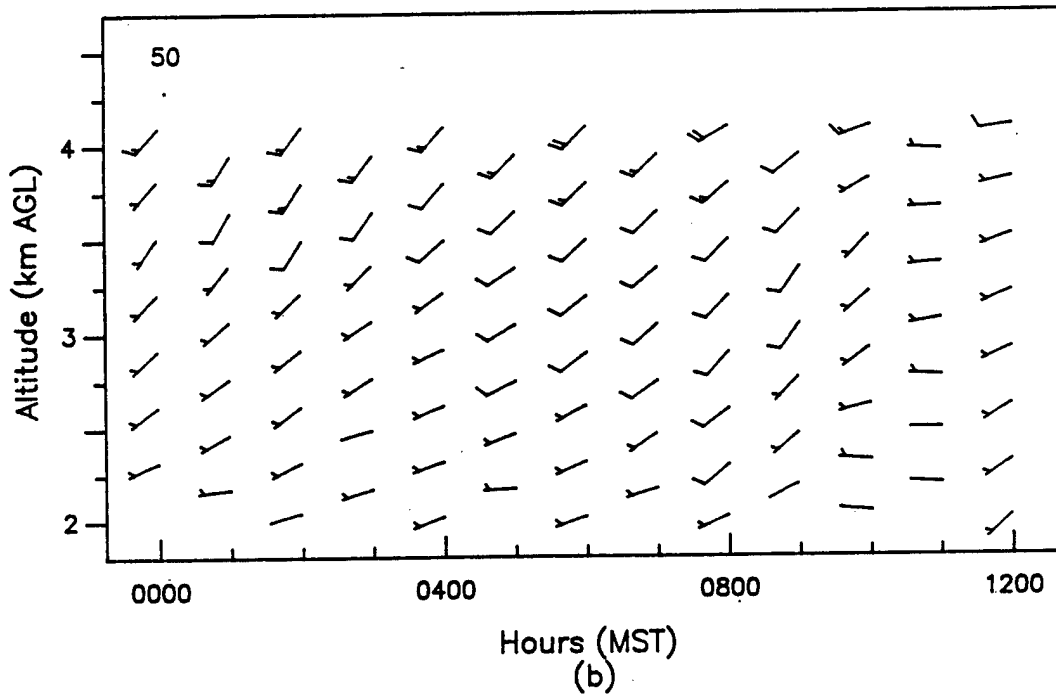
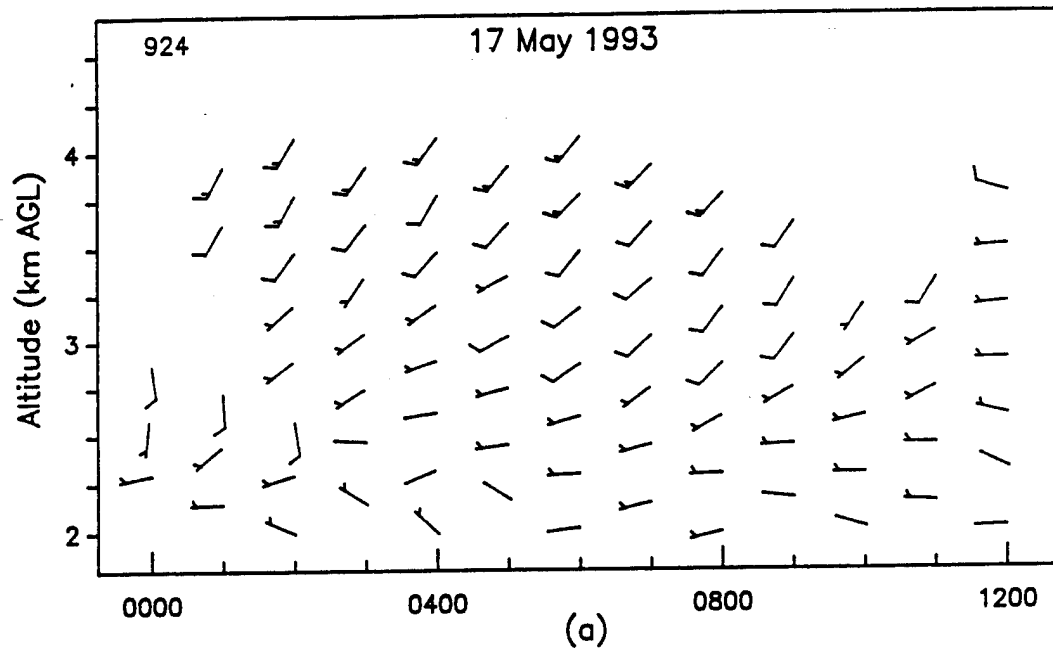


**Figure 24. Hourly average vertical profiles of wind speed and wind direction, as measured with the (a) 924- and (b) 50-MHz profilers, APRF complex, WSMR, 0000 to 1200 MST, 17 May 93.**

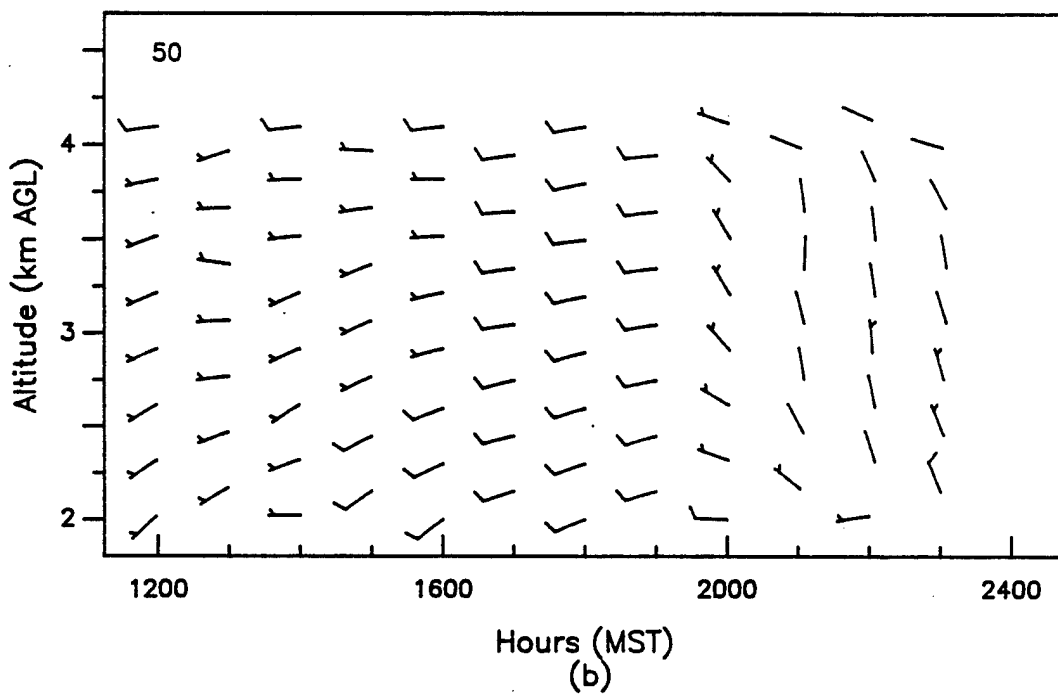
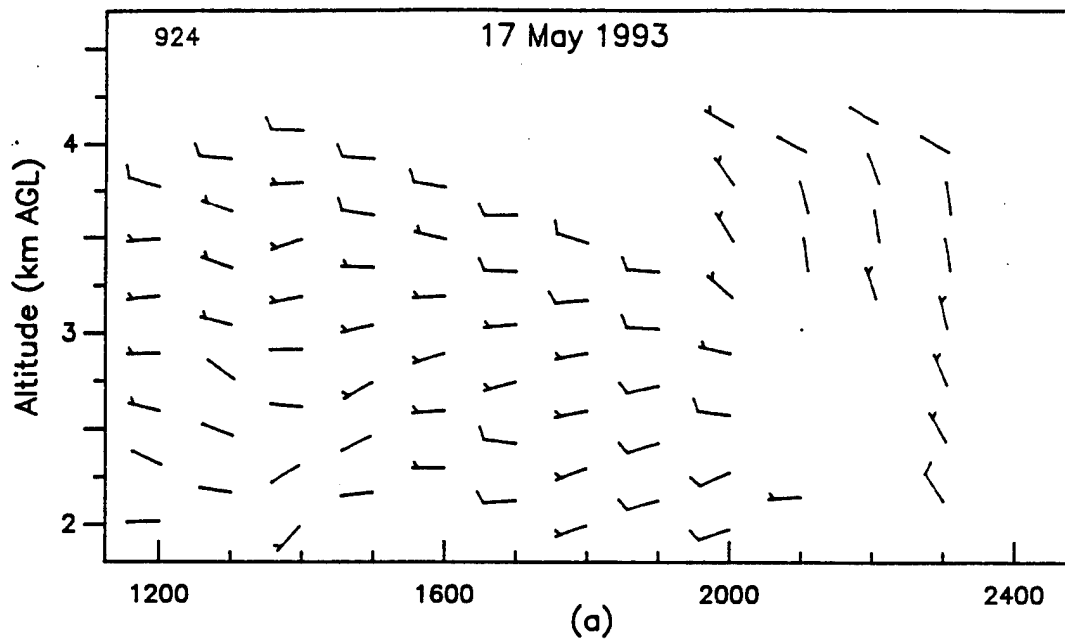


**Figure 25. Hourly average vertical profiles of wind speed and wind direction, as measured with the (a) 924- and (b) 50-MHz profilers, APRF complex, WSMR, 1200 to 2400 MST, 17 May 93.**

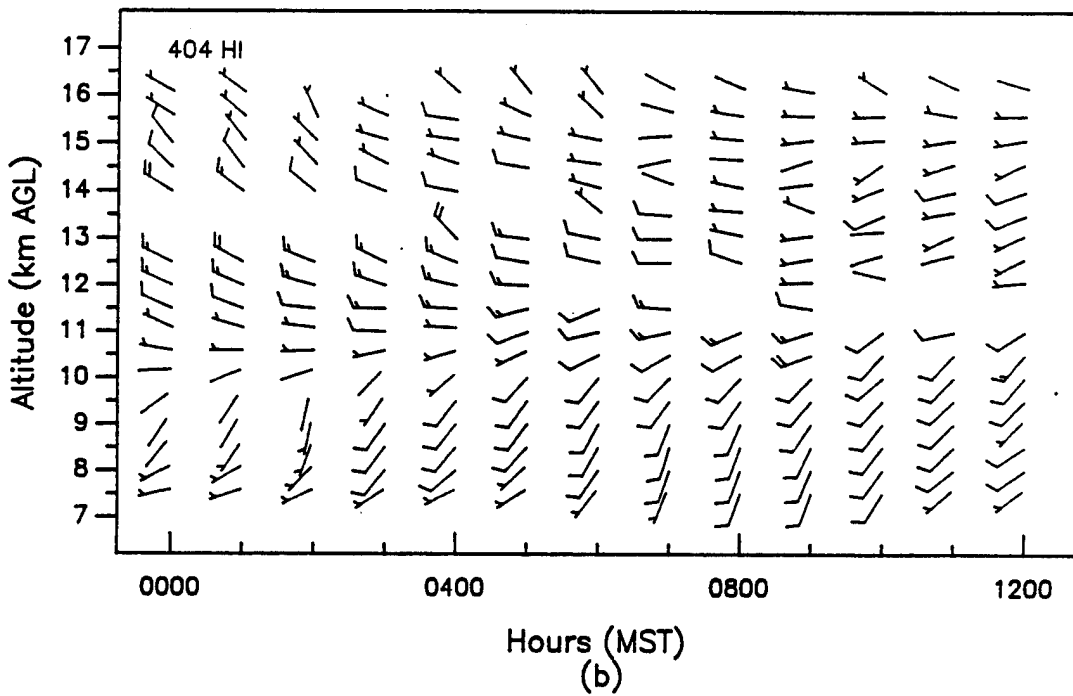
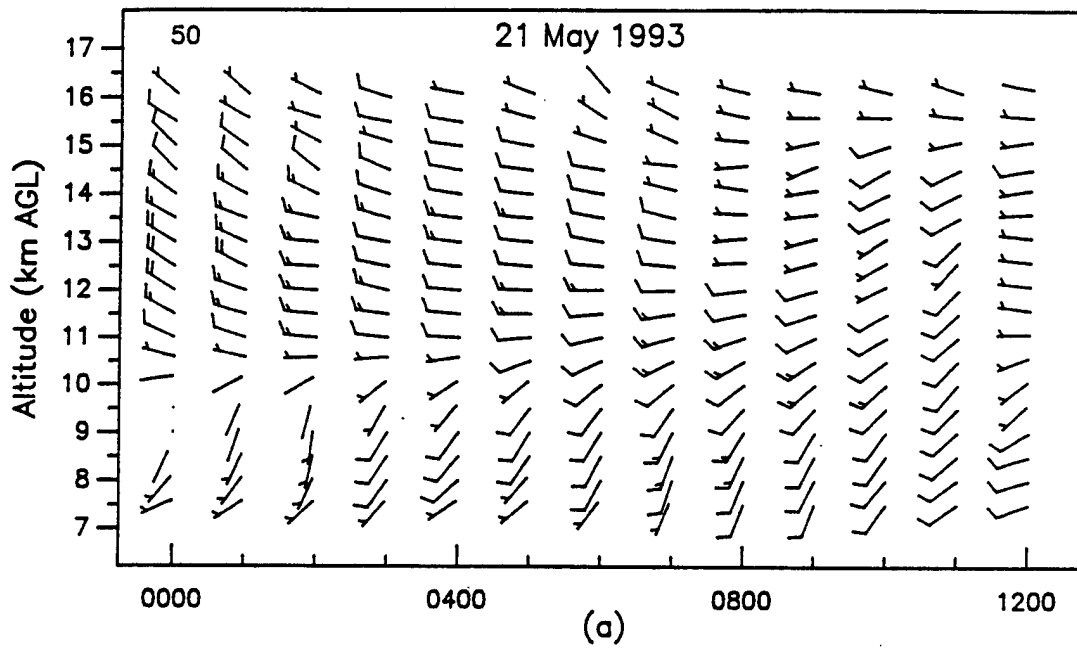


**Figure 26. Hourly average vertical profiles of wind speed and wind direction, as measured with the (a) 50- and (b) 404- (high mode) MHz profilers, APRF complex, WSMR, 0000 to 1200 MST, 21 May 93.**

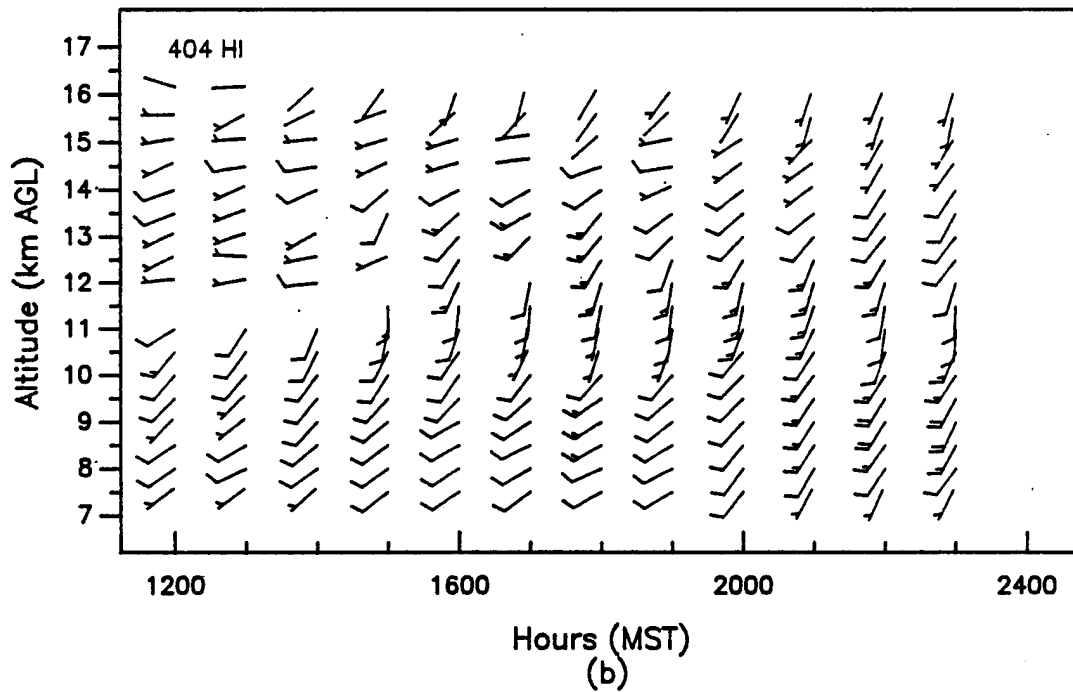
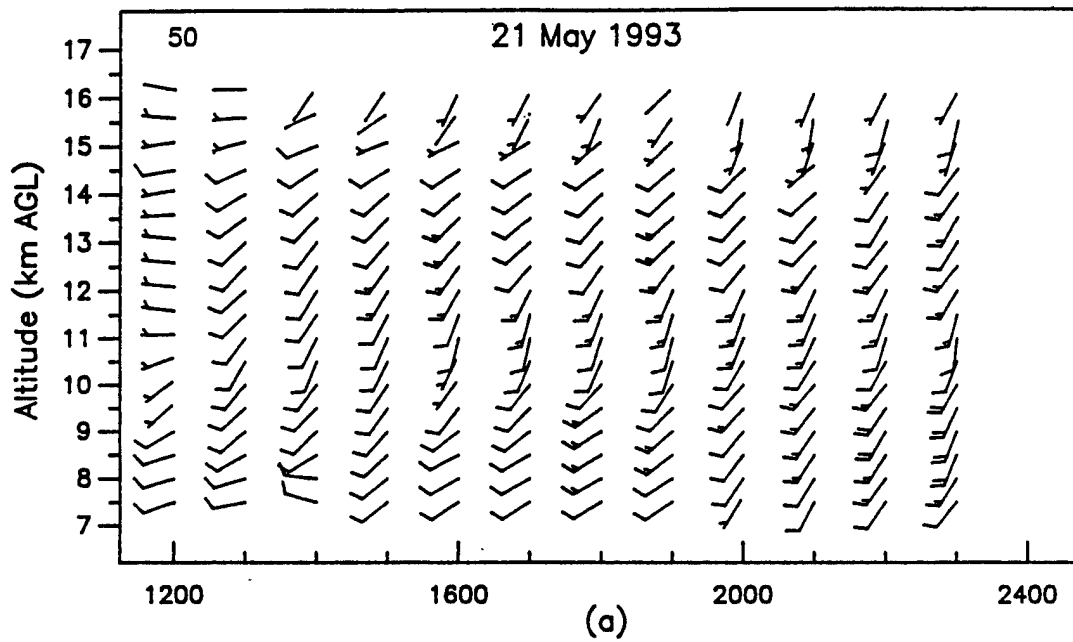


**Figure 27. Hourly average vertical profiles of wind speed and wind direction, as measured with the (a) 50- and (b) 404- (high mode) MHz profilers, APRF complex, WSMR, 1200 to 2400 MST, 21 May 93.**

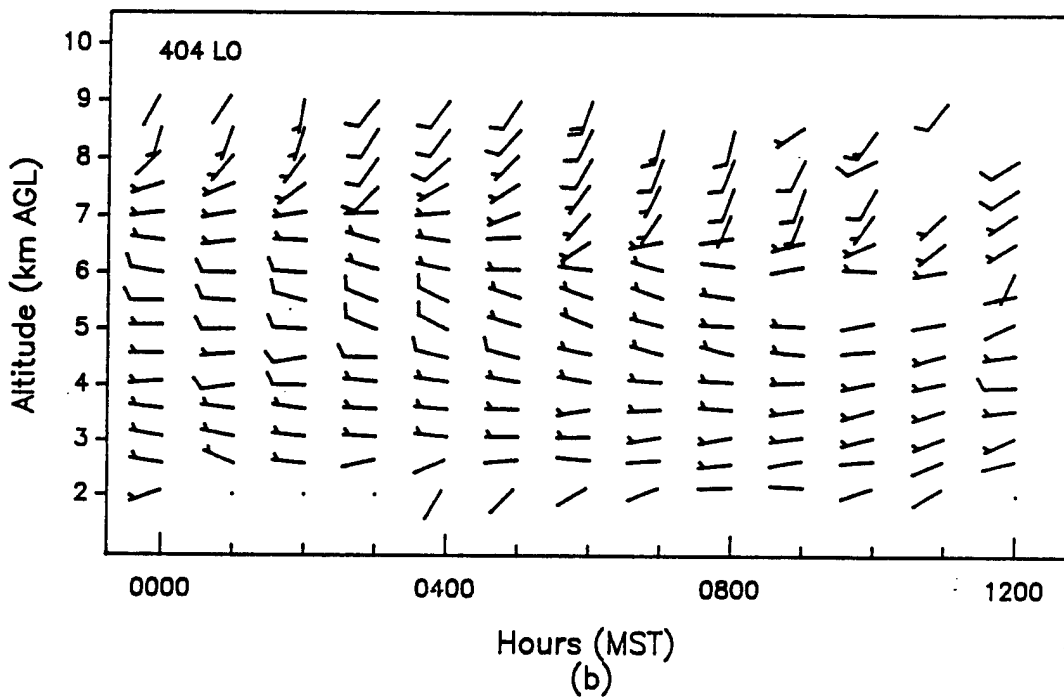
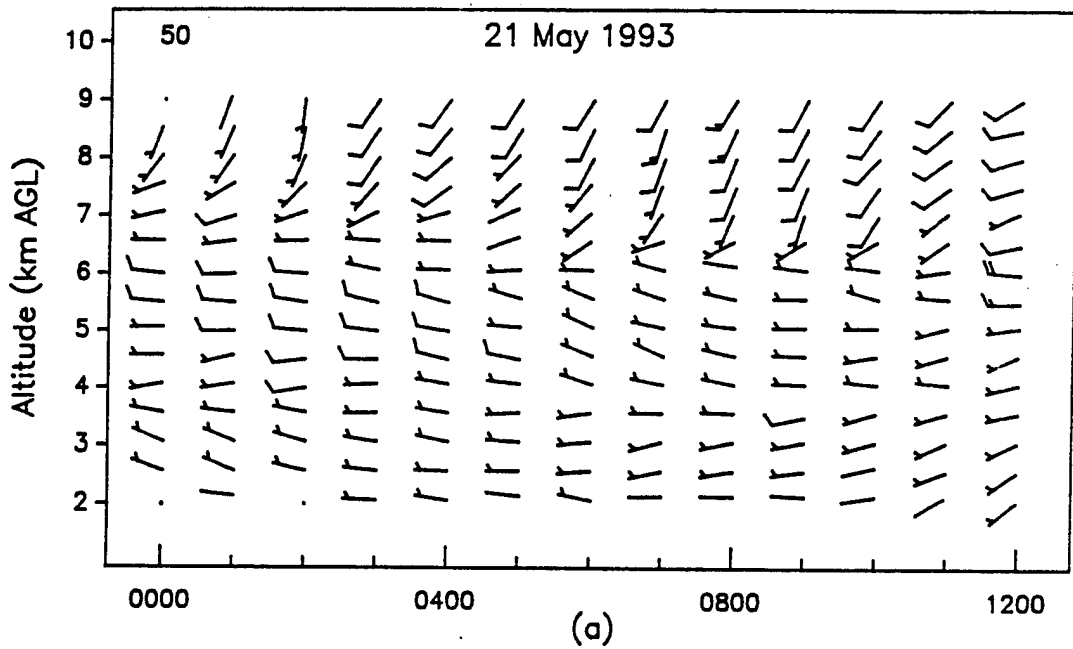


**Figure 28. Hourly average vertical profiles of wind speed and wind direction, as measured with the (a) 50- and (b) 404- (low mode) MHz profilers, APRF complex, WSMR, 0000 to 1200 MST, 21 May 93.**

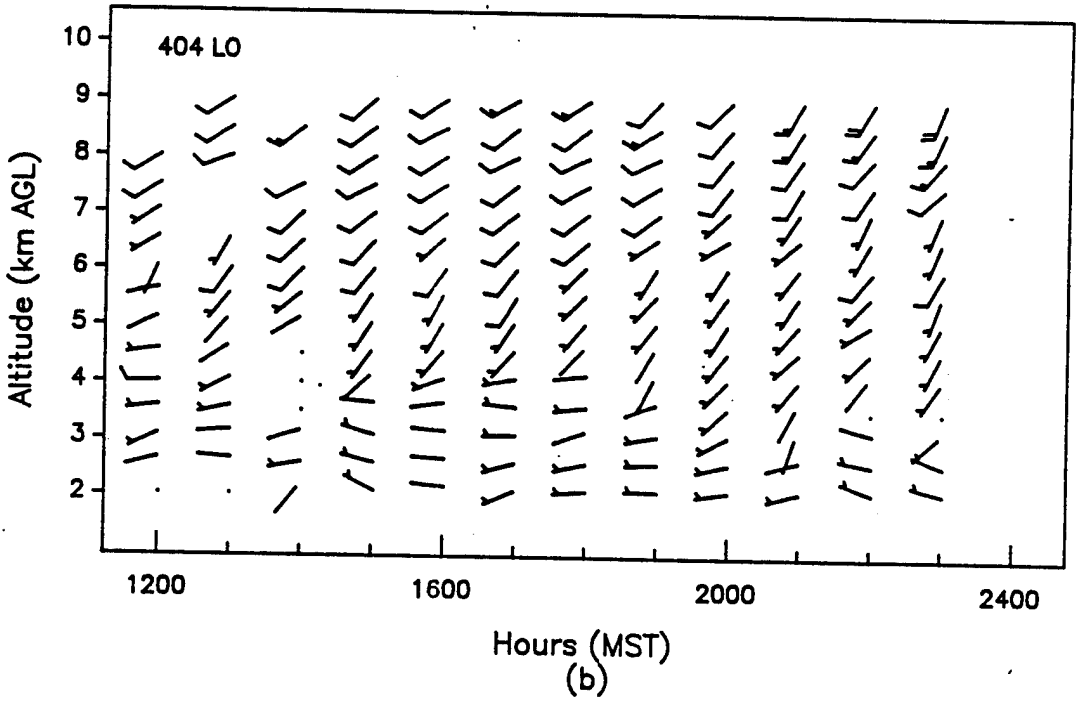
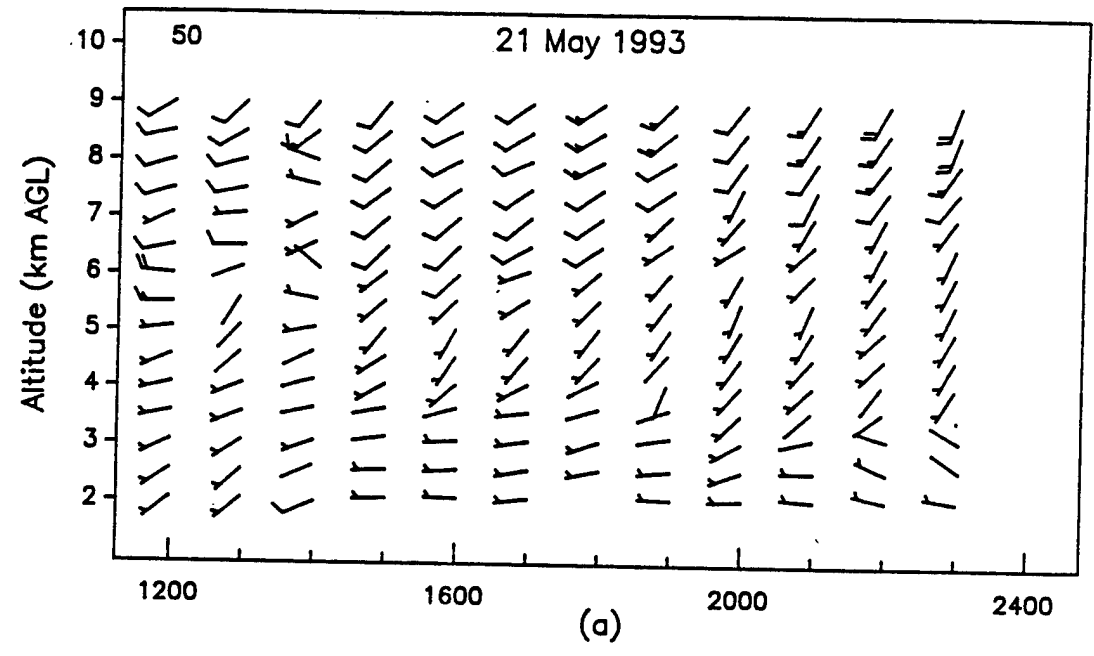


**Figure 29. Hourly average vertical profiles of wind speed and wind direction, as measured with the (a) 50- and (b) 404- (low mode) MHz profilers, APRF complex, WSMR, 1200 to 2400 MST, 21 May 93.**

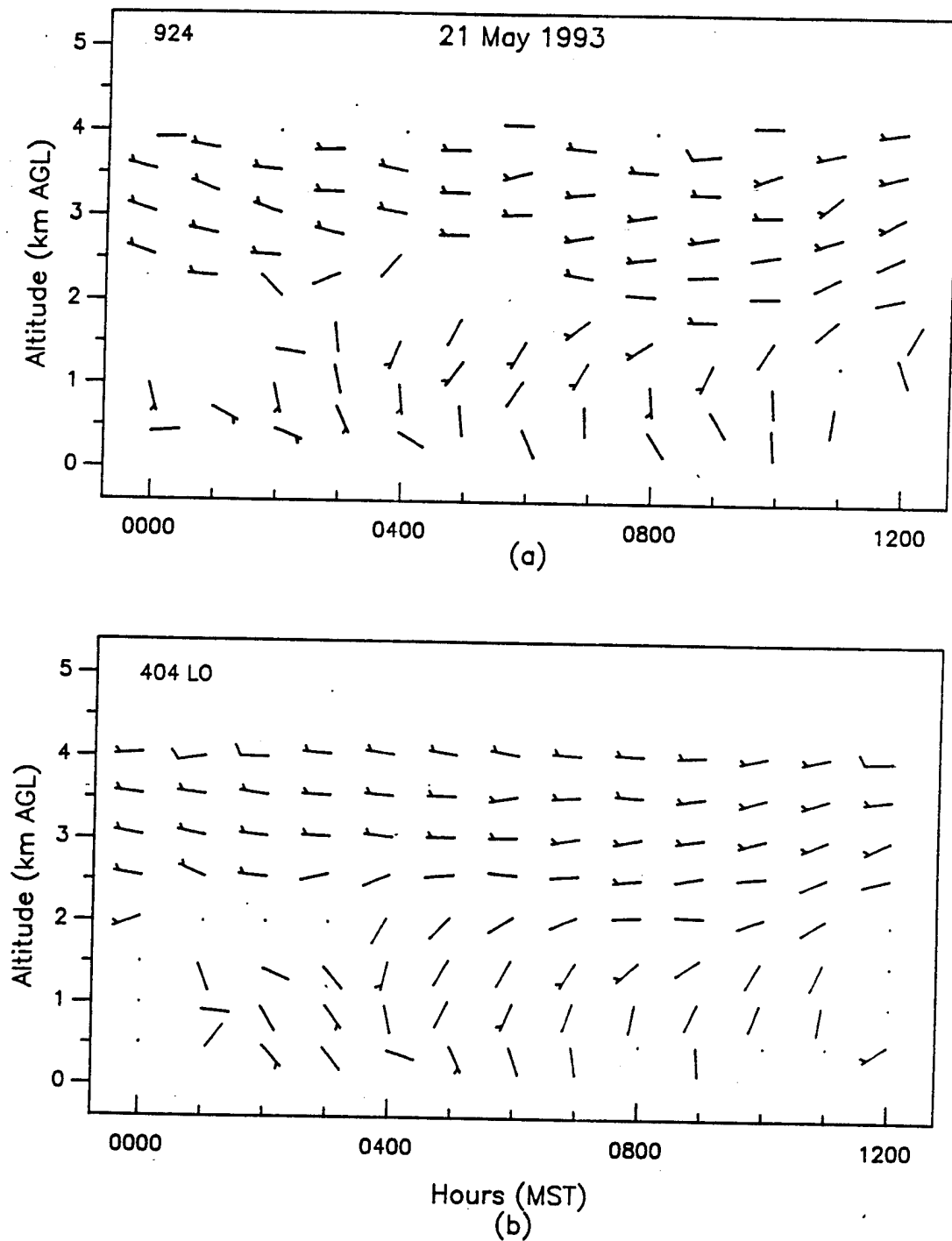


**Figure 30. Hourly average vertical profiles of wind speed and wind direction, as measured with the (a) 924- and (b) 404- (low mode) MHz profilers, APRF complex, WSMR, 0000 to 1200 MST, 21 May 93.**

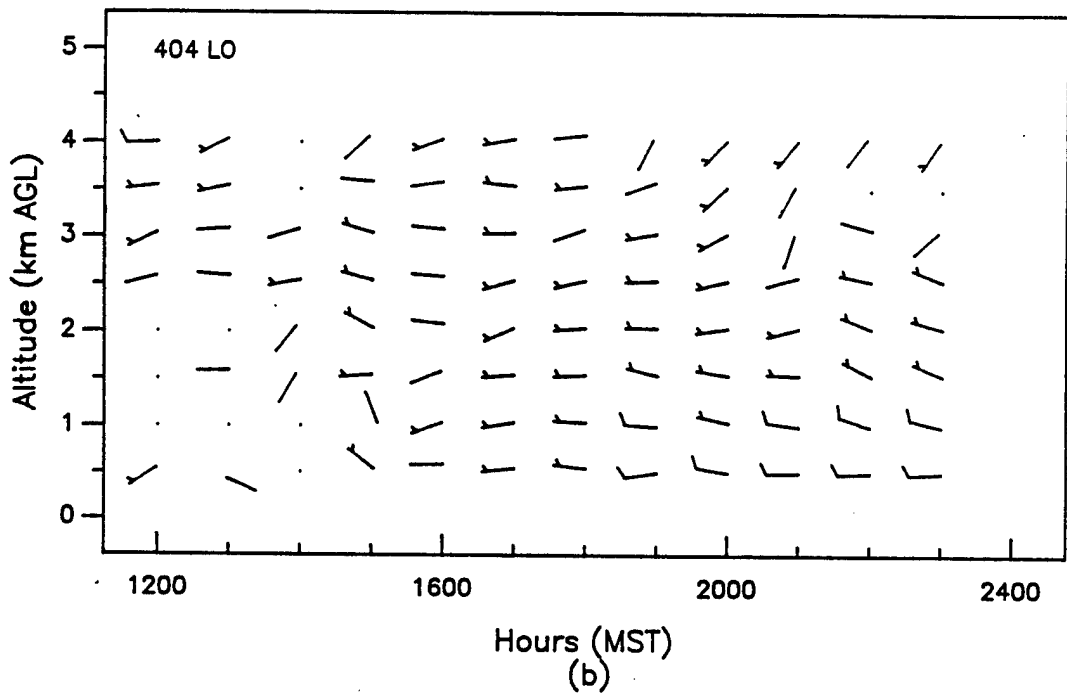
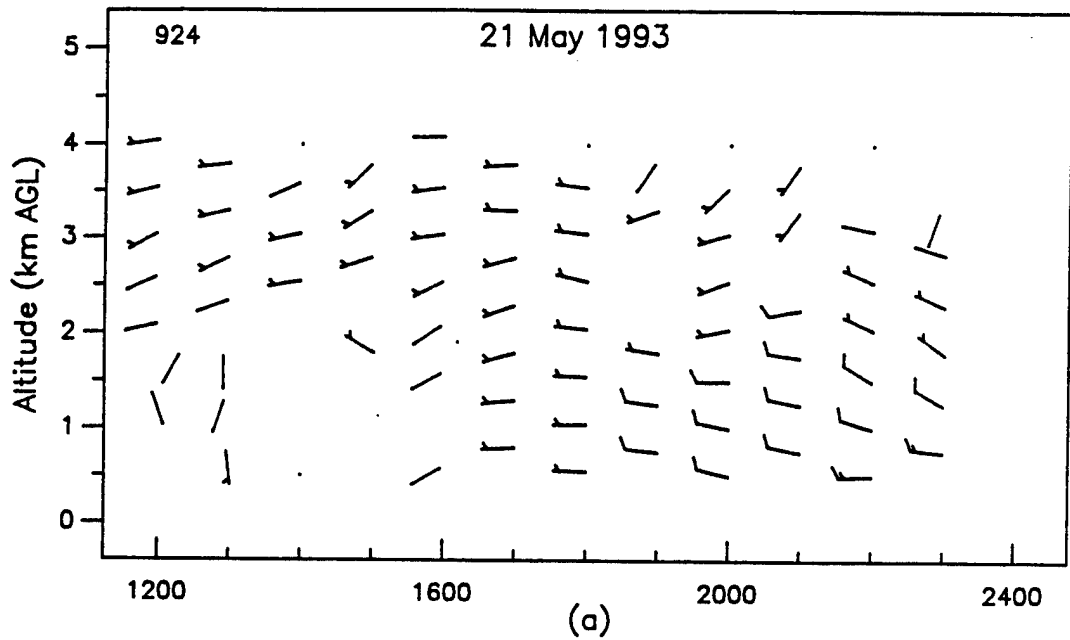


**Figure 31. Hourly average vertical profiles of wind speed and wind direction, as measured with the (a) 924- and (b) 404- (low mode) MHz profilers, APRF complex, WSMR, 1200 to 2400 MST, 21 May 93.**

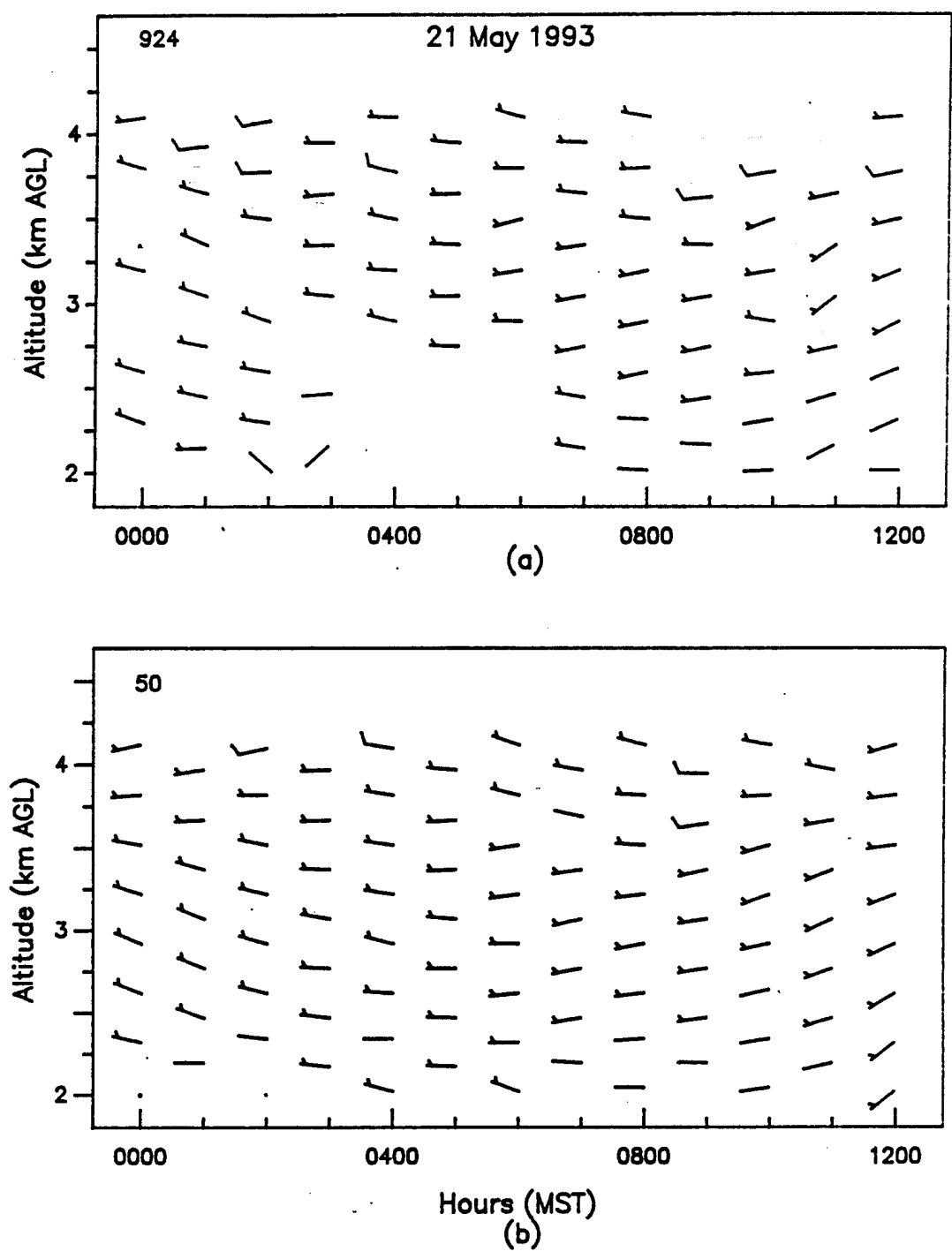


**Figure 32. Hourly average vertical profiles of wind speed and wind direction, as measured with the (a) 924- and (b) 50-MHz profilers, APRF complex, WSMR, 0000 to 1200 MST, 21 May 93.**

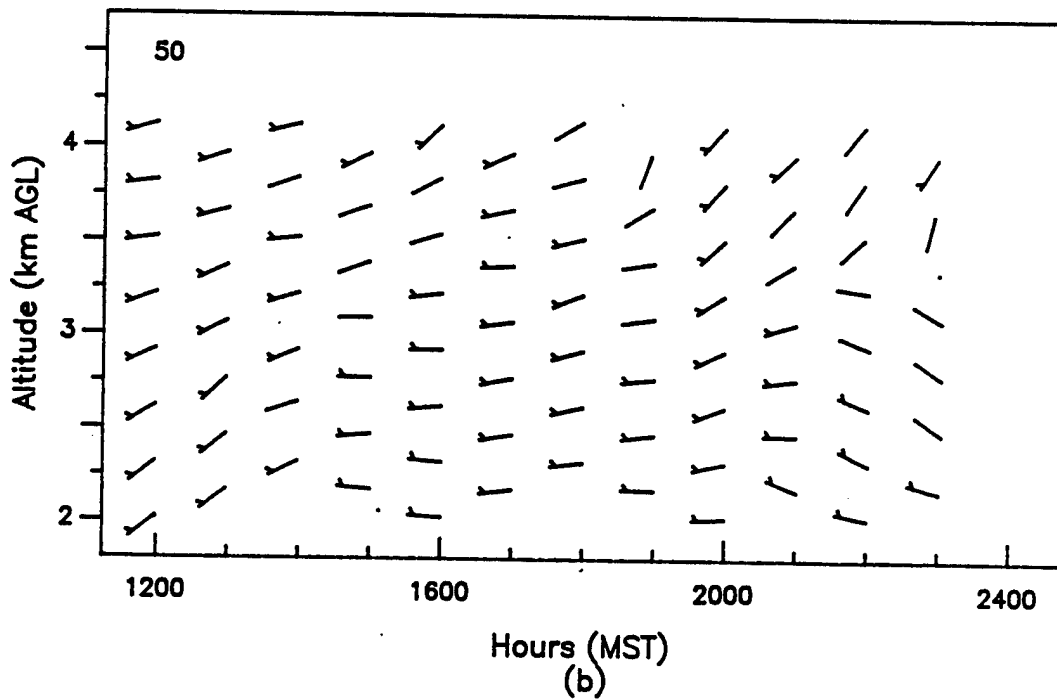
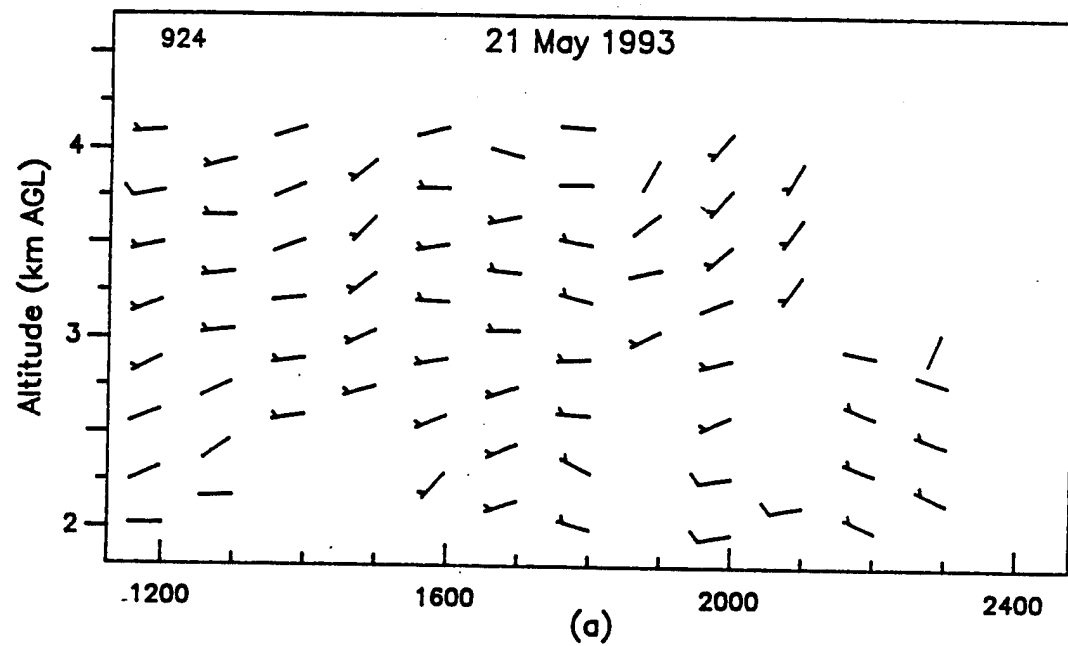


**Figure 33. Hourly average vertical profiles of wind speed and wind direction, as measured with the (a) 924- and (b) 50-MHz profilers, APRF complex, WSMR, 1200 to 2400 MST, 21 May 93.**

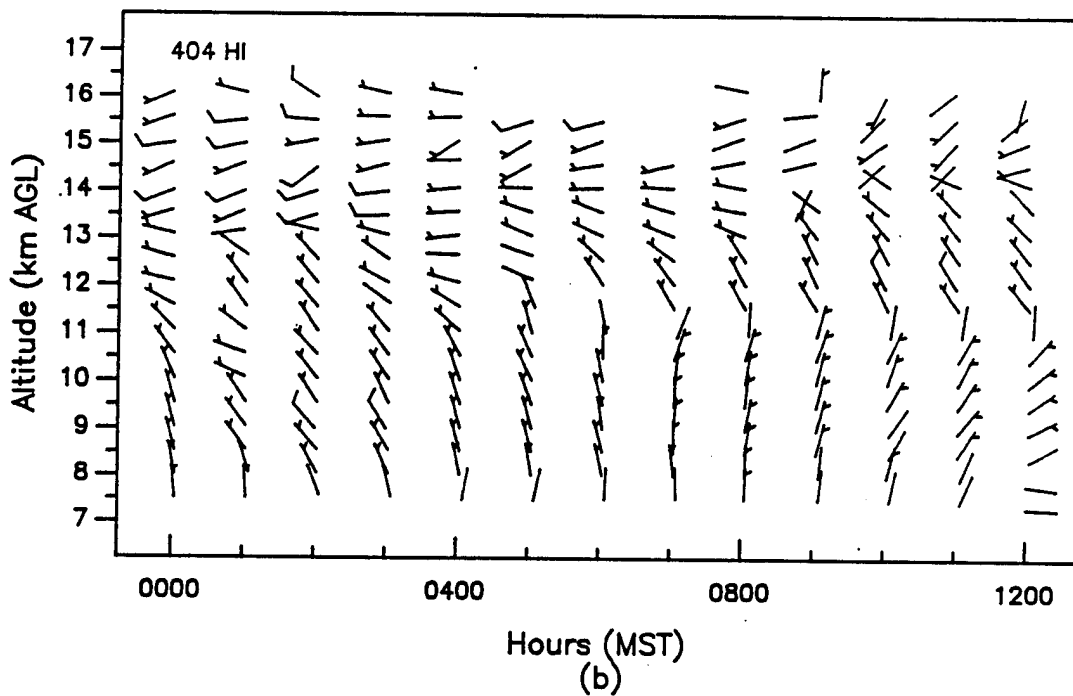
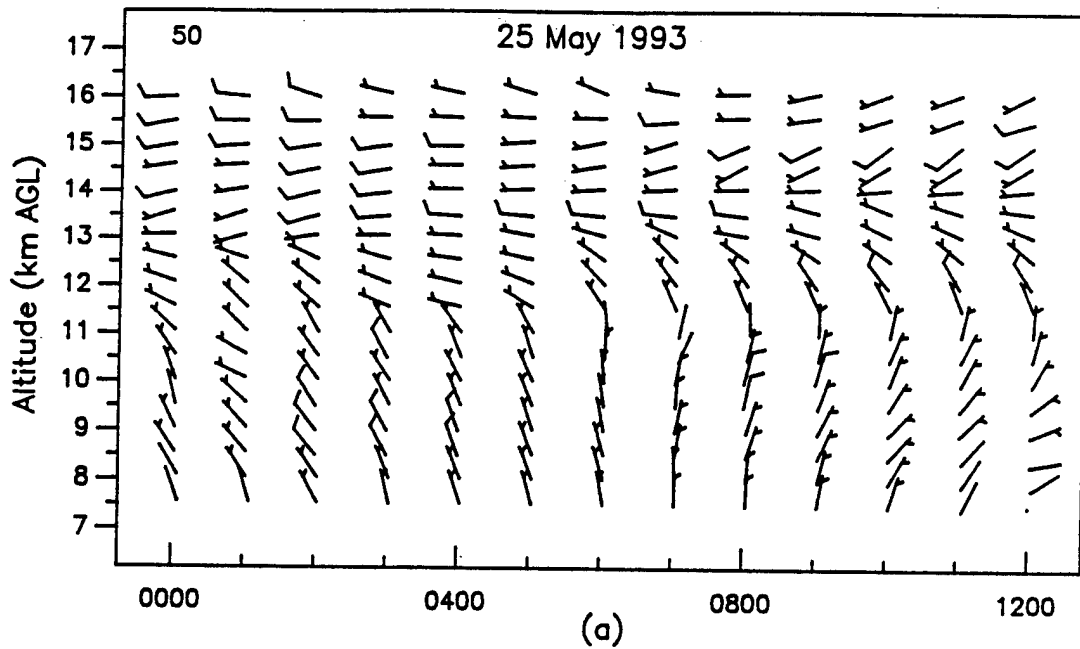


**Figure 34. Hourly average vertical profiles of wind speed and wind direction, as measured with the (a) 50- and (b) 404- (high mode) MHz profilers, APRF complex, WSMR, 0000 to 1200 MST, 25 May 93.**

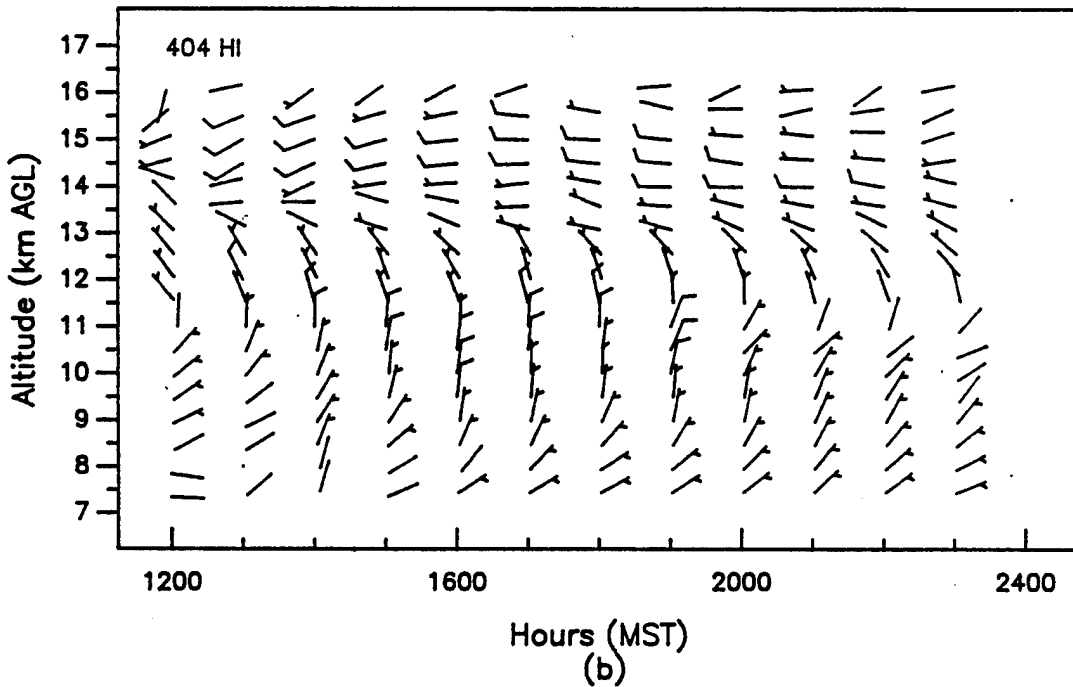
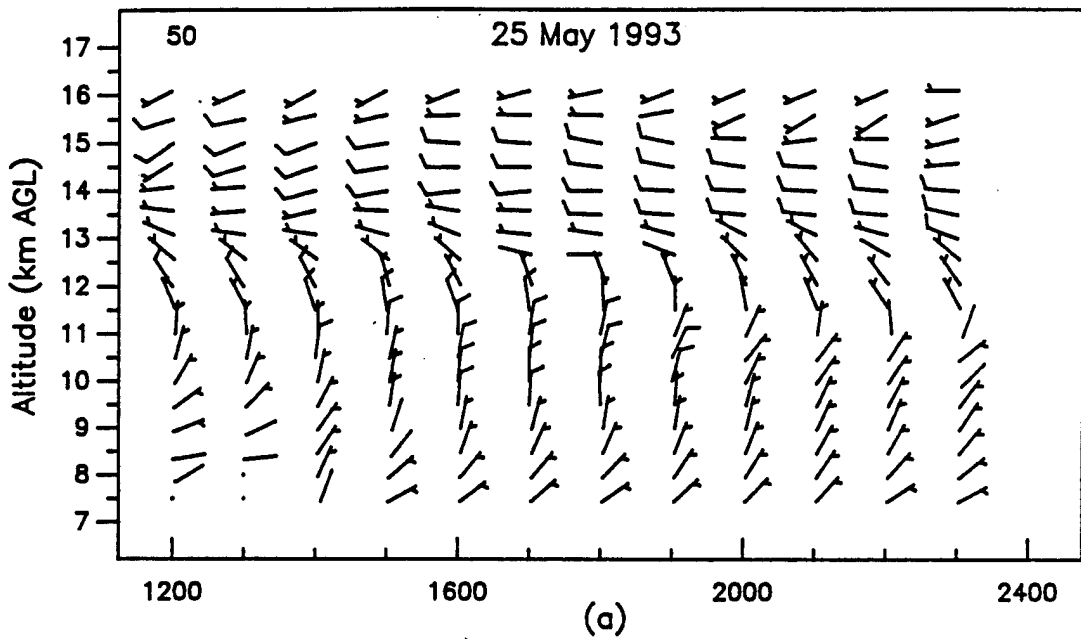


**Figure 35. Hourly average vertical profiles of wind speed and wind direction, as measured with the (a) 50- and (b) 404- (high mode) MHz profilers, APRF complex, WSMR, 1200 to 2400 MST, 25 May 93.**

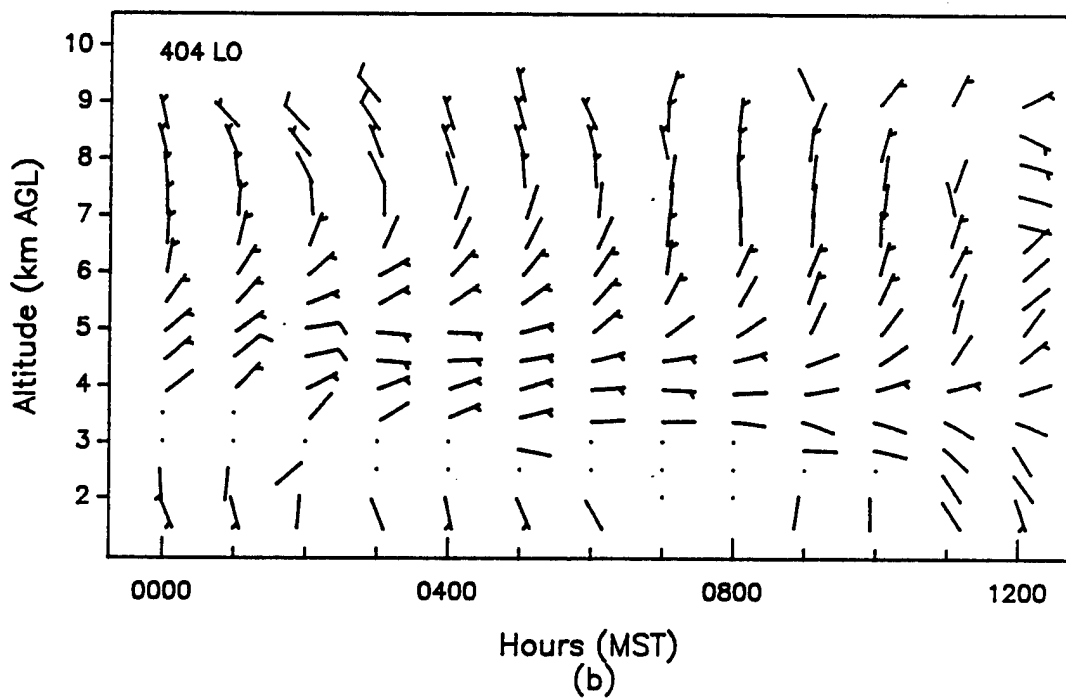
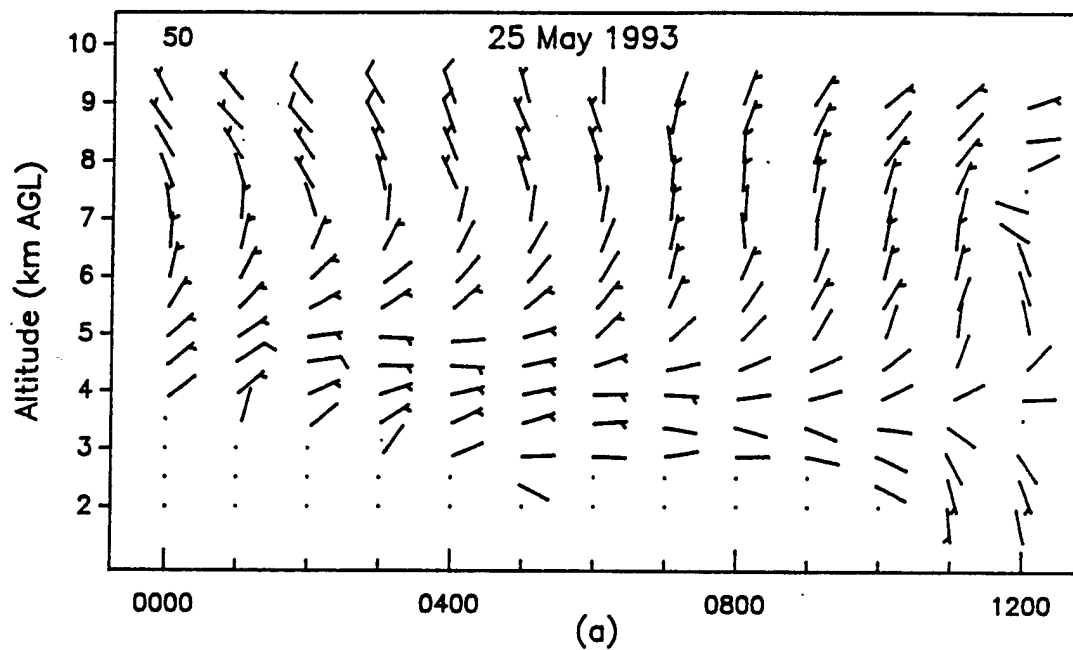


**Figure 36. Hourly average vertical profiles of wind speed and wind direction, as measured with the (a) 50- and (b) 404- (low mode) MHz profilers, APRF complex, WSMR, 0000 to 1200 MST, 25 May 93.**

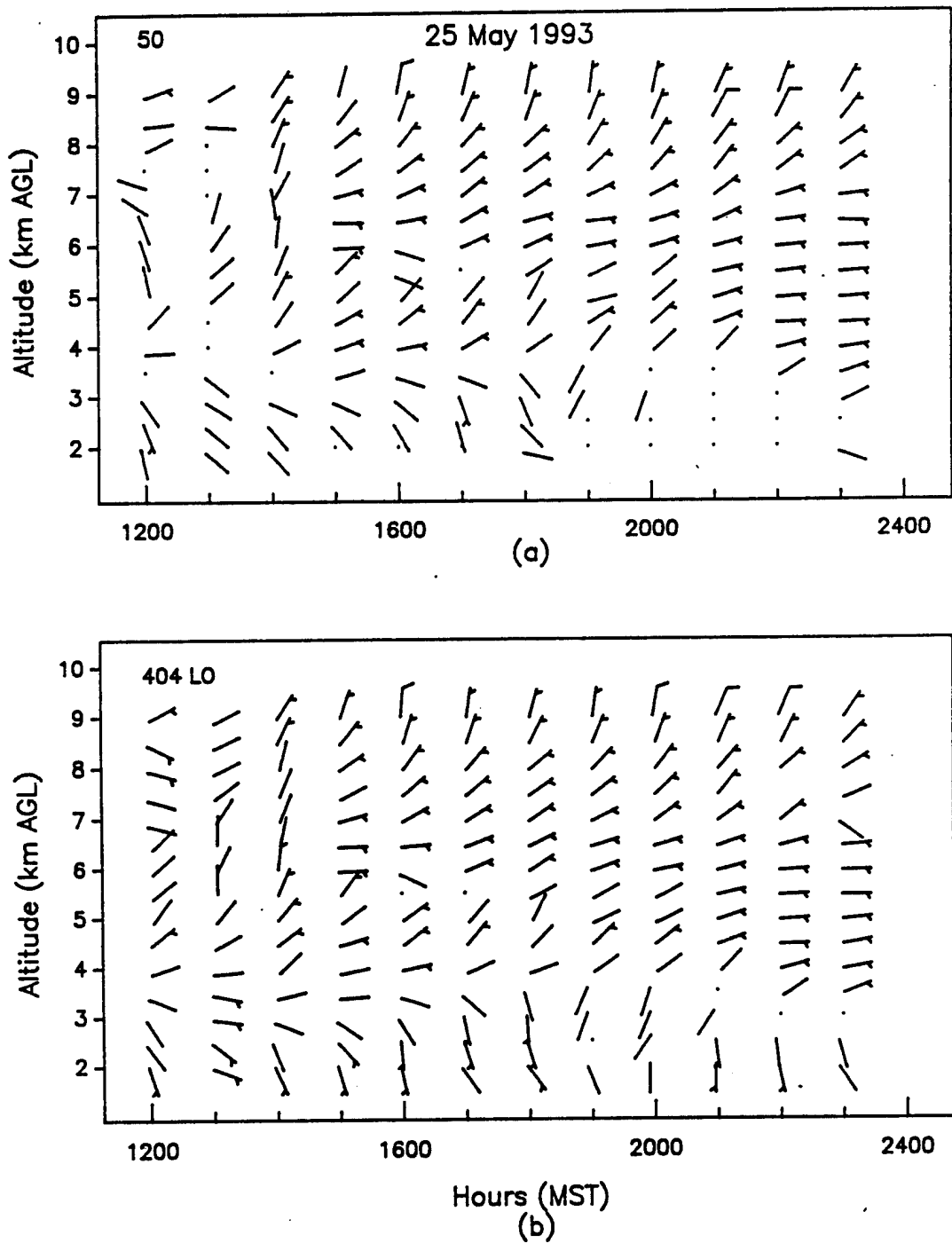


**Figure 37. Hourly average vertical profiles of wind speed and wind direction, as measured with the (a) 50- and (b) 404- (low mode) MHz profilers, APRF complex, WSMR, 1200 to 2400 MST, 25 May 93.**

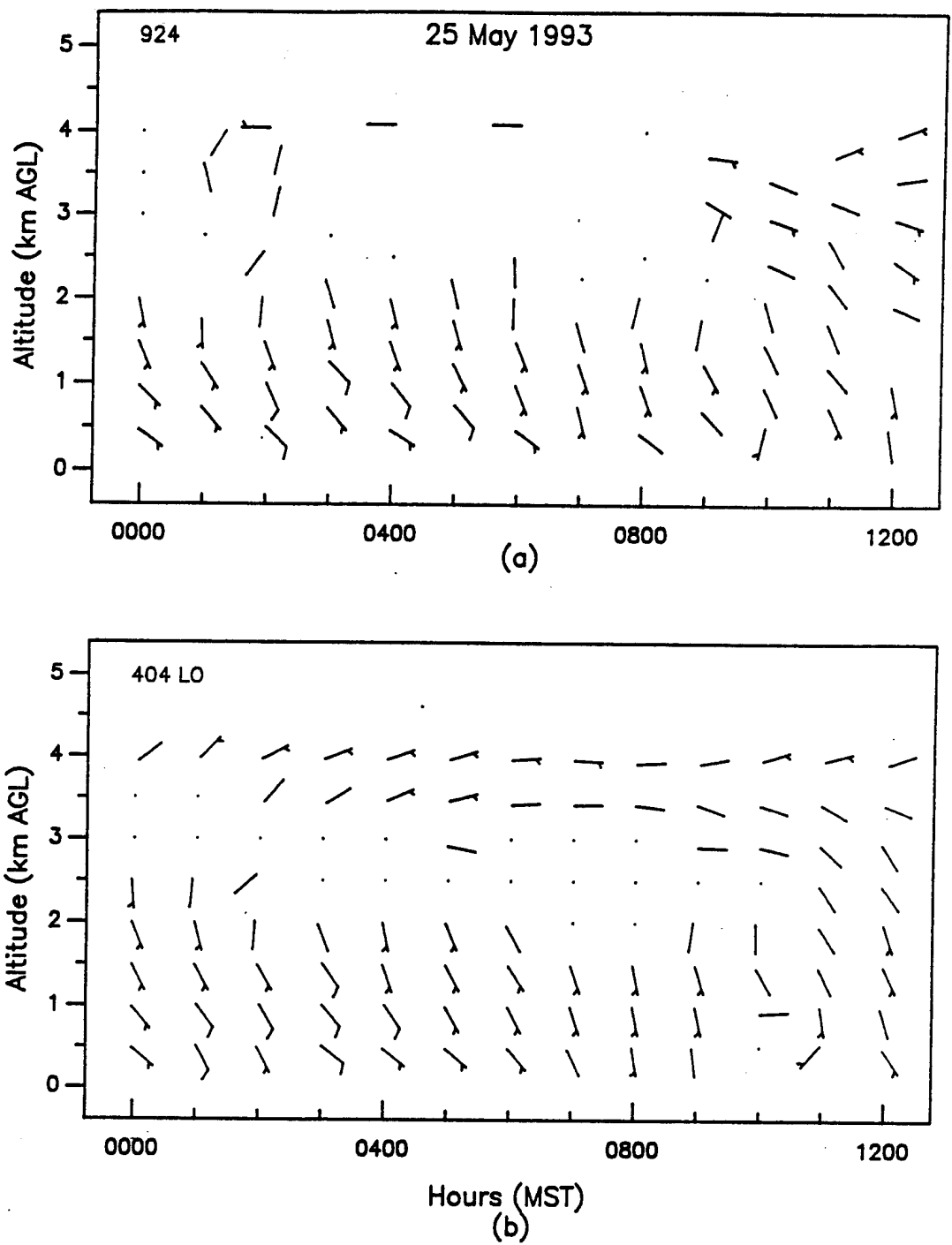


**Figure 38. Hourly average vertical profiles of wind speed and wind direction, as measured with the (a) 924- and (b) 404- (low mode) MHz profilers, APRF complex, WSMR, 0000 to 1200 MST, 25 May 93.**

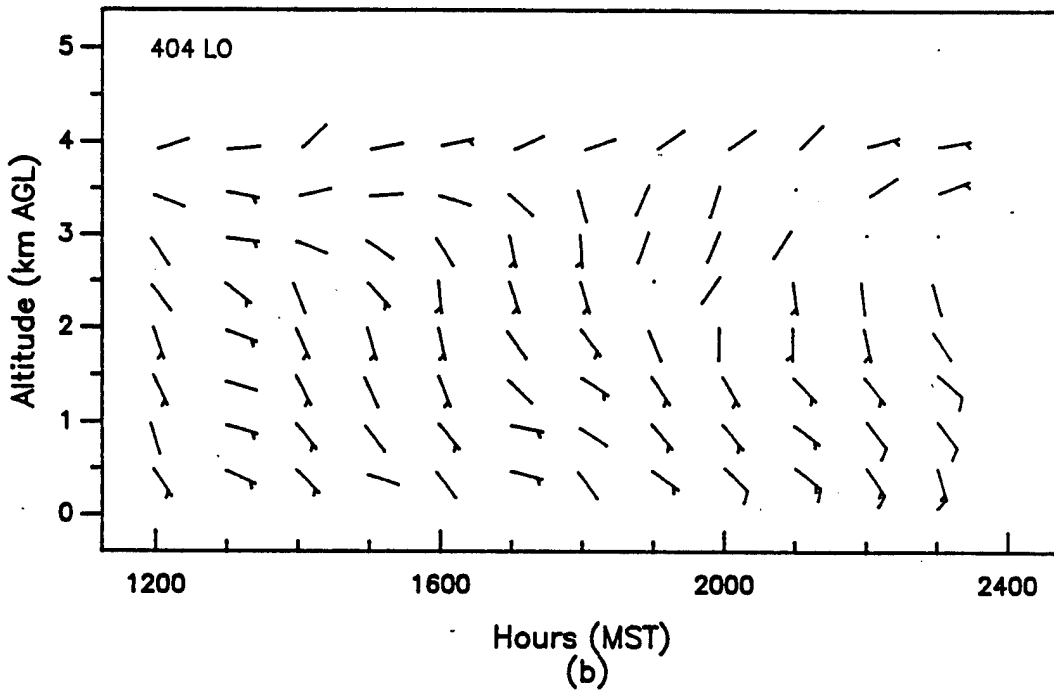
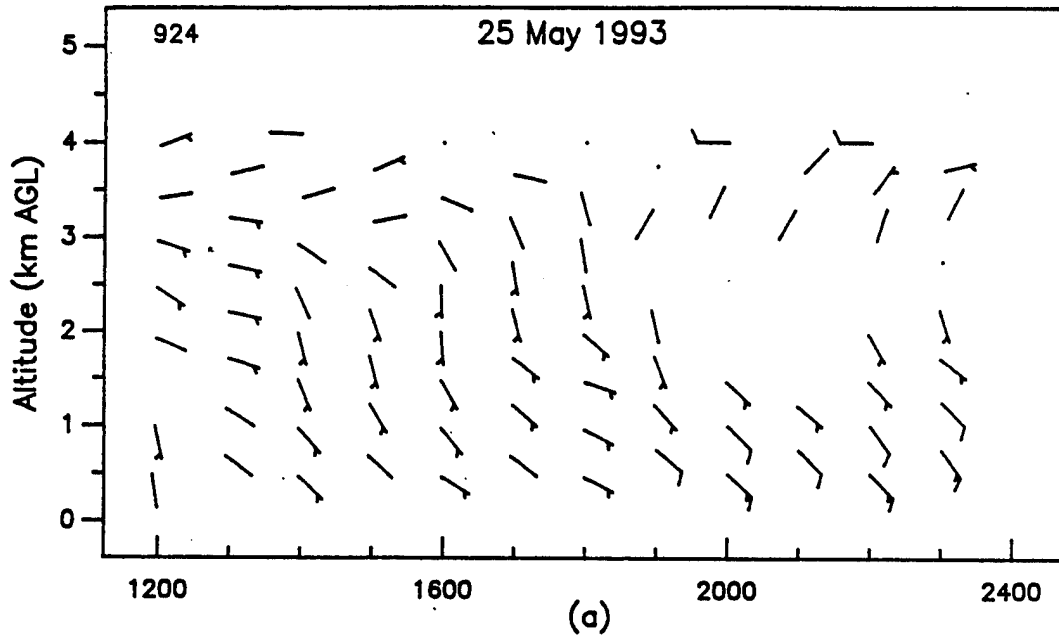


**Figure 39. Hourly average vertical profiles of wind speed and wind direction, as measured with the (a) 924- and (b) 404- (low mode) MHz profilers, APRF complex, WSMR, 1200 to 2400 MST, 25 May 93.**

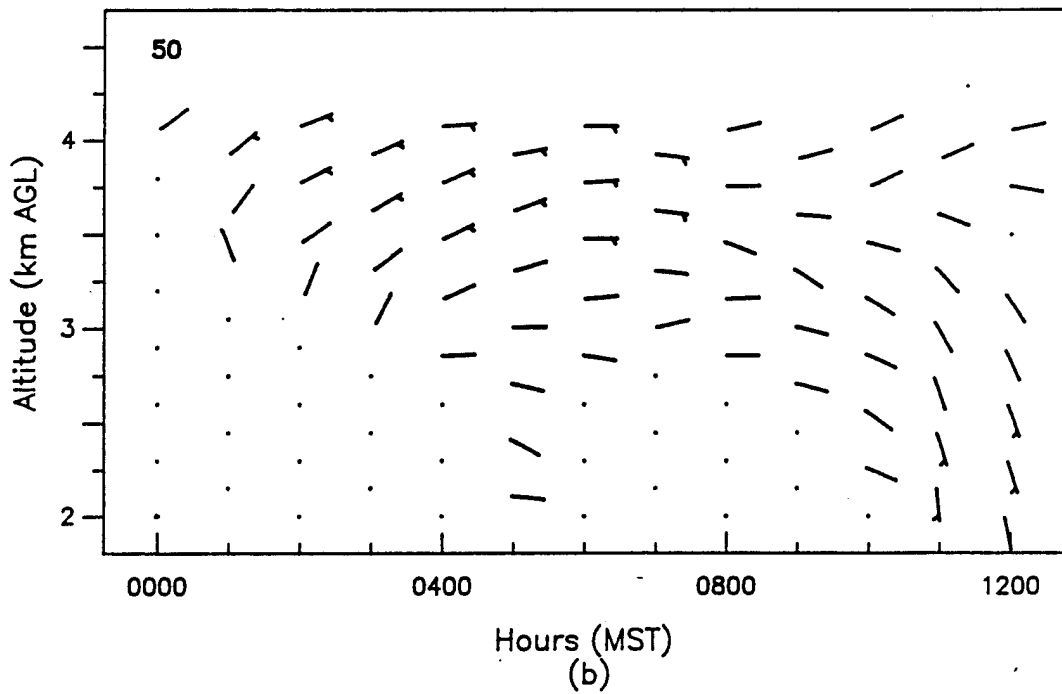
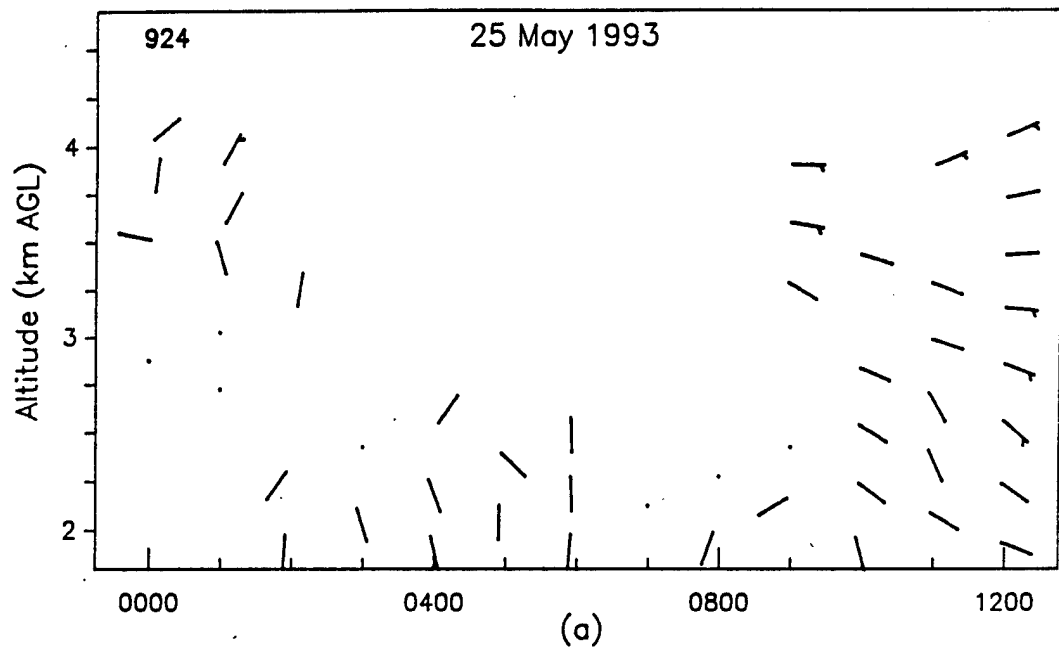


**Figure 40. Hourly average vertical profiles of wind speed and wind direction, as measured with the (a) 924- and (b) 50-MHz profilers, APRF complex, WSMR, 0000 to 1200 MST, 25 May 93.**

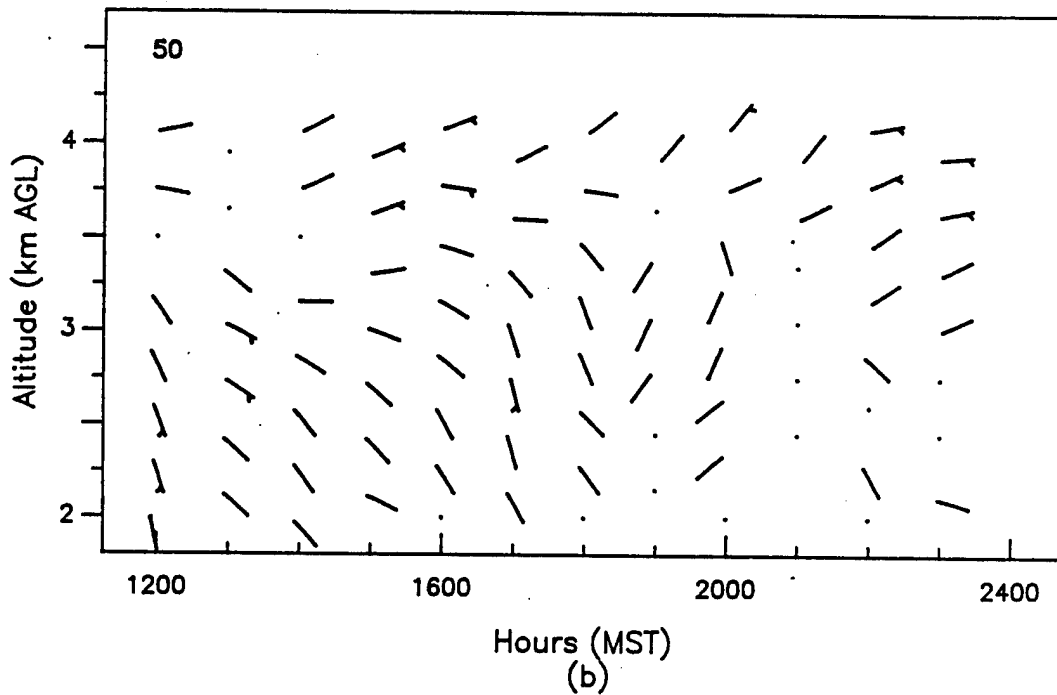
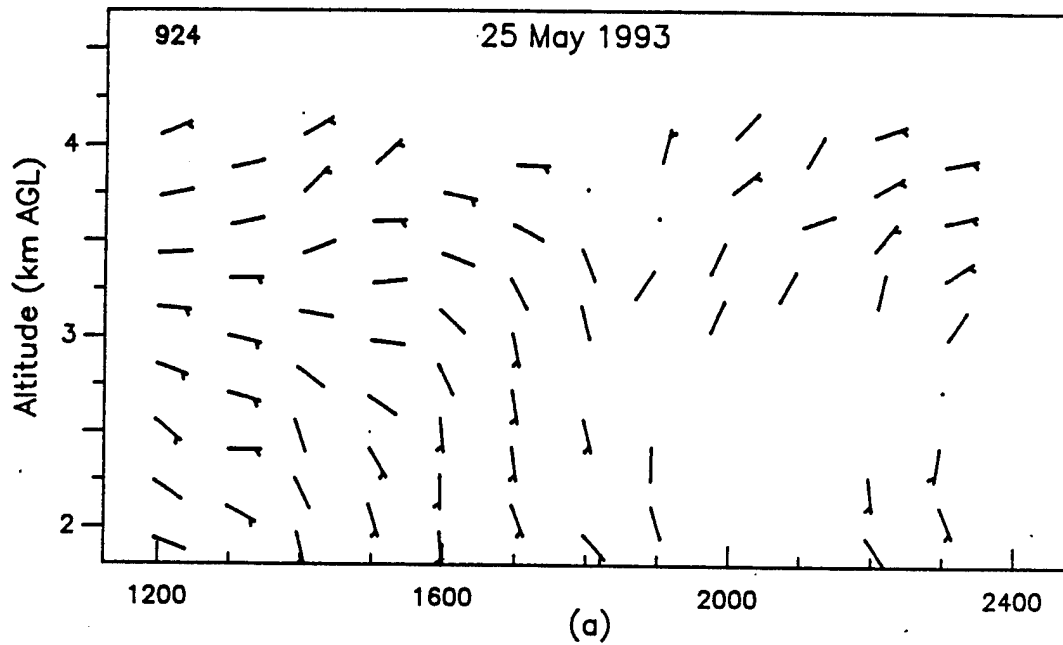


**Figure 41. Hourly average vertical profiles of wind speed and wind direction, as measured with the (a) 924- and (b) 50-MHz profilers, APRF complex, WSMR, 1200 to 2400 MST, 25 May 93.**

### 3.5.2 Statistics

The assessment of the relative accuracies of the wind data from the 50- and 404-MHz systems is based on the Pearson product-moment (correlation) coefficient, the root MSE the bias, and the F-test. In the simpler case of the temperature data (section 4.0) in which there are no individual components to be resolved, as in the case for winds, one could reasonably expect a linear correlation between profiler temperature data and radiosonde temperature data. Regression statistics were obtained for comparisons of each profiler with individual radiosonde flights, as well as for the composite of all flights. The test for the significance of the regression is obtained from the analysis of variance (ANOVA) table from which an F-statistic is calculated. Similarly, wind speed statistics were obtained for individual days and the composite of all days, although only the variances among the profilers in the altitudes at which overlapping measurements were available were studied. The statistics were computed using the Statistical Analysis Software (SAS) commercial statistics package.

The Pearson product-moment (correlation) coefficient ( $\rho$ ), is expressed as

$$\rho = \frac{\sum_1^n (x_{50} - \bar{x}_{50})(x_{404} - \bar{x}_{404})}{(n - 1) \sqrt{\sum_1^n (x_{50} - \bar{x}_{50})^2 \sum_1^n (x_{404} - \bar{x}_{404})^2}}, \quad (1)$$

and the root MSE is expressed as

$$\text{root MSE} = \sqrt{\left( \frac{\sum_1^n [(x_{50} - x_{404}) - B]^2}{n - p} \right)}, \quad (2)$$

where

$n$  = number of observations

$p$  = number of parameters (in this case, 2)

$B$  = bias or expected value of the difference ( $E(x_{50} - x_{404})$ ),

$$B = E(x_{50} - x_{404}) = \frac{\sum_1^n (x_{50} - x_{404})}{n}. \quad (3)$$

The F-test probability (Prob > |F|) as

$$F = \frac{\sum_1^k N_i (\bar{x}_i - \bar{x})^2}{\sum_1^k (N_i - 1) S_i^2} \quad (4)$$

where

$S_i^2$  = variance of group i about its mean.

In this case, we only have two groups the 50 and 404 MHz.

$$S^2 = \frac{\sum_1^n (x_i - \bar{x})^2}{n-1}. \quad (5)$$

The Pearson product-moment (correlation) coefficient and F-test are discussed in more detail in sections 3.5.2.1 and 3.5.2.2.

**3.5.2.1 Correlation Coefficient.**—To investigate linear relationships or offsets between the profilers, the SAS package was used to compute the Pearson product-moment (correlation) coefficient  $\rho$  for each of the five days and a composite of the five days. Figures 42 through 45 show scatter diagrams of the composite five-day intercomparisons. Standard least squares regression was used rather than the median of least squares regression, because significance tests indicated that parametric statistics were appropriate.

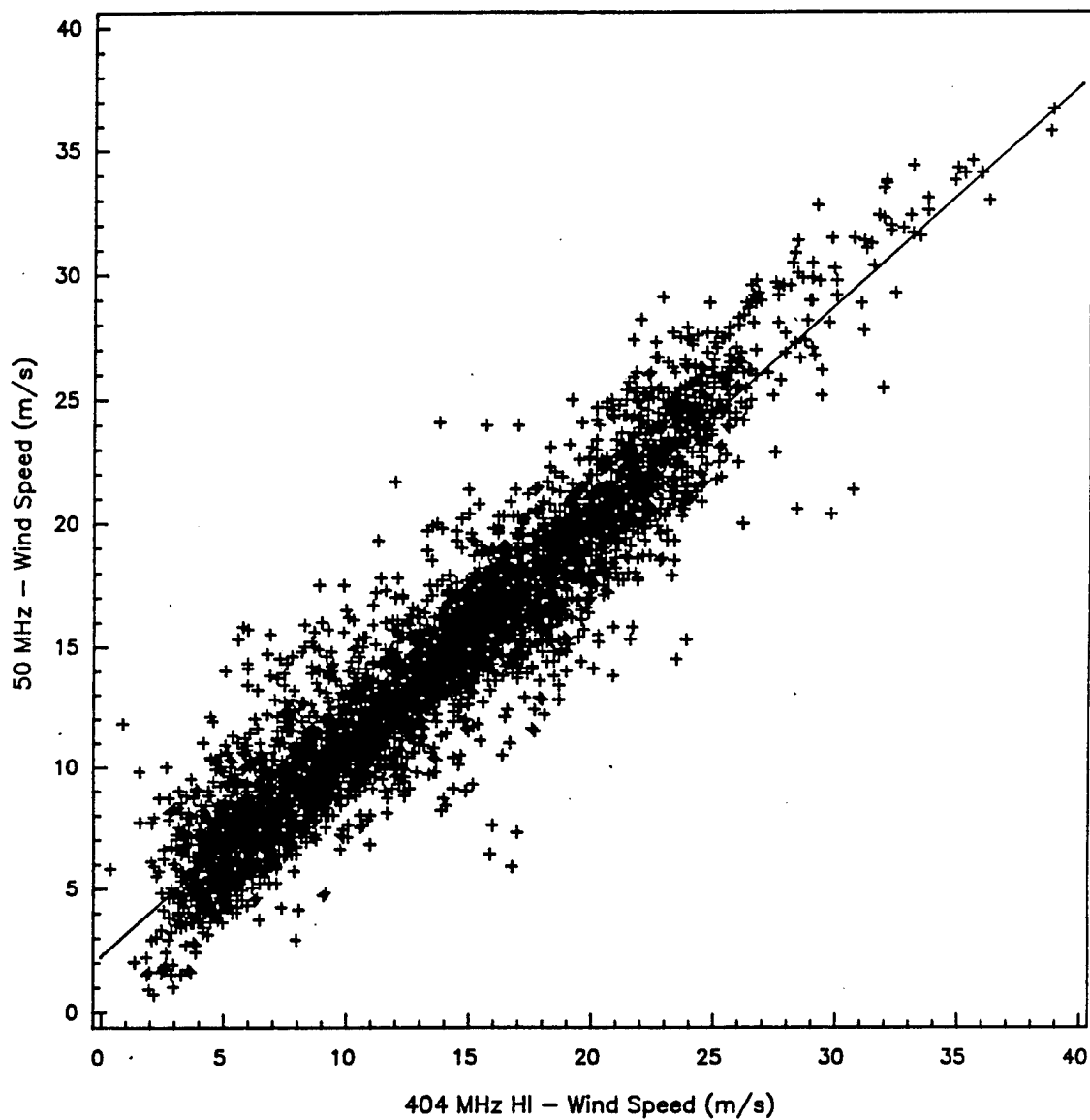


**Figure 42. Composite scatter diagram of the horizontal wind speed estimated from the 50- and 404- (high mode) MHz data from the APRF complex, WSMR, 7 Mar, 16, 17, 21, and 25 May 93.**

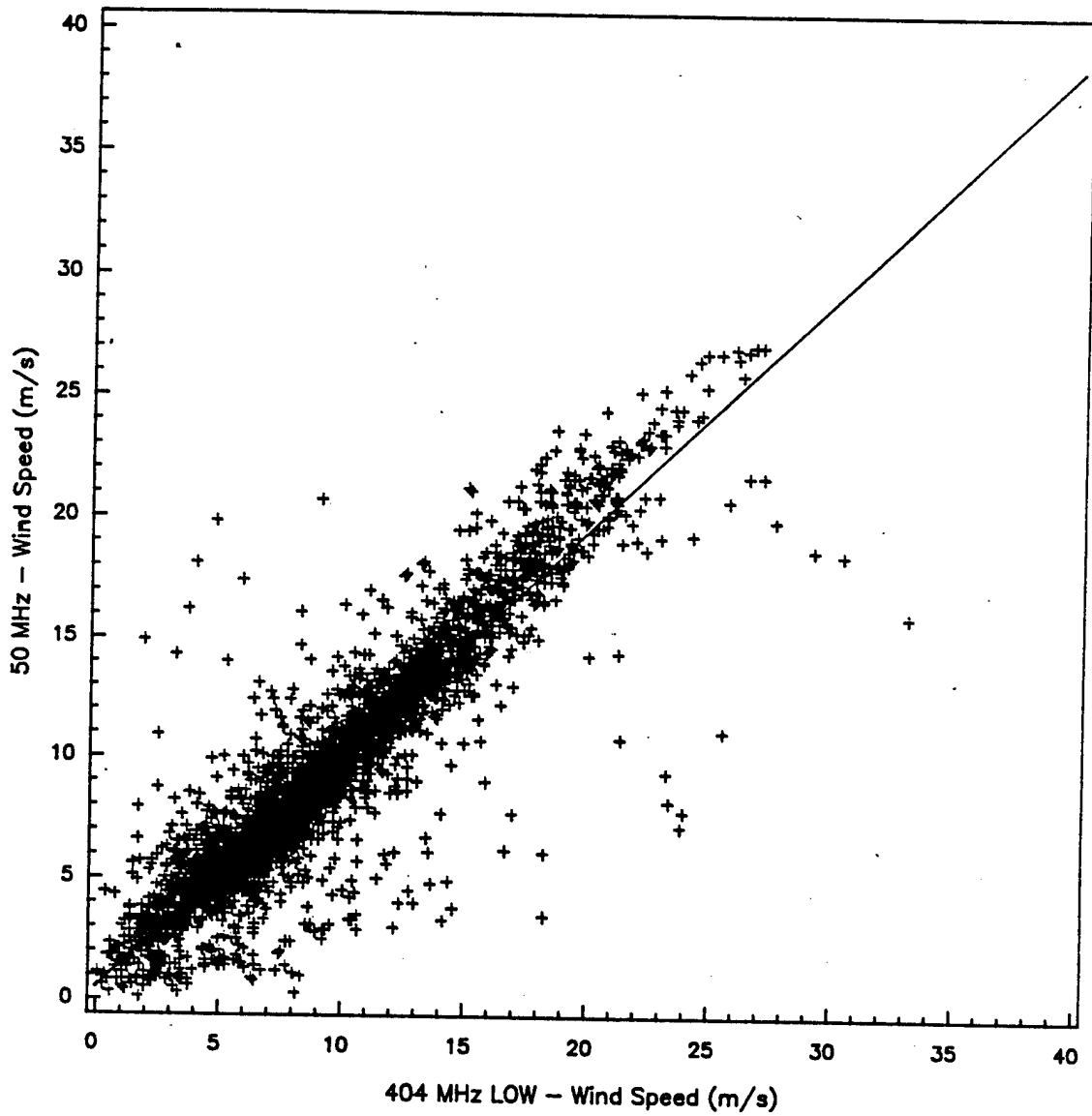


**Figure 43. Composite scatter diagram of the horizontal wind speed estimated from the 50- and 404- (low mode) MHz data from the APRF complex, WSMR, 7 Mar, 16, 17, 21, and 25 May 93.**

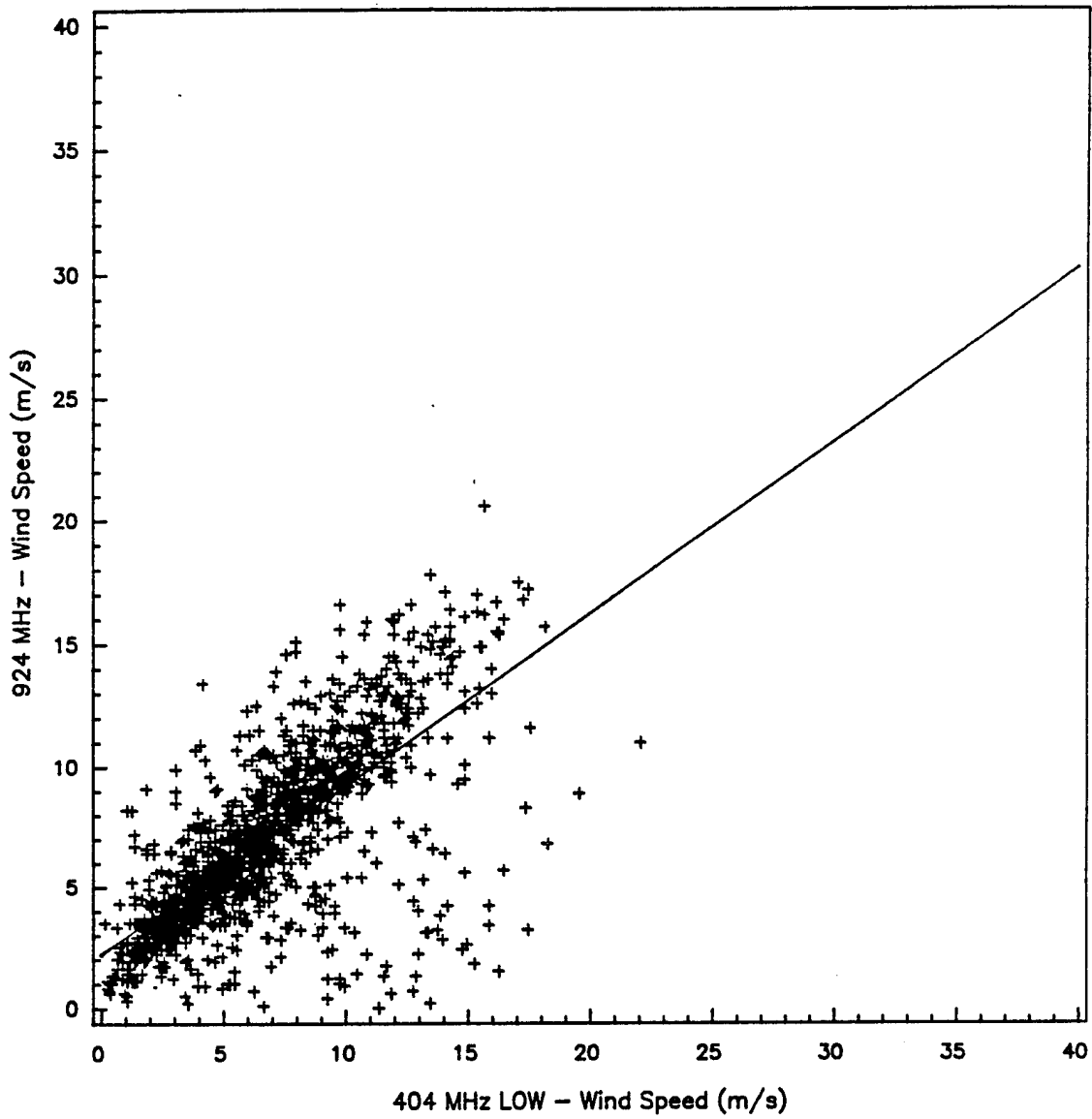


**Figure 44. Composite scatter diagram of the horizontal wind speed estimated from the 924- and 404- (low mode) MHz data from the APRF complex, WSMR, 16, 17, 21, and 25 May 93.**

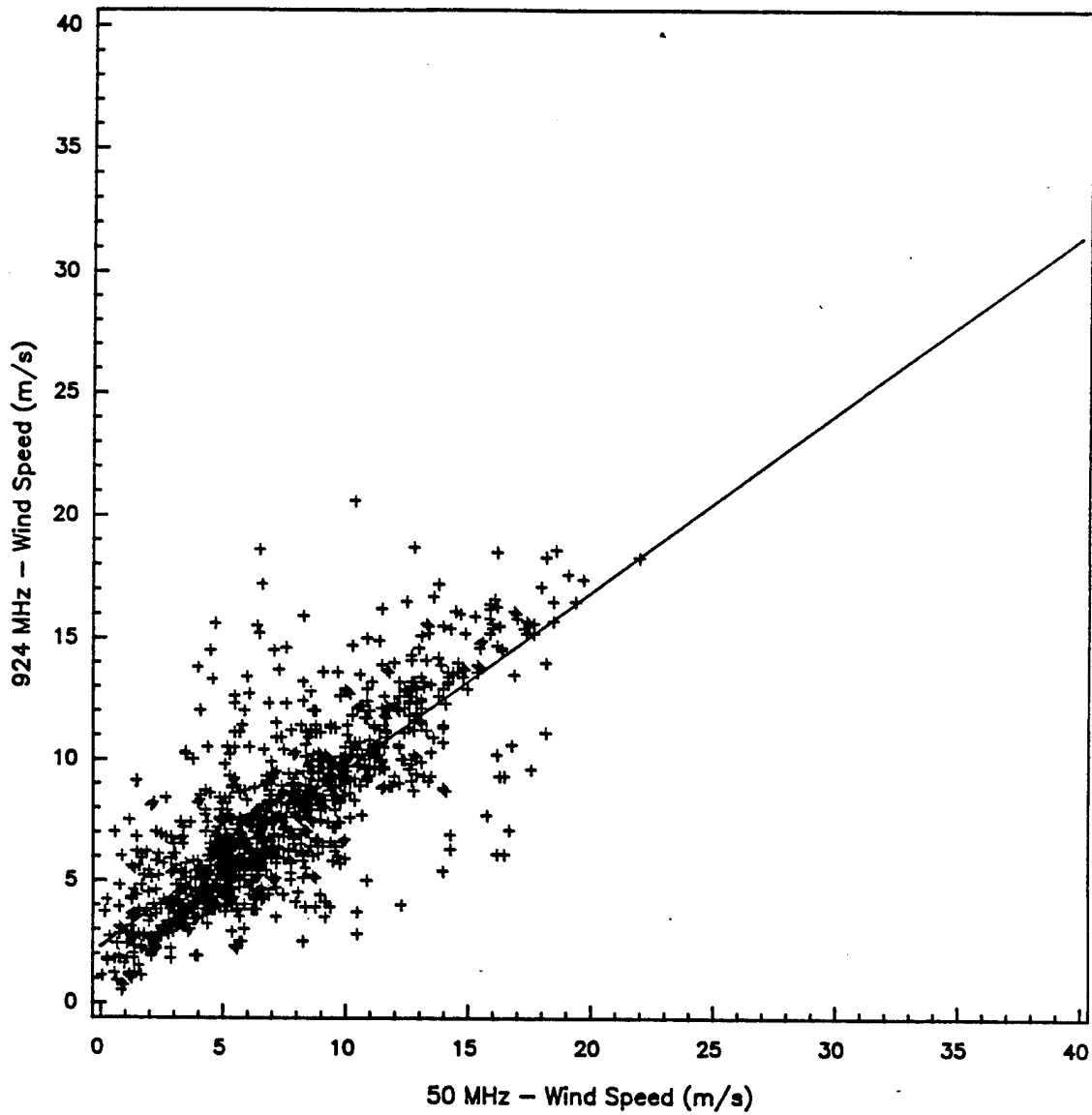


**Figure 45. Composite scatter diagram of the horizontal wind speed estimated from the 924- and 50-MHz data from the APRF complex, WSMR, 16, 17, 21, and 25 May 93.**

3.5.2.2 *F-test.*—The basic question is whether a significant difference exists between the wind speed variances measured over approximately equal time intervals and height ranges by the 50- and 404-MHz profilers. The F-test is used to compare the U and V component variances and the resultant wind speed variances of the 50- and 404-MHz profilers.

The significance level of the F-statistic is the probability of obtaining an F-statistic at least as large as the one computed if the population variances were equal. Refer to any standard text for further discussion of this statistic; it suffices to say that it is the ratio of the sum of squares between instruments to the sum of squares within instruments, each divided by its corresponding degrees of freedom.

The smaller the significance value, the greater the probability that the variances from the two systems are not equal.

Tables 6 through 9 list the statistical comparisons of the U and V components and the resultant speed. Tables 10 through 13 list the corresponding composite statistics.

**Table 6. Statistical comparisons of the 50- and 404- (high mode) MHz wind speeds, APRF complex, WSMR, 1993**

Statistic	7 Mar	16 May	17 May	21 May	25 May
$\rho$ : U	0.89	0.93	0.90	0.86	0.95
$\rho$ : V	0.93	0.92	0.92	0.92	0.93
$\rho$ : S	0.95	0.91	0.90	0.87	0.74
root MSE	1.78	2.07	1.98	1.89	1.52
$E[x_{50} - x_{404}]$	0.16	0.79	0.10	1.07	1.30
95% C. I.	0.03	0.63	-0.04	0.92	1.18
	0.29	0.95	0.23	1.21	1.41
Prob >   F   :U	0.0001	0.0001	0.0001	0.0001	0.0001
Prob >   F   : V	0.0001	0.0001	0.0001	0.0001	0.0001
Prob >   F   : S	0.0001	0.0001	0.0001	0.0001	0.0001

**Table 7. Statistical comparisons of the 50- and 404- (low mode) MHz wind speeds, APRF complex, WSMR, 1993**

Statistic	7 Mar	16 May	17 May	21 May	25 May
$\rho: U$	0.78	0.89	0.92	0.75	0.91
$\rho: V$	0.88	0.87	0.95	0.89	0.89
$\rho: S$	0.87	0.89	0.93	0.81	0.77
root MSE	1.63	1.95	2.20	2.14	1.50
$E[x_{50} - x_{404}]$	0.03	0.10	0.46	0.12	-0.48
95% C. I.	-0.13	-0.04	0.28	-0.05	-0.60
	0.19	0.25	0.64	0.30	-0.36
Prob >  F  : U	0.0001	0.0001	0.0001	0.0001	0.0001
Prob >  F  : V	0.0001	0.0001	0.0001	0.0001	0.0001
Prob >  F  : S	0.0001	0.0001	0.0001	0.0001	0.0001

**Table 8. Statistical comparisons of the 404- (low mode) and 924-MHz wind speeds, APRF complex, WSMR, 1993**

Statistic	16 May	17 May	21 May	May 25
$\rho: U$	0.62	-0.18	0.84	0.53
$\rho: V$	0.77	0.00	0.68	0.90
$\rho: S$	0.63	-0.24	0.71	0.87
root MSE	2.99	3.39	2.08	1.49
$E[x_{404} - x_{924}]$	0.14	-1.46	0.70	0.22
95% C. I.	-0.22	-2.49	0.46	0.05
	0.51	-0.43	0.93	0.40
Prob >  F  : U	0.0001	0.0760	0.0001	0.0001
Prob >  F  : V	0.0001	0.9877	0.0001	0.0001
Prob >  F  : S	0.0001	0.0163	0.0001	0.0001

**Table 9. Statistical comparisons of the 50- and 924-MHz wind speeds, APRF complex, WSMR, 1993**

Statistic	16 May	17 May	21 May	May 25
$\rho: U$	0.58	0.79	0.77	0.81
$\rho: V$	0.57	0.85	0.67	0.74
$\rho: S$	0.48	0.79	0.70	0.62
root MSE	2.88	2.22	1.39	1.39
$E[x_{50} - x_{924}]$	0.27	-0.31	0.30	1.18
95% C. I.	-0.17	-0.58	0.13	0.99
	0.70	-0.05	0.47	1.38
Prob >   F   : U	0.0001	0.0001	0.0001	0.0001
Prob >   F   : V	0.0001	0.0001	0.0001	0.0001
Prob >   F   : S	0.0001	0.0001	0.0001	0.0001

**Table 10. Composite statistical summary of the 50- and 404- (high mode) MHz wind profiler wind speed comparison, APRF complex, WSMR, 7 Mar, 16, 17, 21, and 25 May 93**

Statistic	Composite
$\rho: U$	0.96
$\rho: V$	0.97
$\rho: S$	0.95
root MSE	1.92
$E[x_{50} - x_{404}]$	0.69
95% C. I.	0.63
	0.75
Prob >   F   : U	0.0001
Prob >   F   : V	0.0001
Prob >   F   : S	0.0001

**Table 11. Composite statistical summary of the 50- and 404- (low mode) MHz wind profiler wind speed comparison, APRF complex, WSMR, 7 Mar, 16, 17, 21, and 25 May 93**

Statistic	Composite
$\rho: U$	0.96
$\rho: V$	0.96
$\rho: S$	0.92
root MSE	2.02
$E[x_{50} - x_{404}]$	0.03
95% C. I.	-0.04
	0.10
Prob >   F   : U	0.0001
Prob >   F   : V	0.0001
Prob >   F   : S	0.0001

**Table 12. Composite statistical summary of the 404- (low mode) and 924-MHz wind profiler wind speed comparison, APRF complex, WSMR, 16, 17, 21, and 25 May 93**

Statistic	Composite
$\rho: U$	0.77
$\rho: V$	0.72
$\rho: S$	0.66
root MSE	2.64
$E[x_{404} - x_{924}]$	0.18
95% C. I.	0.00
	0.36
Prob >   F   : U	0.0001
Prob >   F   : V	0.0001
Prob >   F   : S	0.0001

**Table 13. Composite statistical summary of the 50- and 924-MHz wind profiler wind speed comparison, APRF complex, WSMR, 16, 17, 21, and 25 May 93**

Statistic	Composite
$\rho: U$	0.90
$\rho: V$	0.84
$\rho: S$	0.80
root MSE	2.19
$E[x_{50} - x_{924}]$	0.31
95% C. I.	0.16
	0.45
Prob >   F   : U	0.0001
Prob >   F   : V	0.0001
Prob >   F   : S	0.0001

### 3.6 Meteorological Conditions

The discussion of the meteorological conditions is divided into three paragraphs for each of the five days. The first paragraph summarizes the pattern of winds aloft over the western United States and is based on the circulation at the 500-mbar pressure height level ( $\cong$  4600 m AGL) at 0500 MST as depicted in the Daily Weather Map series published by the Climate Analysis Center in Washington, DC.

The second paragraph presents a summary of the surface weather conditions over southern New Mexico at 0500 MST as shown in the aforementioned Daily Weather Map series.

The third paragraph summarizes the meteorological conditions in the vicinity of the APRF complex and were extracted from the surface weather observations taken at "C" Station, a site located approximately 7 km south of the APRF complex. The observations are generally taken only between 0400 and 1900 MST. No precipitation was recorded at "C" Station during the five days.

### **3.6.1 7 Mar 93**

A high-pressure ridge over the Pacific coast states and a trough of low pressure over the Mississippi River valley resulted in light to moderate northwesterly flow over south-central New Mexico.

Boundary layer flow over southern New Mexico was dominated by high pressure. The closest frontal activity was a cold/stationary front extending from Minnesota westward to the Pacific Ocean.

At the APRF complex, skies were clear throughout the day, surface winds ranged from calm to light and variable, and dewpoints generally were in the midteens. The maximum temperature was 75 °F, and the minimum temperature was 30 °F.

### **3.6.2 16 May 93**

At the 500-mbar level ( $\cong$  4600 m AGL), at 0500 MST, a weak ridge line extended from the Big Bend area of Texas to the Washington/Idaho area. This resulted in light southwesterly flow over south-central New Mexico at that level at that time.

At the surface, a weak, low-pressure area was over extreme southeastern New Mexico. A northeast-southwest oriented trough line extended through the low. A stationary front extended from north-central Texas northwestward through Wyoming.

Skies over WSMR were partly cloudy to broken, surface winds ranged from calm to light and variable, and dewpoints ranged from the mid-40's to the mid-20's. Convective activity, possibly associated with the trough line, was observed primarily toward the northeast through south of "C" Station. Distant rain showers were observed, but no precipitation was recorded at "C" Station. The maximum temperature was 91 °F, and the minimum temperature was 64 °F.

### **3.6.3 17 May 93**

At the 500-mbar level ( $\cong$  4600 m AGL), at 0500 MST, there was a trough extending from southwestern Arizona northeastward to southwestern Colorado. This resulted in moderate southwesterly flow over south-central New Mexico at that level at that time.

At the surface, the trough line of the previous day had dissipated and the stationary front had moved slightly eastward. The result was a very weak area of low pressure over New Mexico.

The skies at WSMR were partly cloudy, surface winds were generally light and variable and dewpoints ranged from the mid-40's to the mid-20's. Convective clouds (cumulus and cumulonimbus) were in evidence toward the northeast. The maximum temperature was 91 °F, and the minimum temperature was 53 °F.

### **3.6.4 21 May 93**

At the 500-mbar level ( $\cong$  4600 m AGL), at 0500 MST, there was a ridge line extending from western New Mexico north through the Canadian border. This resulted in west-northwesterly flow over south-central New Mexico at that level at that time.

At the surface, there was a stationary front along the eastern border of New Mexico and a cold front extending from western Montana southwestward to southern California.

Skies over WSMR were partly cloudy, surface winds ranged from calm to light and variable, and dewpoints ranged from the upper 40's to the upper 30's. Cumulonimbus clouds were observed toward the north through northeast. The maximum temperature was 93 °F, and the minimum temperature was 60 °F.

### **3.6.5** *25 May 93*

At the 500-mbar level ( $\cong$  4600 m AGL), at 0500 MST, there was a weak ridge line extending from western New Mexico northwestward to southern Idaho. This resulted in a light easterly flow over south-central New Mexico at that level at that time.

At the surface, pressure gradients were weak across southern New Mexico. A stationary front extended from northern Texas northwestward to northern Utah.

At WSMR, skies were partly cloudy to broken, surface winds ranged from calm to light and variable, and dewpoints ranged from the lower 50's to the mid-30's. There was some convective activity, including midafternoon rain showers, in the vicinity of "C" Station. The maximum temperature was 88 °F, and the minimum temperature was 57 °F.

## **3.7 Discussion**

For comparison purposes, dates were chosen in this study of the APRF instrumentation when there were nearly complete data sets available.

### **3.7.1** *7 Mar 93*

The 0500 MST 500-mbar pattern showed a ridge to the west and a trough to the east of WSMR. The profiler and two available rawinsonde runs indicated that the pattern was stationary throughout the 24-h period. Above the 500-mbar level, the winds generally exhibited a more northerly component.

Except for the U component correlation coefficient between the 50- and 404- (low mode) MHz systems of 0.78,  $\rho$  ranged from 0.87 to 0.95 for the 50- and 404-MHz comparisons.

### **3.7.2 16 May 93**

A high-pressure ridge extended from the Big Bend area of Texas to the Washington/Idaho area at 0500 MST. The trough resulted in light to moderate southwesterly flow from the surface to over 16 km AGL. The direction and speed showed little change during the course of the day.

The correlation coefficients for the 50- and 404- (high mode) and 50- and 404- (low mode) MHz U and V components and resultant wind speed data ranged between 0.87 and 0.93.

### **3.7.3 17 May 93**

A low-pressure trough was to the west of WSMR at 0500 MST. The trough resulted in southwesterly flow from near the ground to over 16 km AGL. The flow was confirmed by the radar profilers and the lone rawinsonde taken at WSMR (0359 MST from the small missile range; located approximately 12 km northwest of the APRF complex). As the day progressed, the trough line moved eastward, and at 1300 MST the trough line passed over WSMR. The passage resulted in a veering of the tropospheric winds aloft from southwesterly to northwesterly.

The correlation coefficients for the 50- and 404- (high mode) and 50- and 404- (low mode) MHz U and V components and resultant wind speed data ranged between 0.90 and 0.95.

### **3.7.4 21 May 93**

The weak, high-pressure ridge extending north from New Mexico drifted slowly eastward through the course of the day, but the effect was not consistent at all levels. Above 10 km, there was a gentle backing of the wind from northwesterly to southwesterly through about 0800 MST. As the ridge line moved slowly eastward during the day, the winds aloft at the APRF complex shifted from northwesterly to southwesterly.

The correlation coefficients for the 50- and 404- (high mode) and 50- and 404- (low mode) MHz U and V components and resultant wind speed data generally were low, ranging from 0.75 to 0.92.

### **3.7.5 25 May 93**

At midnight, the vertical wind profile showed generally light winds that backed from southeasterly at the surface to northeasterly at about 6 km AGL to northerly up to about 10 km and then westerly up to 16 km AGL. As the day progressed, the layer of northeasterly flow deepened to 11.5 km AGL 24 h later.

Although the correlation coefficients for the U and V components were high for the 50- and 404- (high mode) and 50- and 404- (low mode) MHz comparisons, the corresponding resultant speed correlation coefficients were the lowest of the five-day period.

## 4. Virtual Temperature

The virtual temperature is the temperature that dry air would have if it had the same pressure and density as a given sample of moist air. Thus, the virtual temperature always exceeds the air temperature. The difference is very small in dry air, but can exceed 3 °C in very moist tropical air. For the dry conditions usually prevailing over south-central New Mexico, the difference between the virtual temperature and air temperature is usually very small.

The RASS couples acoustic sources with wind profilers to obtain vertical profiles of the virtual temperature (May et al. 1990). Virtual temperature profiles were obtained at the APRF complex with RASS systems attached to the 50-, 404-, and 924-MHz wind-profiling radars.

In the case of the RASS data, an intercomparison of virtual temperature data from the three RASS systems was not practical because the ranges of overlap were small. In the case of the 50- and 404-MHz systems, the overlap was 1500 m (4250-m 50-MHz lower limit, 5750-m 404-MHz upper limit), and in the case of 404- and 924-MHz systems, the overlap was 1100 m (500-m 404-MHz lower limit, 1600-m 924-MHz upper limit). Therefore, for the radiosonde flights (released from Oasis Site) accompanied by nearly concurrent virtual temperature data from all three RASS systems, the composite RASS vertical profile of virtual temperature was compared to the virtual temperature profile as computed from the corresponding radiosonde run.

The following expression was used to compute the virtual temperature from the radiosonde measurements of air temperature and moisture:

$$T_v = (1 + 0.61q)T_a \quad (6)$$

where

$T_v$  = virtual temperature

$T_a$  = air temperature

$q$  = specific humidity of the air

where

$$q = \frac{w}{1 + w} \quad (7)$$

where

$w$  = mixing ratio

$$w = 0.622 \frac{e}{p - e} \quad (8)$$

where

$e$  = vapor pressure

$p$  = atmospheric pressure.

The vapor pressure is computed from the Goff-Gratch formulation (List 1963).

Appendix B lists the gate information for the three RASS systems.

## 4.1 System Comments

Table 14 summarizes the characteristics and operating parameters for the three wind-profiling radars. The virtual temperature data have been corrected for vertical air motion (Martner et al. 1993).

**Table 14. RASS characteristics for the three radar profilers**

Profiler (MHz)	Acoustic Frequency (Hz)	Acoustic Power <sup>a</sup> (W)	Acoustic Beamwidth (°)
50	110	2400	60
404	900	125	18
924	2100-2183	50	8

<sup>a</sup>Total electrical input

#### **4.1.1 50-MHz Profiler**

The 50-MHz system has 64 gates. The higher the wind speed (May et al. 1989) and the dryer the atmosphere, the less data are acquired.

RASS virtual temperature data are acquired over a several-minute span at approximately ½-h intervals.

#### **4.1.2 404-MHz Profiler**

The 404-MHz system has 22 gates. Because of various technical problems beyond the scope of this report, good data are sparse above about 3250 m AGL (Hoidale et al. 1995).

RASS virtual temperature data represent 1-min averages acquired at 6-min intervals.

#### **4.1.3 924-MHz Profiler**

The 924-MHz system has 15 gates. The 924-MHz profiler reports RASS data to a maximum height of 1600 m AGL. Data from the higher range gates are often missing or discontinuous because of lower signal return.

RASS virtual temperature data represent 5-min averages acquired at ½-h intervals.

#### 4.1.4 Radiosonde

Although radiosonde data are acquired from a number of sites at WSMR, only those from Oasis Site were used in this study because that release point is the closest to the APRF complex.

The rise rate of the balloon is approximately 300 m/min. The radiosonde package reaches an altitude of 12 km AGL, the approximate upper limit of data acquisition with the 50-MHz RASS system, about 40 min after release.

#### 4.2 Availability of Data

From 30 Mar 93, when the new 924-MHz wind profiler was installed at the APRF complex, until 30 Jun 93, there were 21 radiosonde releases from the Oasis Site for which there were corresponding RASS data from all three radar profiler systems. Subsequent examination revealed that four of the radiosonde runs did not extend to the lower height of the 50-MHz data, and on two occasions no 924-MHz data were within 1 h of the radiosonde. The releases are identified in table 15.

**Table 15. Radiosonde releases from Oasis Site for which there were virtual temperature data from all three profiler systems**

Date (1993)	Radiosonde Release Times (MST)		
May 13	0803	1409	
14	0923	1323	1400
18	1345	1747	
26	0630		
27	1020		
June 3	0356		
5	0758	1335	
9	0355	1255	
10	0850	1254	
11	1258		
14	0400		
15	0359	1137	
17	0357		

### 4.3 Quality Control

The RASS data were quality controlled using the previously discussed continuity method and the control parameters shown in table 16. However, a preliminary quality control procedure was applied to the 50- and 404-MHz RASS data.

In the case of the 50-MHz RASS data, three exclusion criteria were applied:

1. The spectral power had to range between -25 and +15 dB.
2. The spectral width had to range between 0.25 and 4.0 °C (not the width at the half height, but the width at the noise floor).
3. The virtual temperatures for a given gate had to fall within a specified range of air temperatures. The range of air temperatures was based on the ensemble of radiosonde data acquired at Oasis Site from Jan 92 through Mar 93. For each gate, the differences between the absolute maximum temperature and the 15-month mean temperature and the absolute minimum temperature and the 15-month mean temperature were plotted as a function of altitude. Both curves were fit with straight lines; therefore, absolute maximum temperature was less than or equal to the value of the straight line fit at the altitude, and the minimum temperature was always greater than or equal to the value of the straight line fit at the altitude for a given altitude.

**Table 16. Control parameters for the continuity method of quality control of the RASS data**

Profiler (MHz)	dy	gd	dx(1)	dx(2)	nmin
50	2.5	30	2.25	3.25	30
404 <sup>a</sup>	2.0	20	1.25	2.25	25
924	2.0	20	2.25	1.25	5

<sup>a</sup>high and low modes

The expressions for determining the lower limit (LL) in degrees Celcius and upper limit (UL) in degrees Celcius as a function of gate height ( $z_i$ ) in meters AGL for the 50-MHz system are as follows:

$$LL_{50} = x + z_i * 0.000886 - 25.2536$$

$$UL_{50} = x + z_i * 0.000204 + 12.4086$$

where

$x$  = mean temperature ( $^{\circ}\text{C}$ ) at  $z_i$ .

Data falling outside these ranges were excluded from the data set prior to further processing.

Criteria 1 and 2 were not used in the quality control of the 404-MHz RASS data. However, criterion 3 was in the quality control of the operational data. The corresponding expressions for determining the LL and UL in degrees Celcius as a function of  $z_i$  in meters AGL are as follows:

$$LL_{404} = x + z_i * 0.000915 - 23.8876$$

$$UL_{404} = x + z_i * 0.001001 + 18.4963$$

where

$x$  = mean temperature ( $^{\circ}\text{C}$ ) at  $z_i$ .

#### **4.4 Spatial and Temporal Averaging**

For statistical comparisons of the data, the samples were temporally and spatially paired as closely as possible. It should be emphasized that the RASS and radiosonde data are not actually simultaneous. As already mentioned, the 50-MHz RASS data are averages over several minutes taken at intervals of 30 min or so, the 404-MHz RASS data are 1-min averages taken at 6-min intervals, the 924-MHz RASS data represent 5-min averages taken at 30-min intervals, and the radiosondes take about 40 min to ascend from the surface to 12 km AGL. The air temperature and moisture data are reported every 10 s as the balloon rises. The RASS data are temporally paired with the radiosonde data by selecting the averaging period that most closely overlaps the portion of the radiosonde flight pertaining to that RASS system.

Radiosonde data were matched to RASS data with respect to gate height. Radiosonde temperature readings within  $\pm 50$  m of the midpoint of any given RASS gate were paired with the RASS temperatures from that gate.

Figures 46 through 56 show vertical profiles of virtual temperature for the profilers and radiosondes.

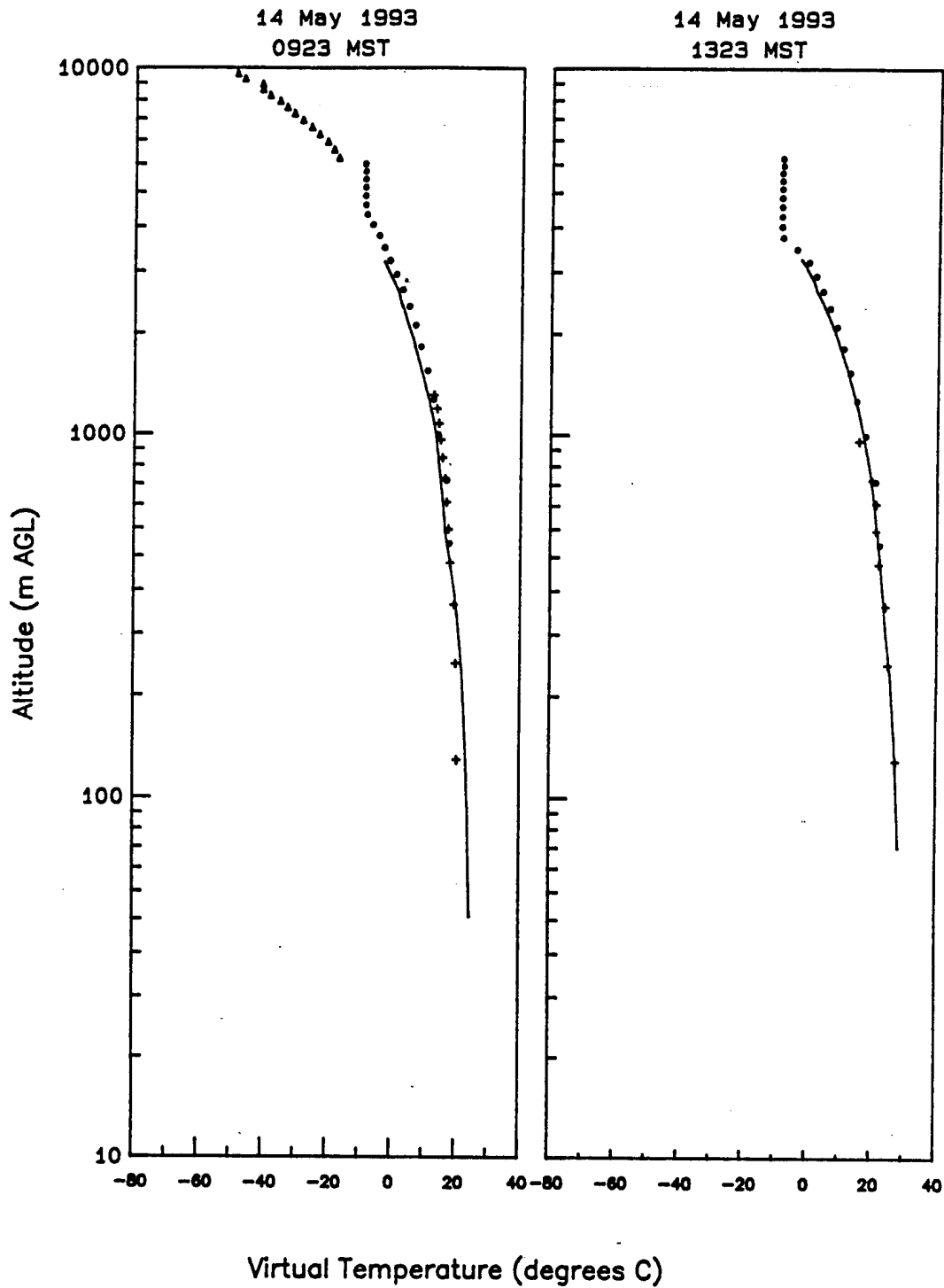
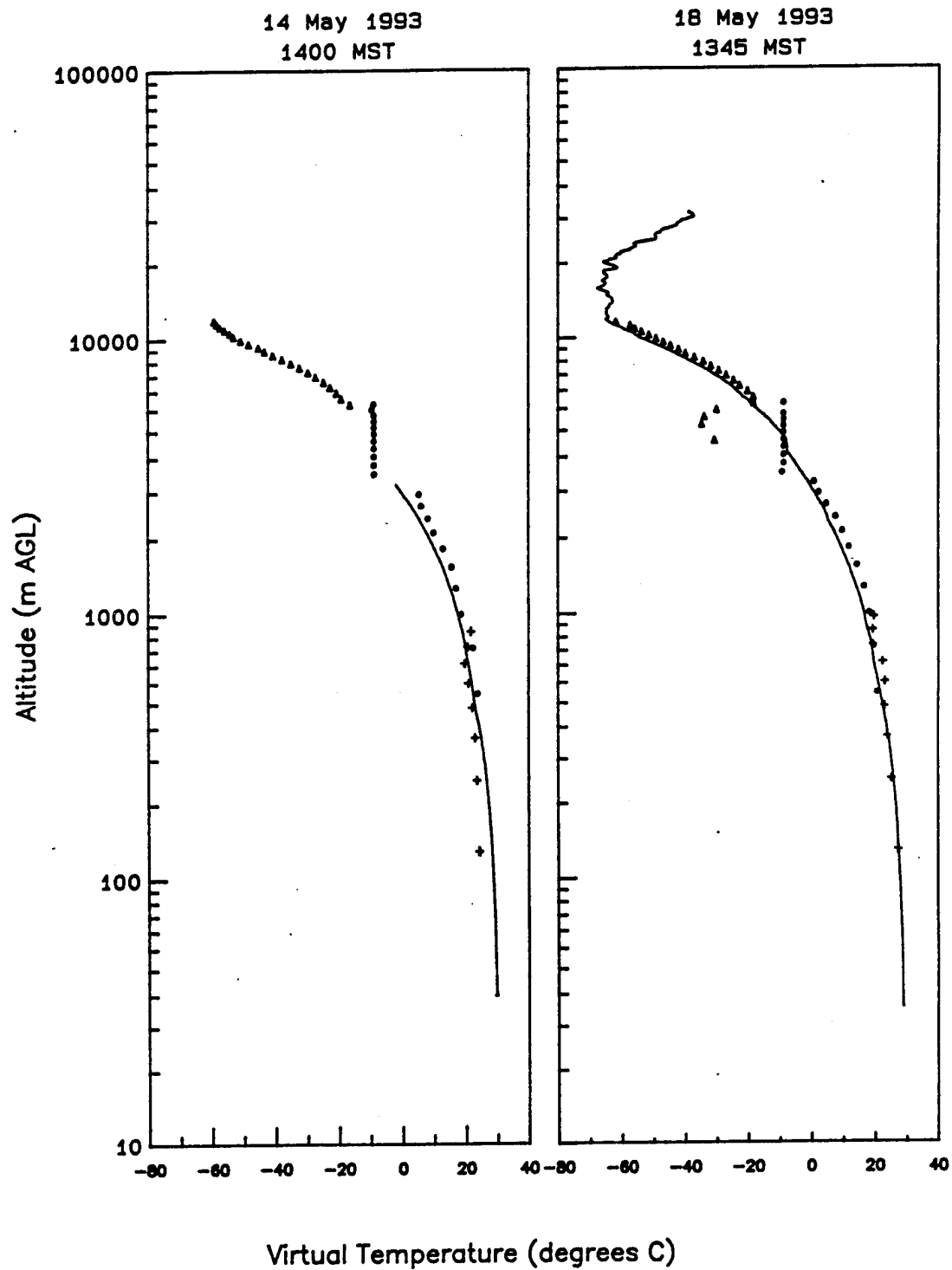
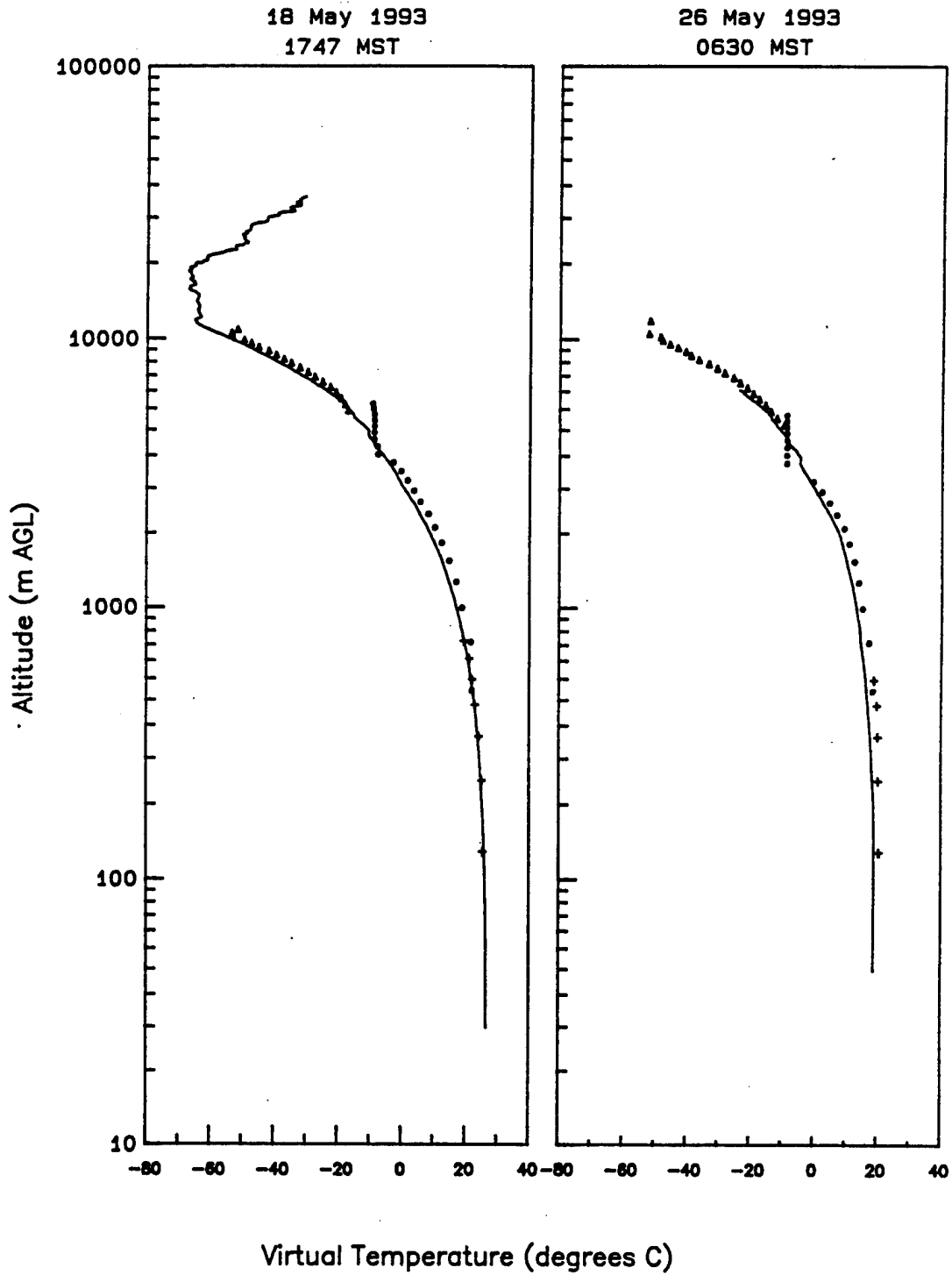


Figure 47. Virtual temperature vertical profiles computed from 924- (+), 404- (•), and 50- (▲) MHz RASS profilers, APRF complex, and radiosonde (—) data, Oasis Site, WSMR, 14 May 93.



**Figure 48. Virtual temperature vertical profiles computed from 924- (+), 404- (•), and 50- (▲) MHz RASS profilers, APRF complex, and radiosonde (—) data, Oasis Site, WSMR, 14 and 18 May 93.**



**Figure 49. Virtual temperature vertical profiles computed from 924- (+), 404- (•), and 50- (▲) MHz RASS profilers, APRF complex, and radiosonde (—) data, Oasis Site, WSMR, 18 and 26 May 93.**

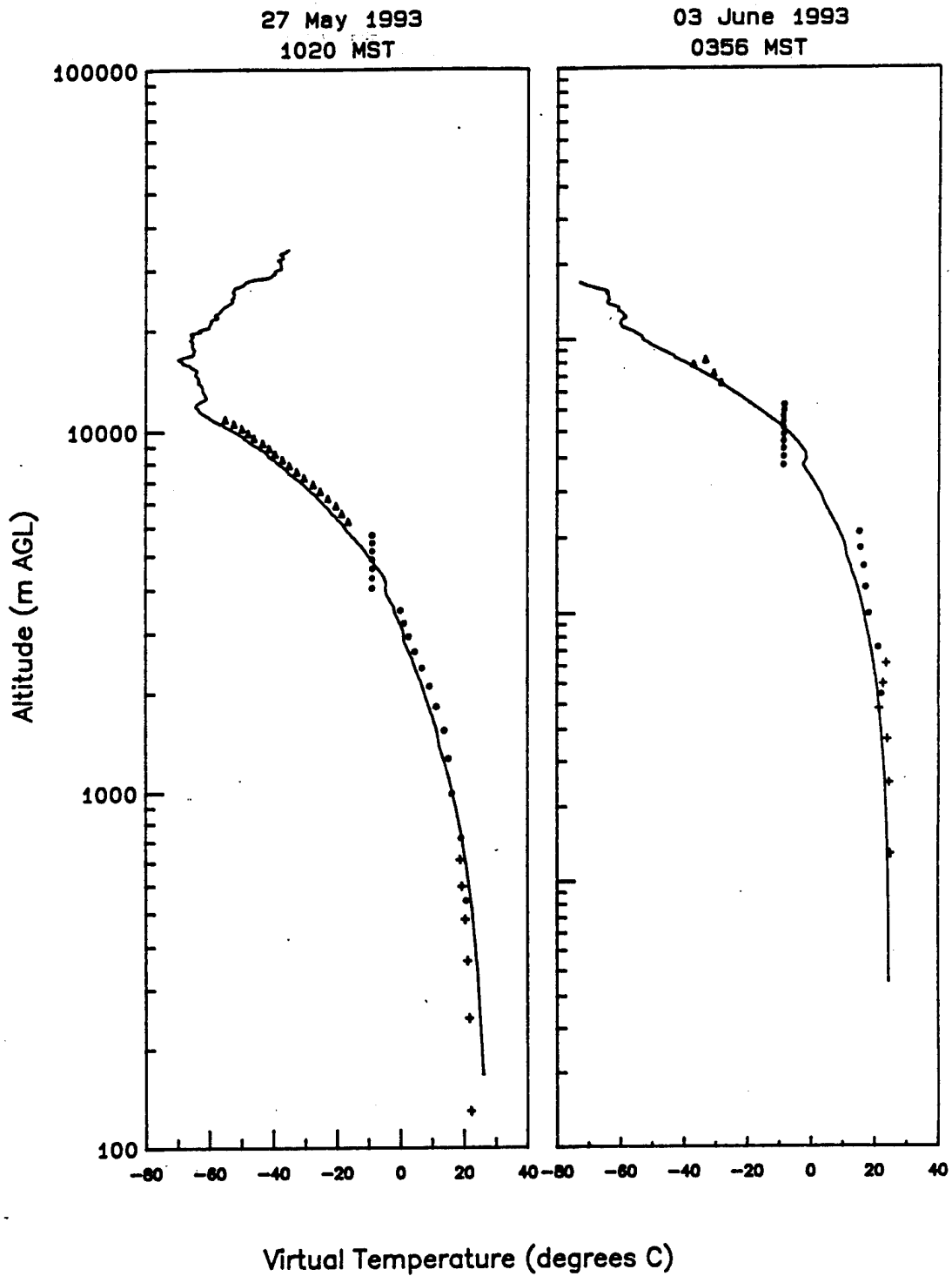


Figure 50. Virtual temperature vertical profiles computed from 924- (+), 404- (•), and 50- (▲) MHz RASS profilers, APRF complex, and radiosonde (—) data, Oasis Site, WSMR, 27 May and 3 Jun 93.

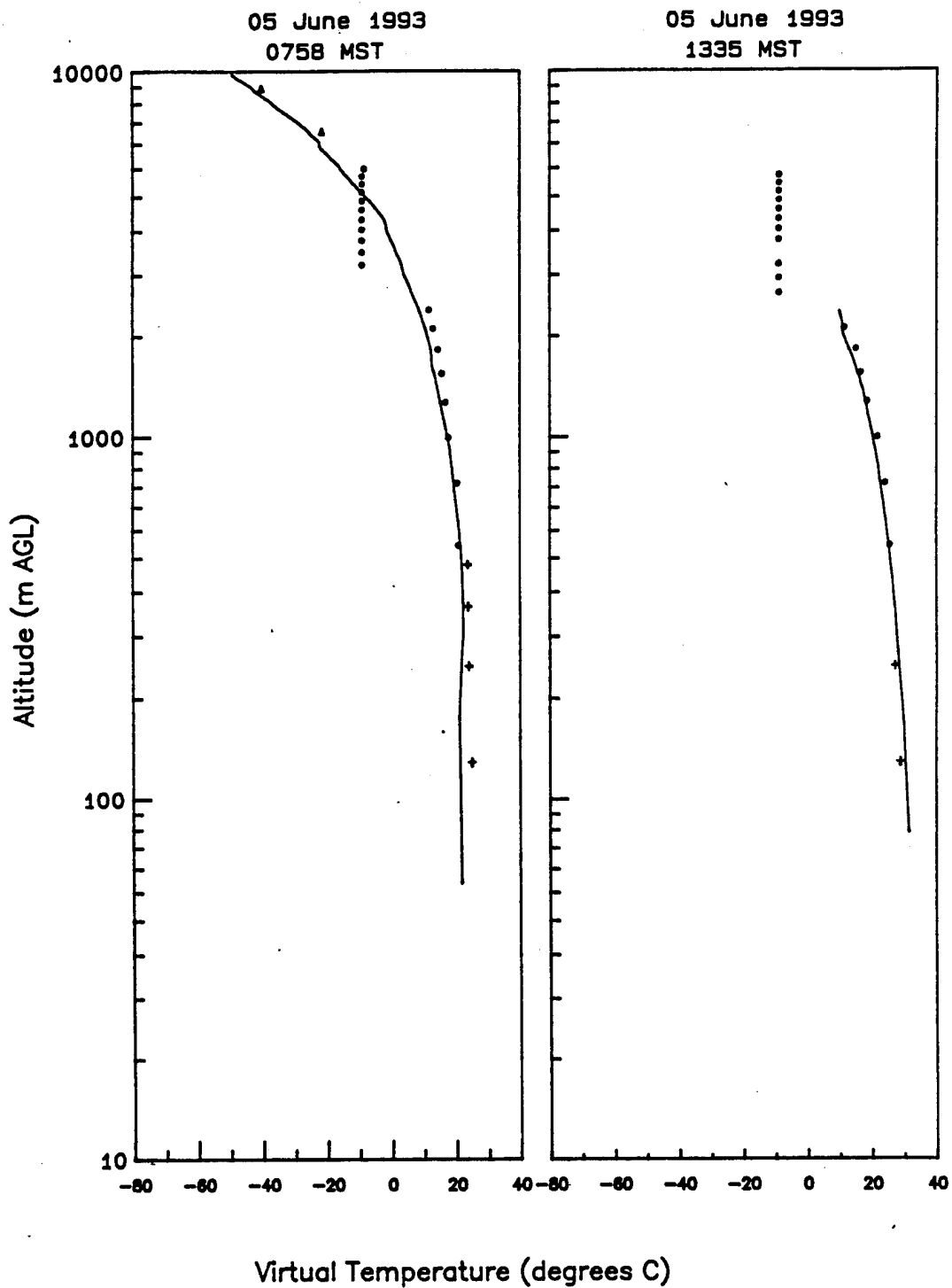


Figure 51. Virtual temperature vertical profiles computed from 924- (+), 404- (•), and 50- (▲) MHz RASS profilers, APRF complex, and radiosonde (—) data, Oasis Site, WSMR, 5 Jun 93.

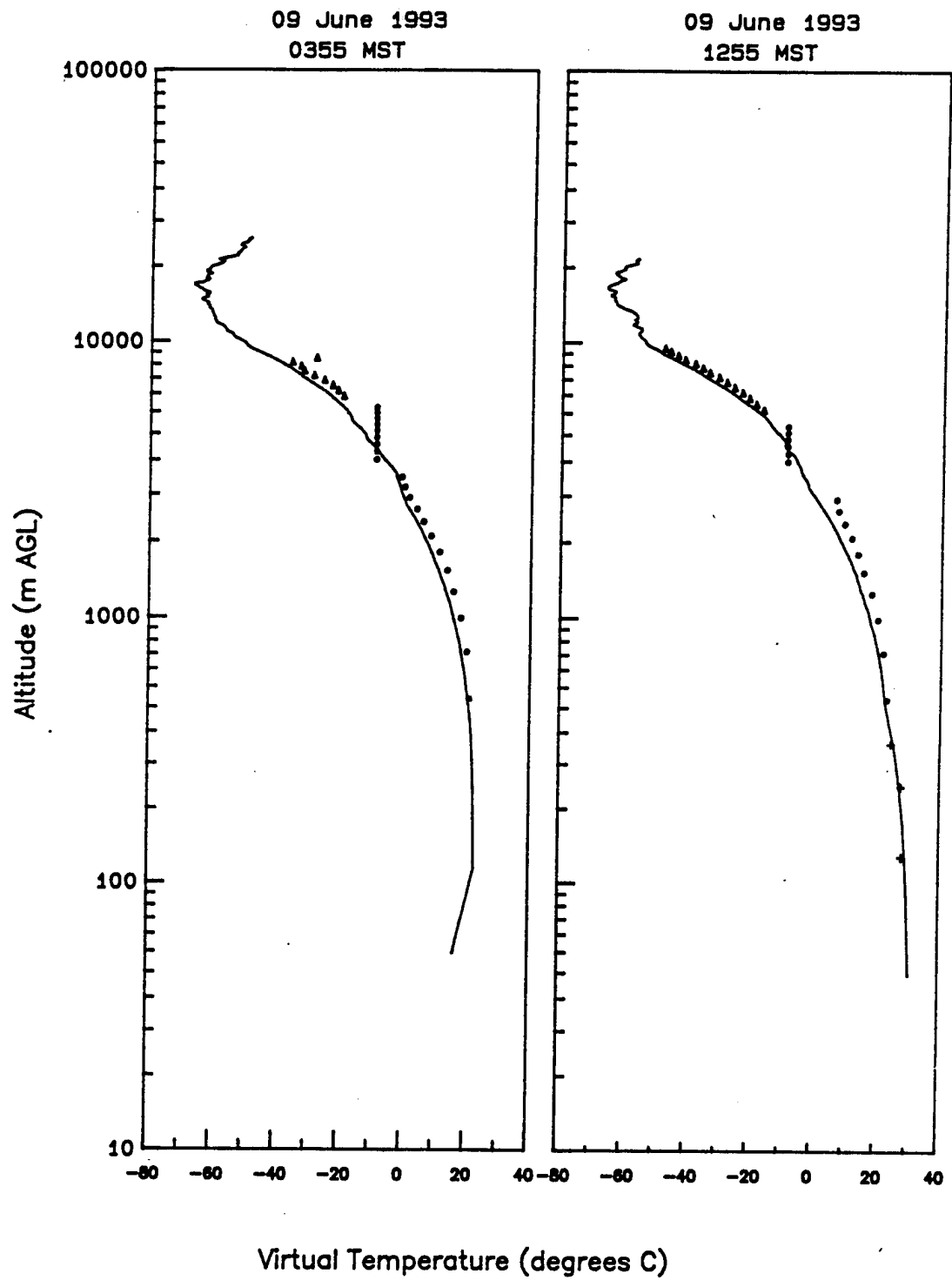


Figure 52. Virtual temperature vertical profiles computed from 924- (+), 404- (•), and 50- (▲) MHz RASS profilers, APRF complex, and radiosonde (—) data, Oasis Site, WSMR, 9 Jun 93.

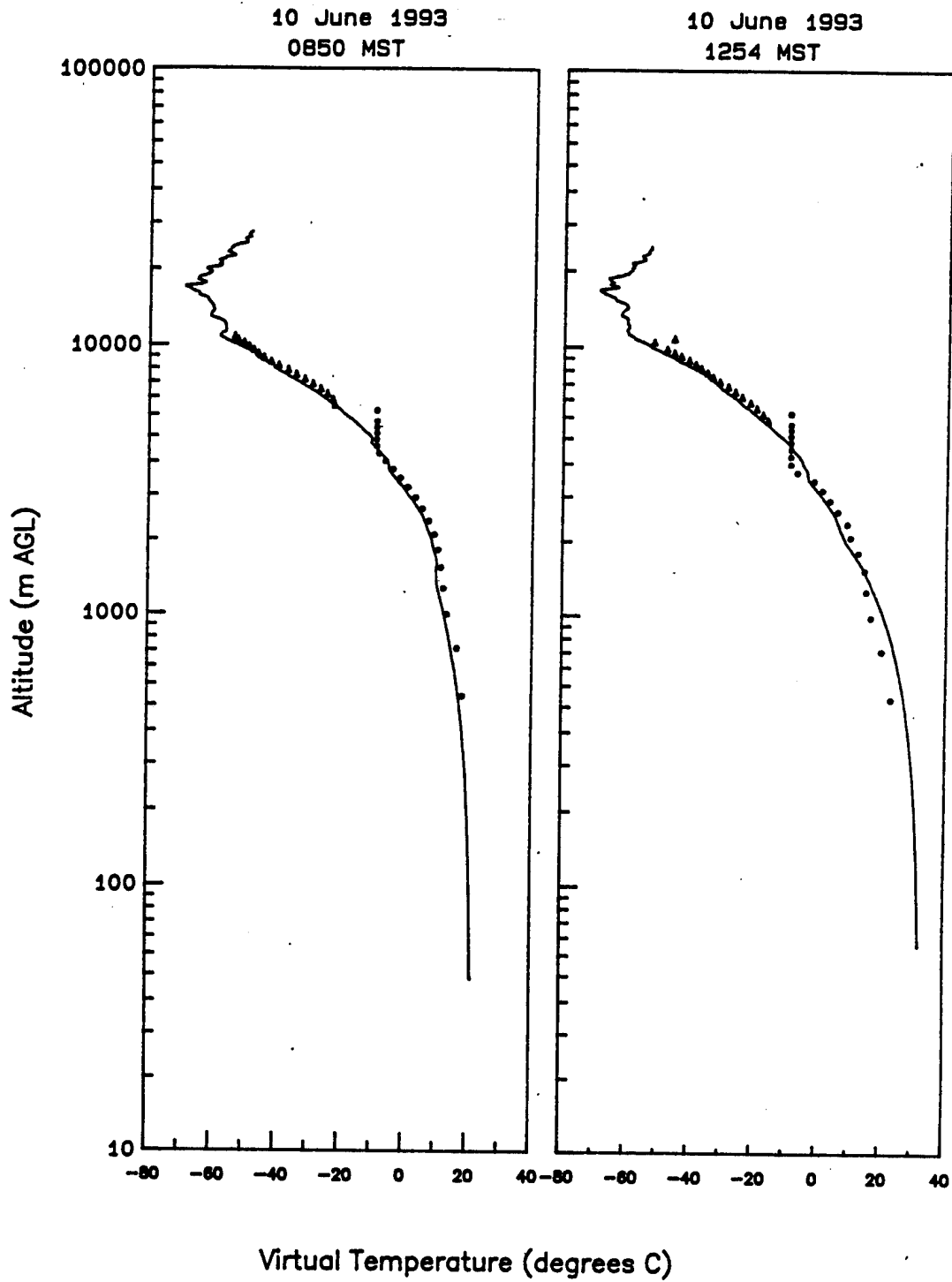


Figure 53. Virtual temperature vertical profiles computed from 924- (+), 404- (•), and 50- (▲) MHz RASS profilers, APRF complex, and radiosonde (—) data, Oasis Site, WSMR, 10 Jun 93.

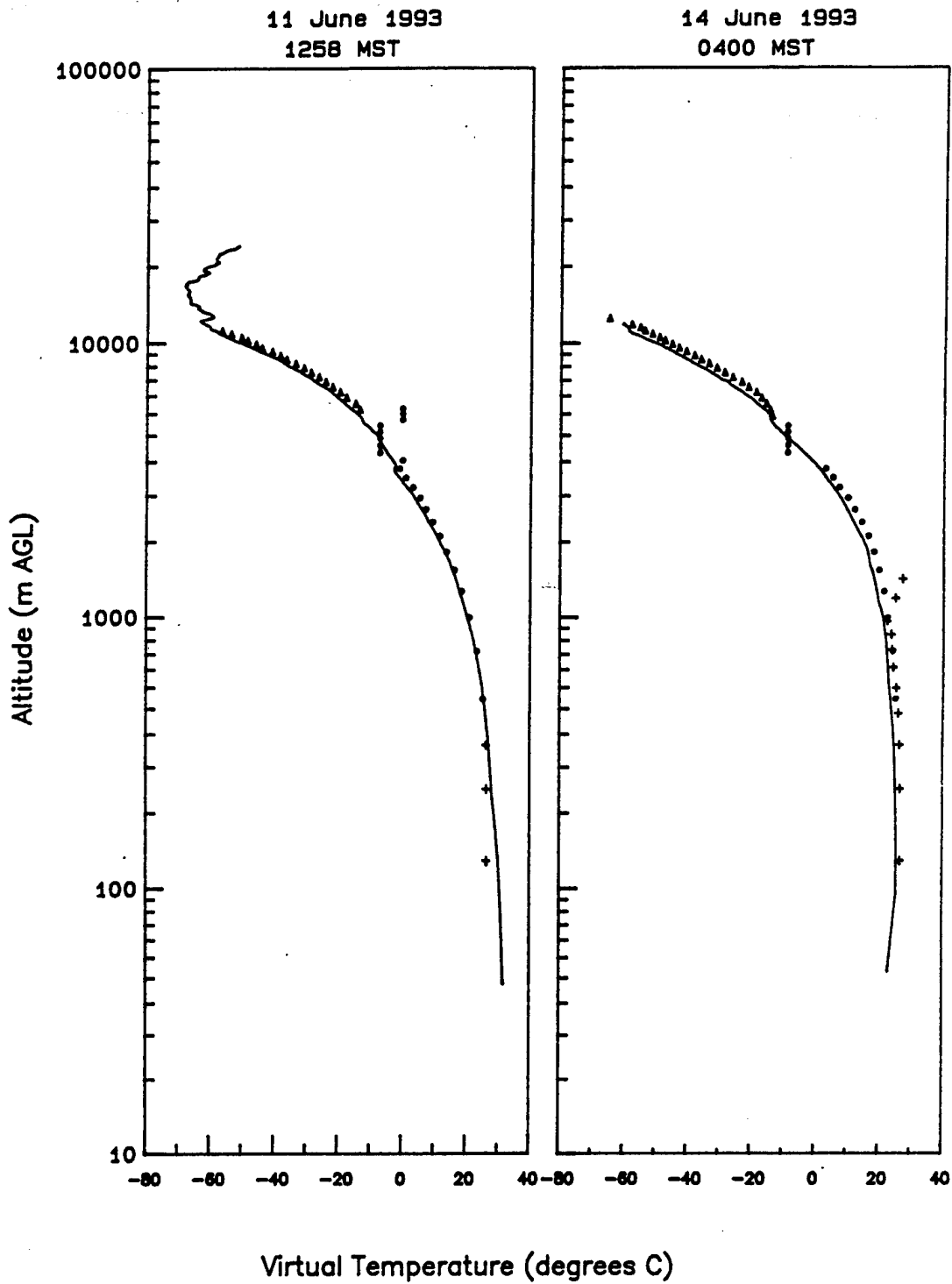
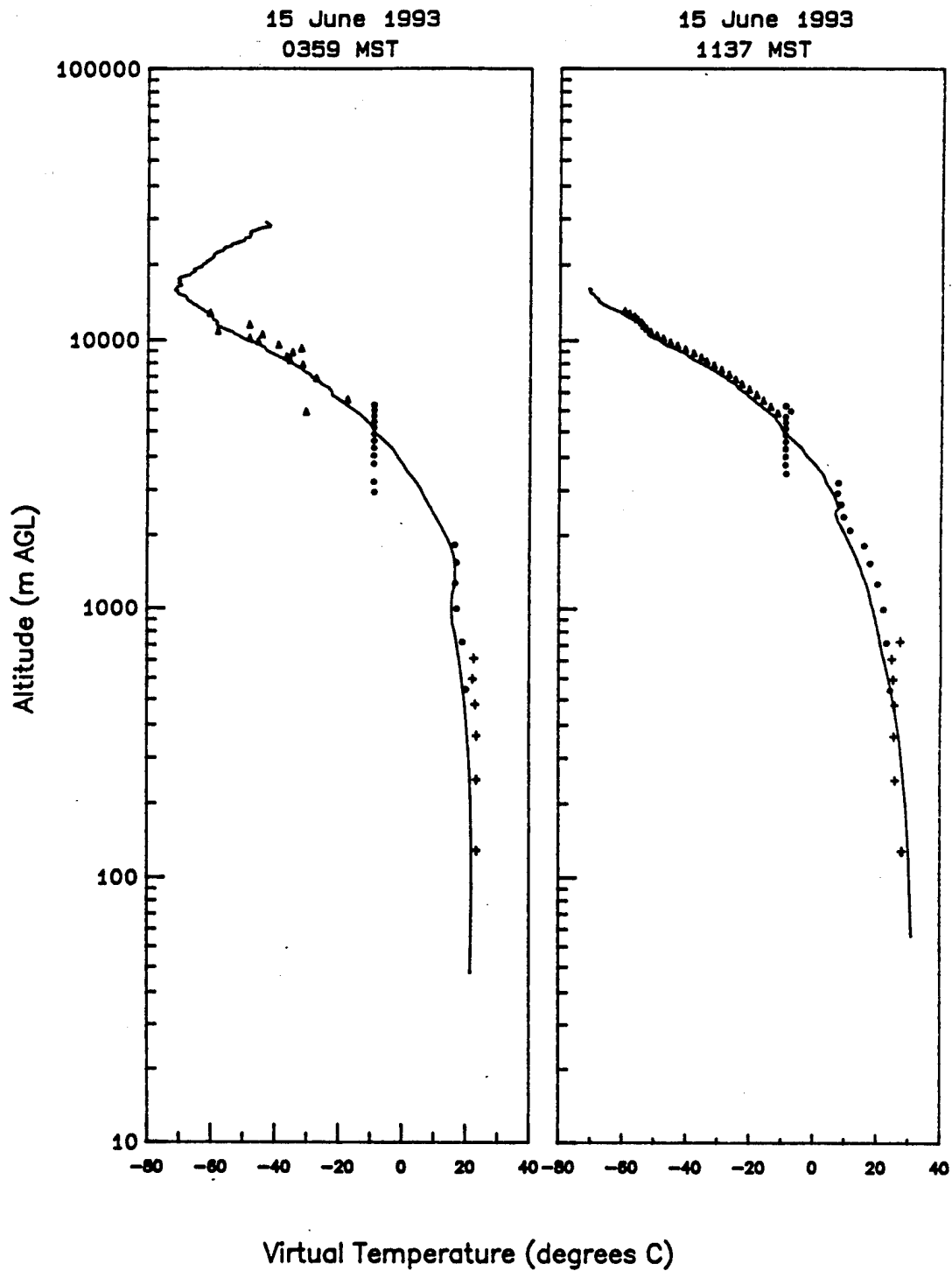
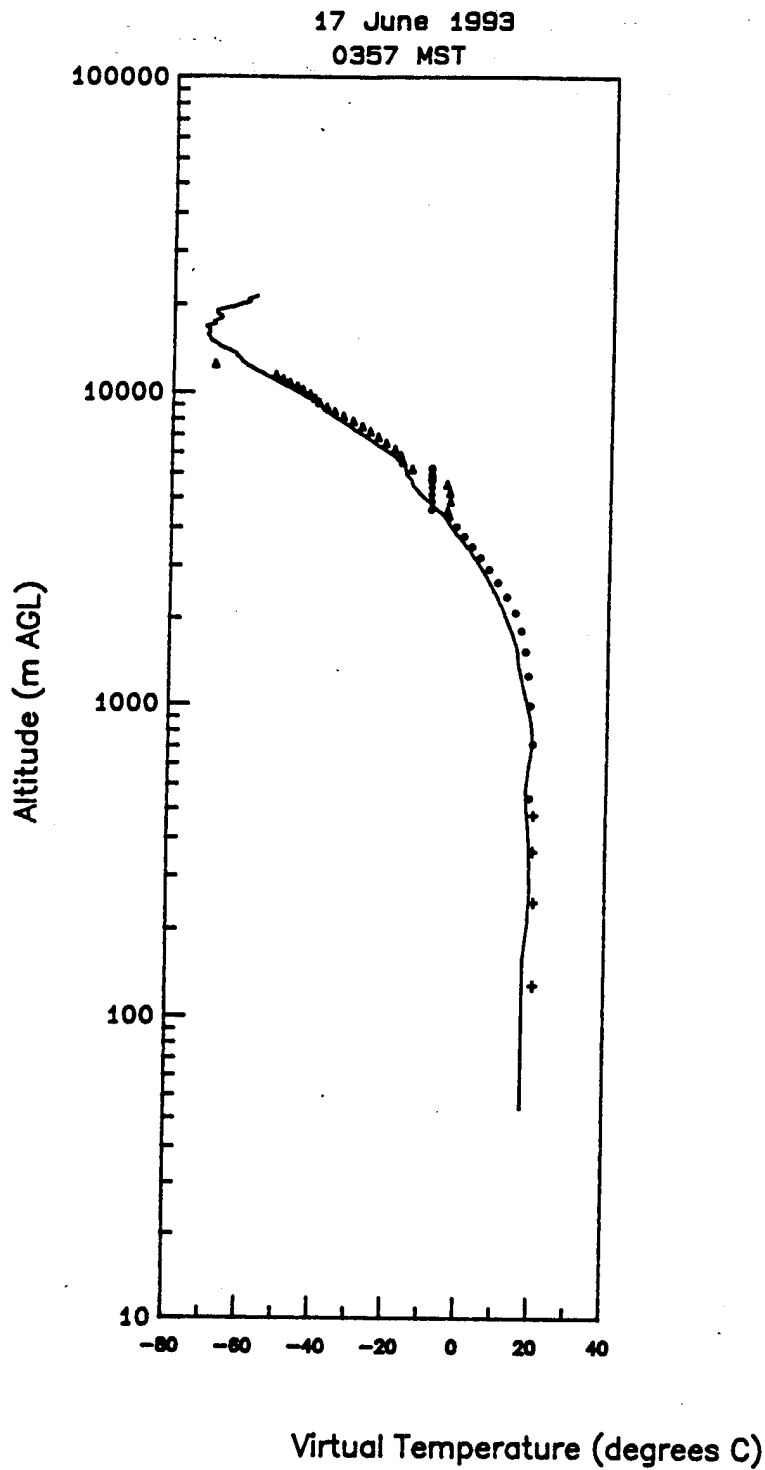


Figure 54. Virtual temperature vertical profiles computed from 924- (+), 404- (•), and 50- (▲) MHz RASS profilers, APRF complex, and radiosonde (—) data, Oasis Site, WSMR, 11 and 14 Jun 93.



**Figure 55. Virtual temperature vertical profiles computed from 924- (+), 404- (•), and 50- (▲) MHz RASS profilers, APRF complex, and radiosonde (—) data, Oasis Site, WSMR, 15 Jun 93.**



**Figure 56. Virtual temperature vertical profiles computed from 924- (+), 404- (•), and 50- (▲) MHz RASS profilers, APRF complex, and radiosonde (—) data, Oasis Site, WSMR, 17 Jun 93.**

## 4.5 Relative Accuracies

As noted in section 3.5, the measurement accuracy is limited by the atmosphere and the radar systems themselves. The term "functional precision" was coined to describe the root mean square difference between measurements made by identical instruments at as nearly as possible the same time, from as nearly as practical the same point in the atmosphere.

Implicit in the analyses of the profiler RASS data is the assumption that the RASS acoustic field is uniform across the entire vertical beam at a given height and over a specified averaging interval.

The assessment of the relative accuracies of the RASS data from the 50-, 404-, and 924-MHz systems is based on the root MSE, the Pearson product-moment (correlation) coefficient, and the F-test computed using the SAS commercial statistics package. Additionally, the classic slope and intercept parameters were determined so the intercept may be considered the temperature offset or bias between the given profiler RASS and the radiosonde system.

A linear correlation between profiler and radiosonde temperature data can be expected. In fact, a slope of nearly 1.0 for a least squares regression line, possibly with slight instrument offset or bias, can be expected. Regression statistics were obtained for comparisons of each profiler with individual radiosonde flights and the composite of all flights. The test for the significance of the regression is obtained from the ANOVA table from which an F-statistic is calculated. Table 17 shows a summary of the comparison statistics.

Appendix C provides the composite SAS statistical runs used to generate the composite portion of table 17.

**Table 17. Statistical summary of the RASS and radiosonde temperature data comparisons, APRF complex/Oasis Site, WSMR**

Date (1993)	Time (MST)	Profiler (MHz)	Root MSE	$\rho$	m	b	Prob >  F
13 May	0803	50	3.58	0.83	0.47	-16.47	0.0001
		404	1.77	0.98	0.94	2.11	0.0001
		924	0.96	0.93	1.07	1.69	0.0001
	1409	50	1.13	0.99	0.96	1.54	0.0001
		404	2.05	0.98	0.83	0.19	0.0001
		924 <sup>a</sup>	-	1.00	0.97	-1.39	-
14 May	0923	50 <sup>b</sup>	N/A	N/A	N/A	N/A	N/A
		404	0.60	1.00	1.00	1.95	0.0001
		924	0.57	0.97	0.59	6.67	0.0001
	1323	50 <sup>b</sup>	N/A	N/A	N/A	N/A	N/A
		404	0.56	1.00	0.92	0.43	0.0001
		924	0.64	0.99	1.19	-4.61	0.0015
	1400	50 <sup>b</sup>	N/A	N/A	N/A	N/A	N/A
		404	1.13	0.99	0.94	3.32	0.0001
		924	0.54	0.97	0.64	6.83	0.0003
18 May	1345	50	6.40	0.86	0.64	-14.03	0.0001
		404	2.27	0.98	0.95	1.09	0.0001
		924	0.55	0.98	0.81	3.61	0.0001
	1747	50	0.95	1.00	0.95	1.29	0.0001
		404	2.63	0.98	0.91	2.39	0.0001
		924	0.64	0.97	1.09	-2.28	0.0002
26 May	0630	50	0.05	1.00	0.95	1.29	0.0001
		404	2.59	0.97	1.05	1.39	0.0001
		924 <sup>c</sup>	0.43	0.84	0.55	10.02	0.0741
27 May	1020	50	0.61	1.00	0.99	2.69	0.0001
		404	2.46	0.89	1.00	0.86	0.0001
		924 <sup>d</sup>	0.35	0.95	0.36	11.93	0.0516
3 Jun	0356	50 <sup>e</sup>	3.53	0.90	0.96	1.72	0.0055
		404	5.35	0.93	1.07	1.11	0.0001
		924 <sup>c</sup>	0.56	-0.78	-0.42	32.92	0.1166

<sup>a</sup>n = 2 where n = sample size.

<sup>b</sup>The radiosonde data does not extend to the base of the 50-MHz data.

<sup>c</sup>n = 5 where n = sample size.

<sup>d</sup>n = 4 where n = sample size.

<sup>e</sup>n = 7 where n = sample size.

<sup>f</sup>n = 3 where n = sample size.

<sup>g</sup>There are no 924 data within one hour of radiosonde release time.

<sup>h</sup>n = 11 where n = sample size.

<sup>i</sup>n = 335 where n = sample size.

<sup>j</sup>n = 555 where n = sample size.

<sup>k</sup>n = 111 where n = sample size.

**Table 17. Statistical summary of the RASS and radiosonde temperature data comparisons, APRF complex/Oasis Site, WSMR (continued)**

Date (1993)	Time (MST)	Profiler (MHz)	Root MSE	$\rho$	m	b	Prob >  F
5 Jun	0758	50 <sup>a</sup>	N/A	1.00	0.71	-3.29	N/A
		404	5.21	0.92	1.09	-2.36	0.0001
		924 <sup>d</sup>	0.43	-0.84	-1.24	51.39	0.1581
	1335	50 <sup>b</sup>	N/A	N/A	N/A	N/A	N/A
		404 <sup>d</sup>	0.33	1.00	0.67	7.46	0.0045
		924 <sup>a</sup>	N/A	1.00	0.65	8.83	-
9 Jun	0355	50	1.90	0.94	0.91	1.65	0.0001
		404	2.76	0.97	0.87	2.78	0.0001
		924 <sup>a</sup>	-	1.00	9.00	-175.4	-
	1255	50	1.46	0.99	1.05	4.34	0.0001
		404	2.79	0.97	1.00	1.95	0.0001
		924 <sup>f</sup>	0.05	1.00	0.68	7.22	0.0194
10 Jun	0850	50	1.04	1.00	0.96	0.68	0.0001
		404	2.19	0.97	0.82	1.57	0.0001
		924 <sup>g</sup>					
	1254	50	0.66	1.00	0.96	1.06	0.0001
		404	2.88	0.96	0.74	0.74	0.0001
		924 <sup>g</sup>					
11 Jun	1258	50	1.65	0.98	0.93	-0.18	0.0001
		404	0.97	0.99	0.80	2.28	0.0001
		924 <sup>f</sup>	0.11	0.75	0.06	24.92	0.4591
14 Jun	0400	50	1.30	1.00	0.96	2.56	0.0001
		404	2.20	0.99	1.07	1.16	0.0001
		924 <sup>h</sup>	1.66	0.25	0.17	21.31	0.4613

<sup>a</sup>n = 2 where n = sample size.

<sup>b</sup>The radiosonde data does not extend to the base of the 50-MHz data.

<sup>c</sup>n = 5 where n = sample size.

<sup>d</sup>n = 4 where n = sample size.

<sup>e</sup>n = 7 where n = sample size.

<sup>f</sup>n = 3 where n = sample size.

<sup>g</sup>There are no 924 data within one hour of radiosonde release time.

<sup>h</sup>n = 11 where n = sample size.

<sup>i</sup>n = 335 where n = sample size.

<sup>j</sup>n = 555 where n = sample size.

<sup>k</sup>n = 111 where n = sample size.

**Table 17. Statistical summary of the RASS and radiosonde temperature data comparisons, APRF complex/Oasis Site, WSMR (continued)**

Date (1993)	Time (MST)	Profiler (MHz)	Root MSE	$\rho$	m	b	Prob >  F
15 Jun	0359	50	4.11	0.95	0.73	-10.43	0.0001
		404	4.92	0.94	0.98	0.53	0.0001
		924	0.25	0.99	0.76	6.76	0.0001
	1137	50	0.75	1.00	1.03	3.36	0.0001
		404	4.64	0.93	1.05	0.34	0.0001
		924 <sup>e</sup>	1.10	0.44	0.15	24.28	0.3172
17 Jun	0357	50	1.48	0.99	1.00	2.01	0.0001
		404	1.94	0.99	0.91	2.61	0.0001
		924 <sup>e</sup>	0.51	-0.07	-0.04	21.47	0.8892
		Composite	50 <sup>i</sup>	3.73	0.95	0.86	-3.34
		404 <sup>j</sup>	3.25	0.96	0.94	1.36	0.0001
		924 <sup>k</sup>	2.05	0.87	0.78	5.45	0.0001

<sup>a</sup>n = 2 where n = sample size.

<sup>b</sup>The radiosonde data does not extend to the base of the 50-MHz data.

<sup>c</sup>n = 5 where n = sample size.

<sup>d</sup>n = 4 where n = sample size.

<sup>e</sup>n = 7 where n = sample size.

<sup>f</sup>n = 3 where n = sample size.

<sup>g</sup>There are no 924 data within one hour of radiosonde release time.

<sup>h</sup>n = 11 where n = sample size.

<sup>i</sup>n = 335 where n = sample size.

<sup>j</sup>n = 555 where n = sample size.

<sup>k</sup>n = 111 where n = sample size.

#### 4.5.1 Altitude Dependence

Because there was very little vertical overlap among the three profilers, the altitude dependence becomes more of a comparison of radiosonde/profiler data as a function of the profiler.

#### 4.5.2 *Stability (Day Versus Night) Dependence*

Because of the skewed temporal distribution of the radiosonde release times (table 18) and the paucity of comparative data, there was no attempt to investigate the stability dependence.

**Table 18. Temporal distribution of 21 radiosonde releases during May and Jun 93, Oasis Site, WSMR**

0000-0600 MST	0600-1200 MST	1200-1800 MST	1800-2400 MST
5	7	9	0

#### 4.6 **Meteorological Conditions**

Section 3.6 summarizes the discussion of the meteorological conditions attending each of the 13 days. No precipitation was recorded at "C" Station during the 13 days.

##### 4.6.1 *13 May 93*

A weak, high-pressure ridge extended over the Rocky Mountains from the Canadian border to the Mexican border.

At the surface, a weak, high-pressure area was over Colorado with a ridge extending south over eastern New Mexico and west Texas.

There were scattered to broken low, middle, and high clouds throughout the daylight hours. Weak convective activity was noted in the form of cumulonimbus clouds to the north after about noon. There was no precipitation. The maximum temperature was 84 °F, and the minimum temperature was 57 °F. Dewpoints ranged from 44 °F during mid-morning to 33 °F shortly after sunset. Surface winds generally were light and variable.

#### **4.6.2 14 May 93**

A weak, high-pressure ridge extended from an apex in northern Idaho to a broad base over the Southwest.

At the surface, a weak, high-pressure area was over northwestern New Mexico and northeastern Arizona. In addition, a trough line extended from eastern South Dakota to eastern New Mexico.

There were scattered low, middle, and high clouds throughout the daylight hours. Weak convective activity in the form of cumulonimbus clouds was noted to the north beginning about noon. The maximum temperature was 88 °F, and the minimum temperature was 53 °F. Dewpoints ranged from 46 °F at 0900 MST to the mid-30's after 1400 MST. Surface winds generally were calm to light and variable.

#### **4.6.3 18 May 93**

The winds aloft were dominated by a high-pressure ridge over the Great Basin, which resulted in light to moderate northwesterly flow over southern New Mexico.

At 0500 MST, the surface weather map showed a southeast-northwest oriented cold front over south-central New Mexico. According to the surface weather observations at "C" Station, the front apparently passed "C" Station at 0312 MST.

Skies became increasingly cloudy as the day progressed with clear skies near sunrise and scattered to overcast low, middle, and high clouds near sunset. Convective activity was limited to towering cumulus clouds during mid to late afternoon and distant cumulonimbus late in the afternoon. The maximum temperature was 87 °F, and the minimum temperature was 58 °F. Dewpoints ranged from the mid-40's during the morning to the low 40's after 1300 MST. Surface winds generally were light and variable.

#### **4.6.4 26 May 93**

There was a high-pressure ridge aloft extending from the Texas Panhandle to northern Montana.

A surface high-pressure area over Missouri resulted in southeasterly flow over much of New Mexico. The surface weather map also revealed an upper north-south oriented cold front across western Arizona.

Generally, there were scattered to broken, low and high clouds throughout the sampling period. Cumulonimbus clouds were reported to the northeast beginning about 1500 MST. The maximum temperature was 89 °F, and the minimum temperature was 57 °F. Dewpoints ranged from the mid-40's during the morning to near 40 during the afternoon and early evening. Surface winds generally were from the southeast and gusting to 14 kn around noon.

#### **4.6.5 27 May 93**

A high-pressure area aloft over the southeastern United States resulted in southerly to southeasterly flow over much of New Mexico.

At the surface, a low-pressure trough extended from south-central South Dakota to the Texas Panhandle and a north-south oriented cold front through Las Vegas, NM.

Generally, there were scattered to broken, low, middle, and high clouds throughout the sampling period. Convective activity was limited to cumulonimbus clouds over the Sacramento mountains to the east. The maximum temperature was 92 °F, and the minimum temperature was 55 °F. Dewpoints ranged from the mid-40's during the morning to mid-30's during the afternoon and early evening. Surface winds ranged from calm to light and variable.

#### **4.6.6 3 Jun 93**

A low-pressure trough aloft over the Great Basin resulted in moderate westerly to southwesterly winds over New Mexico.

At the surface, there was a southeast-northwest oriented stationary front through extreme northeastern New Mexico and a northeast-southwest oriented cold front through extreme northwestern New Mexico.

The sky cover ranged from clear to scattered, high clouds. There was no convective activity, but blowing sand was reported to the north and smoke to the southeast through south during midday. The maximum temperature was 95 °F, and the minimum temperature was 65 °F. Dewpoints were variable and ranged from 29 to 18 °F. Surface winds ranged from calm in the early morning to moderate southwesterly to westerly winds with gusts as high as 28 kn after sunrise.

#### **4.6.7 5 Jun 93**

A closed, low-pressure system aloft off the northern California coast resulted in moderate to strong southwesterly flow over New Mexico.

At the surface, there was a north-south oriented stationary front over eastern New Mexico.

Sky conditions ranged from clear to scattered middle or low clouds. There was no evidence of convective activity. The maximum temperature was 94 °F, and the minimum temperature was 54 °F. Dewpoints ranged from the mid-teens to the mid-20's. Except for moderate southwesterly winds during the middle of the afternoon, winds generally were light southeasterly.

#### **4.6.8 9 Jun 93**

A low-pressure trough aloft extending from Minnesota to Baja, CA, resulted in moderate southwesterly flow over New Mexico and slight warm air advection.

At the surface, there was a northeast-southwest oriented cold front across southern New Mexico.

Skies generally were clear throughout the period of record. There was virtually no evidence of convective activity. Smoke or haze was observed up through 1000 MST. The maximum temperature was 90 °F, and the minimum temperature was 53 °F. Dewpoints ranged from the upper teens to the upper

20's. Surface winds ranged from calm in the early morning to light westerly after midmorning.

#### **4.6.9 10 Jun 93**

A weak, low-pressure trough aloft extending from Colorado to New Mexico resulted in westerly winds over most of New Mexico.

At the surface, there was a weak, high-pressure area over Colorado and a northeast-southwest oriented stationary front from central Illinois to west Texas.

The sky condition ranged from clear to scattered, low and high clouds. Haze was noted to the north, east, and south until late morning. Convective activity was limited to cumulonimbus clouds over the Sacramento Mountains to the northeast. The maximum temperature was 92 °F, and the minimum temperature was 52 °F. Dewpoints increased rapidly from 30 °F at 0500 MST to 48 °F at 1000 MST and decreased to 32 °F at 1900 MST. Surface winds generally were light and variable.

#### **4.6.10 11 Jun 93**

A closed, low-pressure system aloft over western Washington and an associated wave over northwest Texas resulted in northwesterly flow over southern New Mexico.

At the surface, frontal activity generally was confined to the northern half of the United States. The pressure gradient over southern New Mexico and west Texas suggested light southeasterly flow.

Skies basically were clear. There was no convective activity. The maximum temperature was 95 °F, and the minimum temperature was 57 °F. Dewpoints ranged from 50 °F at 0800 MST to 30 °F at 1600 and 1700 MST. Surface winds generally were light and variable.

#### **4.6.11 14 Jun 93**

A high-pressure ridge aloft over the Great Basin resulted in light easterly to northeasterly flow over New Mexico.

At the surface, there was a southeast-northwest oriented cold front over northeastern New Mexico and a trough line from northeastern New Mexico through El Paso and into northern Mexico.

There were clear to scattered, middle clouds until 1200 MST, then scattered to broken low, middle, and high clouds. Convective activity began about 1100 MST and developed into distant cumulonimbus, rain showers, and lightning mainly to the west through north through east. The maximum temperature was 102 °F, and the minimum temperature was 67 °F. Dewpoints were consistently in the 60's through 1100 MST. For the remainder of the observation period, the dewpoints were in the 30's. Surface winds generally were calm to light and variable through 1400 MST and light southeasterly thereafter.

#### **4.6.12 15 Jun 93**

A high-pressure dome aloft extended from Louisiana to the southern Arizona and northern Mexico border.

At the surface, there was a southeast-northwest oriented cold front extending across extreme northeastern New Mexico. The pressure gradient indicated weak southerly flow over southern New Mexico.

Skies were clear through 1000 MST. Scattered, low and high clouds occurred through 2100 MST. Convective activity was limited to distant cumulonimbus clouds beginning at 1100 MST and distant rain showers beginning at 1700 MST. The maximum temperature was 96 °F, and the minimum temperature was 63 °F. Dewpoints ranged from the mid-50's in the morning and evening to the mid-40's during the afternoon. Morning winds at the surface were calm to light and variable, and afternoon winds were moderate southeasterly.

#### 4.6.13 17 Jun 93

A closed, low-pressure system centered over western Utah resulted in southwesterly flow aloft over New Mexico.

At the surface, there was a low-pressure system centered over southwestern Colorado and southeastern Utah. A cold front extended southwestward from the low, and a stationary front extended eastward from the low. The pressure gradient indicated southeasterly flow over southern New Mexico.

Skies ranged from clear during the midmorning hours to generally scattered layers of low, middle, and high clouds. Convective activity was limited to cumulonimbus clouds to the north and east. The maximum temperature was 96 °F, and the minimum temperature was 60 °F. Dewpoints were in the 50's through noon and 40's for the remainder of the observations. Surface winds were light and variable during the morning and gusty southeasterly to southwesterly during the afternoon.

### 4.7 Discussion

On the whole, RASS data from the 924-, 404-, and 50-MHz profilers correlates well with the temperature data from the radiosondes during the study period ( $\rho \geq 0.87$ ). Only the 924-MHz profiler shows occasional marked disagreement. The occasional marked disagreement of the individual 924-MHz data with radiosonde data is a function of the small data sample available for individual days, which contain flyers that have passed internal sanity checks on the profiler itself. The very high offset seen on certain days in the 924-MHz data (5 Jun 93) is due to the fact that the correlation with the radiosonde, though high, is negative. Even in this case, the correlation is significant at the 85 percent level; there is only a 15.8 percent chance that the results are due to randomness. Although the correlation is high, there is a marked temperature offset with the profiler reported temperature; about 1 °C higher than the radiosonde on the whole for the 404-MHz data, 3 °C less than the radiosonde on the whole for the 50-MHz data, and about 5.5 °C higher than the radiosonde for the 924-MHz data.

Limited resources precluded an investigation of the relationship between the statistical data and the meteorological information for each day; however, as an example, we may take the case of 9 Jun 93, characterized by clear skies, no convective activity, and a high boundary layer. The temperature data from the afternoon radiosonde flight compared favorably with the 50- and 404-MHz profiler data with correlation coefficients of 0.99 and 0.97, respectively. The temperatures from both systems were high with an offset bias of 4 and 2 °C, respectively. It may well be that the radiosonde temperature is low at altitude, although the temperature sensor is calibrated at the surface before the flight. The 50- and 404-MHz correlations are significant at the 99.99 percent level. The 924-MHz profiler temperature data had an offset about 7 °C higher than the radiosonde with virtually a perfect correlation, the correlation is significant at the 98.1 percent level.

The limited number of 924-MHz data points compared to those available for the 404- and 50-MHz systems are responsible for some of the errant statistics, and a further comparison of 924-MHz and radiosonde data using 1994 data is warranted, as was done with 404-MHz data (Hoidale et al. 1995).

## 5. Refractive Index Structure Parameter

The refractive index structure parameter ( $C_n^2$ ) is of fundamental concern in understanding acoustic, optical, and radio propagation in the atmosphere; therefore, it is of great interest in many remote sensing efforts. The study of atmospheric refraction transitions over several regions including the surface, boundary layer, troposphere, and stratosphere. Phenomena such as gravity waves (Nastrom and Eaton, 1993), convective plumes, fluxes, drifting insects, wave activity, and frontal passages are studied using small-scale  $C_n^2$  measurements to help determine atmospheric effects on systems and models.

Astronomers have long been concerned with the effect of optical turbulence on "seeing" conditions at observatories. They quantify the effect by the transverse coherence length ( $r_o$ ), a quantity derived from  $C_n^2$  (Eaton et al. 1988a). The isoplanatic angle ( $\theta_o$ ), defined as the maximum angular extent of an extended object that can be viewed through turbulence while the spatial frequency content of the object remains unchanged, is also dependent on  $C_n^2$  profiles. The main difference between the two quantities,  $r_o$  and  $\theta_o$ , is that  $r_o$  is inversely related to the integrated  $C_n^2$  profile while  $\theta_o$  is inversely related to the  $C_n^2$  profile weighted by the range to the five-thirds power.

Clear-air radars and sodars measure backscatter or reflectivity from the atmosphere and can be calibrated for  $C_n^2$ . In addition, path-averaging and in situ point sensors provide near-surface direct  $C_n^2$  measurements or derived  $C_n^2$  data. The detailed profiles measured with these systems and sensors allow proper interpretation of the contribution of  $C_n^2$  versus altitude to such parameters as  $r_o$  and  $\theta_o$ . Eaton et al. (1988b) made comparisons of  $C_n^2$ ,  $r_o$ , and  $\theta_o$  from measurements taken with a suite of instruments including a 50-MHz radar, an  $r_o$  system, an isoplanometer ( $\theta_o$ ), a stellar scintillometer, and a thermosonde system at WSMR in a mountainous terrain. Additionally, measured profiles have been compared favorably to profiles computed using the NOAA Aeronomy Laboratory's  $C_n^2$  model as described in Warnock et al. (1985).

Five of the seven APRF systems mentioned in the Introduction are equipped and calibrated to remotely measure  $C_n^2$ : 50-MHz radar wind profiler, sodar, tower-mounted spatial temperature ( $C_T^2$ ) devices and scintillometers, tethered balloon, and FM-CW radar.

Although the tethered balloon and the FM-CW radar are used at the APRF to provide calibrated  $C_n^2$  profiles, neither system is routinely operated to measure wind or virtual temperature; therefore, they have not been mentioned. The tethered balloon system provides comparison profiles from an in situ  $C_T^2$  instrument while the FM-CW radar is used extensively to measure uniquely ultrahigh-resolution  $C_n^2$  profiles.

Although not calibrated, the 404- and 924-MHz radar wind profilers provide an uncalibrated value of radar return power, quantified as the 0th moment; however, they are not routinely used for  $C_n^2$  measurements. Eaton et al. (1992) discussed the feasibility of empirically calibrating the 404-MHz radar system (30 others are deployed by NOAA across the United States) by intercomparison with a collocated and calibrated 50-MHz radar system.

The combination of systems provides vertical profile data over various ranges extending from near the surface to just under 19 km AGL. The measurement systems are described, and the methods of calibration are discussed. A series of graphical representations is used to illustrate the capabilities of the various systems in the measurement of  $C_n^2$ .

## 5.1 System Comments

Table 19 summarizes salient characteristics of the 50-MHz, sodar, tower, FM-CW, and tethered balloon systems. More complete information on the systems and instrumentation are provided in Hines et al. (1993b), McLaughlin (1992), and Nastrom and Eaton (1993).

**Table 19. Features of the 50-MHz, sodar, tower, FM-CW, and tethered balloon systems**

System	Source	Height Range <sup>a</sup> (m AGL)	Vert. Resol. (m)	Temp. Resol. (s)	Typ. Avg. Int. (min)
50 MHz	Tycho	2000-18500	150	180	60
Sodar	Radian	50-850	4	30	15
Tower	ARL	point	point	10	15
FM-CW	Radian	0-4000	1-4	2-10	N/A
Tethered Balloon	A.I.R.	0-2000	N/A	10	N/A

<sup>a</sup>Midpoints of the gate extremes

### 5.1.1 50-MHz Radar Profiler

The three-beam 50-MHz profiler is of the mesosphere, stratosphere, troposphere type. The radar operates at a 49.25-MHz central frequency with two fixed coaxial-collinear antennas overlaid at right angles. One beam is directed toward the zenith. The other two beams are directed 15° from the zenith, one toward the south and the other toward the west, permitting the resolution of the horizontal and vertical components of the wind and other parameters. The antenna is about 150 m in diameter and produces a one-way beamwidth of 2.9°.

Received power, from which  $C_n^2$  is ultimately derived, is observed for 1 min along each of the three beams. Signal processing techniques produce three moment quantities for each beam: the 0th or total received power, the 1st or radial Doppler velocity, and the 2nd or velocity spectral width. The 0th moment from each oblique beam is used to compute a full  $C_n^2$  profile every 3 min. Pulse coding applied to the 8- $\mu$ s transmitted pulses produces 1- $\mu$ s nominal pulse lengths to give 150-m resolution along each beam axis. In normal operation, 112 range gates are used to sample from 2,000 to approximately 18,500 m AGL.

The transmitted peak power is 250 kW and with the large antenna (15,600 m<sup>2</sup>) leads to a power aperture product of 1 X 10<sup>8</sup> W/m<sup>2</sup>. Consequently, the signal-to-noise ratio is high at all levels sampled.

The radar equation used for the measurement of  $C_n^2$  by the 50-MHz radar is

$$C_n^2 = \frac{112.16 \lambda^{1/3} r^2 P_r}{\Delta P_t L_t A_{em}} \quad (9)$$

where

$\lambda$  = radar wavelength

$r$  = range

$P_r$  = received signal power

$\Delta$  = range resolution

$P_t$  = peak power at the transmitter

$L_t$  = total receiver and transmission line loss and antenna efficiency

$A_{em}$  = effective antenna area.

The radar is calibrated for computations of  $C_n^2$  using the first principles approach by injecting a known source produced with a noise generator into the forward monitor port of the antenna. During this procedure, the high power amplifier is turned off, and the system is set to 0 dBm. The noise generator is disconnected, and the power amplifier is turned on. Moments computed using the noise generator are compared to those acquired during normal operation. All other gains and losses, as well as the transmitted power, are measured and used in the standard way to modify the radar equation.

Comparisons between the two oblique antennas of the radar indicate that small differences exist between the south and west beams of the radar system. It is necessary to increase mean  $C_n^2$  values in the west beam by 2 dB to match the mean values in the south beam. The profiler operates nearly continuously with occasional outages caused by equipment failure.

Manufacturer's tests of the 50-MHz system indicate that the relative accuracy of the  $C_n^2$  measurement falls within a  $\pm 1.5$ -dB window. The antenna is believed to be calibrated within  $\pm 0.5$  dB, but the 2-dB difference between the two oblique beams must be included.

Figure 57 shows an example of total received signal power (0th moment) measured with the 50-MHz radar for a 24-h period beginning at 0600 universal time coordinate (UTC) on 16 May 93.

Figure 58 shows an example of calibrated  $C_n^2$  data corresponding to the total received signal power measured from 0000 to 0100 UTC on 16 May 93 (figure 57). Note the layers centered at 5 and 7 km MSL in comparison with figure 57. A typical wind-barb chart is inserted to emphasize the 150-m resolution of the 50-MHz system (figure 59).

### 5.1.2 *Sodar*

The sodar (sonic detection and ranging) system is an Echosonde model, three-axis system manufactured by Radian Corporation. The sodar is equipped with 1.5-m-diameter antenna apertures. Acoustic energy is directed vertically and  $18^\circ$  from the zenith toward the north and east, permitting the vertical and two horizontal wind components to be resolved. Each of the antenna assemblies consists of an acoustical transducer positioned at the focus of a 1.5-m-diameter parabolic dish housed in an acoustical enclosure optimized to maximize detection of a backscattered returned signal at 1850 Hz. The sodar system typically is operated at 250-W transmitted power with a 150-ms pulse length.

Backscattered signals measured by the vertical antenna are averaged every 30 s (equivalent to two sequential cycles) in 200 range gates to obtain a profile of the temperature structure parameter,  $C_T^2$ , from 50 to 850 m AGL.

Radar Signal Power (0th Moment)

NORTH BEAM

ALL MODES

ARL 50MHz WSMR, NM 1223 M

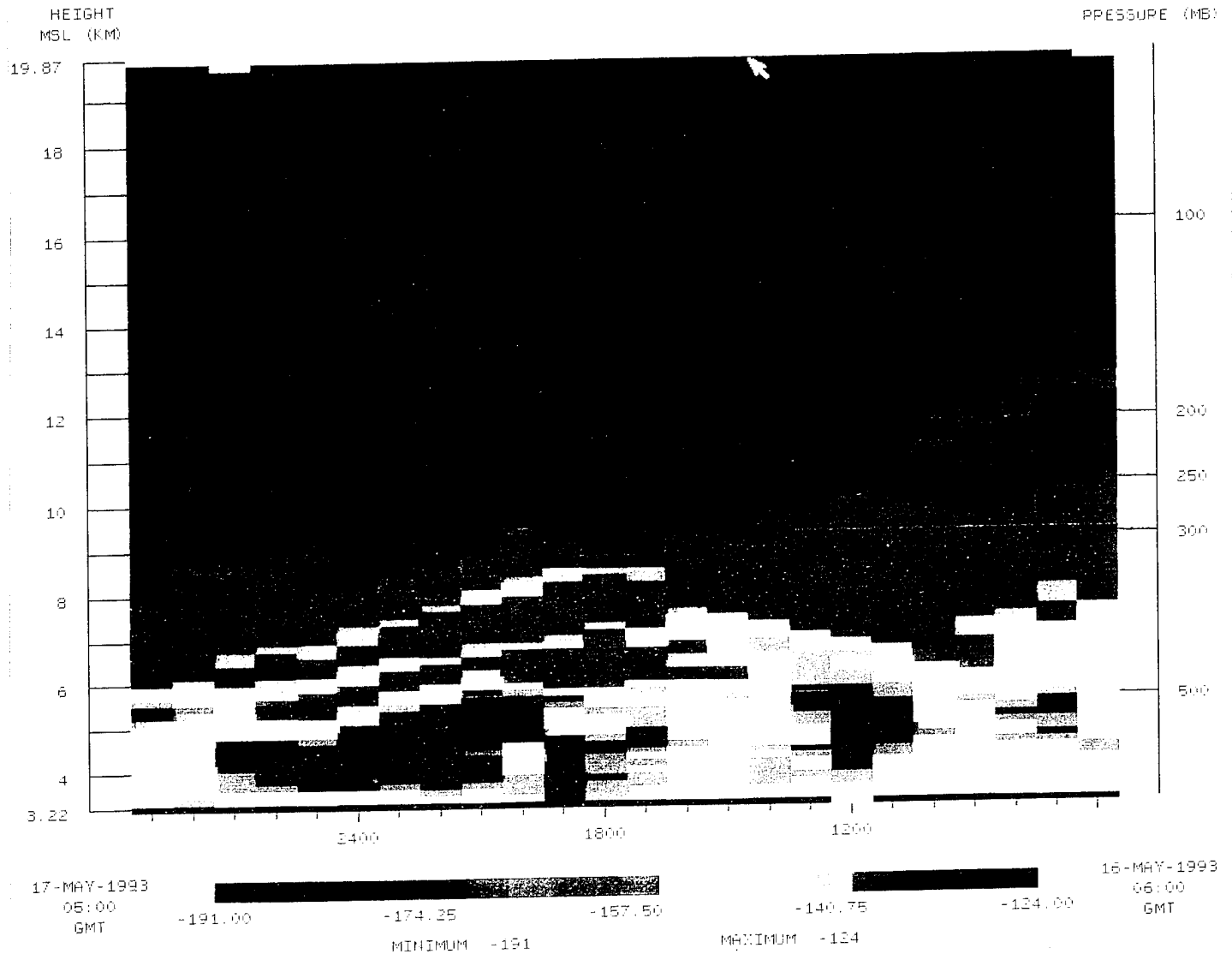


**Figure 57. Radar signal power measured with the north/south beam of the 50-MHz radar, APRF, 0600 UTC 16 May to 0500 UTC 17 May 93. The received power ranges from -191 to -124 dB.**

Ch2 Profile - Normal ALL MODES

ARL 50Mhz WSMR, NM 1222 M

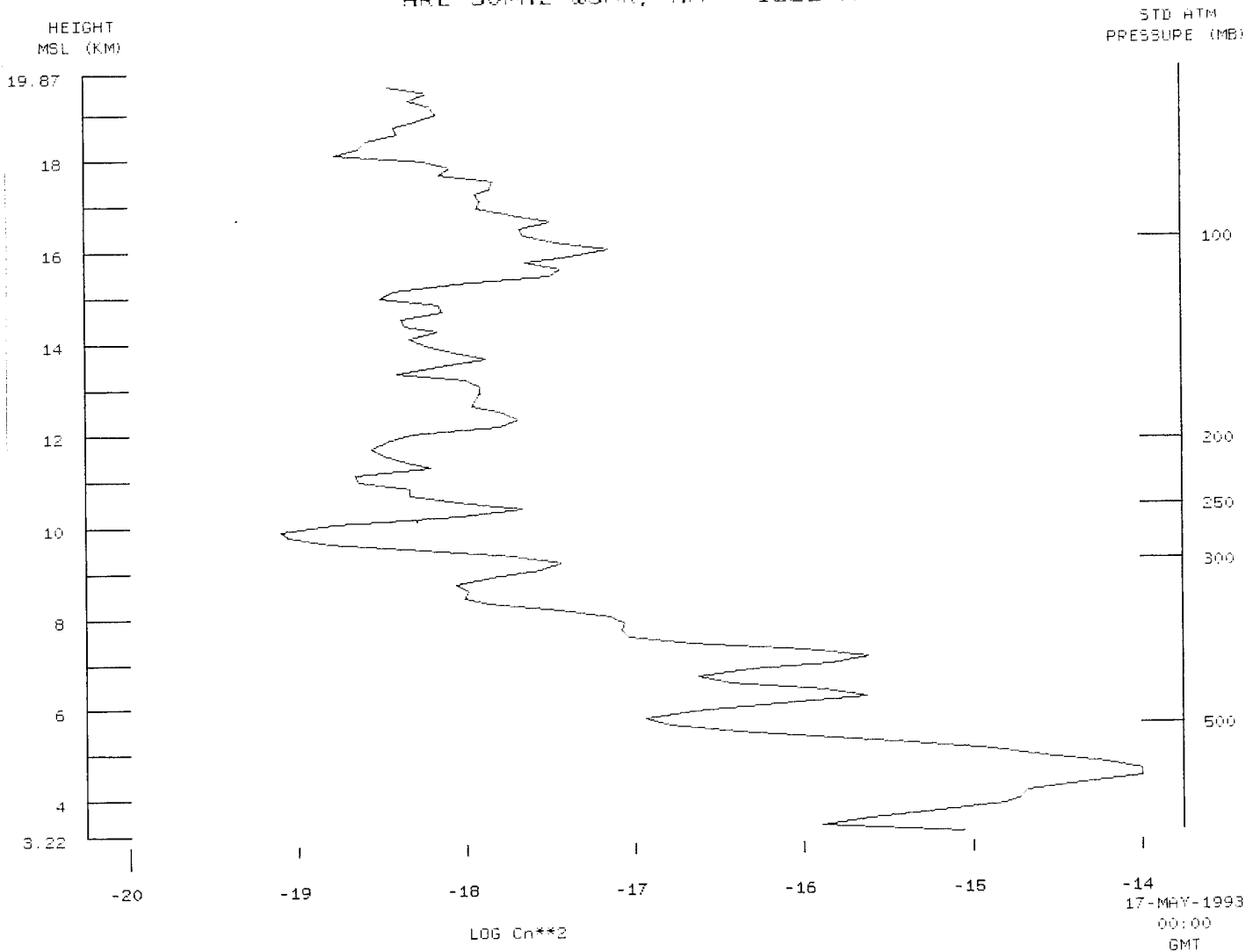


Figure 58. Vertical profile of calibrated  $C_n^2$  data derived from the 50-MHz radar signal power, APRF, 0000 to 0100 UTC, 17 May 93.

Wind Speed and Direction (Wind Barbs) ALL MODES

ARL 50MHz WSMR, NM 1222 M

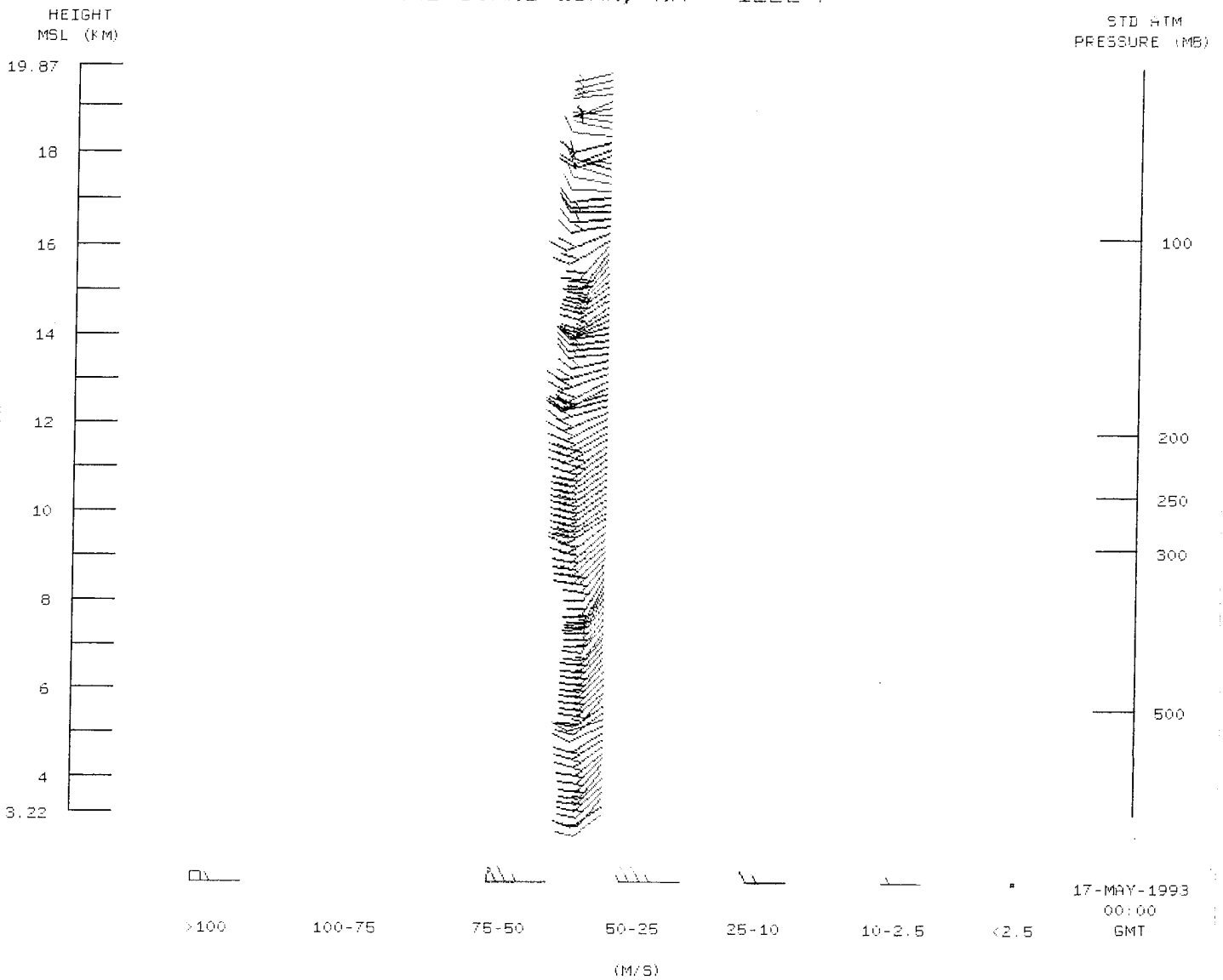


Figure 59. The corresponding wind profile for the period shown in figure 58 emphasizes the resolution of the 50-MHz system.

The sodar equation employed is

$$C_T^2 (\text{sodar}) = \frac{P_r T_o^2 e^{2\bar{\alpha}r} L_e}{E_r [P_t E_t] \left[ \left( \frac{c\tau}{2} \right) \left( \frac{A}{r^2} G \right) \right] [0.0039k^{1/3}]} \quad (10)$$

where

- $C_T^2$  = temperature structure coefficient
- $T_o$  = surface temperature
- $P_r$  = received signal power
- $\bar{\alpha}$  = total (molecular + classical) atmospheric attenuation coefficient
- $r$  = range
- $L_e$  = excess attenuation coefficient: effective efficiency due to losses caused by excess attenuation (function of  $C_n^2$ ) and wind speed -- set to a value of 1 at this time
- $E_r$  = receiver efficiency
- $P_t$  = the peak power at the transmitter
- $E_t$  = transmitter efficiency
- $c$  = speed of sound
- $\tau$  = pulse length
- $A$  = antenna aperture
- $G$  = antenna directivity
- $k$  = wave number ( $2\pi/\lambda$ ).

The measured  $C_T^2$  values are converted to the optical index of refraction structure parameter ( $C_n^2$ ) values by

$$C_n^2 = C_T^2 \left[ (79 \times 10^{-6}) \frac{P}{T^2} \right]^2 \quad (11)$$

where

- $P$  = ambient pressure (mbar)
- $T$  = ambient temperature (K).

Some researchers obtain calibrated  $C_T^2$  values from sodars by comparing the backscattered signals to in situ measurements of  $C_T^2$  taken on towers. Calibration of the sodar is accomplished using the first principles approach by relating received signal power including gains and efficiencies of the various acoustic system components to  $C_T^2$ , similar to the method used for calibrating radar returns. The troublesome, but difficult to theoretically quantify, problem of "excess attenuation," caused by forward beam scatter by the atmospheric turbulence, as well as beam refraction by a horizontal wind, is not addressed. The accuracy of the calibration method usually is checked against the results determined from in situ microthermal (spatial temperature) measurements, as discussed in Forbes et al. (1988).

Most sodar displays, typically as time-height maps, have been used to identify atmospheric features or patterns such as those produced by drainage flows, frontal passages, circulation, storms, or wave activity as well as to show diurnal variations. A personal computer is used for data recovery and processing.

During the summer of 1994, the sodar was relocated at the Apache Peak Observatory (APO). APO is located at about 2750 m MSL in the Sacramento Mountains some 65-km northeast of the APRF. The site is surrounded by trees near the western edge of the mountains. Figure 60 shows examples of received backscatter power as measured by the sodar at APO. The examples reflect the effects of rainfall, convective plumes, an inversion, and the neutral period. Each vertical trace is an average of two soundings from the vertical antenna.

Figure 61 shows an example of calibrated  $C_n^2$  data, also acquired at APO, as measured by the sodar at three heights.

### 5.1.3 *Tower Systems*

Two towers are associated with the APRF complex: a 152-m triangular-steel-type tower located near the APRF and a 20-m scaffold-type tower located adjacent to the 50-MHz radar profiler.

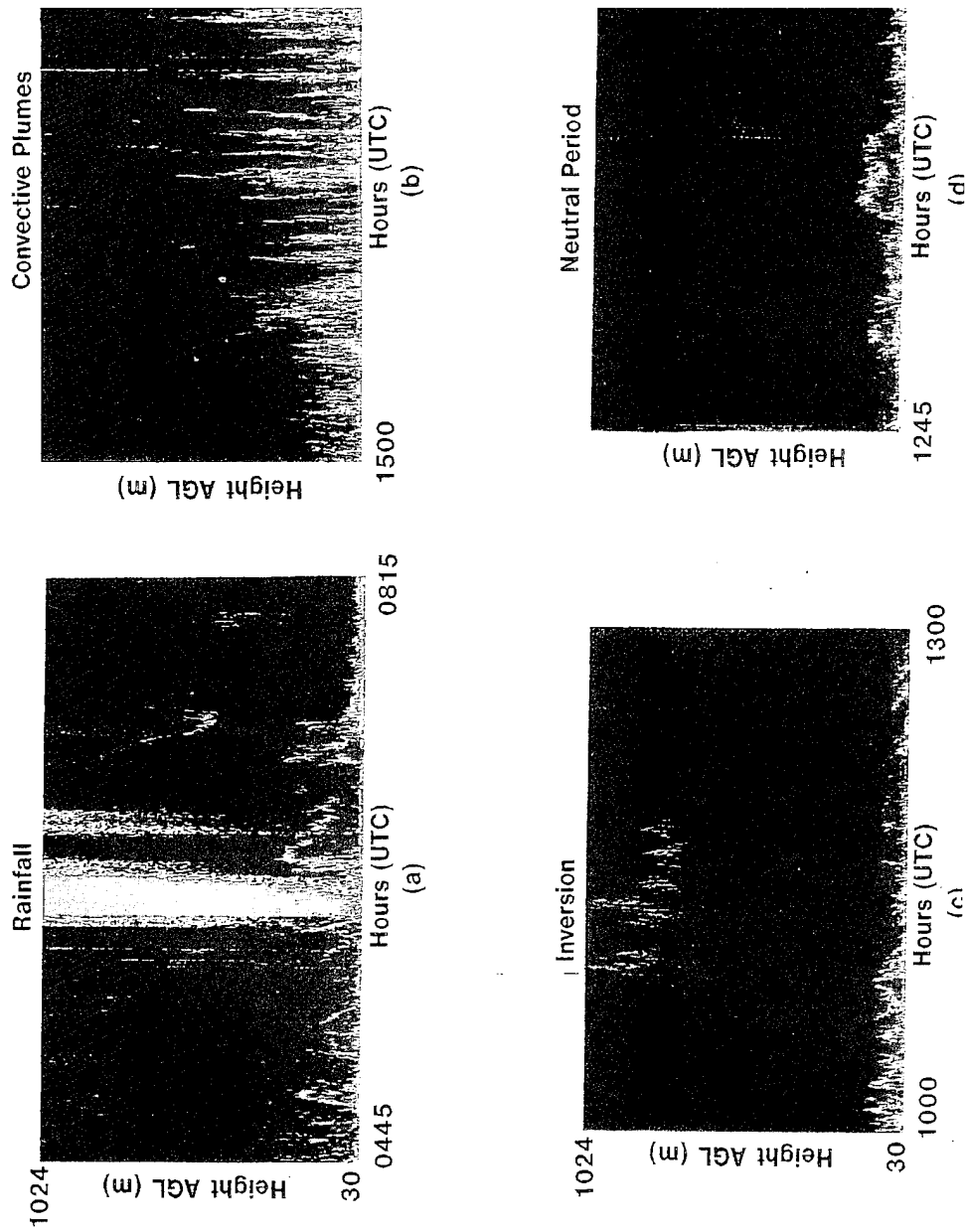
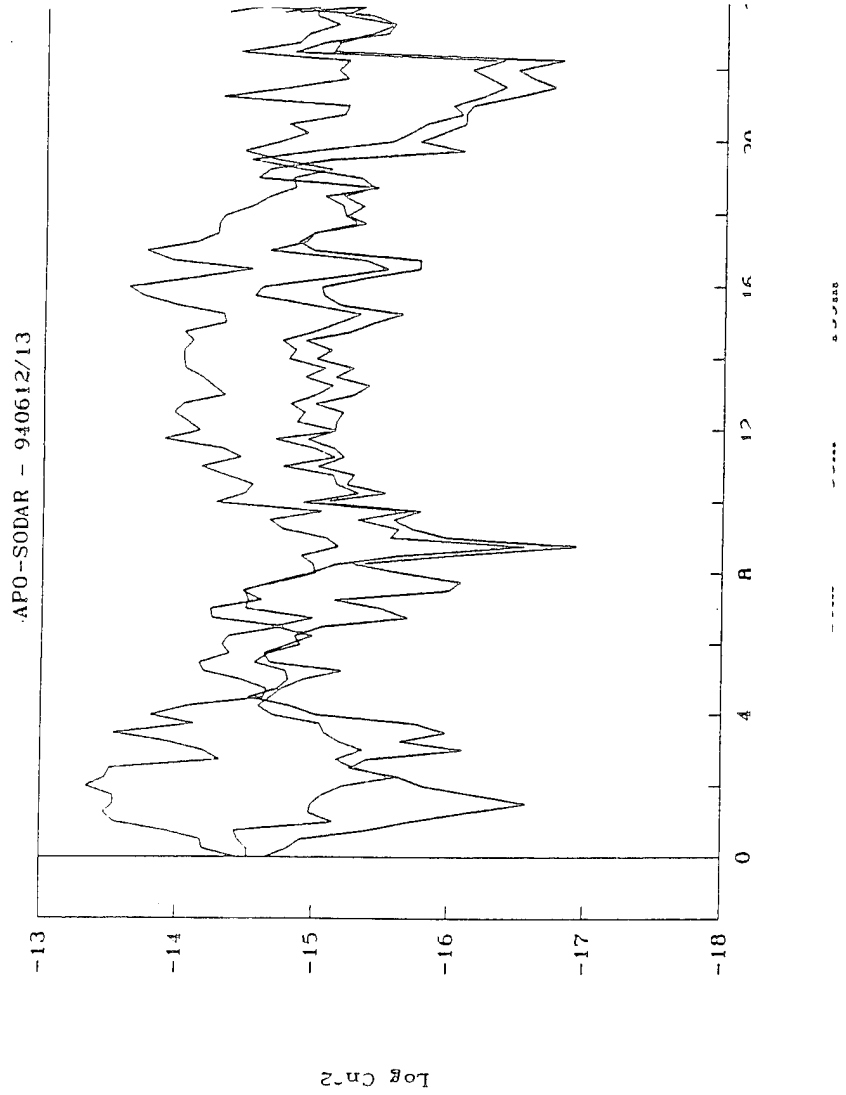


Figure 60. Received power backscatter measured by the sodar during four meteorological conditions: (a) rainfall, (b) convective plumes, (c) inversion, and (d) neutral period, APO, 22 Jul 94. The color scale ranges from the darkest red, corresponding to the return of  $\geq +100$ -dB signal, to black, corresponding to 0-dB signal.



The 152-m tower is instrumented at eight levels, and the 20-m tower is instrumented at two levels (4 and 20 m) with spatial temperature probes developed by ARL to measure  $C_T^2$  (Hamiter and Favier 1990). In addition, two path-averaging optical scintillometers are located at the two levels of the 20-m tower to provide a direct measurement of  $C_n^2$ . The sources for the two-ended scintillometers at 4 and 20 m are located at horizontal distances of 330 and 1000 m, respectively.

The spatial temperature probes utilize two fine-wire tungsten temperature probes mounted with a 0.2-m separation. Full details of the balanced direct current bridge, associated electronics, and system calibration are found in Hamiter and Favier (1990). Coupled with pressure and temperature sensors, the optical  $C_n^2$  is computed from the pressure, temperature, and  $C_T^2$ . The radar  $C_n^2$  is computed using the method described by Eaton et al. (1988b).

The path-averaging optical scintillometers utilize two spatially separated optical units: a transmitter using a light emitting diode source and a receiver with identical 15-cm aperture optics. Full details of the design, operational characteristics, and system calibration are found in Baxter (1986, 1990).

The spatial temperature probe and scintillometer provide continuous data that are sampled every 10 s by a local data system. Averaged edited data are provided at 15-min increments for subsequent comparison and analyses.

Figure 62 shows an example of integrated path  $C_n^2$  as measured with scintillometers at the APRF on 13 Mar 93. One scintillometer was located at 4 m AGL and the other, a dual scintillometer (single source with matched receivers), was located at 20 m AGL.

During the summer of 1994, five spatial temperature probes were temporarily relocated to the SHORAD Site approximately 35 km east of the APRF. The probes were placed at 0.25, 0.5, 1, 2, and 4 m AGL on a 4-m tower located at the site. Figure 63 shows an example of the diurnal variability of  $C_n^2$  as derived from the spatial temperature probes.

TURBULENCE, APRF TOWER #1  
95079

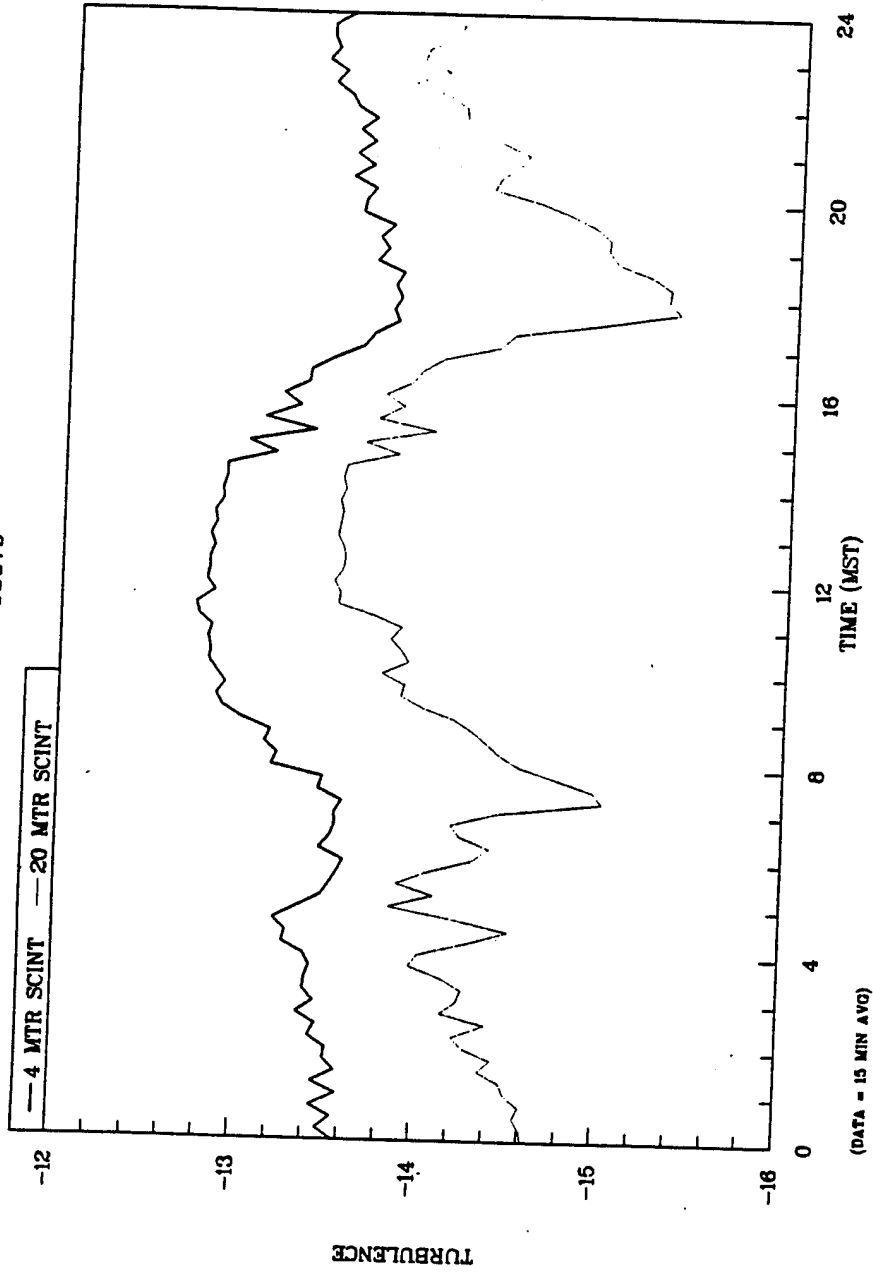


Figure 62. Diurnal variation of integrated path  $C_n^2$  scintillometer measurements, APRF, 4 and 20 m AGL, 0000 to 2400 MST, 20 Mar 95.

LCMS MET DATA - ARL DRAFT

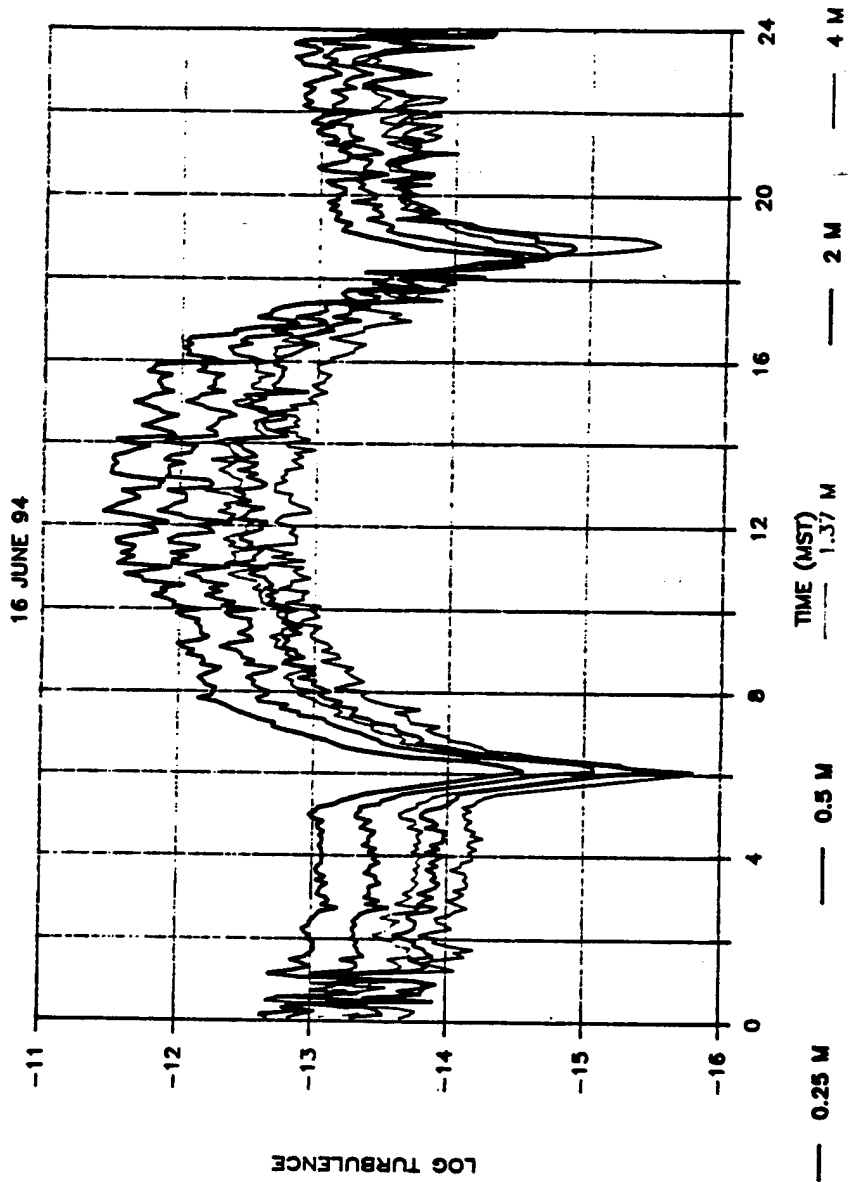


Figure 63. Diurnal variation of  $C_2^2$  measured with five spatial temperature probes at five levels of a 4-m tower, LCMS Site, 16 Jun 94.

#### 5.1.4 *Tethered Balloon System (Tethersonde)*

The tethered balloon system (tethersonde) is a boundary layer sounding system manufactured by Atmospheric Instrumentation Research, Inc. (A.I.R.). The system is designed to measure dry- and wet-bulb temperatures using precision matched thermistors, barometric pressure using a temperature compensated aneroid sensor, wind speed using a 3-cup anemometer, and wind direction using a magnetic compass. In addition, spare channels are available for specialized measurements. One of the channels is used for the  $C_T^2$  sensor. The  $C_T^2$  sensor was developed by ARL and utilizes two fine-wire tungsten temperature probes mounted with a 1-m separation and a miniaturized electronics package similar to that used on the tower systems. Optical and radar  $C_n^2$  are computed as described in Eaton et al. (1988b).

A helium-filled, blimp-shaped balloon, 5.25 or 7.50 m<sup>3</sup>, is used to raise and lower the sounding package suspended 10 to 12 m below the balloon. The altitude of the tethered package is controlled by a variable-speed winch located on the ground.

Measurements are made in one of three modes: (1) slow ascent and descent ( $\sim 10$  m min<sup>-1</sup>), (2) rapid ascent or descent to altitudes of interest and sensing for a few minutes at each altitude, or (3) maintaining the sensing package at a given altitude for approximately ½ h.

The data is telemetered to an A.I.R. Atmospheric Data Acquisition System for realtime logging.

Figure 64 shows an example of a mode 1 vertical profile of  $C_n^2$  as measured at Isabell Site during late morning on a summer day in 1992. Isabell Site is located 2 km north of the APRF.

Figures 65 and 66 show comparative  $C_n^2$  data.

TETHERED BALLOON FLIGHT ISABELL SITE  
 RUN 1 19 AUG 92 09:55-12:49 ASCENT

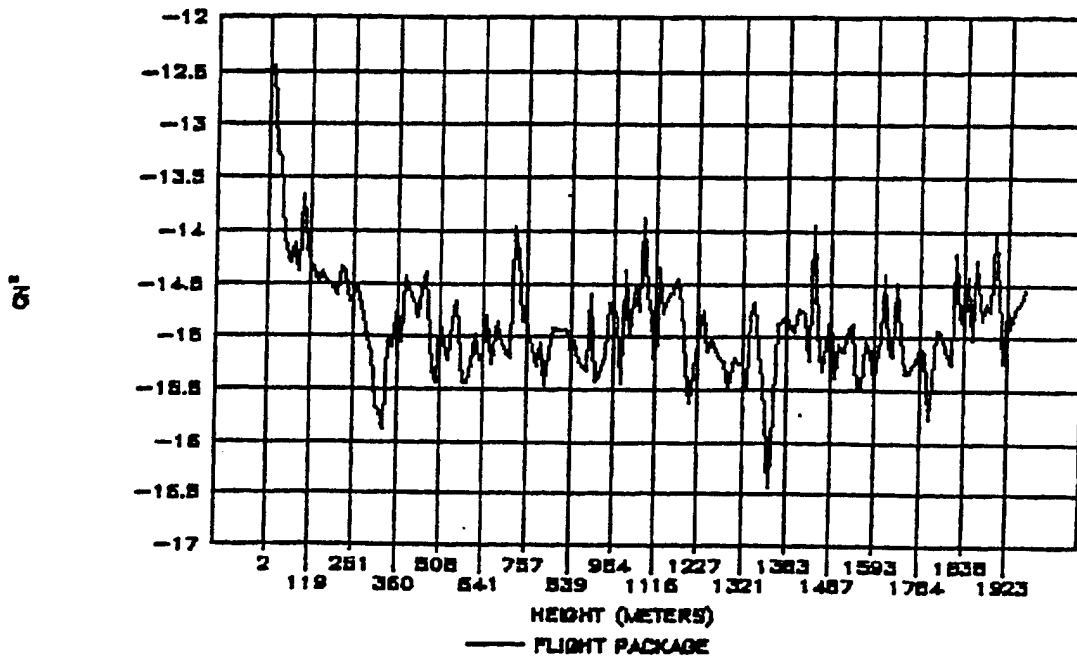


Figure 64. Vertical profile of  $C_n^2$  measured with a tethered balloon sensor at Isabell Site. The data were acquired during the ascent portion of the flight, 0955 to 1249 MST, 19 Aug 92.

Figure 65 shows a comparison of vertical profiles of  $C_n^2$  independently obtained with the tethered balloon (ascent portion of mode 1) at Isabell Site, and the sodar and five tower-mounted spatial temperature devices at the APRF during an approximate 15-min period on 19 Aug 92. The tethered balloon, sodar, and three of the five in situ tower-mounted devices agree reasonably well through a visual interpretation.

## TETHERED BALLOON FLIGHT ISABELL SITE

RUN 1 19 AUG 92 09:55-10:08 ASCENT

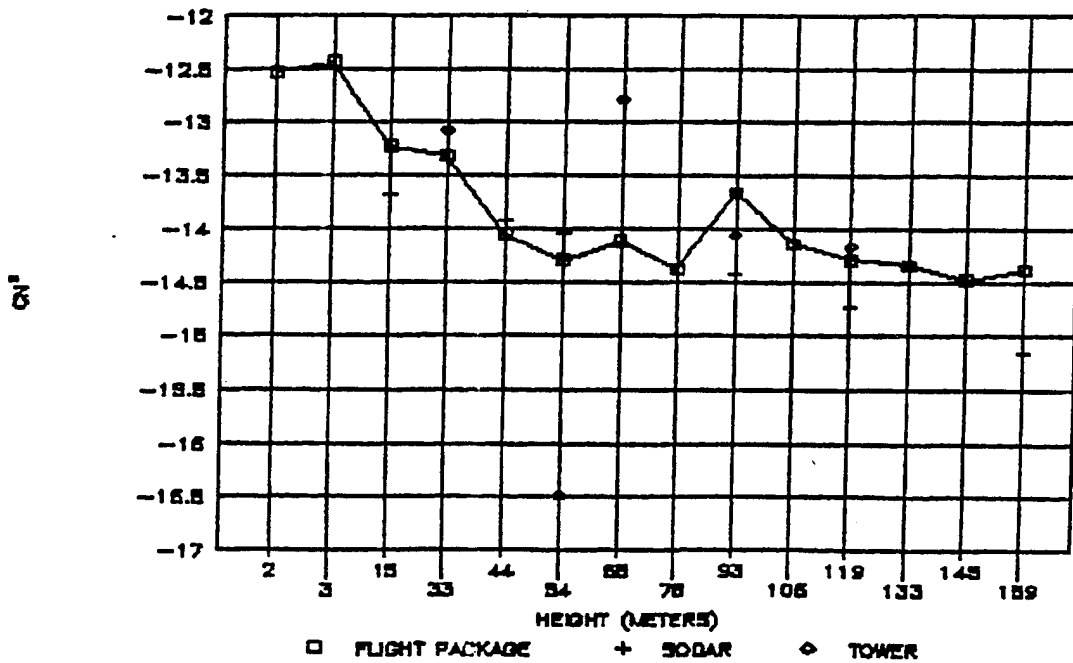


Figure 65. Vertical profiles of  $C_n^2$  measured with a tethered sonde at Isabell Site, and a sodar and five tower-mounted spatial temperature probes at the APRF, 19 Aug 92. The tethered sonde data were acquired during the ascent portion of the flight from 0955 to 1008 MST. The sodar and spatial temperature probe data represent a 15-min average from 1000 to 1015 MST.

Figure 66 shows a comparison of vertical profiles of  $C_n^2$  independently obtained with the tethered sonde (ascent portion) at Isabell Site and sodar during a nearly 30-min period on 13 Jan 93 at the APRF. A single in situ spatial temperature probe is used for surface calibration at Isabell Site and is located at 2 m AGL. The tethered sonde and sodar appear to measure the general trend of turbulence along the entire vertical path. There appears to be good agreement between the tethered sonde and in situ sensors.

TETHERED BALLOON FLIGHT ISABELL SITE  
 RUN 2 13 JAN 93 1048-1116 ASCENT

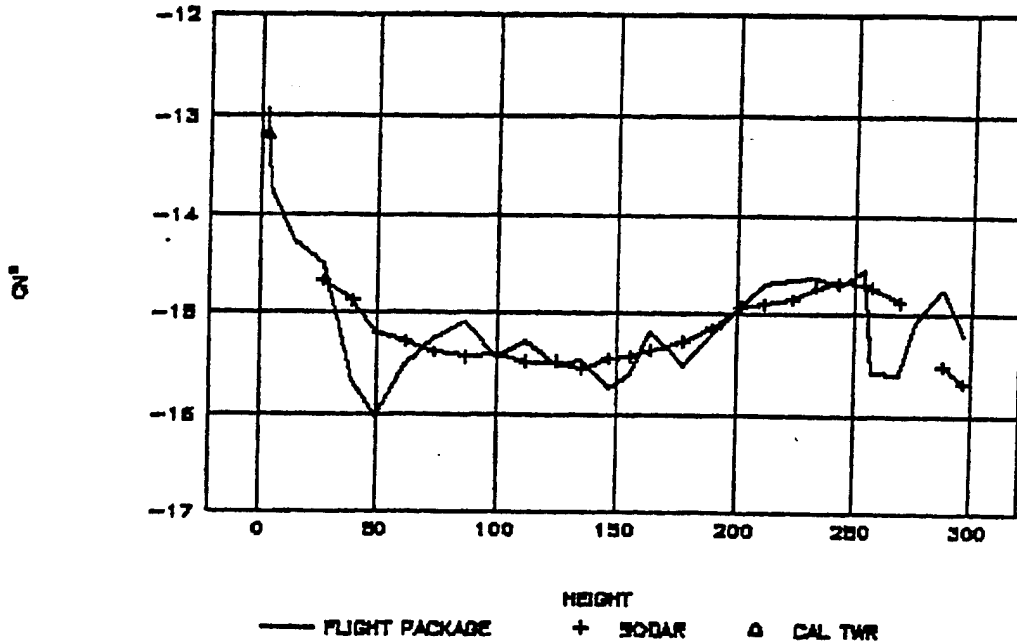


Figure 66. Vertical profiles of  $C_n^2$  measured with a tethered sonde at Isabell Site and a sodar at the APRF, 13 Jan 93. The tethered sonde data were acquired during the ascent portion of the flight from 1048 to 1116 MST. The sodar data represent a 30-min average from 1045 to 1115 MST. Calibration data were obtained with a spatial temperature probe at the 2-m level of a tower at the Isabell Site. The data were obtained over a 10-min period just prior to the tethered sonde flight.

### 5.1.5 FM-CW Radar

The FM-CW radar used at the APRF was designed for studying the planetary boundary layer (PBL) and cloud physics research (McLaughlin 1992). In fact, the high-resolution, ultrasensitive, accurate calibration and sensing near the ground of the FM-CW radar are crucial for modern experimental programs in the PBL (Eaton, McLaughlin, and Hines 1994).

State-of-the-art technology was incorporated throughout, enhancing the temporal and spatial resolution and allowing a more precise calibration

(McLaughlin 1992) than possible with previous FM-CW systems described by Richter (1969) and Chadwick et al. (1976).

The highly linear frequency modulated sweep is generated with a frequency synthesized source instead of a yttrium iron garnet-tuned transistor oscillator as used in earlier systems. All data collection, system calibration, and processing are performed in real-time.

Figure 67 shows the FM-CW radar system (large kettle drum-like antennas, center). The FM-CW system consists of two trailers, one for the data processing/electronics equipment and one for the antennas. The two identical 3-m diameter antennas, one transmitting and one receiving, are mounted on a fully steerable mount. Slow-rate azimuth scans can be made for velocity azimuth display wind profiling, or the antennas can be directed vertically (or lower, e.g. slant path measurements) for high-resolution backscatter profiling. The radar uses a phased-locked-loop digital frequency synthesizer to obtain a highly linear, very low noise 200-MHz sweep over 50 ms as a "sawtooth" wave centered at 2.9 GHz. The final amplifier is a traveling wave tube with a continuous (nearly 100-percent duty cycle) 220-W output. The received signal is homodyned, amplified, filtered, and sampled. The radar continuously sweeps and takes data, processing all data real-time using an Analogic 16-bit Analog-Digital-Converter coupled to a Analogic Array Processor combined with a Hewlett-Packard (HP) 1000 minicomputer. Data is written to tape or disk, graphically to video screens, and in a color FAX type display to an HP PaintJet. Table 20 displays some of the FM-CW key features and operating parameters.

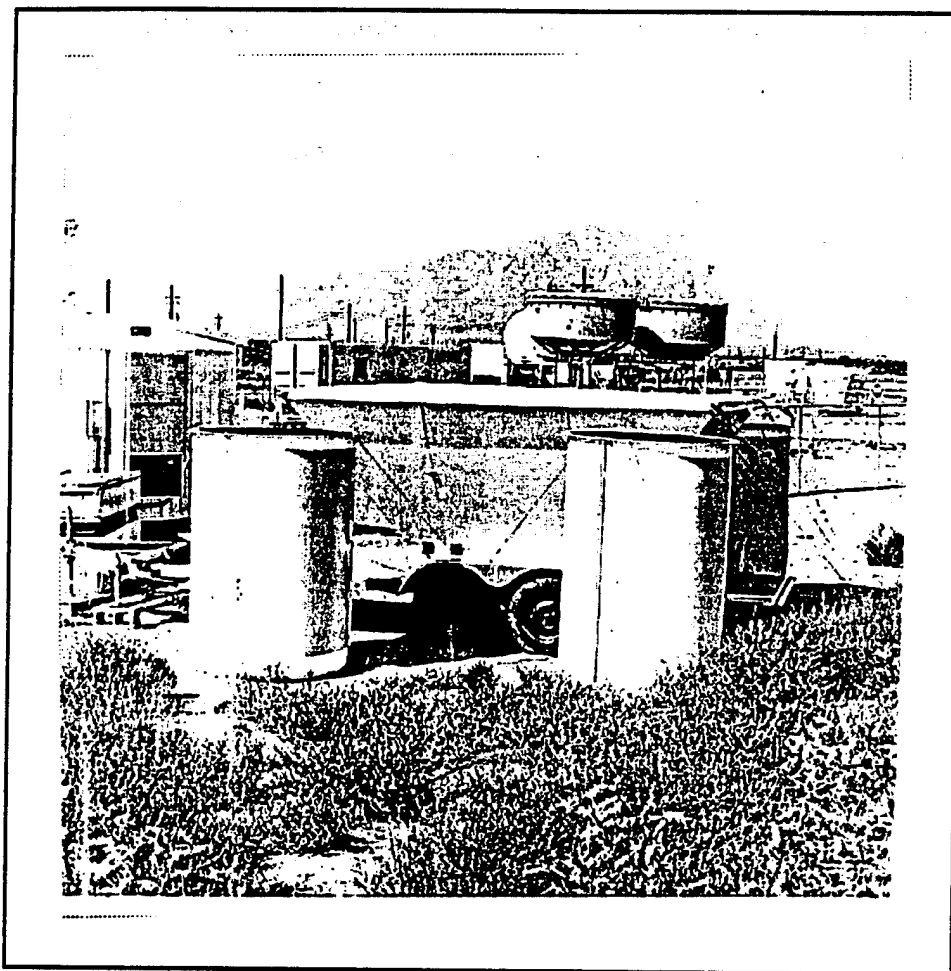


**Figure 67. FM-CW Radar, WSMR (view toward the west with the 924-MHz wind profiler in the foreground and the Organ Mountains in the background).**

**Table 20. Characteristics of the ARL FM-CW radar**

Characteristic	Value
Operating frequency	2.9 GHz $\pm$ 100 MHz
Antenna	
Type	Parabolic
3-dB beamwidth	2.7°
Transmitter	
Type	Traveling wave
Power	220 W continuous
Minimum detectable signal	Less than -165 dBm
Height range	Typically surface to 2-4 km AGL
Number of gates	1024
Resolution	
Spatial	Typically ~2-4 m
Temporal	6-12 s per profile

Absolute calibration of the FM-CW radar system is necessary to relate returned signal power to radar  $C_n^2$ . The FM-CW radar equation can be shown to be

$$P_r = \frac{P_t R_G \left(\frac{D}{R}\right) G^2 \lambda^2 \theta^2 \Delta}{2^9 \ln 2 \pi^2 R^2} \eta \quad (12)$$

where

- $P_r$  = received power
- $P_t$  = transmitted power
- $R_G(D/R)$  = antenna autocorrelation function
- $G$  = antenna gain
- $\lambda$  = radar wavelength
- $\theta$  = antenna 3-dB half-power beamwidth
- $\Delta$  = radar range resolution
- $R$  = radar range
- $\eta$  = radar cross section per unit volume.

After incorporating Ottersten's (1969) relationship,

$$\eta = 0.38 C_n^2 \lambda^{-1/3}, \quad (13)$$

and simplifying system parameters,  $C_n^2$  can be expressed as

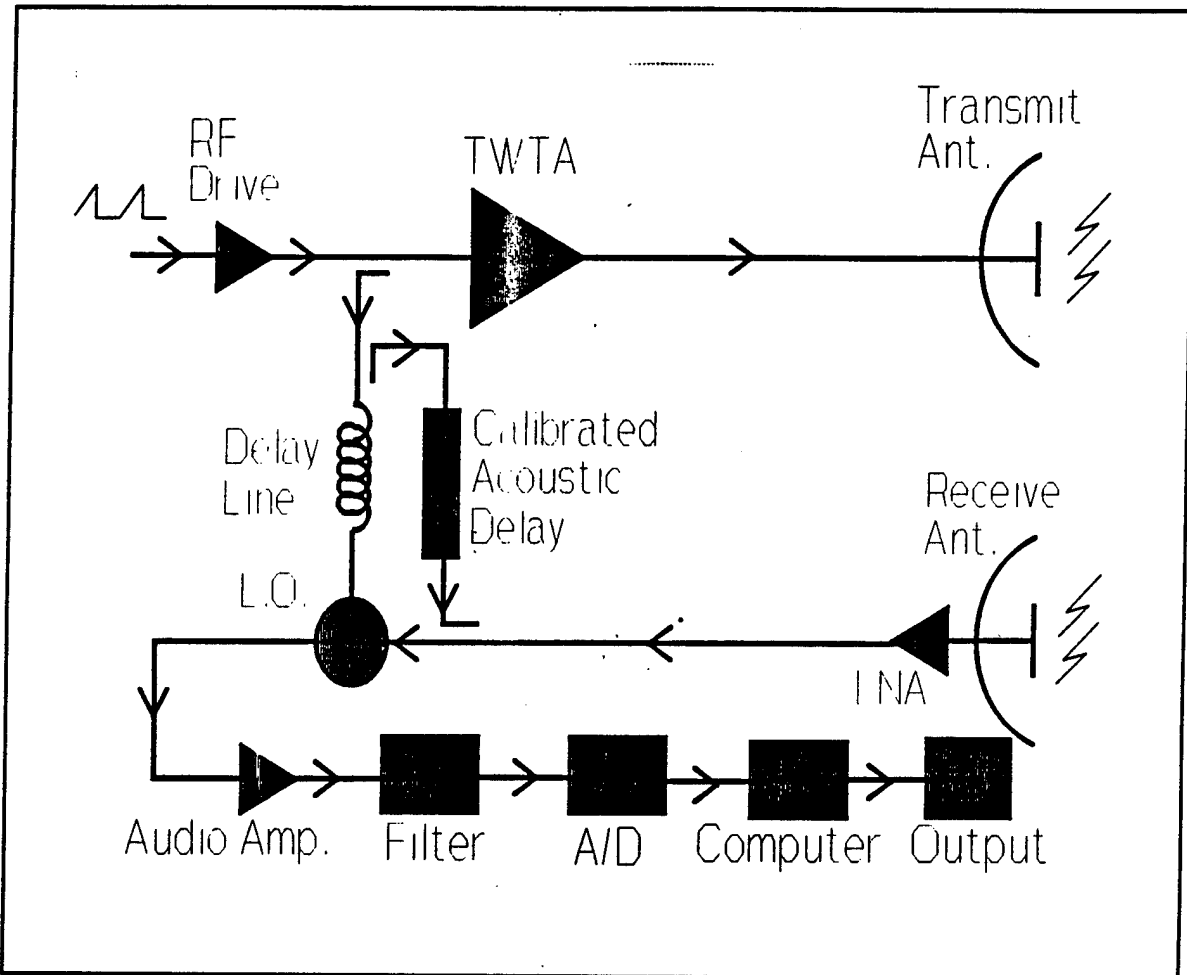
$$C_n^2 = 4.061 \frac{P_r R^2}{P_t R_G \left(\frac{D}{R}\right)}. \quad (14)$$

There is an additional term, not included here, to convert  $P_r$  in watts to "Fast Fourier Transform units" that must be applied to take care of the digital signal processing gains. A similar derivation is applied to calibrate in the cases of hydrometeor backscatter obtaining dBZ (dB = decibels, Z = vertical component) units.

The antenna autocorrelation term  $R_G(D/R)$  accounts for the changing overlap of the transmit and receive beams caused by the bistatic side-by-side arrangement of the two antennas. The correction is computed from the autocorrelation function of the two identical antenna patterns. For ranges less than approximately 500 m, correct  $C_n^2$  calibration depends strongly on accurate knowledge of the antenna autocorrelation. Below approximately 100 m, the weighting function goes to zero. However, the weighting function uses the antenna far-field patterns; therefore, it is only valid above approximately 180 m. The weighting function is applied lower than 180 m to improve data clarity, but an empirical correction for low altitudes is under development utilizing  $C_n^2$  measurements taken from a calibrated sodar, tower measurements, and a tethered balloon.

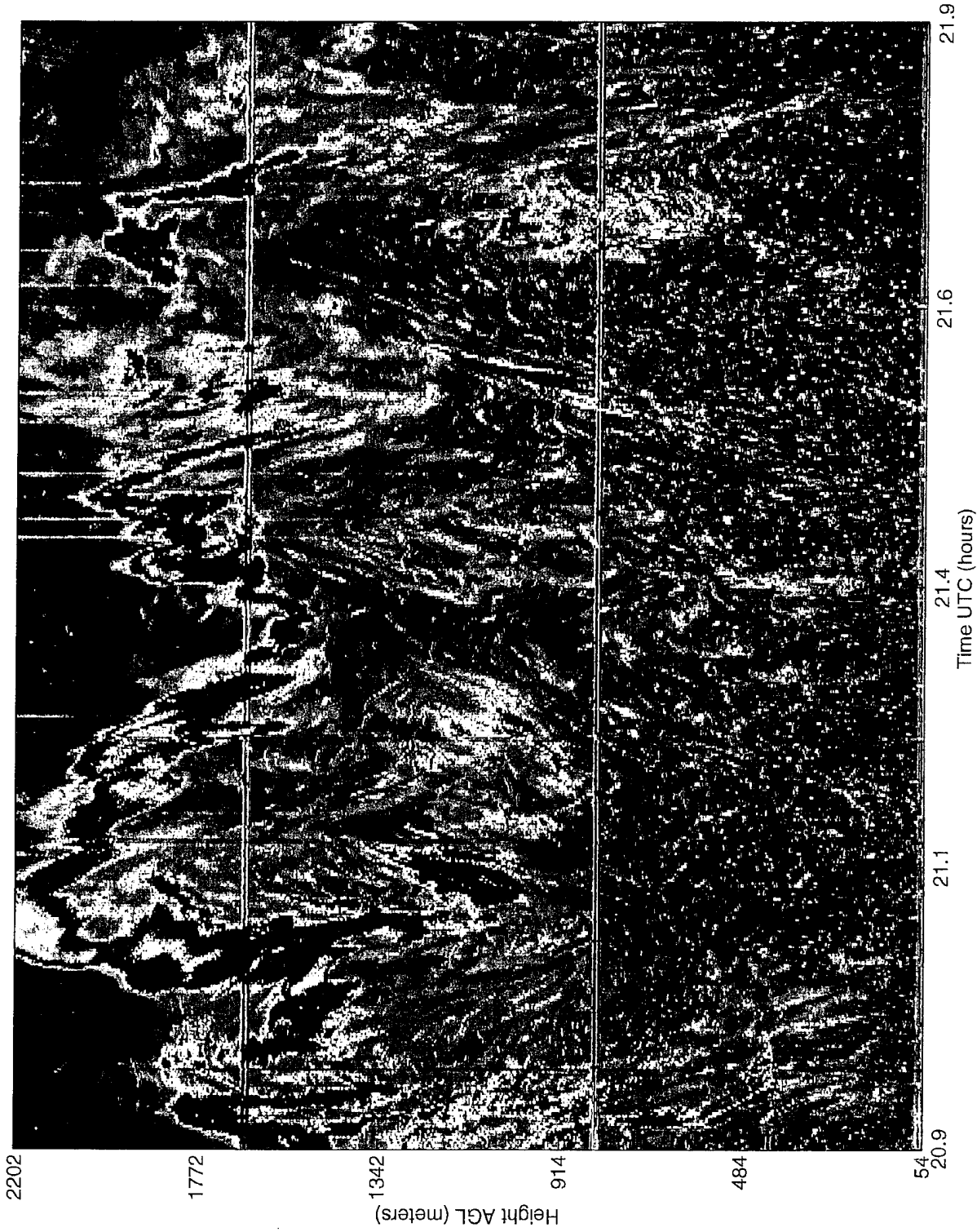
The electronic calibration is performed by taking an attenuated known sample of the transmitted signal, delaying it in an electro-acoustic delay line (equivalent to a target at 675 m), and coupling it into the receiver. Thus, the system can be calibrated from the receiver forward, including the digital signal processing, by using this test signal and resultant output. The gain of the radio frequency preamplifier, antennas, and attenuation of the cable assemblies is measured to complete the calibration.

Figure 68 depicts the calibration technique used for the FM-CW radar. Further intercomparison testing at the APRF is expected to refine the current calibration technique.



**Figure 68. Block diagram displaying the calibration technique for the FM-CW radar.**

Figure 69 shows an example of high-resolution radar backscatter as measured by the FM-CW radar. The small spots and streaks are insects or small birds that act as tracers and delineate the convection cell boundaries and enhance flow visualization. The upper boundary of the cells is shown as a capping layer.



**Figure 69. Boundary layer backscatter measured by the FM-CW radar during a 1-h midday convective period, APRF, 26 Aug 92.**

## 5.2 Availability of Data

Figure 3 summarizes the availability of  $C_n^2$  data from the 50-MHz, sodar, and tower systems. The acquisition of tethered-sonde and FM-CW data is usually tied to specific short-term field experiments.

## 5.3 Quality Control

The quality control techniques used in the processing of the wind and temperature data have not been fully integrated into the processing of the  $C_n^2$  data. As a consequence, the data have not been quality controlled by the continuity method. Because the primary purpose of section 5 is to show the capability of the systems and not to assess the relative accuracy of the  $C_n^2$  measurements, the lack of quality control is not considered critical at this juncture.

## 5.4 Volume and Temporal Averaging

No attempt has been made to adopt the volume averaging techniques discussed in section 3.4. However, temporal averaging was used for the 50-MHz, sodar, and tower systems. The averaging of the tethered-balloon and FM-CW data has not yet been addressed.

## 5.5 Summary

Manufacturer's tests indicate that the relative accuracy of the  $C_n^2$  measurement with the 50-MHz system falls within a  $\pm 1.5$ -dB window. The antenna is believed to be calibrated within  $\pm 0.5$  dB. There is also a 2-dB difference between the average measurement of the two oblique beams, but at present this is assumed to be atmospheric. Because  $C_n^2$  is directly proportional to dB, 1.5 dB is approximately equivalent to a factor of 1.33 in  $C_n^2$ .

Five times during 1993 and 1994, the U.S. Air Force Phillips Laboratory flew an instrumented aircraft over WSMR. The flights occurred between 1100 and 1400 local standard time at various fixed altitudes between 7 and 18 km AGL. Preliminary, unpublished,  $C_n^2$  data obtained during the flights agree quite well with the concurrent  $C_n^2$  data from the 50-MHz system.

Additional experimentation is in progress to help further define the accuracy of the 50-MHz system.

$C_n^2$  data, derived from the sodar backscatter measurements, have repeatedly compared favorably with in situ  $C_T^2$  and  $C_n^2$  profile data. Several system acquisition software changes have improved the availability of high signal-to-noise data. This, in turn, is suggesting improvements in the calibration process. Additional experimentation is in progress to further define the accuracy of the sodar.

Profiles of  $C_n^2$  measured with optical scintillometers and spatial temperature devices repeatedly show good comparison between similar sensors or with remote sensor techniques. Each type of sensor can be influenced by the local environment such as towers, buildings, foliage, and terrain. Sufficient data have been acquired and analyzed to convince us that the sensors are highly accurate under most situations. Because theory does not provide an absolute procedure to define  $C_n^2$  accuracy, repeated successful comparisons between like and different  $C_n^2$  sensors is considered a reasonable method to approximate a definition of accuracy.

Profiles of  $C_n^2$  measured with tethered instrumentations also show reasonably good comparison with fixed  $C_T^2$  sensors and remote volume averaging sensors. Balloon wake effects and mechanical turbulence encountered during flights tend to limit the usefulness of this technique. Patience in choosing flight times results in highly accurate data comparisons. The sensor is a modified version of the tower  $C_T^2$  device and has an excellent record of measurement accuracy within the constraints suggested above.

Radar backscatter/ $C_n^2$  profiles, measured with the FM-CW radar, provide excellent details of boundary layer  $C_n^2$ . Results of calibration comparison studies tend to support the accuracy of the measurements, although future studies are required for a definitive accuracy determination.

Unlike remote sensing techniques for wind and temperature, no known universal measurement technique exists to obtain atmospheric  $C_n^2$  and determine the accuracy of the measurement. The APRF includes an excellent suite of state-of-the-art instrumentation and is addressing the nature, patterns, and persistence

of  $C_n^2$ . Future analyses are expected to resolve this issue within the constraints of current resources.

## 6. Conclusions

The statistical analyses of the wind data from the three radar wind profilers show a high degree of correlation between the 404- and 50-MHz profilers for the high and low modes of the 404-MHz profiler. Correlation coefficients for the composite data from all the study days were above 0.96 for the U and V wind components from the 50-MHz profiler and the 404-MHz high and low modes. The analyses indicate a resultant speed accuracy well within 1 m/s for the 50- and 404-MHz profilers. The 924- and 50-MHz profilers compared less well; the correlation coefficients for the U and V components were in the 0.8 to 0.9 range, but the overall accuracy of the two were within 1 m/s. The poorest overall correlation was between the 404- and 924-MHz profilers, in the range of 0.7 to 0.8; even in this case, the expected wind speed difference between the two was less than 1 m/s over all gates. The poor correlation between the 924- and 50-MHz profilers most likely is due to instrument limitations, the 924-MHz profiler only overlaps the altitude region of the 50-MHz profiler near the top of its range where the backscattered signal-to-noise is poorest. The cause of the poor correlation between the 924- and 404-MHz profilers is undetermined. Future investigation of this discrepancy by ANOVA techniques with respect to height and time of day may resolve the problem.

On the whole, RASS data from the 924-, 404-, and 50-MHz profilers correlates well with the temperature data from the radiosondes during the study period ( $\rho \geq 0.87$ ). Only the 924-MHz profiler shows occasional marked disagreement. Although the correlation is high, there is a marked temperature offset in the case of the 924- and 50-MHz profilers with the profiler reported temperature about 5 °C more and 3 °C less than the radiosonde, respectively. RASS data from the 404-MHz profiler agrees quite well with the radiosonde, a result confirmed by analyses of 1994 404-MHz data (Hoidale et al. 1995).

Although no detailed statistical studies of the turbulence data from profilers has been attempted, qualitative reviews of the available data indicate a general agreement among the instruments.

## References

- Baxter, S., *Auto-Calibrating Atmospheric Scintillometers Model IV-L Operation and Maintenance Manual*, Contractor Report, Lockheed Engineering and Management Services Company, Inc., 1986.
- Baxter, S., *Operation and Maintenance Manual Supplement for Auto-Calibrating Atmospheric Scintillometers Model IV-L and IV-L2*, Contractor Report, Lockheed Engineering and Sciences Company, 1990.
- Biltoft, C. A., "An Analysis of the 150-m ISIE Data," In *Proceedings of 7th Symposium of Meteorological Observations and Instrumentation*, New Orleans, LA, p 409-412, 1991.
- Chadwick, R. B., K. P. Moran, R. G. Strauch, G. E. Morrison, and W. C. Campbell, "A New Radar for Measuring Winds," *Bull. Am. Meteorol. Soc.*, **57**:1120-1125, 1976.
- Eaton, F. D., W. H. Hatch, J. R. Hines, and J. O. Johnson, "Intercomparison of  $C_n^2$  Data Derived from VHF and UHF Radars," *Atmospheric Propagation and Remote Sensing*, In *Proceedings of the SPIE*, **1688**, p 178-184, 1992.
- Eaton, F. D., W. A. Peterson, J. R. Hines, J. J. Drexler, A. H. Waldie, and D. B. Soules, "Comparison of Two Techniques for Determining Atmospheric Seeing," *Optical, Infrared, and Millimeter Wave Propagation Engineering*, In *Proceedings of the SPIE*, **926**, 1988a.
- Eaton, F. D., W. A. Peterson, J. R. Hines, K. R. Peterman, R. E. Good, R. R. Beland, and J. H. Brown, "Comparisons of VHF Radar, Optical, and Temperature Fluctuation Measurements of  $C_n^2$ ,  $r_0$ , and  $\theta_0$ ," *Theor. Appl. Climatol.*, **39**:17-29, 1988b.
- Eaton, F. D., S. A. McLaughlin, and J. R. Hines, "A New FM-CW Radar for Studying Planetary Boundary Layer Morphology," *Rad. Sci.*, (Accepted for publication), 1994.

- Fischler, M. A., and R. C. Boles, "Random Sample Consensus: A Paradigm for Model Fitting Applications to Image Analysis and Automated Cartography," *Commun. Assoc. Comp. Mach.*, **24**:381-395, 1981.
- Flowers, W., L. Parker-Sedillo, G. Hoidale, E. Santantonio, and J. Hines, *Evaluation of a 924-MHz Wind Profiling Radar*, ARL-CR-101, U.S. Army Research Laboratory Contractor Report, White Sands Missile Range, NM, p 202, 1994a.
- Flowers, W., L. Parker-Sedillo, G. Hoidale, E. Santantonio, and J. Hines, *924-MHz Wind Profiling Radar Data Availability, 24 March - 25 August 1992*. U.S. Army Research Laboratory Data Report 2, White Sands Missile Range, NM, p 71, 1994b.
- Forbes, F. F., E. S. Barker, K. R. Peterman, D. D. Cudaback, and D. A. Morse, "High-Altitude Acoustic Soundings, Effect of the Environment on Systems Performance," In *Proceedings of SPIE*, **926**, p 74-87. 1988.
- Hamiter, M. A., and D. L. Favier, *Thermal Turbulence Unit Model C<sup>2</sup>T-1A Operation and Service Manual*, Contractor Report, Physical Sciences Laboratory/Engineering Services/Technical Data Services, 1990.
- Hines, J., and L. Parker-Sedillo, "Assessment of the Performance of Wind Profilers at White Sands Missile Range," Reprints of the 1993 Battlefield Atmospheric Conference, Las Cruces, New Mexico, 345-355, 1993a.
- Hines, J. R., S. A. McLaughlin, F. D. Eaton, and W. H. Hatch, "The U.S. Army Atmospheric Profiler Research Facility: Introduction and Capabilities," *Preprints of Eighth Symposium on Meteorological Observations and Instrumentation*, Anaheim, California, pp 237-242, 1993b.
- Hoidale, G. B., W. L. Flowers, and L. Parker-Sedillo, *An Evaluation of Selected Virtual Temperature Data Acquired at the APRF in 1994*, ARL-CR-199, U.S. Army Research Laboratory Contractor Report, White Sands Missile Range, NM, p 78, 1995.
- Hoehne, W. E., *Precision of National Weather Service Upper Air Measurements*, NOAA Tech. Memo. NWS T&ED-16, p 12, 1980.

- Law, D. C., "Interpretation of Wind Profiler Spectral Moment Data," *Preprints of Seventh Symposium on Meteorological Observations and Instrumentation*, New Orleans, LA, p 389-392, 1991.
- List, R. J., *Smithsonian Meteorological Tables, Sixth Revised Edition*, Publication 4014, 114, The Smithsonian Institution, Washington, DC, 1963.
- May, P. T., R. G. Strauch, T. Sato, M. Yamamoto, S. Kato, T. Tsuda, and S. Fukao, "Errors in the Determination of Wind Speed by Doppler Radar," *J. Atmos. Ocean. Technol.*, 6:235-242, 1989.
- May, P. T., R. G. Strauch, K. P. Moran, and W. L. Ecklund, "Temperature Sounding By RASS With Wind Profiler Radars: A Preliminary Study," *IEEE Trans. Geosci. Remote Sens.*, 28:19-28, 1990.
- McLaughlin, S. A., "The U.S. Army Ultra-High Resolution Turbulence Profiling FM-CW Radar: Description and Data," *Atmospheric Propagation and Remote Sensing*, In *Proceedings of the SPIE*, 1688, p 294-298, 1992.
- Miller, P. A., and M. F. Barth, *Quality Control of Hourly Profiler Winds*. Memorandum for Record, Environmental Research Laboratories, NOAA, Boulder, CO, p 36, 1993.
- Nastrom, G. D., and F. D. Eaton, "The Coupling of Gravity Waves and Turbulence at White Sands, New Mexico, From VHF Radar Observations," *J. Appl. Meteorol.*, 32:81-87, 1993.
- Richter, J. H., "High Resolution Tropospheric Radar Sounding," *Radio Sci.*, 4:1261-1268, 1969.
- Warnock, J. M., T. E. Van Zandt, and J. L. Green, "A Statistical Model to Estimate Mean Values of Parameters of Turbulence In the Free Atmosphere," *Preprints of Seventh Symposium on Turbulence and Diffusion*, New Orleans, LA, p 156-159, 1985.
- Weber, B. L., and D. B. Wuertz, *Quality Control Algorithm for Profiler Measurements of Winds and Temperatures*, NOAA Technical Memo, ERL WPL-212, p 32, 1991.

- Weber, B. L., D. B. Wuertz, D. C. Law, S. S. Frisch, and J. M. Brown, "Effects of Small-Scale Vertical Motion on Radar Measurements of Wind and Temperature Profiles," *J. Atmos. Ocean. Technol.*, 9:193-209, 1992.
- Weber, B. L., D. B. Wuertz, D. C. Welsh, and R. McPeck, "Quality Controls For Profiler Measurements of Winds and RASS Temperatures," *J. Atmos. Ocean. Technol.*, 10:452-464, 1993.
- Wolfe, D. E., D. C. Welsh, B. L. Weber, D. B. Wuertz, J. E. Gaynor, and J. P. Ye, "Comparisons of Quality Control Methods For Low-Level Wind Profiler Data," *Preprints of Eighth Symposium on Meteorological Observations and Instrumentation*, Anaheim, CA, p 257-263, 1993.
- Wuertz, D. B., and B. L. Weber, *Editing Wind Profiler Measurements*, NOAA Technical Report, ERL 438-WPL 62, p 78, 1989.

## Acronyms and Abbreviations

AGL	above ground level
A.I.R.	Atmospheric Instrumentation Research, Inc.
ANOVA	analysis of variance
APO	Apache Peak Observatory
APRF	Atmospheric Profiler Research Facility
ARL	Army Research Laboratory
$C_n^2$	refractive index structure parameter
$C_T^2$	tower-mounted spatial temperature
FM-CW	frequency modulated continuous wave
HP	Hewlett-Packard
LL	lower limit
MSE	mean square error
MSL	mean sea level
NOAA	National Oceanic and Atmospheric Administration
PBL	planetary boundary layer
RASS	Radio Acoustic Sounding System
RF	radio frequency
SAS	Statistical Analysis Software
UL	upper limit
UTC	universal time coordinate
WSMR	White Sands Missile Range

## Bibliography

- Jasperson, W. H., "Mesoscale Time and Space Wind Variability," *J. Appl. Meteorol.*, **21**:831-839, 1982.
- Lawrence, T. R., B. F. Weber, M. J. Post, R. M. Hardesty, R. A. Richter, N. L. Abshire, and F. F. Hall, Jr., *A Comparison of Doppler Lidar, Rawinsonde, and 915-MHz UHF Wind Profiler Measurements of Tropospheric Winds*, NOAA Tech. Memo., ERL WPL-130, Boulder, CO, p 55, 1986.
- Martner, B. E., D. B. Wuertz, B. B. Stankov, R. G. Strauch, E. R. Westwater, K. S. Gage, W. L. Ecklund, C. L. Martin, and W. F. Dabberdt, "An Evaluation of Wind Profiler, RASS, and Microwave Radiometer Performance," *Bull. Am. Meteorol. Soc.*, **74**:599-613, 1993.
- May, P. T., and R. G. Strauch, "An Examination of Wind Profiler Data Processing Algorithms," *J. Atmos. Ocean. Technol.*, **6**:731-735, 1989.
- May, P. T., K. P. Moran, and R. G. Strauch, "The Accuracy of RASS Temperature Measurements," *J. Appl. Meteorol.*, **28**:1329-1335, 1989.
- Ottersten, H., "Atmospheric Structure and Radar Back-Scattering in Clear Air," *Radio Sci.*, **4**:1179-1193, 1969.
- Peters, G., H. Timmermann, and H. Hinzpeter, "Temperature Sounding In the Planetary Boundary Layer By RASS - System Analysis and Results," *Int. J. Remote Sens.*, **4**:49-63, 1983.
- Schroeder, J. A., "A Comparison of Temperature Soundings Obtained From Simultaneous Radiometric, Radio-Acoustic, and Rawinsonde Measurements," *J. Atmos. Ocean. Technol.*, **7**:495-503, 1990.
- Strauch, R. G., B. L. Weber, A. S. Frisch, C. G. Little, D. A. Merritt, K. P. Moran, and D. C. Welsh, "The Precision and Relative Accuracy of Profiler Wind Measurements," *J. Atmos. Ocean. Technol.*, **4**:563-571, 1987.

**Appendix A**  
**Range Gate Information for the Wind Profilers**

Wind speed and direction vertical profiles were obtained with 50-, 404-, and 924-MHz profilers. Tables A-1 through A-4 list the gate numbers and the corresponding gate heights and height ranges for the 50-, 404- (high and low modes), and 924-MHz profilers.

**Table A-1. Gates for the 50-MHz wind profiler**

Gate No.	Gate Height (m AGL)	Height Range (m AGL)
1	2000	1925-2075
2	2150	2075- 2224
3	2299	2224- 2374
4	2449	2374- 2524
5	2599	2524- 2674
6	2749	2674- 2824
7	2899	2824- 2974
8	3049	2974- 3124
9	3199	3124- 3274
10	3349	3274- 3424
11	3499	3424- 3574
12	3648	3574- 3723
13	3798	3723- 3873
14	3948	3873- 4023
15	4098	4023- 4173
16	4248	4173- 4323
17	4398	4323- 4473
18	4548	4473- 4623
19	4698	4623- 4773
20	4848	4773- 4923
21	4998	4923- 5073
22	5147	5073- 5222
23	5297	5222- 5372
24	5447	5372- 5522
25	5597	5522- 5672
26	5747	5672- 5822
27	5897	5822- 5972
28	6047	5972- 6122
29	6197	6122- 6272
30	6347	6272- 6422
31	6497	6422- 6572
32	6646	6572- 6721
33	6796	6721- 6871

**Table A-1. Gates for the 50-MHz wind profiler  
(continued)**

Gate No.	Gate Height (m AGL)	Height Range (m AGL)
34	6946	6871- 7021
35	7096	7021- 7171
36	7246	7171- 7321
37	7396	7321- 7471
38	7546	7471- 7621
39	7696	7621- 7771
40	7846	7771- 7921
41	7995	7921- 8070
42	8145	8070- 8220
43	8295	8220- 8370
44	8445	8370- 8520
45	8595	8520- 8670
46	8745	8670- 8820
47	8895	8820- 8970
48	9045	8970- 9120
49	9195	9120- 9270
50	9345	9270- 9420
51	9494	9420- 9569
52	9644	9569- 9719
53	9794	9719- 9869
54	9944	9869-10019
55	10094	10019-10169
56	10244	10169-10319
57	10394	10319-10469
58	10544	10469-10619
59	10694	10619-10769
60	10843	10769-10918
61	10993	10918-11068
62	11143	11068-11218
63	11293	11218-11368
64	11443	11368-11518
65	11593	11518-11668
66	11743	11668-11818
67	11893	11818-11968
68	12043	11968-12118
69	12193	12118-12268
70	12342	12268-12417
71	12492	12417-12567
72	12642	12567-12717
73	12792	12717-12867

**Table A-1. Gates for the 50-MHz wind profiler  
(continued)**

Gate No.	Gate Height (m AGL)	Height Range (m AGL)
74	12942	12867-13017
75	13092	13017-13167
76	13242	13167-13317
77	13392	13317-13467
78	13542	13467-13617
79	13692	13617-13767
80	13841	13767-13916
81	13991	13916-14066
82	14141	14066-14216
83	14291	14216-14366
84	14441	14366-14516
85	14591	14516-14666
86	14741	14666-14816
87	14891	14816-14966
88	15041	14966-15116
89	15190	15116-15265
90	15340	15265-15415
91	15490	15415-15565
92	15640	15565-15715
93	15790	15715-15543
94	15940	15543-16015
95	16090	16015-16165
96	16240	16165-16315
97	16390	16315-16465
98	16540	16465-16615
99	16689	16615-16764
100	16839	16764-16914
101	16989	16914-17064
102	17139	17064-17214
103	17289	17214-17364
104	17439	17364-17514
105	17589	17514-17664
106	17739	17664-17814
107	17889	17814-17964
108	18039	17964-18114
109	18188	18114-18264
110	18338	18264-18413
111	18488	18413-18563

**Table A-2. High-mode gates for the 404-MHz wind profiler**

Gate No.	Gate Height (m AGL)	Height Range (m AGL)
1	7500	7000-8000
2	7750	7250-8250
3	8000	7500-8500
4	8250	7750-8750
5	8500	8000-9000
6	8750	8250-9250
7	9000	8500-9500
8	9250	8750-9750
9	9500	9000-10000
10	9750	9250-10250
11	10000	9500-10500
12	10250	9750-10750
13	10500	10000-11000
14	10750	10250-11250
15	11000	10500-11500
16	11250	10750-11750
17	11500	11000-12000
18	11750	11250-12250
19	12000	11500-12500
20	12250	11750-12750
21	12500	12000-13000
22	12750	12250-13250
23	13000	12500-13500
24	13250	12750-13750
25	13500	13000-14000
26	13750	13250-14250
27	14000	13500-14500
28	14250	13750-14750
29	14500	14000-15000
30	14750	14250-15250
31	15000	14500-15500
32	15250	14750-15750
33	15500	15000-16000
34	15750	15250-16250
35	16000	15500-16500
36	16250	15750-16750

**Table A-3. Low-mode gates for the 404-MHz wind profiler**

Gate No.	Gate Height (m AGL)	Height Range (m AGL)
1	500	312.5- 687.5
2	750	562.5- 937.5
3	1000	812.5-1187.5
4	1250	1062.5-1437.5
5	1500	1312.5-1687.5
6	1750	1562.5-1937.5
7	2000	1812.5-2187.5
8	2250	2062.5-2437.5
9	2500	2312.5-2687.5
10	2750	2562.5-2937.5
11	3000	2812.5-3187.5
12	3250	3062.5-3437.5
13	3500	3312.5-3687.5
14	3750	3562.5-3937.5
15	4000	3812.5-4187.5
16	4250	4062.5-4437.5
17	4500	4312.5-4687.5
18	4750	4562.5-4937.5
19	5000	4812.5-5187.5
20	5250	5062.5-5437.5
21	5500	5312.5-5687.5
22	5750	5562.5-5937.5
23	6000	5812.5-6187.5
24	6250	6062.5-6437.5
25	6500	6312.5-6687.5
26	6750	6562.5-6937.5
27	7000	6812.5-7187.5
28	7250	7062.5-7437.5
29	7500	7312.5-7687.5
30	7750	7562.5-7937.5
31	8000	7812.5-8187.5
32	8250	8062.5-8437.5
33	8500	8312.5-8687.5
34	8750	8562.5-8937.5
35	9000	8812.5-9187.5
36	9250	9062.5-9437.5

**Table A-4. Gates for the 924-MHz wind profiler**

Gate No.	Gate Height (m AGL)	Height Range (m AGL)
1	140	89.5-190.5
2	241	190.5-291.5
3	342	291.5-392.5
4	443	392.5-493.5
5	544	493.5-594.5
6	645	594.5-695.5
7	746	695.5-796.5
8	847	796.5-897.5
9	948	897.5-998.5
10	1049	998.5-1099.5
11	1150	1099.5-1200.5
12	1251	1200.5-1301.5
13	1352	1301.5-1402.5
14	1453	1402.5-1503.5
15	1554	1503.5-1604.5
16	1655	1604.5-1705.5
17	1756	1705.5-1806.5
18	1857	1806.5-1907.5
19	1958	1907.5-2008.5
20	2059	2008.5-2109.5
21	2160	2109.5-2210.5
22	2261	2210.5-2311.5
23	2362	2311.5-2412.5
24	2463	2412.5-2513.5
25	2564	2513.5-2614.5
26	2665	2614.5-2715.5
27	2766	2715.5-2816.5
28	2867	2816.5-2917.5
29	2968	2917.5-3018.5
30	3069	3018.5-3119.5
31	3170	3119.5-3220.5
32	3271	3220.5-3321.5
33	3372	3321.5-3422.5
34	3473	3422.5-3523.5
35	3574	3523.5-3624.5
36	3675	3624.5-3725.5
37	3776	3725.5-3826.5
38	3877	3826.5-3927.5
39	3978	3927.5-4028.5
40	4079	4028.5-4129.5

**Table A-4. Gates for the 924-MHz wind profiler  
(continued)**

Gate No.	Gate Height (m AGL)	Height Range (m AGL)
41	4180	4129.5-4230.5
42	4281	4230.5-4331.5
43	4382	4331.5-4432.5
44	4483	4432.5-4533.5
45	4584	4533.5-4634.5
46	4685	4634.5-4735.5
47	4786	4735.5-4836.5
48	4887	4836.5-4937.5
49	4988	4937.5-5038.5
50	5089	5038.5-5139.5

## **Appendix B**

### **Range Gate Information for the Virtual Temperature Profilers**

Virtual temperature vertical profiles were obtained with the RASS system associated with the 50-, 404-, and 924-MHz profilers. Tables B-1 through B-3 list the gate numbers and corresponding gate heights and height ranges.

The gate information for the 50-MHz RASS system was nominally the same as for the 50-MHz wind profiler. However, antenna problems precluded acquisition of reliable data below 5 km AGL, and weak signal strength generally precluded acquisition of reliable data above about 12 km AGL.

**Table B-1. Gates for the 50-MHz RASS system and the mean air temperature for each gate as determined from radiosondes released from Oasis Site from Jan 92 through Mar 93**

Gate No.	Gate Height (m AGL)	Height Range (m AGL)	Mean Air Temperature (°C)
1	4200	4125-4275	-10.0
2	4350	4275-4425	-11.1
3	4500	4425-4575	-12.0
4	4650	4575-4725	-13.1
5	4800	4725-4875	-14.1
6	4950	4875-5025	-15.0
7	5100	5025-5175	-16.2
8	5250	5175-5325	-17.1
9	5400	5325-5475	-18.2
10	5550	5475-5625	-19.2
11	5700	5625-5775	-20.3
12	5850	5775-5925	-21.5
13	6000	5925-6075	-22.5
14	6150	6075-6225	-23.6
15	6300	6225-6375	-24.7
16	6450	6375-6525	-25.8
17	6600	6525-6675	-26.9
18	6750	6675-6825	-28.1
19	6900	6825-6975	-29.1
20	7050	6975-7125	-30.3
21	7200	7125-7275	-31.4
22	7350	7275-7425	-32.5
23	7500	7425-7575	-33.5
24	7650	7575-7725	-34.7
25	7800	7725-7875	-35.8

**Table B-1. Gates for the 50-MHz RASS system and the mean air temperature for each gate as determined from radiosondes released from Oasis Site from Jan 92 through Mar 93 (continued)**

Gate No.	Gate Height (m AGL)	Height Range (m AGL)	Mean Air Temperature (°C)
26	7950	7875-8025	-36.8
27	8100	8025-8175	-37.9
28	8250	8175-8325	-38.9
29	8400	8325-8475	-39.9
30	8550	8475-8625	-40.9
31	8700	8625-8775	-41.8
32	8850	8775-8925	-42.8
33	9000	8925-9075	-43.6
34	9150	9075-9225	-44.7
35	9300	9225-9375	-45.5
36	9450	9375-9525	-46.4
37	9600	9525-9675	-47.2
38	9750	9675-9825	-48.0
39	9900	9825-9975	-48.8
40	10050	9975-10125	-49.6
41	10200	10125-10275	-50.5
42	10350	10275-10425	-51.3
43	10500	10425-10575	-51.9
44	10650	10575-10725	-52.6
45	10800	10725-10875	-53.3
46	10950	10875-11025	-53.9
47	11100	11025-11175	-54.5
48	11250	11175-11325	-55.1
49	11400	11325-11475	-55.7
50	11550	11475-11625	-56.3
51	11700	11625-11775	-56.9
52	11850	11775-11925	-57.4
53	12000	11925-12075	-58.0
54	12150	12075-12225	-58.5
55	12300	12225-12375	-59.0
56	12450	12375-12525	-59.5
57	12600	12525-12675	-60.0
58	12750	12675-12825	-60.5
59	12900	12825-12975	-61.0
60	13050	12975-13125	-61.5
61	13200	13125-13275	-62.0
62	13350	13275-13425	-62.6
63	13500	13425-13575	-63.1
64	13650	13575-13725	-63.5

**Table B-2. Gates for the 404-MHz RASS system and the mean air temperature for each gate as determined from radiosondes released from Oasis Site from Jan 92 through Mar 93**

Gate No.	Gate Height (m AGL)	Height Range (m AGL)	Mean Air Temperature (°C)
1	500	312.5-687.5	16.5
2	750	562.5- 937.5	14.7
3	1000	812.5-1187.5	12.7
4	1250	1062.5-1437.5	10.8
5	1500	1312.5-1687.5	8.8
6	1750	1562.5-1937.5	6.9
7	2000	1812.5-2187.5	5.0
8	2250	2062.5-2437.5	3.2
9	2500	2312.5-2687.5	1.5
10	2750	2562.5-2937.5	-0.3
11	3000	2812.5-3187.5	-1.9
12	3250	3062.5-3437.5	-3.6
13	3500	3312.5-3687.5	-5.4
14	3750	3562.5-3937.5	-7.0
15	4000	3812.5-4187.5	-8.8
16	4250	4062.5-4437.5	-10.4
17	4500	4312.5-4687.5	-12.0
18	4750	4562.5-4937.5	-13.8
19	5000	4812.5-5187.5	-15.4
20	5250	5062.5-5437.5	-17.2
21	5500	5312.5-5687.5	-18.9
22	5750	5562.5-5937.5	-20.7

**Table B-3. Gates for the 924-MHz RASS system**

Gate No.	Gate Height (m AGL)	Height Range (m AGL)
1	127	74-180
2	233	180-285
3	338	285-390
4	442	390-494
5	548	494-600
6	652	600-704
7	757	704-810
8	863	810-915
9	967	915-1019
10	1072	1019-1125
11	1178	1125-1231
12	1283	1231-1336
13	1388	1336-1460
14	1492	1460-1544
15	1597	1544-1649

**Appendix C**  
**SAS Statistical Runs for Table 17**

RAOB vs. 50 MHz RASS DATA  
 ALL RAOB vs. 50 MHz RASS DATA - study days

Correlation Analysis

2 'VAR' Variables: B\_TEMP A\_TEMP

Simple Statistics

Variable	N	Mean	Std Dev	Sum
B_TEMP	555	-34.909910	11.779966	-19375
A_TEMP	555	-36.827333	13.037956	-20439

Simple Statistics

Variable	Minimum	Maximum	Label
B_TEMP	-68.500000	-11.300000	50 MHz RASS
A_TEMP	-63.670000	-5.200000	RAOB RASS title RAOB vs. 50 MHz RASS D

Pearson Correlation Coefficients / Prob > |R| under Ho: Rho=0 / N = 555

	B_TEMP	A_TEMP
B_TEMP 50 MHz RASS	1.00000 0.0	0.94868 0.0001
A_TEMP RAOB RASS title RAOB vs. 50 MHz RASS D	0.94868 0.0001	1.00000 0.0

RAOB vs. 50 MHz RASS DATA  
 ALL RAOB vs. 50 MHz RASS DATA - study days RASS

Univariate Procedure

Variable=TEMP

Moments

N	555	Sum Wgts	555
Mean	1.917423	Sum	1064.17
Std Dev	4.164758	Variance	17.34521
Skewness	-3.69329	Kurtosis	15.39902
USS	11649.71	CSS	9609.244
CV	217.2059	Std Mean	0.176784
T:Mean=0	10.84613	Pr> T	0.0001
Num ^= 0	555	Num > 0	512
M(Sign)	234.5	Pr>= M	0.0001
Sgn Rank	59297.5	Pr>= S	0.0001
W:Normal	0.533726	Pr<W	0.0001

99% Confidence Interval

N	ALPHA	MEAN	UPPER	LOWER
555	0.01	1.91742	2.37282	1.46203

95% Confidence Interval

N	ALPHA	MEAN	UPPER	LOWER
555	0.05	1.91742	2.26392	1.57093

RAOB vs. 50 MHz RASS DATA  
 ALL RAOB vs. 50 MHz RASS DATA - study days RASS

Analysis of Variance Procedure

Dependent Variable: B\_TEMP

Source	DF	Sum of Squares	Mean Square	F Value	Pr > F
Model	440	76659.855495	174.226944	91.36	0.0001
Error	114	217.400000	1.907018		
Corrected Total	554	76877.255495			
	R-Square	C.V.	Root MSE	B_TEMP Mean	
	0.997172	-3.955748	1.3809481	-34.909910	

Source	DF	Anova SS	Mean Square	F Value	Pr > F
A_TEMP	440	76659.855495	174.226944	91.36	0.0001

RAOB vs. 404 MHz RASS DATA  
 ALL RAOB vs. 404 MHz RASS DATA - study days

Correlation Analysis

2 'VAR' Variables: B\_TEMP A\_TEMP

Simple Statistics

Variable	N	Mean	Std Dev	Sum
B_TEMP	339	3.803540	11.286227	1289.400000
A_TEMP	339	2.603923	11.530957	882.730000

Simple Statistics

Variable	Minimum	Maximum	Label
B_TEMP	-9.100000	25.000000	404 MHz RASS
A_TEMP	-20.200000	27.000000	RAOB RASS title RAOB vs. 404 MHz RASS

Pearson Correlation Coefficients / Prob > |R| under Ho: Rho=0 / N = 339

	B_TEMP	A_TEMP
B_TEMP	1.00000	0.95787
404 MHz RASS	0.0	0.0001
A_TEMP	0.95787	1.00000
RAOB RASS title RAOB vs. 404 MHz RASS	0.0001	0.0

RAOB vs. 404 MHz RASS DATA  
 ALL RAOB vs. 404 MHz RASS DATA - study days RASS

Univariate Procedure

Variable=TEMP

Moments

N	339	Sum Wgts	339
Mean	1.199617	Sum	406.67
Std Dev	3.320441	Variance	11.02533
Skewness	-0.59629	Kurtosis	2.330554
USS	4214.41	CSS	3726.562
CV	276.7919	Std Mean	0.180342
T:Mean=0	6.651911	Pr> T	0.0001
Num ^= 0	338	Num > 0	261
M(Sign)	92	Pr>= M	0.0001
Sgn Rank	14442.5	Pr>= S	0.0001
W:Normal	0.931385	Pr<W	0.0001

99% Confidence Interval

N	ALPHA	MEAN	UPPER	LOWER
339	0.01	1.19962	1.66418	0.73506

95% Confidence Interval

N	ALPHA	MEAN	UPPER	LOWER
339	0.05	1.19962	1.55309	0.84615

RAOB vs. 404 MHz RASS DATA  
 ALL RAOB vs. 404 MHz RASS DATA - study days RASS

Analysis of Variance Procedure

Dependent Variable: B\_TEMP

Source	DF	Sum of Squares	Mean Square	F Value	Pr > F
Model	322	43015.490752	133.588481	55.39	0.0001
Error	16	38.585000	2.411563		
Corrected Total	338	43054.075752			

R-Square	C.V.	Root MSE	B_TEMP Mean
0.999104	40.82830	1.5529206	3.8035398

Source	DF	Anova SS	Mean Square	F Value	Pr > F
A_TEMP	322	43015.490752	133.588481	55.39	0.0001

RAOB vs. 924 MHZ RASS DATA  
 ALL RAOB vs. 924 MHZ RASS DATA - study days

Correlation Analysis

2 'VAR' Variables: B\_TEMP A\_TEMP

Simple Statistics

Variable	N	Mean	Std Dev	Sum
B_TEMP	111	21.700000	4.210096	2408.700000
A_TEMP	111	20.886126	4.731393	2318.360000

Simple Statistics

Variable	Minimum	Maximum	Label
B_TEMP	11.200000	30.400000	924 MHZ RASS
A_TEMP	9.650000	30.700000	RAOB RASS title RAOB vs. 924 MHZ RASS

Pearson Correlation Coefficients / Prob > |R| under Ho: Rho=0 / N = 111

	B_TEMP	A_TEMP
B_TEMP	1.00000	0.87429
924 MHZ RASS	0.0	0.0001
A_TEMP	0.87429	1.00000
RAOB RASS title RAOB vs. 924 MHZ RASS	0.0001	0.0

RAOB vs. 924 MHz RASS DATA  
 ALL RAOB vs. 924 MHz RASS DATA - study days RASS

Univariate Procedure

Variable=TEMP

Moments

N	111	Sum Wgts	111
Mean	0.813874	Sum	90.34
Std Dev	2.297839	Variance	5.280062
Skewness	0.414306	Kurtosis	1.002759
USS	654.3322	CSS	580.8068
CV	282.3335	Std Mean	0.218101
T:Mean=0	3.731634	Pr> T	0.0003
Num ^= 0	111	Num > 0	72
M(Sign)	16.5	Pr>= M	0.0022
Sgn Rank	1183	Pr>= S	0.0004
W:Normal	0.978378	Pr<W	0.4109

99% Confidence Interval

N	ALPHA	MEAN	UPPER	LOWER
111	0.01	0.81387	1.37570	0.25205

95% Confidence Interval

N	ALPHA	MEAN	UPPER	LOWER
111	0.05	0.81387	1.24135	0.38640

RAOB vs. 924 MHz RASS DATA  
 ALL RAOB vs. 924 MHz RASS DATA - study days RASS

Analysis of Variance Procedure

Dependent Variable: B\_TEMP

Source	DF	Sum of Squares	Mean Square	F Value	Pr > F
Model	98	1845.850000	18.8352041	2.18	0.0667
Error	12	103.890000	8.6575000		
Corrected Total	110	1949.740000			
	R-Square	C.V.	Root MSE	B_TEMP Mean	
	0.946716	13.55928	2.9423630	21.700000	

Source	DF	Anova SS	Mean Square	F Value	Pr > F
A_TEMP	98	1845.850000	18.8352041	2.18	0.0667

## Distribution

	Copies
NASA MARSHAL SPACE FLT CTR ATMOSPHERIC SCIENCES DIV E501 ATTN DR FICHTL HUNTSVILLE AL 35802	1
NASA SPACE FLT CTR ATMOSPHERIC SCIENCES DIV CODE ED 41 1 HUNTSVILLE AL 35812	1
ARMY STRAT DEFNS CMND CSSD SL L ATTN DR LILLY PO BOX 1500 HUNTSVILLE AL 35807-3801	1
ARMY MISSILE CMND AMSMI RD AC AD ATTN DR PETERSON REDSTONE ARSENAL AL 35898-5242	1
ARMY MISSILE CMND AMSMI RD AS SS ATTN MR H F ANDERSON REDSTONE ARSENAL AL 35898-5253	1
ARMY MISSILE CMND AMSMI RD AS SS ATTN MR B WILLIAMS REDSTONE ARSENAL AL 35898-5253	1
ARMY MISSILE CMND AMSMI RD DE SE ATTN MR GORDON LILL JR REDSTONE ARSENAL AL 35898-5245	1
ARMY MISSILE CMND REDSTONE SCI INFO CTR AMSMI RD CS R DOC REDSTONE ARSENAL AL 35898-5241	1

ARMY MISSILE CMND AMSMI REDSTONE ARSENAL AL 35898-5253	1
CMD 420000D C0245 ATTN DR A SHLANTA NAVAIRWARCENWPNDIV 1 ADMIN CIR CHINA LAKE CA 93555-6001	1
PACIFIC MISSILE TEST CTR GEOPHYSICS DIV ATTN CODE 3250 POINT MUGU CA 93042-5000	1
LOCKHEED MIS & SPACE CO ATTN KENNETH R HARDY ORG 91 01 B 255 3251 HANOVER STREET PALO ALTO CA 94304-1191	1
NAVAL OCEAN SYST CTR CODE 54 ATTN DR RICHTER SAN DIEGO CA 92152-5000	1
METEOROLOGIST IN CHARGE KWAJALEIN MISSILE RANGE PO BOX 67 APO SAN FRANCISCO CA 96555	1
DEPT OF COMMERCE CTR MOUNTAIN ADMINISTRATION SPPRT CTR LIBRARY R 51 325 S BROADWAY BOULDER CO 80303	1
DR HANS J LIEBE NTIA ITS S 3 325 S BROADWAY BOULDER CO 80303	1
NCAR LIBRARY SERIALS NATL CTR FOR ATMOS RSCH PO BOX 3000 BOULDER CO 80307-3000	1

DEPT OF COMMERCE CTR 1  
325 S BROADWAY  
BOULDER CO 80303

DAMI POI 1  
WASH DC 20310-1067

MIL ASST FOR ENV SCI OFC 1  
OF THE UNDERSEC OF DEFNS  
FOR RSCH & ENGR R&AT E LS  
PENTAGON ROOM 3D129  
WASH DC 20301-3080

DEAN RMD 1  
ATTN DR GOMEZ  
WASH DC 20314

ARMY INFANTRY 1  
ATSH CD CS OR  
ATTN DR E DUTOIT  
FT BENNING GA 30905-5090

AIR WEATHER SERVICE 1  
TECH LIBRARY FL4414 3  
SCOTT AFB IL 62225-5458

USAFETAC DNE 1  
ATTN MR GLAUBER  
SCOTT AFB IL 62225-5008

HQ AWS DOO 1  
SCOTT AFB IL 62225-5008

PHILLIPS LABORATORY 1  
PL LYP  
ATTN MR CHISHOLM  
HANSCOM AFB MA 01731-5000

ATMOSPHERIC SCI DIV 1  
GEOPHYSICS DIRCTR  
PHILLIPS LABORATORY  
HANSCOM AFB MA 01731-5000

PHILLIPS LABORATORY 1  
PL LYP 3  
HANSCOM AFB MA 01731-5000

RAYTHEON COMPANY 1  
ATTN DR SONNENSCHNEIN  
528 BOSTON POST ROAD  
SUDBURY MA 01776  
MAIL STOP 1K9

ARMY MATERIEL SYST 1  
ANALYSIS ACTIVITY  
AMXSY  
ATTN MP H COHEN  
APG MD 21005-5071

ARMY MATERIEL SYST 1  
ANALYSIS ACTIVITY  
AMXSY AT  
ATTN MR CAMPBELL  
APG MD 21005-5071

ARMY MATERIEL SYST 1  
ANALYSIS ACTIVITY  
AMXSY CR  
ATTN MR MARCHET  
APG MD 21005-5071

ARL CHEMICAL BIOLOGY 1  
NUC EFFECTS DIV  
AMSRL SL CO  
APG MD 21010-5423

ARMY MATERIEL SYST 1  
ANALYSIS ACTIVITY  
AMXSY  
APG MD 21005-5071

ARMY MATERIEL SYST 1  
ANALYSIS ACTIVITY  
AMXSY CS  
ATTN MR BRADLEY  
APG MD 21005-5071

ARMY RESEARCH LABORATORY 1  
AMSRL D  
2800 POWDER MILL ROAD  
ADELPHI MD 20783-1145

ARMY RESEARCH LABORATORY 1  
AMSRL OP SD TP  
TECHNICAL PUBLISHING  
2800 POWDER MILL ROAD  
ADELPHI MD 20783-1145

ARMY RESEARCH LABORATORY AMSRL OP CI SD TL 2800 POWDER MILL ROAD ADELPHI MD 20783-1145	1
ARMY RESEARCH LABORATORY AMSRL SS SH ATTN DR SZTANKAY 2800 POWDER MILL ROAD ADELPHI MD 20783-1145	1
ARMY RESEARCH LABORATORY AMSRL 2800 POWDER MILL ROAD ADELPHI MD 20783-1145	1
NATIONAL SECURITY AGCY W21 ATTN DR LONGBOTHUM 9800 SAVAGE ROAD FT GEORGE G MEADE MD 20755-6000	1
OIC NAVSWC TECH LIBRARY CODE E 232 SILVER SPRINGS MD 20903-5000	1
ARMY RSRC OFC AMXRO GS ATTN DR BACH PO BOX 12211 RTP NC 27709	1
DR JERRY DAVIS NCSU PO BOX 8208 RALEIGH NC 27650-8208	1
US ARMY CECRL CECRL GP ATTN DR DETSCH HANOVER NH 03755-1290	1
ARMY ARDEC SMCAR IMI I BLDG 59 DOVER NJ 07806-5000	1
ARMY SATELLITE COMM AGCY DRCPM SC 3 FT MONMOUTH NJ 07703-5303	1

ARMY COMMUNICATIONS ELECTR CTR FOR EW RSTA AMSEL EW D FT MONMOUTH NJ 07703-5303	1
ARMY COMMUNICATIONS ELECTR CTR FOR EW RSTA AMSEL EW MD FT MONMOUTH NJ 07703-5303	1
ARMY DUGWAY PROVING GRD STEDP MT DA L 3 DUGWAY UT 84022-5000	1
ARMY DUGWAY PROVING GRD STEDP MT M ATTN MR BOWERS DUGWAY UT 84022-5000	1
DEPT OF THE AIR FORCE OL A 2D WEATHER SQUAD MAC HOLLOMAN AFB NM 88330-5000	1
PL WE KIRTLAND AFB NM 87118-6008	1
USAF ROME LAB TECH CORRIDOR W STE 262 RL SUL 26 ELECTR PKWY BLD 106 GRIFFISS AFB NY 13441-4514	1
AFMC DOW WRIGHT PATTERSON AFB OH 0334-5000	1
ARMY FIELD ARTLLRY SCHOOL ATSF TSM TA FT SILL OK 73503-5600	1
NAVAL AIR DEV CTR CODE 5012 ATTN AL SALIK WARMINISTER PA 18974	1

ARMY FOREGN SCI TECH CTR CM 220 7TH STREET NE CHARLOTTESVILLE VA 22901-5396	1
NAVAL SURFACE WEAPONS CTR CODE G63 DAHLGREN VA 22448-5000	1
ARMY OEC CSTE EFS PARK CENTER IV 4501 FORD AVE ALEXANDRIA VA 22302-1458	1
ARMY CORPS OF ENGRS ENGR TOPOGRAPHICS LAB ETL GS LB FT BELVOIR VA 22060	1
ARMY TOPO ENGR CTR CETEC ZC 1 FT BELVOIR VA 22060-5546	1
LOGISTICS CTR ATCL CE FT LEE VA 23801-6000	1
SCI AND TECHNOLOGY 101 RESEARCH DRIVE HAMPTON VA 23666-1340	1
ARMY NUCLEAR CML AGCY MONA ZB BLDG 2073 SPRINGFIELD VA 22150-3198	1
USATRADOC ATCD FA FT MONROE VA 23651-5170	1
ARMY TRADOC ANALYSIS CTR ATRC WSS R WSMR NM 88002-5502	1
ARMY RESEARCH LABORATORY AMSRL BE S BATTLEFIELD ENVIR DIR WSMR NM 88002-5501	1

ARMY RESEARCH LABORATORY AMSRL BE W BATTLEFIELD ENVIR DIR WSMR NM 88002-5501	1
ARMY RESEARCH LABORATORY AMSRL BE ATTN MR VEAZY BATTLEFIELD ENVIR DIR WSMR NM 88002-5501	1
DTIC 8725 JOHN J KINGMAN RD SUITE 0944 FT BELVOIR VA 22060-6218	1
ARMY MISSILE CMND AMSMI REDSTONE ARSENAL AL 35898-5243	1
ARMY DUGWAY PROVING GRD STEDP 3 DUGWAY UT 84022-5000 USATRADO ATCD FA FT MONROE VA 23651-5170	1  1
WSMR TECH LIBRARY BR STEWIS IM IT WSMR NM 88001	1
Record Copy	2
TOTAL	77